frontiers | Research Topics

Hazardous pollutants in the environment: Analysis, assessment and remediation

Edited by
Jun Wu, Xiaohu Wen, Jian-Hua Wang and Antonio Miranda

Published in
Frontiers in Environmental Science

ISSN 1664-8714
ISBN 978-2-8325-3285-0
DOI 10.3389/978-2-8325-3285-0

About Frontiers

Frontiers is more than just an open access publisher of scholarly articles: it is a pioneering approach to the world of academia, radically improving the way scholarly research is managed. The grand vision of Frontiers is a world where all people have an equal opportunity to seek, share and generate knowledge. Frontiers provides immediate and permanent online open access to all its publications, but this alone is not enough to realize our grand goals.

Frontiers journal series

The Frontiers journal series is a multi-tier and interdisciplinary set of open-access, online journals, promising a paradigm shift from the current review, selection and dissemination processes in academic publishing. All Frontiers journals are driven by researchers for researchers; therefore, they constitute a service to the scholarly community. At the same time, the *Frontiers journal series* operates on a revolutionary invention, the tiered publishing system, initially addressing specific communities of scholars, and gradually climbing up to broader public understanding, thus serving the interests of the lay society, too.

Dedication to quality

Each Frontiers article is a landmark of the highest quality, thanks to genuinely collaborative interactions between authors and review editors, who include some of the world's best academicians. Research must be certified by peers before entering a stream of knowledge that may eventually reach the public - and shape society; therefore, Frontiers only applies the most rigorous and unbiased reviews. Frontiers revolutionizes research publishing by freely delivering the most outstanding research, evaluated with no bias from both the academic and social point of view. By applying the most advanced information technologies, Frontiers is catapulting scholarly publishing into a new generation.

What are Frontiers Research Topics?

Frontiers Research Topics are very popular trademarks of the *Frontiers journals series*: they are collections of at least ten articles, all centered on a particular subject. With their unique mix of varied contributions from Original Research to Review Articles, Frontiers Research Topics unify the most influential researchers, the latest key findings and historical advances in a hot research area.

Find out more on how to host your own Frontiers Research Topic or contribute to one as an author by contacting the Frontiers editorial office: frontiersin.org/about/contact

Hazardous pollutants in the environment: Analysis, assessment and remediation

Topic editors

Jun Wu — Harbin Engineering University, China

Xiaohu Wen — Northwest Institute of Eco-Environment and Resources, Chinese Academy of Sciences (CAS), China

Jian-Hua Wang — University of Chinese Academy of Sciences, China

Antonio Miranda — Federal University of São Paulo, Brazil

Citation

Wu, J., Wen, X., Wang, J.-H., Miranda, A., eds. (2023). *Hazardous pollutants in the environment: Analysis, assessment and remediation*. Lausanne: Frontiers Media SA. doi: 10.3389/978-2-8325-3285-0

Table of contents

frontiers | Frontiers in Environmental Science

TYPE Original Research
PUBLISHED 14 November 2022
DOI 10.3389/fenvs.2022.1025027

OPEN ACCESS

EDITED BY
Jun Wu,
Harbin Engineering University, China

REVIEWED BY
Danrui Sheng,
Chinese Academy of Sciences (CAS), China
Li Leiming,
Qinghai Institute of Salt Lakes (CAS), China

*CORRESPONDENCE
Mei Li,
mli@pku.edu.cn

SPECIALTY SECTION
This article was submitted to Toxicology, Pollution and the Environment, a section of the journal Frontiers in Environmental Science

RECEIVED 22 August 2022
ACCEPTED 27 October 2022
PUBLISHED 14 November 2022

CITATION
Zhang R, Li M and Ma H (2022), Comparative study on numerical simulation based on CALPUFF and wind tunnel simulation of hazardous chemical leakage accidents. *Front. Environ. Sci.* 10:1025027. doi: 10.3389/fenvs.2022.1025027

Comparative study on numerical simulation based on CALPUFF and wind tunnel simulation of hazardous chemical leakage accidents

Rongqian Zhang, Mei Li* and Hancong Ma

Institute of Remote Sensing and Geographical Information System, Peking University, Beijing, China

CALPUFF, as a Lagrangian puff modeling system, is mostly used in the field of atmospheric environment research and risk assessment. CALPUFF performs well for short-term and short-range release scenarios over complex terrain, as well as long-term and long-range transportation. Therefore, this article uses the CALPUFF model to simulate a toxic gas leakage accident in a hazardous chemical plant in an urban area, focusing on the influence of local buildings. Wind tunnel experiments are performed in accordance with the CALPUFF experiments to assess the model's accuracy in cases of chemical leakage accidents. The results of the wind tunnel experiment are superimposed on the map of CALPUFF calculation, and the quantitative analysis is also performed. The comparative results show that the simulation results of the CALPUFF are mainly affected by factors such as wind direction, wind speed, and the complexity of the surface environment. With less influence of buildings, such as the south and north wind, the CALPUFF simulation is consistent with the wind tunnel experiment, having a correlation coefficient of over 0.7 in most cases, while under the east wind, the consistency is significantly lower due to the influence of buildings. In addition, it is found that the wind tunnel experiment is more accurate in the near field of the pollution source, while CALPUFF is more suitable for simulating the overall trend of gas dispersion. The comparison and evaluation of the capabilities of different methods on gas dispersion simulation are helpful in guiding the emergency response during hazardous chemical leakage accidents.

KEYWORDS

hazardous chemical leakage accident, gas dispersion model, CALPUFF, wind tunnel data validation, building downwash

1 Introduction

A gas dispersion model studies the complex hydrodynamic processes of pollutants, such as diffusion, transportation, transformation, and deposition in the atmosphere. A gas dispersion model usually can be described as a set of computable mathematical formulas through reasonable physical and chemical assumptions. Generally, gas dispersion models can be divided into the box model, Gaussian model, Lagrangian model, Euler model, and computational fluid dynamics model (Holmes et al., 2006), according to the fundamental principles. The last four types of models are most commonly used.

The Gaussian model includes a plume model and a puff model, and the model systems of this type commonly used are ADMS (Carruthers et al., 1994), AERMOD (Cimorelli et al., 2004), and ALOHA (NOAA and EPA, 2007). The plume model considers gas emitted continuously, and the pollutant concentration distribution is compliant with the rule of Gaussian distribution, while the puff model considers the continuously emitted plume as a series of discrete pollutant masses, namely, the air mass. The emission of air mass is instantaneous, whose movement is affected by the wind direction and wind speed. The concentration distribution of the air masses conforms to Gaussian distribution, and the concentration of the pollutant at each receptor point is the linear superposition of the concentration value of each air mass here (Yuan et al., 2013). The Lagrangian model includes a particle model and a puff model, whose common model systems include HYSPLIT (Stein et al., 2015) and NAME (Jones et al., 2007). The particle model is a dispersion model based on the statistical theory of turbulence, which calculates the temporal and spatial probability distribution of particles by recording the movement track of the labeled particles so as to estimate the variation of the pollutant concentration. In the puff model, it is assumed that the concentration distribution of the puff satisfies Gaussian distribution in both horizontal and vertical directions (Yu and Cao, 2020). The Euler model, similar to the computational fluid dynamics model, is a kind of grid model that uses numerical methods to discretely solve the convection–dispersion equation for the concentration derived from the law of conservation of mass and Fick's Law (Stockie, 2011).

The gas dispersion model can be used not only in regional ecological monitoring and environmental pollution control but also in emergency response management. The research and applications of the gas dispersion model in the emergency field mainly concentrate on the nuclear accident (Liu et al., 2017; Li et al., 2018; Ulimoen et al., 2022), chemical industrial park (Huang et al., 2019; Cheng et al., 2021), gas pipeline (Mishra et al., 2015 CFD; Yan et al., 2016), and road transportation (Fallah-Shorshani et al., 2015; Kota et al., 2013). Compared with the environmental assessment cases, the emergency simulation often requires a near-field, finer spatial-temporal computational grid and further analysis and adjustment of the model parameters (Rzeszutek, 2019).

The validation study on the gas dispersion model is helpful in evaluating its applicability and prediction accuracy in different meteorology, terrain, and pollution source conditions so as to better guide model selection and parameter setting of different simulation scenarios. At present, many verification studies compare the field observation data on sampling points with the model simulation data. For example, Masoud Fallah–Shorshani used the composite model chain combining traffic, emission, and dispersion models to simulate the NO_2 pollution concentration of urban blocks and compared it with the observation data on measurement stations (Fallah-Shorshani et al., 2017). Piotr Holnicki used the CALPUFF model to simulate the annual average concentration of air pollutants in major cities in Warsaw and the hourly average concentration of air pollutants on a certain day and compared with the data on five observation stations, finding that the CALPUFF model has a higher accuracy of simulation on a long-time scale (Holnicki et al., 2016). In order to evaluate the simulation results of AERMOD, CALPUFF, ISC2, and RATCHET models, AS Rood used the dataset of the 1991 experiment in the Rocky Mountains for model verification, in which 140 sampling sites were distributed within 16 km from the pollution source, including 12 independent experiments (Rood, 2014). Although the field experiment can better represent the reality and has high reliability, its operation process is complex and time-consuming, and the number of sampling points is limited. In addition, the location and the pollutant type of field observations are limited. It is impossible to carry out experiments of toxic gases or in crowded areas.

Therefore, some studies use wind tunnel experimental data to verify the gas dispersion models. For example, Dong et al. (2021) carried out wind tunnel experiments in six directions of the Sanmen nuclear power plant area and compared the results of the wind field and concentration field qualitatively and quantitatively with the simulation results of CALMET-RIMPUFF and SWIFT-RIMPUFF models, respectively. Toscano et al. (2021) used the wind tunnel experiment and CFD numerical simulation to evaluate the emission impact of cruise ships berthing at the port of Naples and verified the accuracy of the CALPUFF model. Yassin et al. (2021) conducted the numerical simulation of pollution gas emissions from urban roof chimneys and verified with wind tunnel experiment results both qualitatively and quantitatively. Jiang et al. (2021) carried out wind tunnel experiments in eight directions on leakage and diffusion accidents of high sulfur gas in mountainous terrain and drew the risk distribution map. Comparing with the CFD simulation results, they found that the numerical simulation accuracy was not enough and proposed an improved numerical simulation equation. In wind tunnel experiments, the properties of the gas airflow, such as pressure, velocity, temperature, and density, can

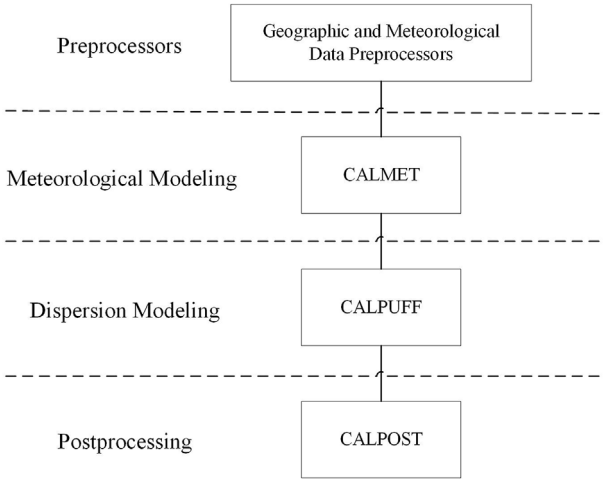

FIGURE 1
Main system modules of the CALPUFF model.

be adjusted easily and accurately. In addition, an indoor experiment is safer and more flexible. So, experiments under different conditions can be carried out at once.

The technical guidelines for the environmental impact assessment-Atmospheric Environment (HJ 2.2-2018) issued by the Ministry of Ecology and Environment of China have recommended gas dispersion models which have been extensively utilized in environmental assessment and the evaluation of atmospheric environmental quality. Among them, the CALPUFF model is suitable for long-scale experimental areas (more than 50 km), comprehensively considering complex terrain, meteorological parameters, and other aspects and has higher accuracy (Li et al., 2020; Ridzuan et al., 2020). Compared with other gas dispersion models, CALPUFF computes more rapidly than the CFD model and supports finer spatial and temporal resolutions than other Gaussian models like AERMOD. Based on the aforementioned factors, the CALPUFF model is selected for emergency simulation in this study.

However, there are few studies that validate the accuracy of CALPUFF in small-scale emergency scenarios, which could offer important reference for many industries like oil and gas field. In this paper, a comparative study between the CALPUFF model and wind tunnel experiment on toxic gas leakage accidents in the near-field area is conducted. An ethylene gas leakage accident case in a national hazardous chemical emergency rescue (training) center is simulated both from the CALPUFF simulation and wind tunnel experiment, followed by qualitative and quantitative comparisons. Finally, the effect of the CALPUFF model on near-field diffusion simulation in urban areas with dense buildings is validated.

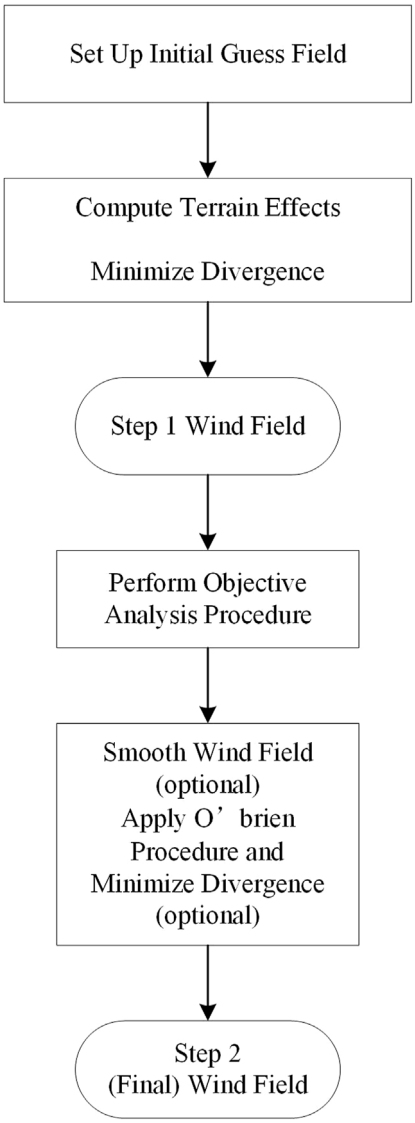

FIGURE 2
Main process of the CALMET module.

2 Methods

2.1 CALPUFF model

The CALPUFF model is a new generation of the unsteady gas phase and air quality modeling system developed by Sigma Corporation of America, as one of the Lagrange–Gaussian puff models (Scire et al., 2011). It divides the pollutants into several puffs according to a certain volume, where the Lagrangian method is used to calculate the trajectory of the puffs, and the Gaussian method is used to calculate the distribution of pollutants inside a puff. Finally, each puff is superimposed to obtain the total concentration field. The model adopts the

meteorological data of the hourly wind field, fully considers the influence of a complex terrain on the dry and wet deposition of pollutants, and simulates the diffusion pattern of pollutants in areas of different scales well. The CALPUFF model is mainly composed of four parts: the geographic and meteorological data preprocessors, meteorological model CALMET, dispersion model CALPUFF, and postprocessor CALPOST, as shown in Figure 1.

2.1.1 Diagnostic wind model

CALMET includes a diagnostic wind model and a micrometeorological model. The workflow of the diagnostic wind model is shown in Figure 2.

The CALMET diagnostic wind model uses two steps to estimate the wind field. It should be noted that the initial gas field can be a three-dimensional wind field or a constant wind field composed of regional average. The regional average wind field can be obtained by means of the vertical average and temporal interpolation of meteorological data from high-altitude observations or can be directly specified by users. If the regional average wind field is calculated, a user needs to specify not only the atmospheric layer for which the average wind field is to be calculated but also the high-altitude sounding stations for calculation. Alternatively, all station data are interpolated inversely to the square of the distance to produce an initial guess wind field with spatial variation. The first step is to calculate the step 1 wind field from the initial gas field, including adjustments for kinematic terrain effects, slope flows, blocking effect and a three-dimensional divergence minimization procedure, and other algorithms. The second step includes an objective analysis that introduces the observation data into the step 1 wind field to generate the final wind field, including interpolation, smoothing, O'Brien adjustment of vertical wind speed, divergence minimization, and other algorithms. We can also use grids to predict the wind field in CALMET, which better reflects some aspects of the regional flow, sea breeze circulation, and slope/valley circulation.

2.1.2 Lagrange–Gaussian puff model

CALPUFF is a puff model that simulates multilayer and multipollutant-type diffusion in unsteady conditions. It can simulate the migration, transformation, and dispersion of pollutants in meteorological conditions that vary temporarily and spatially. The main processes are as follows: retrieving and processing time-averaged data from meteorological and source information files; releasing, transporting, and removing puffs from computational grids; assessing the effects of diffusion, chemical conversion, dry and wet deposition, and subgrid-scale complex topography; and sampling puffs to obtain concentrations and deposition fluxes at the gridded and discrete receptors. Among them, the algorithms dealing with near-source influences include building downwash, transitional plume lifting, partial plume penetration, and subgrid terrain interaction. The algorithms dealing with long distance transmission influences include dry and wet deposition, chemical transformation, vertical wind shear, overwater transport, and coastal interaction effects.

Generally, the puff model evaluates the concentration contribution of a puff to a receptor point through the snapshot method. For example, if the time step is 1 h and the sampling step is 1 min, then the contribution of a puff to the receptor point's 1-h average concentration will be the average of 60 snapshots per minute. The disadvantage of this method is that when the distance between puffs is too large and overlapping is not enough, the simulation results may be inaccurate, that is, the concentration of receptor points located in the gap between puffs at the sampling time will be lower than the real value, while the concentration of those in the center of puffs will be higher. There are two sampling functions in CALPUFF to solve this problem: the first is a radially symmetric Gaussian puff, and the second is a non-circular puff stretched in the direction of the wind, when released, called slug, does not need to release the puff frequently. For most CALPUFF applications, the modeling of emissions as puffs is recommended as it produces similar model results but with significantly shorter run times than the slug approach. However, the slug approach is preferred for causality effects along small spatial and temporal scales, such as an accidental release scenario, and where the transport from the source to the receptor is very short. Therefore, this study chooses the slug function.

The basic equations of the puff sampling function are as follows:

$$c(x,y,z) = \frac{Q}{2\pi\sigma_x\sigma_y} g \cdot exp\left(-\frac{d_a^2}{2\sigma_x^2}\right) exp\left(-\frac{d_b^2}{2\sigma_y^2}\right), \quad (1)$$

$$g = \frac{2}{\sqrt{2\pi}\sigma_z} \sum_{n=-\infty}^{\infty} exp\left(-\frac{(H+2nh)^2}{2\sigma_z^2}\right), \quad (2)$$

where $c(x,y,z)$ is the ground-level concentration of the pollutant at a specific receptor; Q is the pollutant mass in the puff; x, y, and z still represent the along-wind, cross-wind, and vertical directions, respectively; σ_x, σ_y, and σ_z are the standard deviations of the Gaussian distribution in the three directions, respectively; and d_a and d_b are the distances from the puff center to the receptor in the along-wind and cross-wind directions, respectively. g is the vertical term of the Gaussian equation, H is the effective height above the ground of the puff center, and h is the mixed-layer height. The summation in the vertical term, g, accounts for multiple reflections of the mixing lid and the ground. It reduces to the uniformly mixed limit of $1/h$ for $\sigma_z > 1.6h$. In general, puffs within the convective boundary layer meet this criterion within a few hours after release.

For a horizontally symmetric puff, with $\sigma_x = \sigma_y$, Eq. 1 reduces to

$$c(s) = \frac{Q(s)}{2\pi\sigma_y^2(s)} g(s) \cdot exp\left(-\frac{R^2(s)}{2\sigma_y^2(s)}\right), \quad (3)$$

where R is the distance from the center of the puff to the receptor and s is the distance traveled by the puff. An analytical solution to this integral can be obtained if s is the main variable. Generally, σ_y and g are computed at the mid-point of the trajectory segment because at mesoscale distances, the fractional change in the puff size during the sampling step is usually small, and the use of the mid-point values is adequate. This method for mesoscale distances, however, may not be appropriate in the near field, where the fractional puff growth rate can be rapid and plume height may vary. For this reason, the integrated sampling function has been implemented with receptor-specific values for σ_y and g and evaluated at the point of the closest approach of the puff to each receptor.

2.2 Building downwash

The building downwash effect is due to the air disturbance caused by buildings around the pollution source, resulting in the streamline sliding effect of the airflow emitted by the chimney after passing the building, which quickly diffuses to the ground, leading to a high local concentration. In the CALPUFF model, the parameterization of building downwash is suitable for use in the turbulent wake region and is based on the procedures used in the ISC3 model. ISC3 contains two building downwash algorithms:

(1) Huber–Snyder model (Huber and Synder, 1976; Huber, 1977). This model is applied when the source height H_s is greater than H_b+ $0.5L_b$ (H_b is the building height, and L_b is the lesser of the building height or the projected width). The first step is to compute the effective plume height, H_e, due to the momentum rise at a downwind distance of two building heights. If H_e exceeds H_b+$1.5L_b$, building downwash effects are assumed to be negligible. Otherwise, building-induced enhancement of the plume dispersion coefficients is evaluated. For stack heights, H_s, less than $1.2H_b$, and both σ_y and σ_z are enhanced. Only σ_z is enhanced for stack heights above $1.2H_b$ (but below H_b+ $1.5\ L_b$).

For a squat building (that is, the projected building width exceeds its height, i.e., $H_w \geq H_b$), the enhanced σ_y and σ_z can be calculated as follows:

$$\sigma_z' = 0.7H_b + 0.067(x - 3H_b), \quad (4)$$

$$\sigma_y' = 0.35H_w + 0.067(x - 3H_b) \text{when Hw}/\text{Hb} < 5, \quad (5)$$

$$\sigma_y' = 0.35H_b + 0.067(x - 3H_b) \text{ or } \sigma_y' = 1.75H_b + 0.067(x - 3H_b) \text{when } Hw/Hb > 5. \quad (6)$$

For a tall building (that is, the building width exceeds its projected width, $H_b \geq H_w$), the enhanced σ_y and σ_z can be calculated as follows:

$$\sigma_z' = 0.7H_w + 0.067(x - 3H_w), \quad (7)$$

$$\sigma_y' = 0.35H_w + 0.067(x - 3H_w). \quad (8)$$

(2) Schulman–Scire model (Schulman and Scire, 1980; Schulman and Hanna, 1986). This model applies a linear decay factor to the building-included enhancement of the dispersion coefficients and accounts for the effect of downwash on plume rise. It is used for stacks lower in height than H_b+ $0.5L_b$. The main features of the algorithm are that the effects of building downwash on reducing the plume rise are incorporated, and the enhancement of σ_z is a gradual function of the effective plume height rather than a step function. The vertical dispersion coefficient is determined as follows:

$$\sigma_z'' = A\sigma_z', \quad (9)$$

where σ_z' is determined from Eqs 4, 7, and

$$A = \begin{cases} 1 & H_e \leq H_b \\ \frac{H_b - H_e}{2L_b} + 1 & H_b < H_e \leq H_b + 2L_b. \\ 0 & H_b + 2L_b < H_e \end{cases} \quad (10)$$

3 Experiments

3.1 CALPUFF configurations

This experimental area is located at a national hazardous chemical emergency rescue base, as shown in Figure 3. This base is a comprehensive training base integrating training, drill, appraisal, seminar, and competition regarding emergency firefighting. The base has 10 major training areas for fire training, smoke-heat simulation, oil and gas blowout, hazardous chemical leakage, building fire, earthquake prevention and disaster mitigation, three-dimensional desktop deduction, comprehensive physical exercise, water oil spill disposal, water rescue, and the large-scale oil pool fire experimental platform (600 m^2). It can simulate the trainings of more than 130 emergency cases in 13 categories, such as petrochemical industrial leakage, earthquake, high-rise buildings, and water rescue. The base is built in a flat area, with a chemical factory on the westside and a farmland and villages on the other sides. The land covers good vegetation, and the trees are less than 10 m high.

In this experiment, we assume that there is a chimney emitting stable ethylene (C_2H_4) in the middle of the research area. Gas tanks, office buildings, and other buildings around the

FIGURE 3
Remote sensing image of the experimental area.

TABLE 1 Simulation parameters.

Parameter type	Parameter name	Value
Pollution source properties	Stack height (m)	13
	Stack diameter (m)	3
	Exit velocity (m/s)	1
	Exit temperature (K)	300
	Emission rate (g/s)	10
Weather condition	Wind speed (m/s)	3/6
	Wind direction (°)	0/180/270
	Temperature (°C)	25
Simulation time settings	Time step (s)	60
	Run length (h)	2
Simulation range settings	X-direction length (km)	1
	Y-direction length (km)	1
	Grid spacing of the wind field (m)	50
	Grid spacing of the concentration field (m)	25

chimney may block and divert gas dispersion. Configurations in CALPUFF are shown in Table 1.

According to the remote sensing image of the base, the coordinates and height parameters of 14 major buildings, such as oil tanks, office buildings, and gas tanks, are collected and input into the building module of CALPUFF. The heights of the cylindrical tanks are about 10 m, and the heights of other buildings are about 2–8 m. Different discrete receptors are set

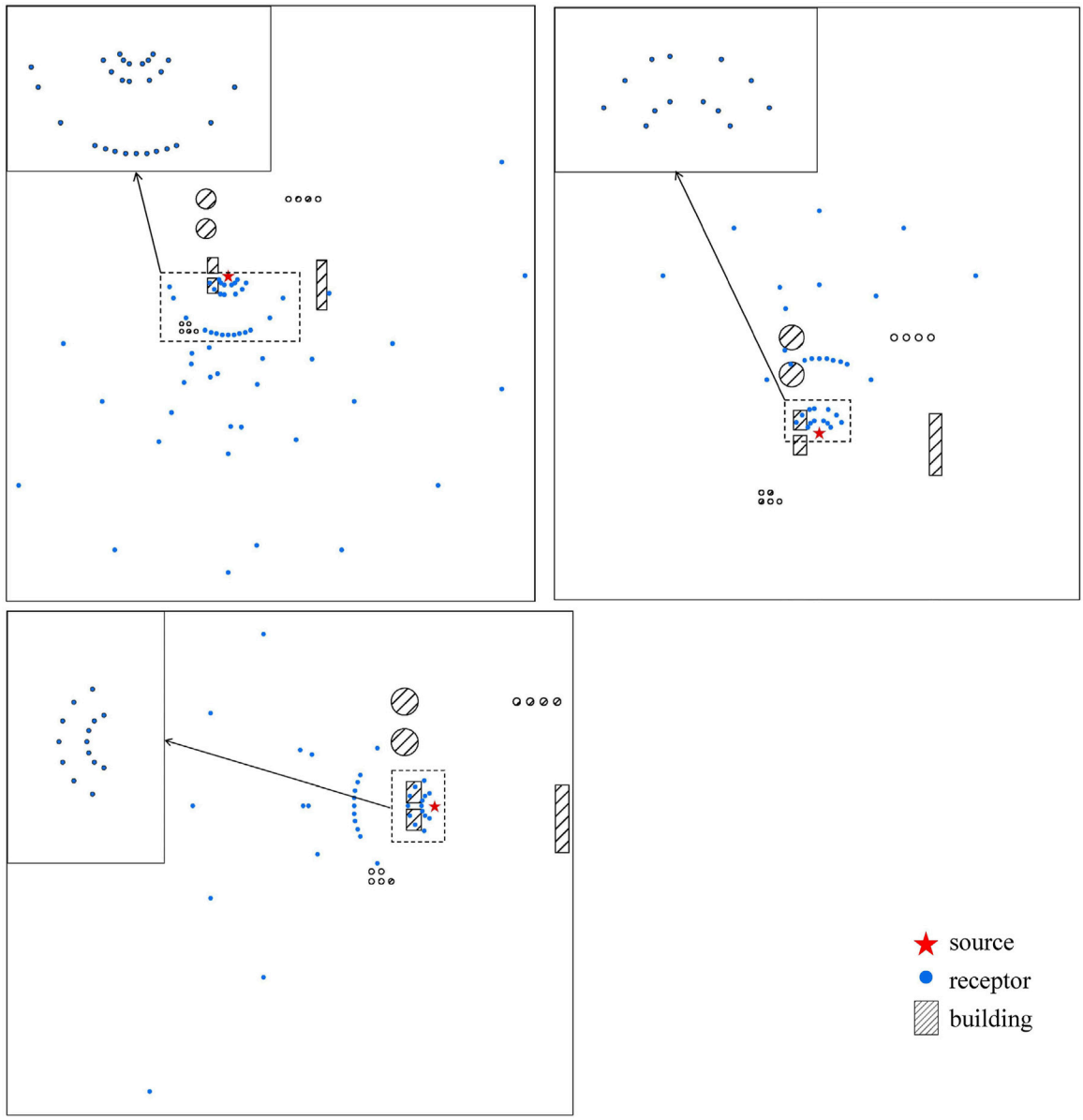

FIGURE 4
Map of measurement points and buildings in the base.

under three wind directions, north, south, and east, and two wind speeds, 3 and 6 m/s (at the height of 10 m above the ground), as shown in Figure 4.

3.2 Wind tunnel experiments

The direct-current down-blowing wind tunnel used in this experiment consists of an inlet section, a drive section, a settling chamber, a contraction section, a test section, and an exhaust section. During the experiment, the airflow flows into the air inlet straightly and passes through the aforementioned sections in sequence and finally flows out of the air outlet. The miniature model of the base is placed in the wind tunnel, and the wind field conditions can be changed through the operating system. The gas dispersion process in the miniature model can be observed and analyzed through the measurement system.

The overall external dimensions of the wind tunnel are 10.4 m × 11.2 m × 81.0 m (width × height × length). The size of the test section is 4 m × 3 m × 20 m (width × height × length). To eliminate the static pressure gradient along the tunnel axis caused by the thickening of the tunnel wall's boundary layer, the

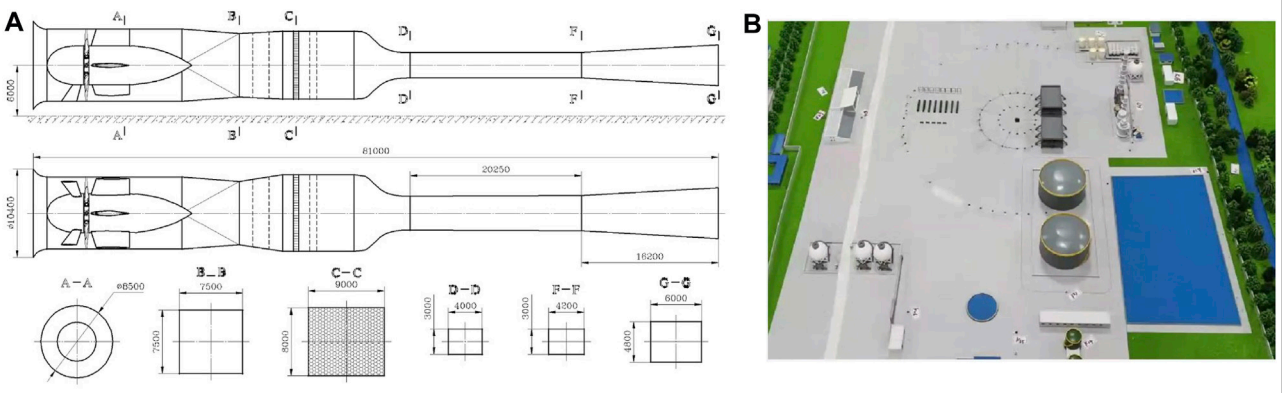

FIGURE 5
Models of the wind tunnel and experimental scene.**(A)** Design of the wind tunnel. **(B)** Physical miniature model.

two side walls have a divergence angle of 0.8° (upper and lower walls are horizontal with no divergence angle). The aerodynamic profile of the wind tunnel is shown in Figure 5A. In this study, three wind directions of north, south, and east and two wind speeds of 3 and 6 m/s are used to form six different sets of wind field conditions.

In the experiment, ethylene (C_2H_4) is used as the tracer to simulate the diffusion of pollutants in the atmosphere. The gas flow rate is 200 ml/min. The initial ethylene concentration is 5×10^5 ppm, and the concentration increases to 10^6 ppm when the gas spreads over a distance of 300 mm.

We use a 1:300 scale experimental miniature model for the base surrounding area of 1 km, as shown in Figure 5B, which is placed in the test section of the wind tunnel in Figure 5A. A total of 128 concentration measurement points are set in the experiment, measuring the gas concentration at the height of 10 m in reality, some of which are evenly distributed around the pollution source in a circular ring, with the distances of 50, 100, 300, 900, and 1,500 mm from the pollution source, whose quantities are 16, 22, 38, 16, and 8, respectively. The others are distributed at densely populated and sensitive locations such as dormitories, office buildings, and equipment as supplementary, with the total number of 28.

3.3 Statistical evaluations

To evaluate the consistency of gas concentrations obtained from CALPUFF simulation and the wind tunnel experiment, we use the quantitative indexes proposed by (Hanna and Chang, 2012; Chang and Hanna, 2004),, which are the fractional bias (FB) and normalized mean square error (NMSE), defined as follows:

$$FB = \frac{2\left(\overline{X_o} - \overline{X_p}\right)}{\overline{X_o} + \overline{X_p}}, \tag{11}$$

$$NMSE = \frac{\overline{\left(X_o - X_p\right)^2}}{\overline{X_o}\,\overline{X_p}}, \tag{12}$$

where the subscript P represents the CALPUFF model simulation result, O represents wind tunnel experiment observation, and $\overline{X_p}$ and $\overline{X_o}$ are the average values of the sampling points. FB and NMSE indexes can reflect the systematic deviation of the total data. In the most ideal scenario, that is, when the model result is completely consistent with the experimental results, both FB and NMSE are equal to 0.

Hanna and Chang also give the reference range of each index according to the characteristics of gas dispersion in urban areas: when $|FB| \le 0.67$ and $NMSE \le 6$, it indicates that the two sets of data fit well.

In addition, we also select the correlation coefficient R to reflect the correlation between two sets of data. If the |R| value is closer to 1, the linear correlation between the two sets of data is higher and *vice versa*.

$$R = \frac{\overline{\left(X_o - \overline{X_o}\right)\left(X_p - \overline{X_p}\right)}}{\sigma_o \sigma_p}, \tag{13}$$

where σ_o and σ_p are the standard deviations of the sampling points by CALPUFF model simulation and wind tunnel observation, respectively, and the meanings of other symbols are the same as before.

In the wind tunnel and CALPUFF experiments, the initial gas concentrations are c_{0m} and c_{0p}, and the gas concentrations at each measurement point are c_m and c_p, respectively. Gas concentrations obtained from the wind tunnel experiment and

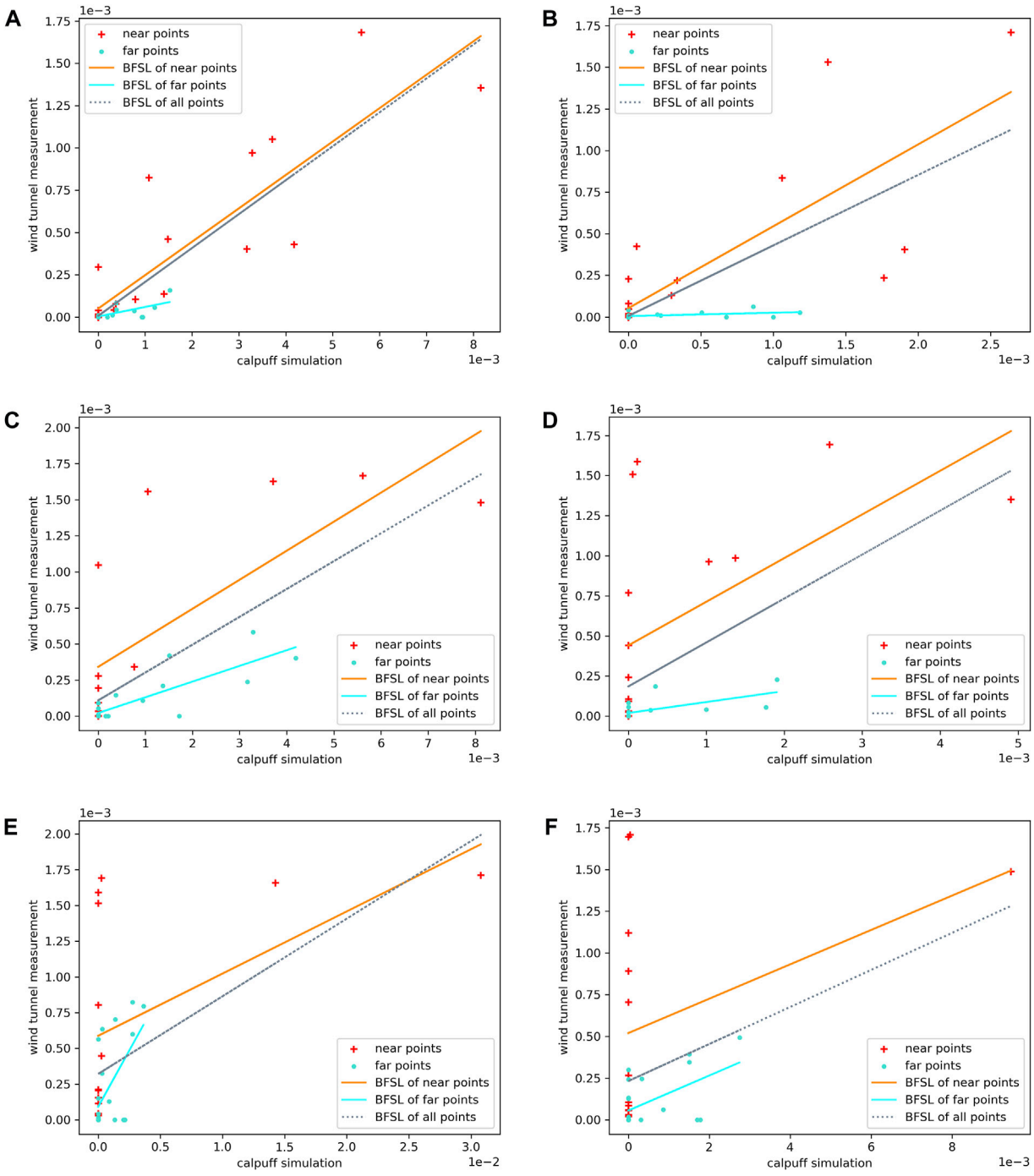

FIGURE 6
Scatter plots for the gas concentration dilution ratio of wind tunnel observation and CALPUFF simulation results: **(A)** N direction, 3 m/s, **(B)** N direction, 6 m/s, **(C)** S direction, 3 m/s, **(D)** S direction, 6 m/s, **(E)** E direction, 3 m/s, and **(F)** E direction, 6 m/s.

CALPUFF simulation cannot be directly compared. Therefore, we calculate the gas concentration dilution ratio for comparison, which is defined as follows:

$$r_m = \frac{c_m}{c_{0m}}, \tag{14}$$

$$r_p = \frac{c_p}{c_{0p}}. \tag{15}$$

At the same measurement point, if r_m and r_p are close, they are consistent with each other, illustrating that they represent a similar diffusion process.

4 Results and discussion

In wind tunnel experiments, it is difficult to avoid the existence of background values, systematic errors, and random errors, leading to outliers and deviations. First, the records of wind tunnel experiments and CALPUFF calculation results are compared with themselves to eliminate the background value. Then, scatter fitting is performed on the remaining measurement points under each wind direction and speed, and the measurement points are divided into two groups in the near field and far field of the pollution source. The scatter plots are shown, respectively, in Figure 6. The points located 100 mm farther from the pollution source (corresponding to 30 m in reality) are designated as far-field measurement points, whose initial emission concentration of ethylene is 10^6 ppm; and those within 100 mm are designated as near-field measurement points, with the initial emission concentration of 5×10^5 ppm.

On the scatter plots, it can be found that the concentration distributions of measurement points in the near-field and far-field show different patterns. We use the best fit straight line (BFSL) to show the linear relationship of CALPUFF simulation and wind tunnel experiment results based on the least-squares estimation method.

As shown in Figures 6A–D, in the south and north wind directions, the slope of the BFSL of the far-field measurement points (blue line) is smaller than that of the near-field measurement points (orange line), which means CALPUFF tends to output higher gas concentration values in the far field than in the near field. The dilution effect of gas at far-field measurement points is more significant, leading to a smaller gas concentration dilution ratio, so the far-field scatter points are gathered near the origin of the coordinates. However, the distribution of near-field measurement points is more scattered, with a larger gas concentration dilution ratio, so the trend of BFSL of all measurement points is more significantly affected by the near-field measurement points. However, in the east wind direction, as shown in Figures 6E,F, contrary to the other wind directions, the slope of the blue line is larger than that of the orange line, which means that CALPUFF tends to output higher gas concentration values in the near field than in the far field. Also, the CALPUFF simulation results of the near-field points show little diversity, mostly clustered near the y-axis, so the trend of the BFSL of all measurement points is more significantly affected by the far-field measurement points. At the same time, it also shows that under east wind, due to the shielding of nearby buildings, gas dispersion is disturbed by a turbulent flow and the regularity of the spatial distribution of the gas concentration is not consistent, showing a more chaotic scatter distribution.

In order to further describe the continuous diffusion trend of polluted gas on the terrain surface, gridded receptors are set in CALPUFF to simulate the gas concentration on the surface layer. The result is overlaid with the concentration dilution ratio of the measurement points in the wind tunnel experiment, visually compared by means of graded coloring, as shown in Figure 7.

Gas concentrations on the earth surface under different wind directions and speeds generally present the similar trend, which is gradually decreasing from the pollution source, and the simulation results show the best consistency with measurement points in the medium-level concentration (0.35×10^{-3} < ratio <3.53×10^{-3} in Figure 7). In addition, with larger wind speed, the horizontal diffusion range of the gas becomes smaller and the propagation distance becomes longer. Therefore, the shape of gas dispersion under the 6 m/s wind condition is narrower and sharper, and the concentration grades change more abruptly.

Under south and north wind directions, as shown in Figures 7A–D, the buildings are parallel to the wind directions, with heights of about 10 m and medium volumes, and the distance between the east and west buildings is about 160 m in reality, which is relatively large, so the diffusion of gas is less hindered by the surroundings. It can be observed that the horizontal distribution of the pollutant concentration is almost symmetrical, and the dilution effect in the downwind direction is smooth. Comparing the measurement points of the wind tunnel experiment and the CALPUFF simulation results of the surface layer, it is shown that their distribution trends are consistent, but the gas dilutes faster in the wind tunnel experiment. The measurement results of the wind tunnel experiment are all smaller than CALPUFF simulation results at the same location, so the diffusion range of the wind tunnel experiment is also smaller.

Under east wind, as shown in Figures 7E,F, an obvious high concentration center appears near the pollution source, covering a large area compared with other wind directions. Two buildings are distributed about 15 m from the pollution source on the leeward side by side and produce a complex turbulence. Relevant studies have shown that when the airflow passes through an area between the windward side and the leeward side that is equivalent to a “door hole,” the airflow accelerates. Also, when the “door hole” shrinks, the airflow speed increases. When the airflow passes buildings, positive pressure will be generated in the windward area and negative pressure will be generated in the side area. The pattern of pollutant concentration distribution is mainly affected by the turbulence. Where the turbulence is severer, the transportation of pollutants is easier to be transported in and out. Where the airflow is more stable, pollutants are harder to be transported to, but once they arrive, an area with high gas concentration may be generated after a period of accumulation (Zhuang, 2014). According to the distribution of results of the CALPUFF surface layer, a high concentration center forms behind the near-field buildings, showing that along the leeward direction from the pollution source, the pollutant concentration first increases and reaches the peak concentration behind the buildings on the midline of the two buildings and then gradually dilutes. This may be due to the

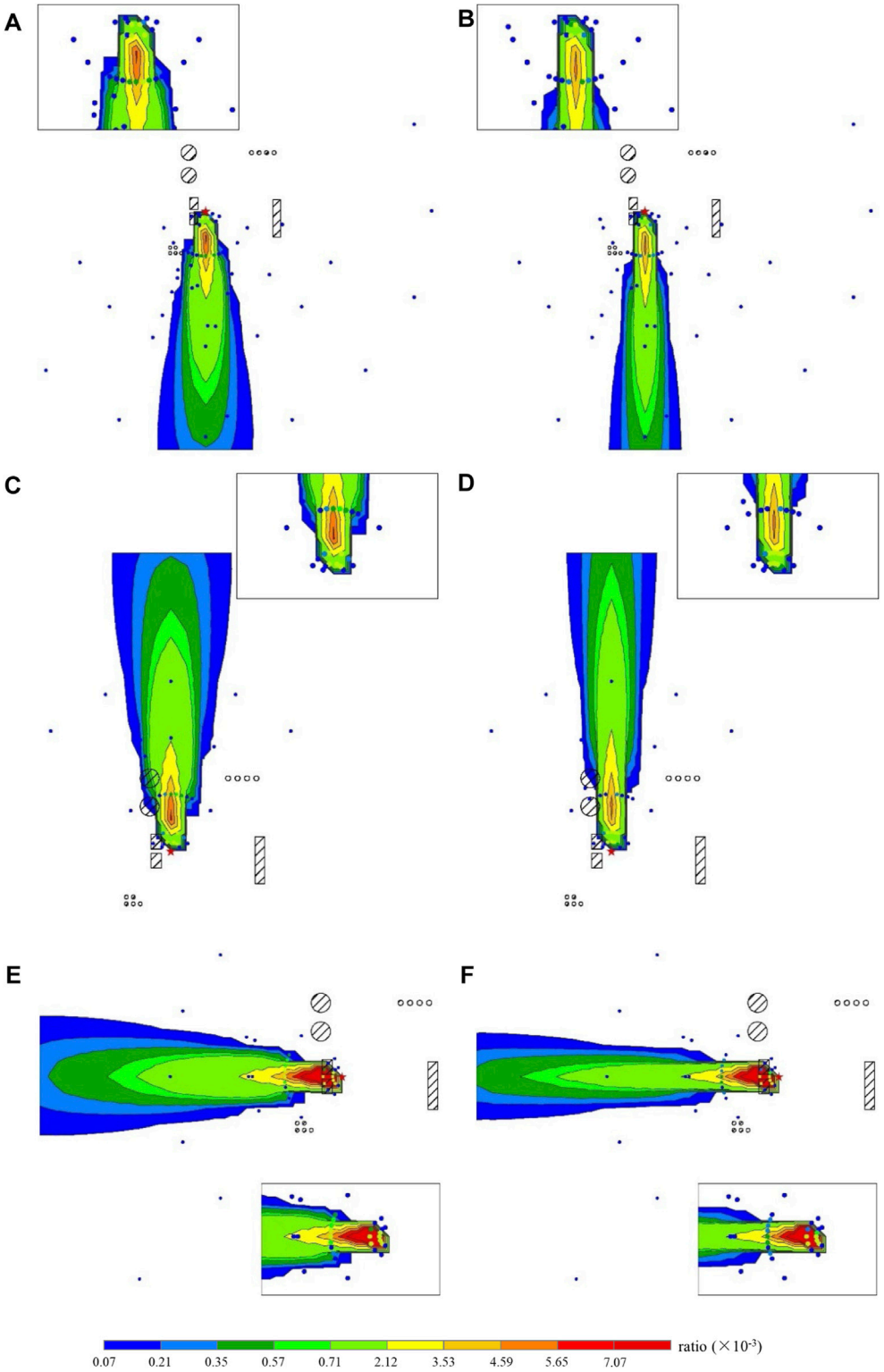

FIGURE 7
Overlaid comparison diagrams of wind tunnel observation and CALPUFF simulation results: **(A)** N direction, 3 m/s, **(B)** N direction, 6 m/s, **(C)** S direction, 3 m/s, **(D)** S direction, 6 m/s, **(E)** E direction, 3 m/s, and **(F)** E direction, 6 m/s.

TABLE 2 Evaluation indexes for the comparison of the wind tunnel experiment and CALPUFF simulation under different wind directions and speeds.

Wind direction	Wind speed (m/s)	Location of the measurement point	FB	NMSE	R
			−0.67 to 0.67	0 to 6	
N	3	Near-field	−1.2325	10.0160	***0.8839***
		Far-field	−1.7380	54.5300	***0.7096***
		Total	−1.3064	17.3451	***0.8874***
	6	Near-field	***−0.4346***	***2.7207***	***0.8021***
		Far-field	−1.7969	93.9663	0.4827
		Total	−0.7617	***5.9892***	***0.7331***
S	3	Near-field	−0.7940	***5.3304***	***0.7516***
		Far-field	−1.5269	18.9997	***0.8224***
		Total	−1.0949	8.8029	***0.7124***
	6	Near-field	***−0.0278***	***3.0404***	0.5698
		Far-field	−1.5264	32.2436	0.6309
		Total	***−0.3759***	***5.3690***	0.5353
E	3	Near-field	−1.2676	30.4333	0.5252
		Far-field	−1.1441	7.4833	0.5882
		Total	−1.2323	39.5744	0.5358
	6	Near-field	***−0.1402***	12.8139	0.3900
		Far-field	−1.2801	12.7308	0.5445
		Total	***−0.6242***	14.4834	0.3799

fact that the east wind in the experiment accelerates and transports a large amount of pollutants when passing through the two buildings in the near field, which deposit and accumulate around the buildings due to the stable airflow. Comparing the CALPUFF dispersion result with the measurement points in the wind tunnel experiment, both the magnitude and distribution trend of the concentration dilution ratio fit well.

In order to quantitatively compare the results of the two methods, for the far- and near-field measurement points under different wind directions and speeds, the results of the evaluation indexes in 3.3 are shown in Table 2.

For the FB and NMSE indexes used in this study, the smaller the value, the better is the consistency of the two groups of data. The FBs and NMSEs in Table 2 within the reference range in 3.3 are bold and italic. For the R index, generally, the R value between 0 and 0.3 indicates a weak positive linear relationship; the value between 0.3 and 0.7 indicates a moderate positive linear relationship; and the value between 0.7 and 1 indicates a strong positive linear relationship (Ratner, 2009). The Rs in Table 2 all exceed 0.3, and the Rs over 0.7 are bold and italic.

From the perspective of FBs and NMSEs, in the four groups of experiments under south and north wind, the order of absolute values is as follows: near field < total < far field. For example, under north wind with the speed of 6 m/s, the order of FBs is $|-0.4346| < |-0.7617| < |-1.7969|$; and under south wind with the speed of 3 m/s, the order of NMSEs is $|5.3304| < |8.8029| < |18.9997|$. It reveals that for the magnitude of the results, the simulation accuracy is the highest of the near-field measurement points but the lowest of the far-field measurement points. Under east wind, there is no such regularity of the order of values, but the results of 6 m/s show better indexes than 3 m/s, with lower FBs and NMSEs in most cases.

From the perspective of the R index, under north wind, the order of values is near field > far field, and the near-field values are over 0.8. For example, the Rs' order of near-field and far-field points under 3 m/s is 0.8839 >0.7096; and under 6 m/s is 0.8021 >0.4827. It illustrates that CALPUFF simulates the concentration distribution in near field well and has the ability to reflect the diffusion regularity of pollutants in space. Under both south and east wind, the orders of Rs are as follows: far field > near field. For example, under south wind with the speed of 3 m/s, the order of far-field and near-field points is 0.8224 > 0.7516. It indicates that CALPUFF simulates better in the far field. However, under east wind, Rs of near-field points are only about 0.4, showing more difficulty and uncertainty for both CALPUFF simulation and the wind tunnel experiment caused by complex buildings.

In addition, from the perspective of different wind speeds, under south and north wind, the performances of the evaluation indexes under the wind speed of 3 m/s are better than those of 6 m/s. Because the higher the wind speed, the more unstable is the airflow, causing more difficulty in data collection, and the credibility of the observations in the wind tunnel experiment may decrease.

5 Conclusion

In this study, a wind tunnel experiment and a CALPUFF simulation experiment of the ethylene gas leakage accident are designed and implemented for a national hazardous chemicals emergency rescue base, with a total of six groups of experimental conditions under three wind directions and two wind speeds. The experiment results of each group are, on one hand, qualitatively compared by visualization methods such as scatter plots and overlay analysis and, on the other hand, quantitatively compared by FB, NMSE, and R indexes, in order to analyze the differences between the results of the two methods. This study leads to the following conclusions:

(1) Generally, the CALPUFF model can simulate the diffusion trend of pollution gas accurately, reflecting the regularity of its spread in space, but in the aspect of magnitude of the results, CALPUFF tends to underestimate the concentration in the near field of the pollution source and overestimate the concentration in the far field.
(2) The CALPUFF model has very limited capabilities of processing the scenes with complex buildings (such as urban environments). Airflow near buildings is fickle, especially when the pollution source is located very close to buildings, leading to inaccurate results.
(3) In wind tunnel experiments, many steps are operated artificially, such as the manufacture of physical models, adjustment of gas emission, and layout of measurement points, which are significantly affected by the experimenters' working ability. They may also lead to deviations in the results, so the measurement points with a poor reference can be filtered and excluded in advance of the analysis. Additionally, extra measurement points can be added at some important locations such as front and behind the near-field buildings, according to specific conditions, so as to inspect the changes in the pollutant diffusion process subtly.

Based on the aforementioned analysis and conclusions, both the wind tunnel experiment and CALPUFF model are important means of simulating gas leakage accidents currently, with their own advantages and disadvantages. The wind tunnel experiment can recur the real scene as more as possible and has lower cost and fewer restrictions than traditional field measurements, so it is more applicable to complex surface conditions and crowded environments, but it also requires more accurate measurement devices and higher ability of experimenters, with more complicacy of error analysis. The CALPUFF model is more convenient to use and can repeatedly adjust and test different experimental parameters with satisfactory accuracy for general emergency plans' requirement. However, the simulation result of CALPUFF is not good enough for fine-scale and complex near-field environments. In future studies, researchers can work on improving the building module of the gas dispersion model to improve its simulation accuracy. Also, more precise equipment and comprehensive solutions can be used in the wind tunnel experiment to improve its reliability. The simulation results of gas leakage accidents should be selectively referred to: if the case is in the near-field area of the pollution source significantly affected by buildings, the wind tunnel experiment is a better reference, but if the case is in the far-field and relatively open area, as well as to simulate an overall concentration distribution, CALPUFF can also provide a more credible reference.

Data availability statement

The raw data supporting the conclusion of this article will be made available by the authors, without undue reservation.

Author contributions

RZ: conceptualization, methodology, validation, and writing—original draft. ML: conceptualization and writing—review and editing. HM: writing—review and editing.

Conflict of interest

The authors declare that the research was conducted in the absence of any commercial or financial relationships that could be construed as a potential conflict of interest.

Publisher's note

References

AERMOD (2019). *User's Guide for the AMS/EPA Regulatory Model (AERMOD) [DB/OL]*. United States: U.S. Environmental Protection Agency

Carruthers, D. J., Holroy, D. R. J., Hunt, J. C. R., Weng, W. S., Robins, A. G., Apsley, D. D., et al. (1994). UK-ADMS: A new approach to modelling dispersion in the earth's atmospheric boundary layer. *J. Wind Eng. Industrial Aerodynamics* 5 (52), 139–153. doi:10.1016/0167-6105(94)90044-2

Chang, J. C., and Hanna, S. R. (2004). Air quality model performance evaluation. *Meteorol. Atmos. Phys.* 87 (1-3), 167–196. doi:10.1007/s00703-003-0070-7

Cheng, K., Zhao, X., Zhou, W., Cao, Y., Yang, S. H., and Chen, J. (2021). Source term estimation with deficient sensors: Traceability and an equivalent source approach. *Process Saf. Environ. Prot.* 152, 131–139. doi:10.1016/j.psep.2021.05.035

Cimorelli, A. J., Perry, S. G., Venkatram, A., Weil, J. C., Paine, R. J., Wilson, R. B., et al. (2004). *Aermod – description of model formulation*. Research Triangle Park, North Carolina: U.S. Environmental Protection Agency

Dong, X., Zhuang, S., Fang, S., Li, H., and Cao, J. (2021). Site-targeted evaluation of SWIFT-RIMPUFF for local-scale air dispersion modeling around Sanmen nuclear power plant based on multi-scenario wind tunnel experiments. *Ann. Nucl. Energy* 164, 108593. doi:10.1016/j.anucene.2021.108593

Fallah Shorshani, M., Seigneur, S., Rehn, P., and Chanut, D. (2015). Atmospheric dispersion modeling near a roadway under calm meteorological conditions. *Transp. Res. Part D Transp. Environ.* 34, 137–154. doi:10.1016/j.trd.2014.10.013

Fallah-Shorshani, M., Shekarrizfard, M., and Hatzopoulou, M. (2017). Integrating a street-canyon model with a regional Gaussian dispersion model for improved characterisation of near-road air pollution. *Atmos. Environ.* 153, 21–31. doi:10.1016/j.atmosenv.2017.01.006

Hanna, S., and Chang, J. (2012). Acceptance criteria for urban dispersion model evaluation. *Meteorol. Atmos. Phys.* 116 (3-4), 133–146. doi:10.1007/s00703-011-0177-1

Holmes, N. S., and Morawska, L. (2006). A review of dispersion modelling and its application to the dispersion of particles: An overview of different dispersion models available. *Atmos. Environ.* 40 (30), 5902–5928. doi:10.1016/j.atmosenv.2006.06.003

Holnicki, P., Kałuszko, A., and Trapp, W. (2016). An urban scale application and validation of the calpuff model. *Atmos. Pollut. Res.* 7 (3), 393–402. doi:10.1016/j.apr.2015.10.016

Huang, Z., Yu, Q., Ma, W., and Chen, L. (2019). Surveillance efficiency evaluation of air quality monitoring networks for air pollution episodes in industrial parks: Pollution detection and source identification. *Atmos. Environ.* 215, 116874. doi:10.1016/j.atmosenv.2019.11687410

Huber, A. H., and Synder, W. H. (1976). "Building wake effects on short stack effluents," in Proceedings of the Preprint volume for the third symposium on atmospheric diffusion and air quality (Boston, Massachusetts: American Meteorological Society).

Huber, A. H. (1977). "Incorporating building/terrain wake effects on stack effluents," in Proceedings of the Preprint volume for the joint conference on applications of air pollution meteorology (Boston, Massachusetts: American Meteorological Society).

Jiang, X., Yang, H., Lin, G., Dang, W., Xin, B., Zhang, J., et al. (2021). Measurements and predictions of harmful releases of the gathering station over the mountainous terrain. *J. Loss Prev. Process Industries* 71 (8), 104485. doi:10.1016/j.jlp.2021.104485

Jones, A., Thomson, D., Hort, M., and Devenish, B. (2007). "The U.K. Met office's next-generation atmospheric dispersion model, NAME III," in *Air pollution modeling and its application XVII*. Editors C. Borrego and A. L. Norman (Boston, MA: Springer). doi:10.1007/978-0-387-68854-1_62

Kota, S. H., Qi, Y., and Zhang, Y. (2013). Simulating near-road reactive dispersion of gaseous air pollutants using a three-dimensional Eulerian model. *Sci. Total Environ.* 454-455 (1), 348–357. doi:10.1016/j.scitotenv.2013.03.039

Li, K., Liang, M., and Su, G. (2018). Data assimilation method for atmospheric dispersion based on a Gaussian puff model. *J. Tsinghua Univ. Technol.* 58 (11), 992–999. doi:10.16511/j.cnki.qhdxxb.2018.22.049

Li, M., Yang, D., and He, W. (2020). Comparison and perspective on theories and simulation results of gas dispersion models AERMOD and CALPUFF. *Geomatics Inf. Sci. Wuhan Univ.* 45 (08), 1245–1254. doi:10.13203/j.whugis20200110

Liu, Y., Li, H., Sun, S., and Fang, S. (2017). Enhanced air dispersion modelling at a typical Chinese nuclear power plant site: Coupling RIMPUFF with two advanced diagnostic wind models. *J. Environ. Radioact.* 175/176, 94–104. doi:10.1016/j.jenvrad.2017.04.016

Ministry of Ecology and Environment of the People's Republic of China (2018). Technical Guidelines for environmental impact assessment—atmospheric Environment HJ 2.2-2018. https://www.mee.gov.cn/ywgz/fgbz/bz/bzwb/other/pjjsdz/201808/W020180814672740551977.pdf

Mishra, K. B., and Wehrstedt, K. D. (2015). Underground gas pipeline explosion and fire: CFD based assessment of foreseeability. *J. Nat. Gas Sci. Eng.* 24, 526–542. doi:10.1016/j.jngse.2015.04.010

NOAA and EPA (2007). ALOHA user's manual. February, 2007. Retrieved from: https://nepis.epa.gov/Exe/ZyPDF.cgi/P1003UZB.PDF?Dockey=P1003UZB.PDF

Ratner, B. (2009). The correlation coefficient: Its values range between +1/1, or do they? *J. Target. Meas. Anal. Mark.* 17 (2), 139–142. doi:10.1057/jt.2009.5

Ridzuan, N., Ujang, U., Azri, S., and Choon, T. L. (2020). Visualising urban air quality using AERMOD, CALPUFF and CFD models: A critical review *The International Archives of the Photogrammetry, Remote Sensing and Spatial Information Sciences*. XLIV-4/W3-2020, 355–363. doi:10.5194/isprs-archives-xliv-4-w3-2020-355-2020

Rood, A. S. (2014). Performance evaluation of AERMOD, CALPUFF, and legacy air dispersion models using the Winter Validation Tracer Study dataset. *Atmos. Environ.* 89 (2), 707–720. doi:10.1016/j.atmosenv.2014.02.054

Rzeszutek, M. (2019). Parameterization and evaluation of the calmet/calpuff model system in near-field and complex terrain-terrain data, grid resolution and terrain adjustment method. *Sci. Total Environ.* 689 (1), 31–46. doi:10.1016/j.scitotenv.2019.06.379

Schulman, L. L., and Hanna, S. (1986). Evaluation of downwash modifications to the industrial source complex model. *J. Air Pollut. Control Assoc.* 36, 258–264. doi:10.1080/00022470.1986.10466066

Schulman, L. L., and Scire, J. S. (1980). Buoyant line and point source (BLP) dispersion model user's guide. Final report.Available at: https://www.osti.gov/biblio/5824114

Scire, J. S., Strimaitis, D. G., and Yamartino, R. J. (2011). A user's guide for the Calpuff dispersion model. Available at: http://www.src.com/calpuff/download/CALPUFF_UsersGuide.pdf

Stein, A. F., Draxler, R. R., Rolph, G. D., Stunder, B. J. B., Cohen, M. D., and Ngan, F. (2016). NOAA's HYSPLIT atmospheric transport and dispersion modeling system. *Bull. Am. Meteorol. Soc.* 96, 2059–2077. doi:10.1175/BAMS-D-14-00110.1

Stockie, J. M. (2011). The mathematics of atmospheric dispersion modeling. *SIAM Rev. Soc. Ind. Appl. Math.* 53 (2), 349–372. doi:10.1137/10080991x

Toscano, D., Marro, M., Mele, B., Murena, F., and Salizzoni, P. (2021). Assessment of the impact of gaseous ship emissions in ports using physical and numerical models: The case of Naples. *Build. Environ.* 196, 107812. doi:10.1016/j.buildenv.2021.107812

Ulimoen, M., Berge, E., Klein, H., Salbu, B., and Lind, O. C. (2022). Comparing model skills for deterministic versus ensemble dispersion modelling: The fukushima daiichi npp accident as a case study. *Sci. Total Environ.* 806, 150128. doi:10.1016/j.scitotenv.2021.150128

Yan, X., Guo, X., Liu, Z., and Yu, J. (2016). Release and dispersion behaviour of carbon dioxide released from a small-scale underground pipeline. *J. Loss Prev. Process Industries* 43, 165–173. doi:10.1016/j.jlp.2016.05.016

Yassin, M. F., Alhajeri, N. S., Elmi, A. A., Malek, M. J., and Shalash, M. (2021). Numerical simulation of gas dispersion from rooftop stacks on buildings in urban environments under changes in atmospheric thermal stability. *Environ. Monit. Assess.* 193 (1), 22. doi:10.1007/s10661-020-08798-x

Yu, X., and Cao, L. (2020). A review of the Lagrangian diffusion model for atmospheric pollution. *Environ. Eng.* 38 (09), 145–153. doi:10.13205/j.hjgc.202009024

Yuan, D., Li, S., Huang, Y., and Wu, M. (2013). Research progress on diffusion model of petrochemical industry gas leakage. *Energy Chem. Ind.* 34 (02), 21–26. doi:10.3969/j.issn.1006-7906.2013.02.006

Zhuang, S. (2014). Study on mechanism of gas flow and pollutant dispersion around the buildings. PhD thesis. Shenyang (IL): Northeastern University (Chinese).

frontiers | Frontiers in Environmental Science

TYPE Methods
PUBLISHED 18 November 2022
DOI 10.3389/fenvs.2022.1054839

OPEN ACCESS

EDITED BY
Xiaohu Wen,
Northwest Institute of Eco-Environment and Resources (CAS), China

REVIEWED BY
Lin Mu,
Shenzhen University, China
Qingzhi Hou,
Tianjin University, China

*CORRESPONDENCE
Shu Wang,
ustbwangshu@ustb.edu.cn

SPECIALTY SECTION
This article was submitted to Toxicology, Pollution and the Environment, a section of the journal Frontiers in Environmental Science

RECEIVED 27 September 2022
ACCEPTED 09 November 2022
PUBLISHED 18 November 2022

CITATION
Yang Y-f, Wang S, Zhu Z-d and Jin L-z (2022), Prediction model and consequence analysis for riverine oil spills.
Front. Environ. Sci. 10:1054839.
doi: 10.3389/fenvs.2022.1054839

Prediction model and consequence analysis for riverine oil spills

Yu-feng Yang[1,2], Shu Wang[1]*, Zhen-duo Zhu[3] and Long-zhe Jin[1]

[1]School of Civil and Resource Engineering, University of Science and Technology Beijing, Beijing, China, [2]Pipechina Science and Technology Research Institute, Langfang, China, [3]Department of Civil, Structural and Environmental Engineering, University at Buffalo, Buffalo, NY, United States

Long-distance oil and gas pipelines play an important role in ensuring energy imports, but can cause riverine oil spills and threaten public health and the environment. The emergency disposal of spilled oil is affected by a number of factors such as the difficulty of disposal and the long recovery cycle; however, there are deficiencies in the understanding of river oil spills. In this study, a prediction model of the river oil spill trajectory based on the random walk particle tracking algorithm was constructed. The performance of the model was tested by simulating the Enbridge Line 6B Oil Discharge scenario occurred in the United States in 2010. The temporal and spatial variations of the oil pollution zone in downstream and vertical directions were studied, and the interception effects on the arrival time of oil in key sections were obtained. Results showed that after the spilled oil entered the surface water body, the tiny oil droplets generated by crushing can remain underwater for a long time, making them difficult to detect and intercept. It can further combine with suspended particles in the water, settle, and pollute the riverbed, which has a greater potential for harm and risk. The model offers helpful information for the first-phase emergency response for riverine oil spills.

KEYWORDS

oil pipeline, oil spill, river, oil trajectory simulation, random walk model

1 Introduction

Long oil and gas pipelines play an essential role in ensuring the security of imported energy. To meet the rising energy demand driven by rapid economic growth, China is experiencing a third wave of pipeline construction, with the lengths of crude oil and petroleum product pipelines ranking fourth and third, respectively, in the world (Li et al., 2021). Meanwhile, there is growing concern regarding the effects of oil spills (Zheng and Huang, 2017). Countries such as the United States, Canada, and China have created emergency management systems to guide responses to oil spills (Li et al., 2016).

According to National Transportation Safety Board's (NTSB) reports (National Transportation Safety Board (NTSB)), a total of 486 pipeline incidents occurred in America between 2010 and 2019, of which 151 involved oil spills, accounting for 31% of

the total pipeline incidents. Forty-four of these oil spills reached inland water systems and caused environmental pollution, accounting for 9% of the total pipeline incidents. These incidents spilled more than four million gallons of oil, including diesel, gasoline, and crude oil, damaging fresh water resources, the soil environment, and ecosystems to varying degrees, and causing over 270 million dollars in economic losses. One of the most famous incident is the Enbridge Line 6B Oil Spill incident. The pipeline ruptured at approximately 6 p.m. on 25 July 2010. The crude oil (DilBit) spilled from the ruptured segment, seeped into the ground and the nearby wetland, and flowed to the Talmadge Creek. The emergency response was initiated 17 h after the spill. The discharged DilBit volume was estimated to be approximately 3,192 m^3 (843,444 gallons) and drifted downstream along the Talmadge Creek before entering the Kalamazoo River. The impacted area, including the river, floodplains, and wetlands along the banks, exceeded 20 km^2. River channel restoration lasted until October 2014.

There are more than 175,000 km of onshore oil and gas pipelines in China. Many pipelines cross large rivers within their territory, such as the Yangtze River, the Yellow River, and transboundary rivers, such as the Lancang River. An oil spill from such pipelines could cause serious environmental pollution and even have an international impact (Chang et al., 2014; Beyer et al., 2016). Modeling the fate and transport of discharged oil in inland rivers is critical for risk assessment and oil response (Amir-Heidari et al., 2019) and these efforts date back to the 1970s (Tsahalis, 1979). River morphology (meanders, branches, artificial constructions etc.) and ambient environment variation (rain, wind et al.) significantly influence river flow through multiple aspects (Yapa et al., 1994; Rakesh and B, 2018). The spilled oil may transform into a film, droplet, emulsion, aggregate, or other forms within 24 h of the spill (Afenyo et al., 2016; Brussaard et al., 2016), which brings potential challenges to the modeling field. Compared with the development of tools for oil spills in the ocean (Keramea et al., 2021; Zhao et al., 2021), studies on oil transportation in inland waterways are limited (Goeury et al., 2014; Kvočka et al., 2021), and new attempts at model optimization and calibration are still made by researchers around the world (Jiang et al., 2021; Li et al., 2022).

The longitudinal distribution of oily pollutants is one of the primary concerns in response to an oil spill in a river. Timely calculation will help in the decision-making of appropriate first-phase action to control the expansion of polluted areas and prevent even worse consequences. River hydrodynamics provide basic flow data for particle tracking algorithms. With the long-term development of numerical approaches for the dynamic model, a large number of mature software packages are available, and many researchers have discussed the computational performance of these models in different scenarios and scales (Jowett and Duncan, 2012; Bürgler et al., 2022). The contaminated area, which is significantly influenced by the longitudinal flow velocity, is hundreds of kilometers in length. It is verified that a one-dimensional hydraulic model can provide accurate results with less effort and computational requirements for large-scale modeling tasks if well calibrated (Horritt and Bates, 2002; de Paiva et al., 2013).

In this study, a random walk particle tracking algorithm using one-dimensional unsteady hydrodynamics was constructed. Data of real-time flow fluctuation and variation of atmospheric parameters can be exchanged at high speeds using the random walk model. The performance of the model was tested by simulating the Enbridge Line 6B Oil Discharge scenario. The consequences with and without containment measures were compared to provide insights into the effectiveness and challenges of emergency operations.

2 Methodology

2.1 Hydrodynamic model

The HEC-RAS software (Hydraulic Engineering Center, developed by the United States Army Corps of Engineers), which yields reliable results in the hydrodynamic modeling of natural rivers, was used for one-dimensional unsteady hydrodynamic simulations in this study. The software uses a weighted four-point implicit finite difference method (Gary, 2020) to solve the Saint-Venant equations by discretization and iteration:

$$\frac{\partial A}{\partial t} + \frac{\partial S}{\partial t} + \frac{\partial Q}{\partial x} - q_l = 0 \tag{1}$$

$$\frac{\partial Q}{\partial t} + \frac{\partial (vQ)}{\partial x} + gA\left(\frac{\partial z}{\partial x} + S_f\right) = 0 \tag{2}$$

where t is time, x is the longitudinal distance along the river channel, A is the cross-sectional area of the portion of the channel occupied by the flow, Q is river discharge, S is the cross-sectional area of the portion of the channel without water flow, q_l is lateral incoming flow, v is flow velocity, g is the gravitational acceleration, and S_f is friction slope.

The current study focused on the river segment impacted by the Enbridge Line 6 B Oil Discharge, which stretches from Talmadge Creek near Marshall to downstream Morrow Lake. River bathymetry was created by interpolating the field data from the United States Geological Survey (USGS) report (Reneau et al., 2015) with the bathymetry interpolation tool from Merwade et al. (2008). The bathymetry map was then merged with a digital elevation model (DEM, with a resolution of 1 m × 1 m) published by the USGS in order to produce a corrected elevation map of the study area. The constructed main channel model for the HEC-RAS was 64.27 km in length, with an average slope of 0.72‰. The model contained a total of 3893 cross sections with spacing of 1.4–30.9 m apart. Inflow

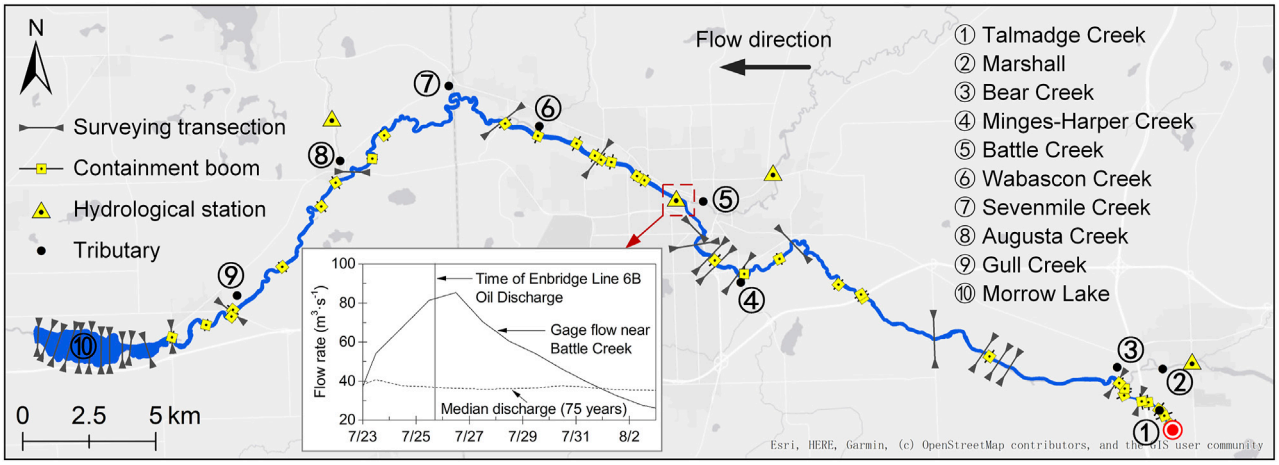

FIGURE 1
Study area.

was applied to nine cross sections, the locations of which are illustrated in Figure 1.

Flow data from the 12th of April to the 16th of April 2013 were used to verify the model (Reneau et al., 2015). The model was calibrated using water surface elevation and discharge data from USGS stations 04105500, SR1485, and SR0585 by adjusting Manning's roughness coefficients. More details can be found in the supplementary data.

2.2 Particle-tracking model

In the Lagrangian scheme, the displacement components of each particle in the longitudinal (x), lateral (y), and vertical (z) directions in Cartesian coordinates at time ($t + \Delta t$) (i.e., $x_i^{t+\Delta t}$, $y_i^{t+\Delta t}$, and $z_i^{t+\Delta t}$) were determined by its location at time t, advective movement, and diffusive transport during the time interval Δt (Wu et al., 2019). The Visser scheme was employed to describe the vertical movement of particles (Visser, 1997). The governing equations are as follows.

$$x_i^{t+\Delta t} = x_i^t + u_i^t \Delta t + R_{-1}^1 \sqrt{2\sigma_R^{-1} D_x^t \Delta t} \tag{3}$$

$$y_i^{t+\Delta t} = y_i^t + v_i^t \Delta t + R_{-1}^1 \sqrt{2\sigma_R^{-1} D_y^t \Delta t} \tag{4}$$

$$z_i^{t+\Delta t} = z_i^t + w_i^t \Delta t + D_z{}' \Delta t + R_{-1}^1 \sqrt{2\sigma_R^{-1} D_{z1}^t \Delta t} \tag{5}$$

Here i is the number index of a particle, Δt is the time step; u_i^t and v_i^t are streamwise and lateral flow velocity components at location (x_i^t, y_i^t) (m·s^{-1}), respectively; w_i^t is the average vertical velocity of the particle between t and $t + \Delta t$, which is calculated using the Stokes equation (m·s^{-1}); R_{-1}^1 is a uniform distribution between −1 and 1; σ_R is the standard deviation of random number R, which is set at 1/3 (Visser, 1997) and D_x^t, D_y^t, and D_z^t denote the streamwise, lateral, and vertical turbulent diffusivity coefficients at time t, respectively.

In the present study, the transverse flow velocity (v_i^t) was ignored because the longitudinal drifting of the oil particles was more valuable for a fast emergency response. The longitudinal velocity (u_i^t) is assumed to obey the law of the wall (Jones and Garcia, 2018), which is written as:

$$\frac{u_i^t}{u_\star} = \frac{1}{\kappa} \ln\left(\frac{u_\star z_i^t}{\nu}\right) + 5.5 \tag{6}$$

where $u_\star$ denotes the shear velocity of the flow (m·s^{-1}); ν denotes the dynamic viscosity of water (m^2·s^{-1}); and κ denotes the von Karman constant (0.41).

The streamwise and lateral diffusions, D_x^t and D_y^t, are given by (Garcia, 2008):

$$D_x^t = D_y^t = 0.6 H u_\star \tag{7}$$

For D_z^t, the parabolic-constant profile (Rijn, 1984) was employed and expressed as:

$$D_z^t = \begin{cases} 0.25\kappa u_\star H & \frac{z}{H} \geq 0.5 \\ z_1\left(1 - \frac{z_1}{H}\right)\kappa u_\star & \frac{z}{H} < 0.5 \end{cases} \tag{8}$$

where H is the water depth (m). In the lower half of the depth, D_z^t is estimated for location z_1, which is given by $z_1 = z_i^t + D_z{}' \Delta t/2$.

A reflective boundary condition was used when the oil particles exceeded the left, right, and bottom boundaries of the channel. When the particles surfaced, they were assumed to be absorbed into the oil slick. The resuspension probability, p,

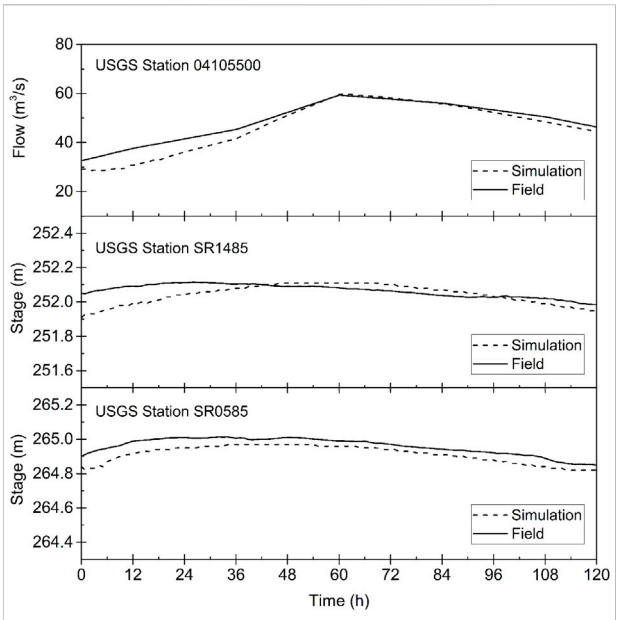

FIGURE 2
Comparison between simulation and survey results.

was calculated to determine whether the particles would reenter the water column (Nordam et al., 2019). p is given by

$$p = 1 - e^{-\Delta t \cdot \lambda} \tag{9}$$

where λ is the lifetime of the oil at the surface (Nordam et al., 2019).

In particular, a random depth is assigned if the particle is resuspended; otherwise, the mass loss of the oil droplet due to evaporation should be calculated during the surfaced duration.

2.3 Spill scenarios

Based on a series of documents released by the National Transportation Safety Board, in the present model, the leakage entered the upstream of Talmadge Creek at the cross section located approximately 2.5 km away from the confluence of Talmadge Creek and the Kalamazoo River, and the start time was 18:00 on 25 July 2010. Oil particles were released at a rate of 720 per hour in the calculation domain for 10 h. Based on the oil droplet size distribution, which was reported in the literature based on the breakup of oil in water (Li et al., 2009; Johansen et al., 2015; Zeinstra-Helfrich et al., 2016), nine oil droplet sizes, that is, diameters of 0.5 mm, 2 mm, 4 mm, 6 mm, 8 mm, 10 mm, 12 mm, 16 mm, and 20 mm, were considered. The density of oil at different temperatures is given by (Berry et al., 2012):

$$\rho_{oil} = \rho_{ref}\left[1.0 - 8.0 \times 10^{-4}\left(T - T_{ref}\right)\right] \tag{10}$$

The density of oil after evaporation was expressed by (Berry et al., 2012),

$$\rho_{oil} = \rho_{ref}\left(1.0 + 0.018F_{ev}\right) \tag{11}$$

where ρ_{oil} is the density of the spilled oil (kg·m^{-3}); ρ_{ref} is the reference density at a reference temperature T_{ref}, which is approximately 920 kg m^{-3} at 20°C; T is the temperature (°C), equal to 23°C; F_{ev} is the mass loss in percentage terms (%); and t is the duration of evaporation (min).

Based on the measured data obtained by Waterman (Waterman, 2015), a fitting function in logarithmic form (R^2 = 0.985) that describes the mass loss due to evaporation was introduced as follows:

$$F_{ev} = 1.961\ln(t) \tag{12}$$

The hydraulic data were calculated using the HEC-RAS software using the flow data between July 25th and 31st, 2010 (Reneau et al., 2015). The particle-tracing algorithm was performed using MATLAB software. The computational time step is 2 s.

Two scenarios, one with containment booms and the other with no measures, were conducted. The containment booms were positioned similarly to those in actual situations and extended 0.05 m deep underwater. Figure 2.

3 Results

3.1 Drift and distribution in scenario with no containment measure

When no containment measure was taken, particles with different sizes exhibited similar drifting trajectories in the simulated domain. Figure 3 illustrates the maps of the particle positions when the particle diameter equals 1 mm. The black arrows in the figure indicate the leading edges of the particle swarm at 1 h, 6 h, 12 h, 24 h, 72 h, and 120 h. The particles arrived at Battle Creek at approximately 19.5 h, which roughly matched the time when a resident reported the appearance of an oil slick near Battle Creek, according to documents released by the National Transportation Safety Board.

Figure 4 shows the statistics for the 10th, 25th, 50th, 75th, and 90th percentiles of the distance drifted downstream of the particle swarm, as well as the temporal variation in the average distance. Overall, the polluted zone continued to expand. The 90th and 10th percentiles represent the positions of the front and rear edges of the polluted zone, respectively. The length of the polluted zone in the downstream direction can then be calculated as the difference between the 90th and 10th percentiles. This was calculated as 12.06 km, 22.81 km, 29.61 km, and 34.96 km, at

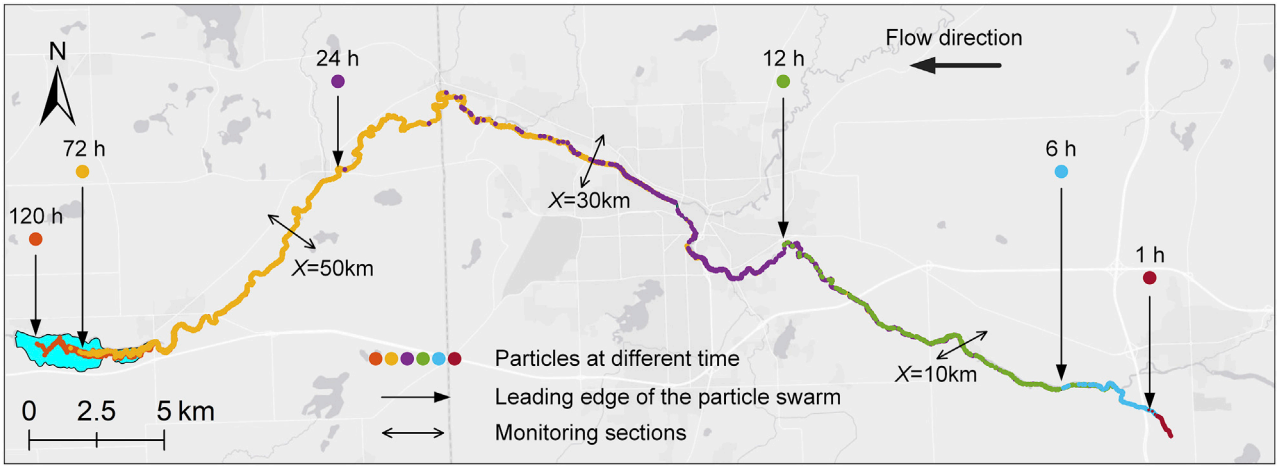

FIGURE 3
Particle position vs. time (particle diameter 0.5 mm).

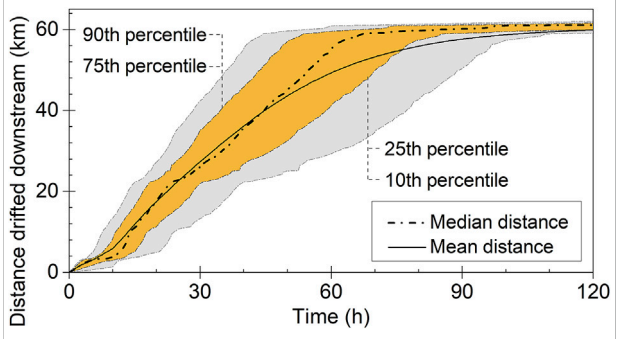

FIGURE 4
Statistics on distance drifted downstream by particles (particle diameter 0.5 mm).

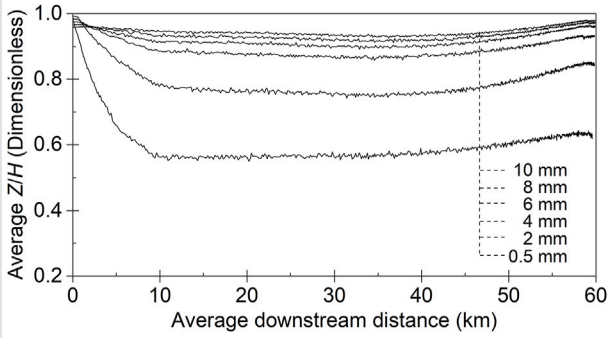

FIGURE 5
Variation in the center of mass of particle swarm (Z/H = 1.0 represents the water surface).

12 h, 24 h, 36 h, and 48 h, respectively, after the oil entered the water. The length of the polluted zone decreased after 48 h, because the front edge arrived at the downstream boundary of the simulated area.

Plotting the means of the particle swarm's longitudinal position (X) and vertical position (Z) at different times provides insight into how the center of the particle swarm varies spatially and temporally. As shown in Figure 5, the dimensionless height Z/H was used as well as $Z/H = 1.0$, which represents the water surface. In general, as the particle size increased from 0.5 mm to 10 mm, the vertical velocity, which is influenced by the buoyancy force, increased. Advective movement driven by buoyancy dominated the vertical position of the particles; thus, more particles (larger than 4 mm) appeared close to the water surface. Small particles were gradually dispersed in water and forced by diffusive movement. After a trip of 10 km downstream, the center of the 0.5 mm particle cloud stabilized at approximately $Z/H = 0.6$.

3.2 Impact of containment measure

After the containment booms were added in the same positions as the actual containment booms that were installed in real response operations, particles with different diameters changed their movement paths. The monitoring sections were set in the model at downstream distances of 10 km, 30 km, and 50 km, as shown in Figure 3. As shown in Figure 6A, the number of particles passing through each section was determined. The

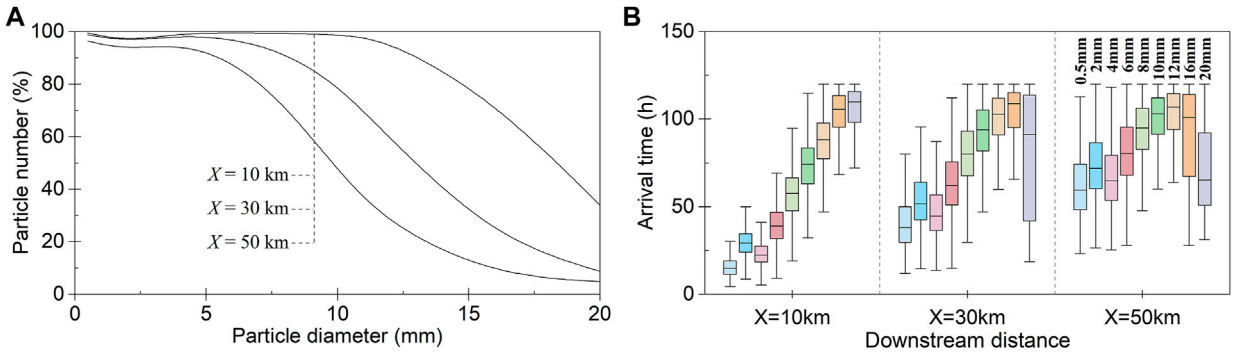

FIGURE 6
Statistics on oil particles at cross-sections located at downstream distance X = 10 km, 20 km, and 30 km respectively: **(A)** Percentage of particles passing through each section; **(B)** Arrival time of particles with different sizes.

containment booms implanted before the monitoring section at a distance of 10 km exhibited a slight interception effect on particles smaller than 10 mm. Approximately 26.12% of the 16 mm particles and 65.93% of the 20 mm particles were contained in the upstream booms. At a distance of 30 km, the containment rates for the 8 mm, 10 mm, and 20 mm particles increased to 7.57%, 19.72%, and 91.23%, respectively. At a distance of 50 km, the corresponding containment rates further increased to 27.54%, 52.55%, and 95.11%, respectively. Unlike large oil droplets, which migrated in the upper part of the water column, small oil droplets were hardly blocked by the implanted booms as these particles were suspended over depth, as revealed in the previous section. The containment effectiveness was enhanced by increasing the number of containment booms. However, their relationship is complex because it is also affected by the actual particle properties and hydraulic conditions.

Statistical analysis was performed for the time when the particles arrived at each monitoring cross section. In the model with no containment measure implanted, the mean time for particles to reach the sections 10 km, 30 km, and 50 km downstream was 11.80 ± 0.41, 35.15 ± 1.34, and 55.01 ± 1.84 h, respectively. The average arrival times in the presence of containment booms are plotted in Figure 6B. We found that the diffusion of oil droplets greater than 6 mm was slowed by the containment booms.

4 Discussion

This study simulated the drifting trajectory of oil droplets in the Kalamazoo River with and without containment measures. Although the sizes of the droplets are artificial to some extent, they provide insight into the difficulty of the cleanup after the spill. Containment measures have an apparent effect on floating slicks. However, as the statistics revealed, small droplets (less than 6 mm in diameter in our simulation) that stayed below the water surface for a long period were hardly stopped by the containment booms. In contrast to their low proportion of leakage volume, these particles, in all probability, potentially pose tremendous hazards, as they would further break into micro-sized particles and coagulate with the suspended solid particles in the water column to form dense aggregates, known as oil–particle aggregates (OPAs). The formed OPAs tend to reach lower waters, deposit on the riverbed, and are resuspended when the water is agitated. With regards to the Enbridge Line 6 B Oil Spill, it took more than 4 years, with costs of up to 1.21 billion dollars, to clean the residual oil from the 56.5-km-long river segment where OPAs were detected. The deposition of OPAs on the downstream riverbed varied with the properties of the oil, sand, and natural environment. Interested readers may refer to our previous study for more information on the formation and transport of OPAs (Wang et al., 2020b; Li et al., 2022).

To obtain a rapid view of the oil fate along the river for a timely emergency response after a spill, a one-dimensional hydrodynamic model by HEC-RAS was employed to provide the depth-averaged streamwise velocities, which were considered as the major factor contributing to the longitudinal transport of particles. The setting enabled fast exchange of data between the real-time flow fluctuations and subsequent particle tracing programs for large-scale river basins. However, it cannot precisely describe the lateral distribution of oil, especially when one is interested in the fate of oil in a lake, reservoir, oxbow, etc. Under these circumstances, two-dimensional or coupled 1D/2D hydrodynamics are required as opposed to a one-dimensional model. In addition, the range of oiled riverbanks cannot be detailed. Using two- or three-dimensional hydrodynamics with a sufficiently fine meshed domain may be used to identify the location where the

particle landed on the bank. Predicting the amount of retained oil along the bank is relatively difficult, as our previous study showed that it is related to multiple factors such as the roughness of the substrate, slope of the bank, hydraulic scouring force, and plant types along the bank (Wang et al., 2020a). Further studies are underway to understand the quantitative relationship between oil retention and the related factors.

The absorption and re-entrainment of oil droplets at the water surface remains unclear. In the present study, a probability function is introduced to describe the resuspension probability of a particle. Although the simplification is not sensitive to the big picture of particle distribution in such a large-scale river basin, further refinement, calibration, and validation of the approach are necessary in the future.

5 Conclusion

Oil spills in inland rivers have serious consequences and cause considerable losses. Modeling the fate and transport of discharged oil in inland rivers, especially the longitudinal distribution, is critical for risk assessment and oil response. In the present work, a random walk particle tracking algorithm was constructed to provide a quick view of oil transport along the river for a timely emergency response after a spill. The main conclusions are as follows.

(1) The model uses one-dimensional hydrodynamics to drive particles. A velocity profile was employed in the vertical direction to correct the streamwise velocity at different positions. A Visser scheme was employed to describe the vertical movement of particles. A probability function was applied to describe the re-entrainment of particles at the water surface.
(2) When no containment measure was taken, particles with different sizes exhibited similar drifting trajectories in the longitudinal direction. Vertical statics revealed that large particles appeared close to the water surface due to advective movement driven by buoyancy, while small particles dispersed in water gradually due to diffusive movement.
(3) Containment measures had an apparent effect on floating slicks. However, small droplets (less than 6 mm in diameter in our simulation) that stayed below the water surface for longer period of time were hardly stopped by containment booms. Although small droplets comprise a low proportion of the leakage volume, these particles potentially pose tremendous hazards.
(4) The model is a tool for calculating the temporal and spatial variations of the impacted zone and the arrival time at key cross-sections after the oil spill and offers helpful information for the first-phase emergency response. Further refinement and calibration of the simplifications employed in the model will be necessary in the future.

Data availability statement

The original contributions presented in the study are included in the article/Supplementary Material, further inquiries can be directed to the corresponding author.

Author contributions

All authors listed have made a substantial, direct, and intellectual contribution to the work and approved it for publication.

Funding

This work was supported by Fundamental Research Funds for the Central Universities (No. FRF-TP-20-003A3), and the National Key R&D Program of China (No. 2016YFC0802104).

Conflict of interest

The authors declare that the research was conducted in the absence of any commercial or financial relationships that could be construed as a potential conflict of interest.

Publisher's note

Supplementary material

The Supplementary Material for this article can be found online at: https://www.frontiersin.org/articles/10.3389/fenvs.2022.1054839/full#supplementary-material

References

Afenyo, M., Veitch, B., and Khan, F. (2016). A state-of-the-art review of fate and transport of oil spills in open and ice-covered water. *Ocean. Eng.* 119, 233–248. doi:10.1016/J.OCEANENG.2015.10.014

Amir-Heidari, P., Arneborg, L., Lindgren, J. F., Lindhe, A., Rosén, L., Raie, M., et al. (2019). A state-of-the-art model for spatial and stochastic oil spill risk assessment: A case study of oil spill from a shipwreck. *Environ. Int.* 126, 309–320. doi:10.1016/J.ENVINT.2019.02.037

Berry, A., Dabrowski, T., and Lyons, K. (2012). The oil spill model OILTRANS and its application to the Celtic Sea. *Mar. Pollut. Bull.* 64, 2489–2501. doi:10.1016/j.marpolbul.2012.07.036

Beyer, J., Trannum, H. C., Bakke, T., Hodson, P. v., and Collier, T. K. (2016). Environmental effects of the deepwater Horizon oil spill: A review. *Mar. Pollut. Bull.* 110, 28–51. doi:10.1016/J.MARPOLBUL.2016.06.027

Brussaard, C. P. D., Peperzak, L., Beggah, S., Wick, L. Y., Wuerz, B., Weber, J., et al. (2016). Immediate ecotoxicological effects of short-lived oil spills on marine biota. *Nat. Commun.* 7 (*1* 7), 11206–11211. doi:10.1038/ncomms11206

Bürgler, M., Vetsch, D. F., Boes, R. M., and Vanzo, D. (2022). Systematic comparison of 1D and 2D hydrodynamic models for the assessment of hydropeaking alterations. *River Res. Appl.* 1–18. doi:10.1002/rra.4051

Chang, S. E., Stone, J., Demes, K., and Piscitelli, M. (2014). Consequences of oil spills: A review and framework for informing planning. *Ecol. Soc.* 19, art26. *Published online: May 09, 2014*. doi:10.5751/ES-06406-190226

de Paiva, R. C. D., Buarque, D. C., Collischonn, W., Bonnet, M.-P., Frappart, F., Calmant, S., et al. (2013). Large-scale hydrologic and hydrodynamic modeling of the Amazon River basin. *Water Resour. Res.* 49, 1226–1243. doi:10.1002/wrcr.20067

Garcia, M. (2008). *Sedimentation Engineering*. Reston, VA, USA: American Society of Civil Engineers. doi:10.1061/9780784408148

Gary, W. B. (2020). *HEC-RAS river analysis system hydraulic reference manual*. Davis, CA, USA: US ARMY CORPS OF ENGINEERS HYDROLOGIC ENGINEERING CENTER HEC. Available at: https://www.hec.usace.army.mil/confluence/rasdocs/ras1dtechref/latest (Accessed October 28, 2022).

Goeury, C., Hervouet, J. M., Baudin-Bizien, I., and Thouvenel, F. (2014). A Lagrangian/Eulerian oil spill model for continental waters. *J. Hydraulic Res.* 52, 36–48. doi:10.1080/00221686.2013.841778

Horritt, M. S., and Bates, P. D. (2002). Evaluation of 1D and 2D numerical models for predicting river flood inundation. *J. Hydrol. X.* 268, 87–99. doi:10.1016/S0022-1694(02)00121-X

Jiang, P., Tong, S., Wang, Y., and Xu, G. (2021). Modelling the oil spill transport in inland waterways based on experimental study. *Environ. Pollut.* 284, 117473. doi:10.1016/J.ENVPOL.2021.117473

Johansen, Ø., Reed, M., and Bodsberg, N. R. (2015). Natural dispersion revisited. *Mar. Pollut. Bull.* 93, 20–26. doi:10.1016/J.MARPOLBUL.2015.02.026

Jones, L., and Garcia, M. H. (2018). Development of a rapid response riverine oil–particle aggregate formation, transport, and fate model. *J. Environ. Eng. New. York.* 144, 04018125. doi:10.1061/(ASCE)EE.1943-7870.0001470

Jowett, I. G., and Duncan, M. J. (2012). Effectiveness of 1D and 2D hydraulic models for instream habitat analysis in a braided river. *Ecol. Eng.* 48, 92–100. doi:10.1016/J.ECOLENG.2011.06.036

Keramea, P., Spanoudaki, K., Zodiatis, G., Gikas, G., and Sylaios, G. (2021). Oil spill modeling: A critical review on current Trends, Perspectives, and challenges. *J. Mar. Sci. Eng.* 9, 181. doi:10.3390/jmse9020181

Kvočka, D., Žagar, D., and Banovec, P. (2021). A review of river oil spill modeling. *Water* 13, 1620. *Page 1620* 13. doi:10.3390/W13121620

Li, P., Cai, Q., Lin, W., Chen, B., and Zhang, B. (2016). Offshore oil spill response practices and emerging challenges. *Mar. Pollut. Bull.* 110, 6–27. doi:10.1016/J.MARPOLBUL.2016.06.020

Li, Q., Zhao, M., Zhang, B., Wen, W., Wang, L., Zhang, X., et al. (2021). Current construction status and development trend of global oil and gas pipelines in 2020 (in Chinese). *Oil Gas Storage Transp.* 40, 1330–1337. doi:10.6047/j.issn.1000-8241.2021.12.002

Li, Y., Zhu, Z., Soong, D. T., Khorasani, H., Wang, S., Fitzpatrick, F., et al. (2022). FluOil: A Novel tool for modeling the transport of oil-particle aggregates in inland waterways. *Front. Water* 3, 180. doi:10.3389/frwa.2021.771764

Li, Z., Lee, K., King, T., Boufadel, M. C., and Venosa, A. D. (2009). Evaluating Chemical dispersant Efficacy in an experimental wave Tank: 2—Significant factors determining *in Situ* oil droplet size distribution. *Environ. Eng. Sci.* 26, 1407–1418. *https://home.liebertpub.com/ees* 26. doi:10.1089/EES.2008.0408

Merwade, V., Cook, A., and Coonrod, J. (2008). GIS techniques for creating river terrain models for hydrodynamic modeling and flood inundation mapping. *Environ. Model. Softw.* 23, 1300–1311. doi:10.1016/J.ENVSOFT.2008.03.005

National Transportation Safety Board (NTSB) (2022). Accident Investigation report. Available at: https://www.ntsb.gov/investigations/AccidentReports/Pages/Reports.aspx?mode=Pipeline (Accessed October 30, 2022).

Nordam, T., Kristiansen, R., Nepstad, R., and Röhrs, J. (2019). Numerical analysis of boundary conditions in a Lagrangian particle model for vertical mixing, transport and surfacing of buoyant particles in the water column. *Ocean. Model. (Oxf).* 136, 107–119. doi:10.1016/j.ocemod.2019.03.003

Rakesh, B., and B, S. W. (2018). Data and calibration challenges for spill response models. *J. Environ. Eng. New. York.* 144, 04017109. doi:10.1061/(ASCE)EE.1943-7870.0001319

Reneau, P. C., Soong, D. T., Hoard, C. J., and Fitzpatrick, F. A. (2015). *Hydrodynamic assessment data associated with the July 2010 line 6B spill into the Kalamazoo River, Michigan, 2012–14*. Report 2015-1205. U.S. Geological Survey Open-File Juneau, AL, USA. doi:10.3133/ofr20151205

Rijn, L. C. van (1984). Sediment transport, Part II: Suspended load transport. *J. Hydraul. Eng.* 110, 1613–1641. doi:10.1061/(asce)0733-9429(1984)110:11(1613)

Tsahalis, D. T. (1979). Contingency planning for oil spills: RIVERSPILL - a river simulation model. *Int. Oil Spill Conf. Proc.* 1979, 27–36. doi:10.7901/2169-3358-1979-1-27

Visser, A. (1997). Using random walk models to simulate the vertical distribution of particles in a turbulent water column. *Mar. Ecol. Prog. Ser.* 158, 275–281. doi:10.3354/meps158275

Wang, S., Xu, S., Yang, Y., Jin, L., Wang, Y., and Zhang, J. (2020a). Retention behavior of spilled oil along river bank. *J. China Univ. Petroleum Ed. Nat. Sci.* 44, 144–150.

Wang, S., Yang, Y., Zhu, Z., Jin, L., and Ou, S. (2020b). Riverine deposition pattern of oil–particle aggregates considering the coagulation effect. *Sci. Total Environ.* 739, 140371. doi:10.1016/j.scitotenv.2020.140371

Waterman, D. M. (2015). *Laboratory Tests of oil-particle Interactions in a Freshwater riverine environment with Cold lake Blend Weathered Bitumen*. Urbana, IL, USA: University of Illinois.

Wu, X., Liang, D., and Zhang, G. (2019). Estimating the accuracy of the random walk simulation of mass transport processes. *Water Res.* 162, 339–346. doi:10.1016/J.WATRES.2019.06.027

Yapa, P. D., Shen, H. T., and Angammana, K. S. (1994). Modeling oil spills in a river—Lake system. *J. Mar. Syst.* 4, 453–471. doi:10.1016/0924-7963(94)90021-3

Zeinstra-Helfrich, M., Koops, W., and Murk, A. J. (2016). How oil properties and layer thickness determine the entrainment of spilled surface oil. *Mar. Pollut. Bull.* 110, 184–193. doi:10.1016/J.MARPOLBUL.2016.06.063

Zhao, L., Nedwed, T., and Mitchell, D. (2021). Review of the Science behind oil spill fate models: Are Updates Needed? *Int. Oil Spill Conf. Proc.* 2021, 687874. doi:10.7901/2169-3358-2021.1.687874

Zheng, H., and Huang, W. (2017). Development status and prospect of safety insurance technologies for oil&gas pipelines and storage and transportation facilities (in Chinese). *Oil Gas Storage Transp.* 36, 1–7. doi:10.6047/j.issn.1000-8241.2017.01.001

frontiers | Frontiers in Environmental Science

TYPE Original Research
PUBLISHED 22 November 2022
DOI 10.3389/fenvs.2022.1077430

OPEN ACCESS

EDITED BY
Jun Wu,
Harbin Engineering University, China

REVIEWED BY
Xueci Xing,
Guangzhou University, China
Elena Neverova-Dziopak,
AGH University of Science and Technology, Poland

*CORRESPONDENCE
Ruya Chen,
chenruya2021@163.com

SPECIALTY SECTION
This article was submitted to Toxicology, Pollution and the Environment, a section of the journal Frontiers in Environmental Science

RECEIVED 23 October 2022
ACCEPTED 08 November 2022
PUBLISHED 22 November 2022

CITATION
Kang Y, Chen Y, Zhou M, Xu Y, Feng H and Chen R (2022), Identification of regional industrial priority pollutants in surface water: A field study in Taihu Lake Basin.
Front. Environ. Sci. 10:1077430.
doi: 10.3389/fenvs.2022.1077430

Identification of regional industrial priority pollutants in surface water: A field study in Taihu Lake Basin

Ying Kang[1,2,3], Yuqi Chen[1], Mengjiao Zhou[1], Yingfeng Xu[1], Huajun Feng[1,2] and Ruya Chen[1]*

[1]School of Environmental Science and Engineering, Zhejiang Gongshang University, Hangzhou, China, [2]Zhejiang Key Laboratory of Ecological and Environmental Big Data, Hangzhou, China, [3]Zhejiang Ecological Environmental Monitoring Center, Hangzhou, China

The current water environment management of China has gradually shifted from reaching water quality standards to preserving water ecological health, and the control focus has extended from traditional nitrogen and phosphorus pollutants to micropollutants, such as heavy metals and emerging pollutants. However, the precise traceability and regulatory system of micropollutants in different regions' watersheds was not yet mature. A five-step strategy of risk assessment and management was proposed this study to successfully construct a list of industrial priority pollutants and a list of 376 priority control discharge enterprises in 13 administrative regions of China's Taihu Lake Basin. Firstly, a preliminary list of 78 pollutants was determined with reference to the emission standards of major regional industrial pollution sources, relevant national environmental regulations and literature reports. Secondly, 22 types of priority control pollutants were re-screened based on the analytical results of surface water samples obtained from 26 monitoring sites in the study area. Then the environmental risk values of the re-screened pollutants were calculated referring to the Chemical Hazard Evaluation for Management Strategy (CHEMS-1) method. Next, the regional environmental risk baseline value was determined and the risk value equivalent (E_Y) for each pollutant was calculated. Finally, according to the E_Y results, the regional priority control pollutants were identified, and the priority control discharge enterprises were confirmed retroactively. The results of this study can provide

Abbreviations: AOX, Absorbable organic halogen; BCF, Bioconcentration factor; DCM, Dichloromethane; DMF, Dimethylformamide; E_Y, Risk value equivalent of pollutant Y; E-E, Exposure effects; HH-E, Human health effects; HV, Total risk value; HV_{OR}, Human acute oral effects; HV_{INH}, Human acute inhalation toxicity effects; HV_{CAR}, Carcinogenicity effects; HV_{other}, Other specific effects; HV_{MAM}, Acute oral effects for terrestrial organisms; HV_{FA}, Acute toxicity effects for fish; HV_{FC}, Chronic toxicity effects for fish; HV_{HYD}, Hydrolytic degradation; HV_{BOD}, Biological oxygen demand; IARC, International Agency for Research on Cancer; Kow, Octanol water partition coefficient; LC_{50}, Lethal Concentration 50%; LD_{50}, Lethal Dose 50%; NOEL, No observable effect level; RWF, Emission weight of pollutants in water; SAR, Safety Assessment Report; USEPA, United States Environmental Protection Agency; WE-E, Water environmental effects; wHV, Risk value based on the discharge; $wHV_{X, Y}$, Risk value of pollutant Y in area X based on the discharge; $wHV_{X, b}$, Environmental risk background value of the benchmark pollutant in area X.

methodological support and a scientific basis for the precise control of micropollutants in surface water from differentiated regions.

KEYWORDS

environmental management, regionalization, industrial sources, priority pollutants, risk assessment

1 Introduction

With the continuous promotion of national ecological environmental protection, the current water environment management of China's surface water environment has gradually shifted from reaching water quality standards to preserving water ecological health, and its control focus has been extended from conventional nitrogen and phosphorus pollutants (Wang, et al., 2015) to micropollutants, such as heavy metals (Cui, et al., 2022; Huang, et al., 2022) and emerging pollutants (Chen, et al., 2021; Li, et al., 2021). As the third largest freshwater lake in China, Taihu Lake plays a pivotal role in the economic development of the lower reaches of the Yangtze River. However, in recent years, toxic and harmful substances discharged by enterprises in heavy polluting industries such as chemical industry, textile printing and dyeing, and ferrous metallurgy in the basin have caused serious damage to the water quality of Taihu Lake (Xu, et al., 2022; Meng, et al., 2018). Currently, there is a lack of regional differential screening and identification methods for such substances, and it is difficult for the environmental protection department to carry out targeted control of pollution in the specific implementation. There is an urgent need for the government to develop a list of localized priority pollutants to support the high-level improvement of water ecological environment quality.

Since the mid-1970s, some developed countries and relevant international organizations have been conducting screening of environmental priority control pollutants (Cui, et al., 2010). The United States Environmental Protection Agency (USEPA) mainly uses the production of pollutants, environmental detection rate, acute and chronic toxicity, as well as the environmental and biological effects of toxicity as assessment indicators, and then combines expert argumentation method to screen priority pollutants (Li, et al., 2018). The EU Water Framework Directive is based on monitoring and model prediction to calculate the exposure score and toxicity effect score of pollutants, and the risk ranking of pollutants according to the total score, and finally the priority pollutants are determined by expert evaluation (EC, 2011). The screening of priority pollutants in the environmental white paper issued by the Japanese government takes into account the toxicity, persistence, and bioconcentration of pollutants (Bu, et al., 2016), and the methodology is objective but does not consider the human health risks associated with environmental exposure.

China had selected a total of 68 types of 14 categories of benzene, phenol, DDT, etc. for the blacklist of priority control pollutants in China's water based on the comprehensive assessment of the acute and chronic toxicity, carcinogenic, teratogenic and mutagenic effects, product yield, and environmental detection rate of pollutants, were (He, et al., 2014). However, the evaluation method is highly subjective, which also lacks model parameters and scoring criteria based on the actual local environmental conditions in China, and does not consider the risk of human health exposure caused by pollutants. Meanwhile, with the rapid development of economy, science and technology, the status quo of pollutants in China's environment and the level of government supervision and control have changed. The blacklist of priority-controlled pollutants in China's water can't meet the requirements of current regional differentiated and precise pollution control.

The specific methods for screening priority pollutants in the environment all over the world include the potential hazard index method, the Hasse graphical method, and the comprehensive scoring method and so on. The potential hazard index method is a method for ranking chemical substances based on their potential hazard level to the environment, which can use various toxicity data to estimate the potential hazard level of chemical substances through a unified model (Du, et al., 2022), which is fast, easy and comparable. The Hasse graphical method is a method that uses vectors to describe the hazards of compounds and graphically shows the relative magnitude of the hazards of compounds and the logical relationship between them (Kudlak, et al., 2014), which can visually represent the relative magnitude of the hazards of compounds and the contradiction of different indicators (Tsakovski, et al., 2010). However, these method does not take into account the state of existence of pollutants in the environment and cannot reflect the diffusion law of chemical substances (Fan, et al., 2016), which needs further improvement. Among the various comprehensive evaluation methods, the Chemical Hazard Evaluation for Management Strategy (CHEMS-1) adopted by EPA is screened based on the pollutants' toxic effects, hazards to the environment and human health and exposure effects, combining with the emission, persistence and bioaccumulation of pollutants in the ecosystem for comprehensive evaluation (USEPA, 1994; Pei, et al., 2013; Zhu, et al., 2013). Then, the list of regional priority pollutants is determined by assigning quantitative evaluation results and ranking. This method has been used in various studies to evaluate and prioritize contaminant risks

(Swanson, et al., 1997; Tobiszewski and Namieśnik, 2015; Guo, et al., 2021). Compared with other evaluation methods, CHEMS-1 technology has the following advantages: 1) it integrates human health effects, environmental hazards and exposure effects, and has a more comprehensive evaluation perspective; 2) the evaluation method is based on the toxicity effects of pollutants, which is more practical for evaluating regions where the main discharged pollutants are relatively toxic pollutants, and is more consistent with the pollution production characteristics of enterprises in heavy pollution industries; 3) based on the emission and persistence of pollutants and other factors, starting from the actual pollution situation, and taking into account the long-term harm degree of pollutants, the selected list of priority pollutants screened out is more time-sensitive and more consistent with the future pollution situation; 4) the calculation process is simpler and easier to implement than other methods, and is currently widely used (Zhang, et al., 2015; Karahan Ozgun, et al., 2016).

This study focused on the pollutants discharged from industrial pollution sources in the water environment of different regions. A five-step method was proposed for identifying regional priority industrial pollutants that need to be controlled urgently referring to EPA's CHEMS-1 technology. On this basis, trace the industrial enterprises that discharge these pollutants in the region and a list of key industrial enterprises was determined. This method is scientific, accurate and operable, making it easier for local governments to control industrial pollution sources and provide technical support for regionalized, differentiated and precise environmental pollution control.

2 Materials and methods

2.1 Study area

The water area of Taihu Lake is about 2338 km^2, with an average depth of 1.9 m and a maximum depth of about 3.4 m (Dai, et al., 2016). The study area covers 13 county-level administrative regions of Zhejiang province in China. The leading industries in this area are paper making, printing and dyeing, tannery, electroplating, pharmaceutical and other heavy pollution industries. Zhejiang area of the Taihu Lake Basin has been one of the key areas for water environment management in China.

2.2 Sampling point layout

There are 13 administrative regions in Zhejiang area of Taihu Basin. The sampling principle was to distribute at least 2 monitoring points in each county-level administrative area, thus a total of 26 monitoring locations were selected for surface water sampling and analysis in August 2020. The monitoring points were all national/provincial/municipal control cross-section points, so the water samples can represent the pollution level of local surface water. Figure 1 shows the distribution of specific sampling points, and Supplementary Table S1 shows the detailed latitude and longitude of sampling points. Sampling methods are shown in Supplementary Text S1 of the Supplementary Material. Monitoring indicators cover 67 contaminants in the initial screening list. Sample collection, pre-treatment, instrument analysis and quality control carried out in accordance with national standard methods or the methods recommended in the "Surface Water Environmental Quality Standards" (GB3838-2002).

2.3 Construction of a priority pollutant identification and assessment method

This study establishes the identification, screening and evaluation method of regional industrial priority control pollutants based on CHEMS-1 method (Figure 2). Specifically, there are five steps: 1) establishing the initial screening list of priority pollutants by referring to national environmental protection laws, industry emissions standards, and regulations and literature reports; 2) sampling and testing of surface water in the study area and re-screening of the pollutants according to the analysis results; 3) evaluating the environmental risk values of pollutants in the re-screening list by referring to the CHEMS-1 evaluation method and calculating the risk values of each pollutant; 4) determining the regional environmental risk benchmark value and calculate the risk value equivalent E_Y for each substance based on the risk benchmark value; 5) for pollutants with $E_Y \geq 1$, determining the priority pollutants to be controlled in the region, and finally determining the regional key industrial enterprises list under control based on the basic emission statistics of regional pollution sources.

2.3.1 Initial screening

In the process of screening and identification of regional industrial priority pollutants, a preliminary screening list of pollutants should be established first. The initial screening principles are as follows: 1) give priority to select pollutants with large production, use and emissions in major industries in the region or basin; 2) give priority to pollutants with high environmental detection rate and resistance to degrade; 3) give priority to pollutants with bioaccumulation and biotoxicity; 4) give priority to pollutants that have certain analytical conditions to be detected by targeted or non-targeted analytical methods. The initial screening lists of pollutants in different surface water environments are mainly based on the blacklist of priority control pollutants in China's water, Surface Water Environmental Quality Standards (GB

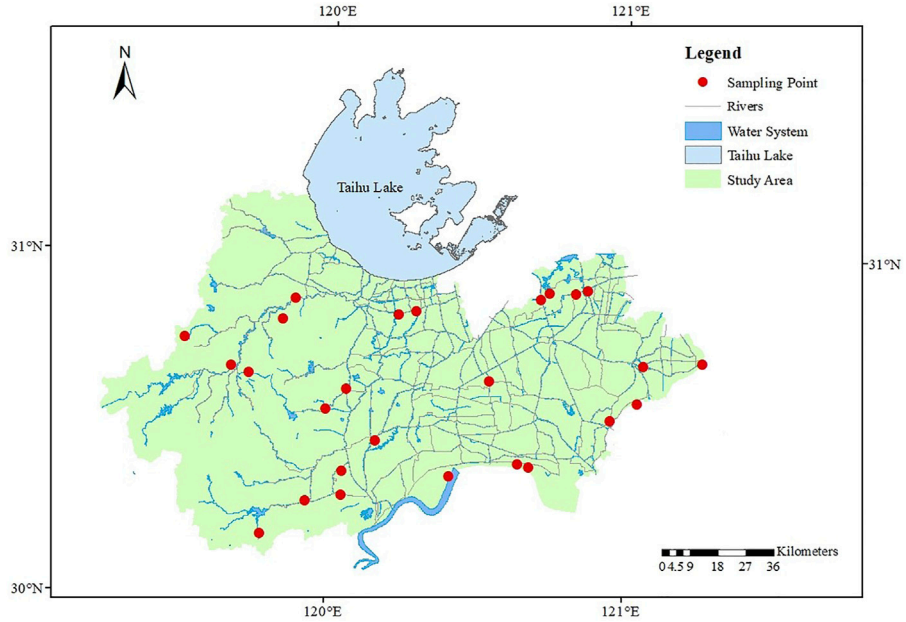

FIGURE 1
Distribution of sampling points.

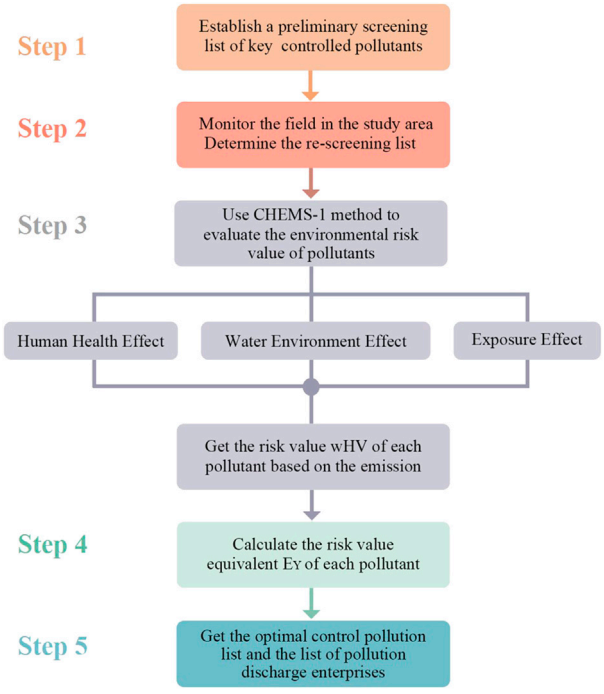

FIGURE 2
Flow chart of the identification of regional industrial priority pollutants.

3838–2002) and wastewater discharge standards of various industries, etc., with reference to relevant pollutant research literature and reports as well as the actual pollution conditions of the studied areas.

2.3.2 Re-screening

Surface water monitoring sections in the study area were selected to conduct point monitoring with the method of 2.2 introduced, and based on the monitoring results, the indicators of the pollutants not detected in the area were eliminated and the priority control pollutants present were re-screened from the initial screening list.

2.3.3 Environmental risk assessment and assignment

The environmental risk assessment and assignment of priority control pollutants refer to the aforementioned CHEMS-1 technique, which integrates the human health effects, water environment effects and exposure effects of the re-screened pollutants, quantifies the evaluation results by assigning scores, and then ranks the pollutant scoring results to finally obtain the priority control pollutant list.

The aquatic animals in Taihu Lake Basin mainly include white fish, white shrimp, silver fish, white chub, chub, crucian carp, grass carp and cyprinid; aquatic plants include bitter grass, spiny bitter grass, whorled black algae, microtooth eyelet,

goldfish algae and Malaysian eye (Gao, et al., 2019). In the risk assignment of pollutants, the corresponding pollutant risk assignment of these aquatic organisms was selected, and the scoring of each risk value was expressed by the continuity equation, and the risk level of each risk item and the calculation method of the assignment are shown in Supplementary Table S2.

The human health effects (HH-E) risk values were calculated by grading the human acute oral risk (LD_{50} of rodent), human acute inhalation toxicity (LC_{50} of rodent), carcinogenicity and other effects, and then scoring. The LD_{50} and LC_{50} data sources were obtained by reviewing the literature based on plant and aquatic animal species in the Taihu Lake Basin. Carcinogenicity was based on the International Agency for Research on Cancer (IARC) and EPA classifications, and was assessed using the Safety Assessment Report (SAR) if neither IARC nor EPA classified the chemical as its carcinogenicity.

HH-E is calculated using the following equation:

$$HH - E = HV_{OR} + HV_{INH} + HV_{CAR} + HV_{other} \quad (1)$$

where HV_{OR} is the human acute oral effects; HV_{INH} is the human acute inhalation toxicity effects; HV_{CAR} is the carcinogenicity effects; and HV_{other} is the other specific effects, including mutagenicity, developmental effects, reproductive effects, neurotoxicity and neurotoxicity.

The calculation of risk values for water environmental effects (WE-E) is based on rodent oral LD_{50}, fish LC_{50} and fish no observable effect level (NOEL). NOEL is used to assess chronic sublethal effects on fish and is estimated from acute toxicity data (i.e. LC_{50} data) and the n-octanol water partition coefficient (Kow) of the chemical, calculated as follows:

When $2 \leq \log Kow < 5$,

$$NOEL = \frac{LC_{50}}{5.3 \times \log(Kow) - 6.6} \quad (2)$$

When $\log Kow \geq 5$,

$$NOEL = 0.05 \times LC_{50} \quad (3)$$

When $\log Kow < 2$,

$$NOEL = 0.25 \times LC_{50} \quad (4)$$

WE-E is calculated using the following equation:

$$WE - E = HV_{MAM} + HV_{FA} + HV_{FC} \quad (5)$$

where HV_{MAM} is the acute oral effects for terrestrial organisms; HV_{FA} is the acute toxicity effects for fish; and HV_{FC} is the chronic toxicity effects for fish.

Exposure effects (E-E) are classified as persistence and bioconcentration. The former is based on the assessment of the half-life of biological oxygen demand (BOD) and the half-life of hydrolytic degradation (HYD) to obtain the residual persistence of pollutants in the environment, calculated with reference to the Hammett and Taft substitution constant method. Bioconcentration factor (BCF) is determined by the quantitative structure-activity relationship (QSAR) equation (Binetin and Devillers, 1994).

E-E is calculated using the following equation:

$$E - E = HV_{BOD} + HV_{HYD} + HV_{BCF} \quad (6)$$

The total risk values for contaminants include HH-E, WE-E and E-E, with the following equations:

$$HV = (HH - E + WE - E) \times E - E \quad (7)$$

$$wHV = HV \times RWF \quad (8)$$

$$RWF = \ln(Emissions) \quad (9)$$

where HV is the total risk value; emission data refers to the 2020 Zhejiang Province Ecological Environment Statistics Annual Report; wHV is the risk value based on emission; RWF is the emission weight of pollutants in water.

2.3.4 Identifying regional priority pollutants and their industrial priority emission sources

As mentioned above, the identification range of priority pollutants was determined through pollutant screening, and then the potential risk value of each pollutant was quantified by constructing a scoring system to obtain its potential risk value to the environment. Due to the lack of evaluation benchmarks for the current risk level of micropollutants in the water environment, an evaluation benchmark needs to be set reasonably to further screen different regional priority pollutants.

Since there were no mercury pollutants discharged from the enterprises involved in the study area, and the long-term monitoring results from the cross-sectional monitoring stations showed that the mercury content in surface water usually met the water quality standard for surface water (category III, GB3838-2002), Therefore, it is assumed that mercury will continue to be at low risk level and can be considered as the benchmark pollutant in the study area. If the pollutants' risk value is lower than that of mercury, the pollutant is considered to be at low risk and can be excluded from the list of regional priority pollutants. Based on the above assumptions, the environmental risk background values of the benchmark pollutant were calculated according to the environmental limit value (0.0001 mg/L) of total mercury in surface waters (category III) of the Surface Water Environmental Quality Standards (GB3838-2002) and the amount of surface water in study area. Due to the algorithm takes into account the different regional surface water environmental capacity, the evaluation results of environmental risk background values are more accurate and more in line with the actual control needs of regional differentiated environmental risks and priority control pollutants.

The risk value of each pollutant in each region is divided by the environmental risk background value to obtain the risk value equivalent of each pollutant in each region relative to the baseline pollutant, expressed by the letter E_Y and E_Y calculated as:

$$E_Y = \frac{wHV_{X,Y}}{wHV_{X,b}} \quad (10)$$

TABLE 1 Priority control pollutant initial screening list.

	Pollutant			Pollutant	
1	Total Nickel	Aniline	27	Dimethyl phthalate	
2	Total Lead		28	Polycyclic Aromatic Hydrocarbons	Naphthalene
3	Total Arsenic				Acenaphthene
4	Total Antimony				Dihydroacenaphthene
5	Total Copper				Anthracene
6	Total Zinc				Fluorene
7	Total Manganese				Faye
8	Total Cobalt				Fluoranthene
9	Total Chromium				Pyrene
10	Total Mercury				Benzo(a)anthracene
11	Total Cadmium				Substances
12	Total Silver				Benz(b) fluoranthene
13	Chloride Ion				Benzo(k)fluoranthene
14	Total fluoride				Benzo(a)pyrene
15	Chlorine Dioxide				Dibenzo (a,h)anthracene
16	Sulfide				Benzo (g,h,i)pyrene
17	AOX				Indeno (1,2,3-cd)pyrene
18	Aniline		29	Perfluorinated compounds	PFHxS
		Dinitroaniline			PFHxA
		2,6-Dinitroaniline			PFBS
		p-Nitroaniline			PFBA
19	Alkylmercury				PFNA
20	Volatile Phenols				PFOS
21	Nitrobenzene	Nitrobenzene			PFDA
		p-Nitrotoluene			PFHpA
		2,4-Dinitrotoluene			PFOA
		Trinitrotoluene			PFHpS
		p-Nitrochlorobenzene			PF-3
		2,4-Dinitrochlorobenzene			7-DMOA
22	Dichloromethane				1H,1H,2H,2H-PFOS
23	Hexavalent Chromium				
24	Total Cyanide				
25	Toluene				
26	DMF				

where Y is the pollutant type; E_Y is the risk value equivalent of pollutant Y; X is each county and urban area of Taihu Lake Basin; $wHV_{X,\ Y}$ is the risk value of pollutant Y in area X based on the discharge; $wHV_{X,\ b}$ is the environmental risk background value of the benchmark pollutant in area X.

The pollutants with risk value equivalent $E_Y \geq 1$ in the region were listed as industrial priority pollutants for control in the region. Combined with the existing environmental statistics database and the results of pollution source census and other information, a list of pollutant sources with priority pollutant emissions in the study area was obtained.

3 Results and discussion

3.1 Primary screening of industrial priority pollutants in Taihu Lake Basin

For the Zhejiang area of Taihu Lake Basin studied in this study, the blacklist of priority pollutants in China's water, Surface Water Environmental Quality Standards (GB 3838–2002) and wastewater discharge standards of paper, printing and dyeing, tannery, electroplating, pharmaceutical, lead battery and other industries are used as benchmarks, and then refer to relevant

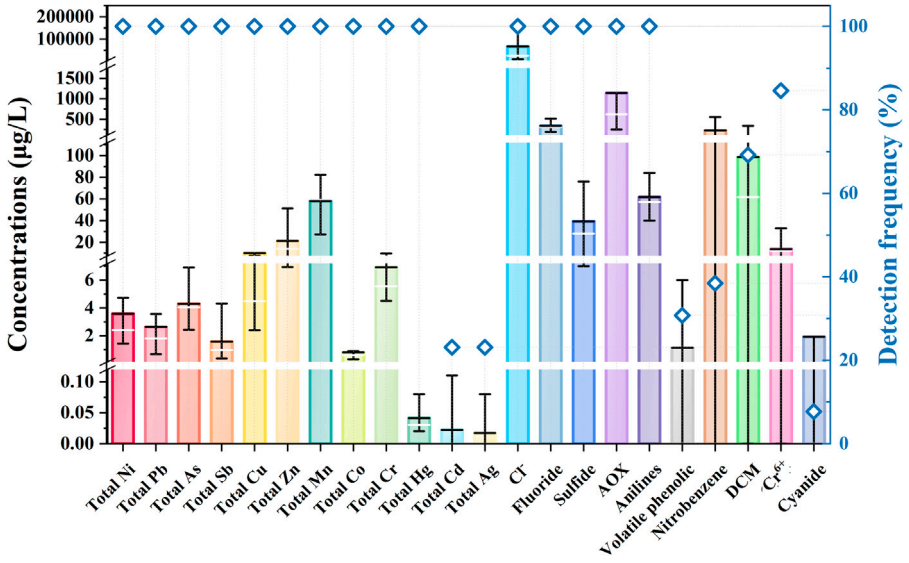

FIGURE 3
The concentration (left Y-axis) and detection frequency (right Y-axis) of the detected pollutants in 13 regions.

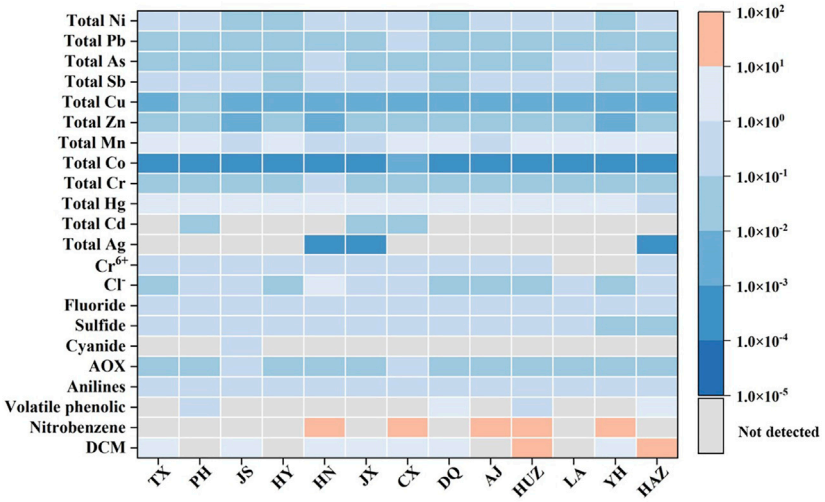

FIGURE 4
The standing-reaching quotient of pollutants in each region.

pollutant research literature and reports, a total of 78 priority pollutants in 34 categories are initially identified, covering conventional pollutants, persistent organic pollutants, emerging pollutants, volatile organic pollutants and inorganic toxic hazardous pollutants, as shown in Supplementary Table S3.

Seven conventional pollutants with lower environmental risk were excluded (including COD, NH_4-N, TN, TP, petroleum, animal and vegetable oils, TOC) and the preliminary screening list of priority control pollutants was obtained as follows (Table 1).

3.2 Re-screening of industrial priority pollutants

The water sample monitoring results of the priority control pollutants in Table 1 are shown in Supplementary Table S4. The

TABLE 2 Re-screening of priority control pollutants list.

	Pollutant		Pollutant	
1	Total Ni	17	Aniline	Aniline
2	Total Pb			Dinitroaniline
3	Total As			2,6-Dinitroaniline
4	Total Sb			p-Nitroaniline
6	Total Zn	18	Volatile Phenols	
7	Total Mn	19	Nitrobenzene	Nitrobenzene
8	Total Co			p-Nitrotoluene
9	Total Cr			2,4-Dinitrotoluene
10	Total Hg			Trinitrotoluene
11	Total Cd			p-Nitrochlorobenzene
12	Total Ag			2,4-Dinitrochlorobenzene
13	Cl^-	20	DMC	
14	F^-	21	Cr^{6+}	
15	Sulfide	22	Total Cyanide	
16	AOX			

mean concentrations and detection rates of the detected pollutants are shown in Figure 3. As shown in Figure 3, total Ni, total Pb, total As, total Sb, total Cu, total Zn, total Mn, total Co, total Cr, total Hg, Cl^-, fluoride, sulfide, AOX and aniline were detected in all regions. Total Cd, total Ag, volatile phenols, nitrobenzene, DMC, Cr^{6+} and total cyanide were detected in some areas, and the detection rates were 23.01%, 23.01%, 30.77%, 38.46%, 69.23%, 84.62% and 7.69%, respectively. The rest of the pollutants in Supplementary Table S4 were below the detection limit and recorded as non-detect.

As shown in Figure 4, the data in the heat map indicate the standing-reaching quotient of each pollutant in surface water, ≥ 1 means exceedance, and <1 means meet the standard. The results show that some of the study regions' levels of nitrobenzene, DCM, volatile phenolic, Cl^-, and total Mn exceeded the surface water environmental quality standards, with DCM levels exceeding the standards in 69.23% of the regions. The detected pollutants were considered to be at risk and were further rescreened as priority control pollutants, including total Ni, total Pb, total As, total Sb, total Cu, total Ag, Cl^-, F^-, sulfide, AOX, aniline, volatile phenols and other 22 types of pollutants (Table 2).

3.3 Environmental risk assessment and assignment of regional industrial priority pollutant

For the 22 types of pollutants in Table 2 of the re-screening list of priority control pollutants in Taihu Lake Basin, the evaluation was carried out from HH-E, WE-E and E-E in accordance with the environmental risk assessment method of priority control pollutants in Section 2.3.3, and assigned points for accounting. The accounting results are detailed in Supplementary Table S5–S8.

Despite the significant differences in human health, environmental health and exposure factors for each pollutant, the total risk value calculated by considering the three factors together gives a better indication of the true risk level. The scoring calculation results show that the risk of Ni was the highest, followed by As, Co and Ag, thus the local contamination with heavy metals was still predominant, while the risk from trace organic pollutants was relatively low (Figure 5).

According to the actual emissions of each pollutant in 13 regions in Taihu Lake Basin (calculated by using environmental statistics and pollutant discharge coefficients), the RWF of pollutants in water was calculated, and then the wHV of pollutants in each region was obtained, and the accounting results of each region are detailed in Supplementary Table S9. The pollutants with the highest wHV are DMC in HAZ region; total Ni in LA region, AJ and CX regions; aniline in YH, DQ, JS and TX regions; total Sb in HUZ, HN and JX regions; and AOX in HY and PH regions, respectively.

3.4 Equivalent risk value accounting of the regional priority pollutants

With the method of risk benchmark values and risk value equivalents described in 2.3.4, the regional environmental risk background values of benchmark pollutants were calculated by taking the environmental limit value of total Hg in surface water (0.0001 mg/L) and referring to the total amount of surface water in 13 administrative areas of Taihu Lake Basin in the Water Resources Bulletin of Zhejiang Province in 2020. The environmental risk background values of each region are shown in Supplementary Table S10.

The pollutants with $E_Y \geq 1$ are listed as priority control pollutants, and the list of industrial priority pollutants in each regions is shown in Figure 6 and Supplementary Table S11. It shows that the three pollutants with the highest frequency in the priority control pollutants in 13 administrative regions in Taihu Lake Basin were aniline, AOX and total antimony, which distributed in 10 regions, 8 regions and 7 regions, respectively. JS region requires the most types of the priority control pollutants, including aniline, total Sb, AOX, DCM, total Cu, total Ni, total Zn. The next is HUZ region whose priority control pollutants include total Sb, aniline, total Cr, AOX, and Cr^{6+}.

The industries with the highest wastewater discharge in Taihu Lake Basin are chemical fiber weaving and processing, chemical fiber fabric dyeing and paper manufacturing industry, which account for 38.5%, 22.5% and 18.7% of the total regional industrial source wastewater discharge, respectively. It can be seen that the regional industrial priority pollutant categories screened by this method are in line with the actual emission status of regional industrial sources.

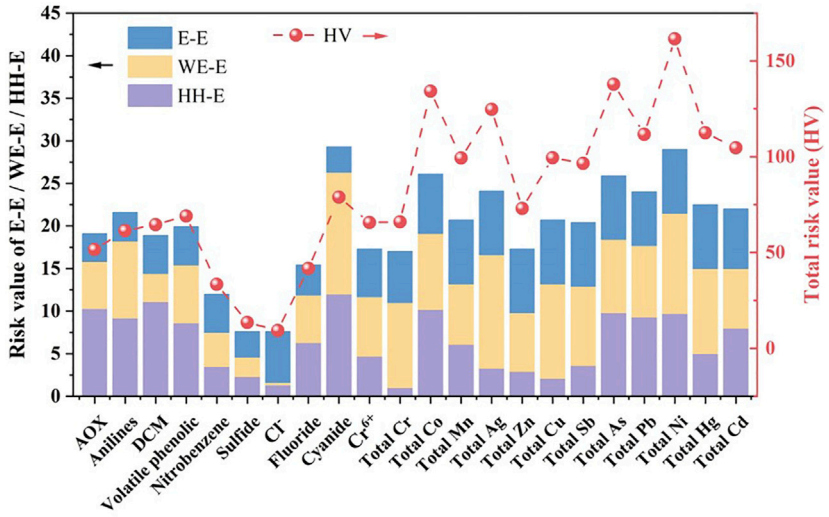

FIGURE 5
The risk values for three types of effects and total risk values of priority pollutants.

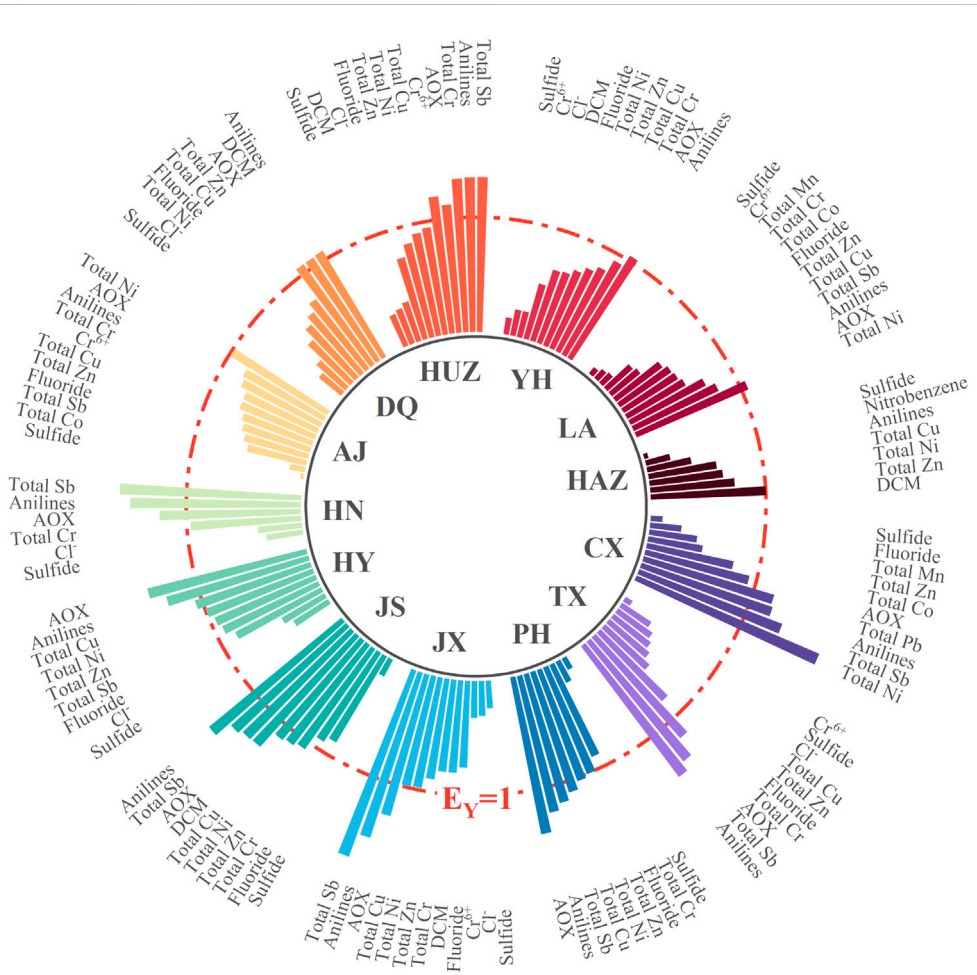

FIGURE 6
E_Y of pollutants in 13 regions.

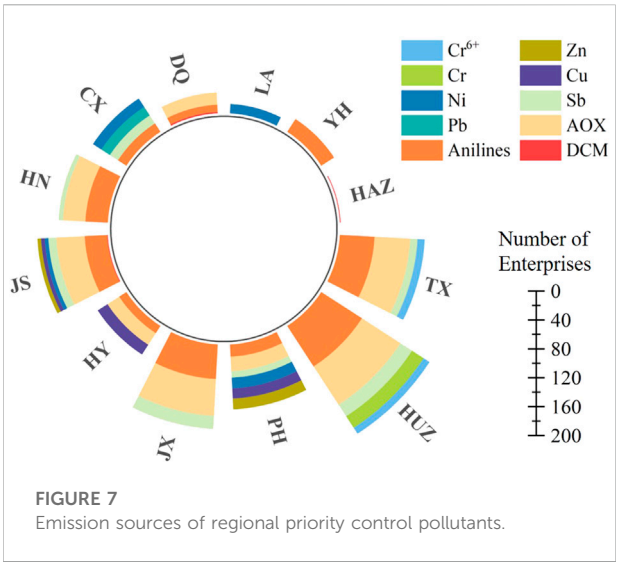

FIGURE 7
Emission sources of regional priority control pollutants.

3.5 List of regional key industrial enterprises

Based on the regional priority control pollutant list, combined with the environmental statistics database and the results of the Second National Pollution Source Census and other information, the priority pollutant emission sources were listed to be priority-controlled in each region. The number of key industrial enterprises in each region is shown in Figure 7 and Supplementary Table S12. A total of 376 priority control discharge enterprises were identified retroactively. From the data, HUZ region has the highest number of key industrial enterprises with 178, followed by JX region 117) and TX region (107), which should be targeted to control to minimize the environmental risks caused by their emission of pollutants.

It is noteworthy that nitrobenzene was not included in the regional priority pollutants in each region after calculating the pollutant emissions from industrial enterprises, which could be due to the fact that the enterprises we investigated did not cover all the sources of nitrobenzene emissions, or there were other potential sources of nitrobenzene besides industrial sources. The number of enterprises involved in the research area of this study was very large, therefore, according to the annual report of environmental statistics, the six industries with the largest amount of wastewater discharge in Zhejiang Province were selected for screening (paper making, textile, tanning, electroplating, medicine, and battery industry). Among the six industries, only the medicine industry has included nitrobenzene in its regulation (Supplementary Table S3). Nitrobenzene is an essential raw material for producing dyes, resins, explosives, pesticides and so on (Min, et al., 2022), so it was likely that nitrobenzene comes from other industries with small wastewater discharge but high nitrobenzene content (such as petrochemical industry, etc.), or from agricultural pollution sources. Similarly, pollutants such as DCM were not classified as a priority pollutant in some exceedance regions. These pollutants require in-depth local traceability in the future study, for example, from raw material production and other directions to identify the source of pollution.

4 Conclusion

The five-step method proposed in this study can successfully establish a regional industrial priority pollutant discharge list in the surface water environment of 13 administrative regions of Taihu Lake Basin. Twenty-two types of industrial priority pollutants were screened out from the initial list of 78 water pollutants in regional water bodies, and 376 priority control discharge enterprises were confirmed on this basis, which provides theoretical guidance for the regional water pollution management and control.

This method takes into account the toxicity, persistence, bioaccumulation and uses the risk value assignment method to quantitatively screen the priority control pollutants in the study area based on risk value equivalents. Given the regional differences in surface water environmental pollution conditions, this study's method can establish a localized industrial priority control pollutant list, which is more conducive to the formation of a differentiated regional priority control pollutant water quality benchmark, with the ultimate goal of protecting aquatic organisms and human health.

Data availability statement

The original contributions presented in the study are included in the article/Supplementary Material, further inquiries can be directed to the corresponding author.

Author contributions

YK: Conceptualization, Methodology, Writing- Reviewing and Editing. YC: Investigation, Validation, Writing—Reviewing and Editing. MZ: Investigation, Formal analysis, Writing, and Editing. YX: Investigation, Formal analysis. HF: Methodology, Supervision, Funding acquisition. RC: Formal analysis, Visualization, Writing—Reviewing and Editing, Supervision.

Funding

This study was supported by the Open Funding of Zhejiang Key Laboratory of Ecological and Environmental Big Data (No. EEBD-2022–03).

Conflict of interest

The authors declare that the research was conducted in the absence of any commercial or financial relationships that could be construed as a potential conflict of interest.

Publisher's note

All claims expressed in this article are solely those of the authors and do not necessarily represent those of their affiliated organizations, or those of the publisher, the editors and the reviewers. Any product that may be evaluated in this article, or claim that may be made by its manufacturer, is not guaranteed or endorsed by the publisher.

Supplementary material

The Supplementary Material for this article can be found online at: https://www.frontiersin.org/articles/10.3389/fenvs.2022.1077430/full#supplementary-material

References

Binetin, S., and Devillers, J. (1994). Qsar for organic chemical sorption in soils and sediments. *Chemosphere* 28 (6), 1171–1188. doi:10.1016/0045-6535(94)90335-2

Bu, Q. W., Wang, D. H., and Wang, Z. J. (2016). A risk-based screening approach for priority organic contaminants at the watershed scale: Method development. *Asian J. Ecotoxicol.* 11 (1), 61–69. doi:10.7524/AJE.1673-5897.20150415007

Chen, R. Y., Li, G. W., He, Y. T., Pan, L. L., Yu, Y., and Shi, B. Y. (2021). Field study on the transportation characteristics of PFASs from water source to tap water. *Water Res.* 198, 117162. doi:10.1016/j.watres.2021.117162

Cui, X. Y., Ding, W. J., Chai, T. Y., and Zhang, F. (2010). *Comparative study on the ranking of environmental and health risks of chemical pollutants at home and abroad*. Beijing: Science Press.

Cui, L., Li, J., Gao, X., Tian, B., and Liu, Z. (2022). Human health ambient water quality criteria for 13 heavy metals and health risk assessment in Taihu Lake. *Front. Environ. Sci. Eng* 16, 4. doi:10.1007/s11783-021-1475-6

Dai, X. L., Qian, P. Q., Ye, L., and Song, T. (2016). Changes in nitrogen and phosphorus concentrations in lake Taihu, 1985-2015. *J. Lake Sci.* 28 (5), 935–943. doi:10.18307/2016.0502

Du, Y. J., Xu, X., Liu, Q. Z., Bai, L., Hang, K. X., and Wang, D. H. (2022). Identification of organic pollutants with potential ecological and health risks in aquatic environments: Progress and challenges. *Sci. Total Environ.* 806 (3), 150691. doi:10.1016/j.scitotenv.2021.150691

EC (2011). Guidance Document No. 27. Technical Guidance For Deriving Environmental Quality Standards. Brussels: European Communities.

Fan, W., Zhou, J. L., and Zeng, Y. Y. (2016). Research progress on screening methods for priority pollutants for control of water environment. *Ground Water* 38 (3), 94–96.

Gao, H. L., Cheng, H. F., Zhan, M. H., and Wang, B. Y. (2019). Research progress of aquatic plants in Taihu Lake. *Wetl. Sci.* 17 (1), 11–17. doi:10.13248/j.cnki.wetlandsci.2019.01.002

Guo, Q., Wei, D., Wang, F., Chen, M., and Du, Y. (2021). A novel risk score-based prioritization method for pollutants in reclaimed water. *Sci. Total Environ.* 795, 148833. doi:10.1016/j.scitotenv.2021.148833

He, W., Qin, N., Kong, X. Z., Liu, W. X., He, Q. S., Wang, Q. M., et al. (2014). Water quality benchmarking (wqb) and priority control screening (pcs) of persistent toxic substances (ptss) in China: Necessity, method and a case study. *Sci. Total Environ.* 472, 1108–1120. doi:10.1016/j.scitotenv.2013.11.119

Huang, T. B., Chen, Y., Lu, J. A., Xia, T., and Xu, N. (2022). Evaluation of heavy metal pollution characteristics in sediments of Taihu Lake basin. *J. Nanjing tech Univ. Nat. Sci. Ed.* 44 (4), 443–449.

Karahan Ozgun, O., Basak, B., Eropak, C., Abat, S., Kirim, G., Girgin, E., et al. (2016). Prioritization methodology of dangerous substances for water quality monitoring with scarce data. *Clean. Technol. Environ. Policy* 19 (1), 105–122. doi:10.1007/s10098-016-1194-z

Kudlak, B., Tsakovski, S., Simeonov, V., Sagajdakow, A., Wolska, L., and Namiesnik, J. (2014). Ranking of ecotoxisity tests for underground water assessment using the Hasse diagram technique. *Chemosphere* 95, 17–23. doi:10.1016/j.chemosphere.2013.05.049

Li, Q. F., Lv, Y. L., Wang, P., and Zhang, Y. Q. (2018). Selection of priority contaminants in a watershed using risk ranking methodology. *Environ. Sci.* 39 (10), 4472–4478. doi:10.13227/j.hjkx.201802135

Li, Y., Wang, X. P., and Gong, P. (2021). Combined risk assessment method based on spatial interaction: A case for polycyclic aromatic hydrocarbons and heavy metals in Taihu Lake sediments. *J. Clean. Prod.* 328, 129590. doi:10.1016/j.jclepro.2021.129590

Meng, C., Qiang, W., Shan, G., Zhu, L., Yang, L., and Liu, M. (2018). Occurrence, partitioning and bioaccumulation of emerging and legacy per- andpolyfluoroalkyl substances in Taihu Lake, China. *Science of the TotalEnvironment* 634, 251–259. doi:10.1016/j.scitotenv.2018.03.301

Min, X. B., Chu, C., Luo, Z. H., Ma, J. Y., Fu, Y. F., Wei, Z. S., et al. (2022). Transformation of phenol and nitrobenzene by superoxide radicals: Kinetics and mechanisms. *Chem. Eng. J.* 442, 136134. doi:10.1016/j.cej.2022.136134

Pei, S. W., Zhou, J. L., and Liu, Z. T. (2013). Research progress on screening of environment priority pollutants. *J. Environ. Eng. Technol.* 3 (4), 363–368.

Swanson, M. B., Davis, G. A., Kincaid, L. E., Schultz, T. W., Bartmess, J. E., Jones, S. L., et al. (1997). A screening method for ranking and scoring chemicals by potential human health and environmental impacts. *Environ. Toxicol. Chem.* 16, 372–383. doi:10.1002/etc.5620160237

Tobiszewski, M., and Namieśnik, J. (2015). Scoring of solvents used in analytical laboratories by their toxicological and exposure hazards. *Ecotoxicol. Environ. Saf.* 120, 169–173. doi:10.1016/j.ecoenv.2015.05.043

Tsakovski, S., Astel, A., and Simeonov, V. (2010). Assessment of the water quality of a river catchment by chemometric expertise. *J. Chemom.* 24 (11-12), 694–702. doi:10.1002/cem.1333

USEPA (1994). *Chemical hazard evaluation management strategies: A method for ranking and scoring chemicals by potential human health and environmental impacts*. Washington: United States Environmental Protection Agency.

Wang, D. C., Xie, W. P., and Cao, J. (2015). Characterization of nitrogen and phosphorus pollution in typical rivers entering Taihu Lake and analysis of pollution sources. *Pollut. Control Technol.* 28 (2), 71–75.

Xu, L., Liu, S., and Tang, Y. (2022). Long-term dechlorination of polychlorinated biphenyls (PCBs) in Taihu Lake sediment microcosms: Identification of new pathways, PCB-driven shifts of microbial communities, and insights into dechlorination potential. *Environmental Science and Technology* 56 (2), 938–950. doi:10.1021/acs.est.1c06057

Zhang, X. M., Li, B., Liu, R. X., Zeng, P., Song, Y. H., and Yang, Y. Z. (2015). Identification of priority pollutants in river polluted by effluents from printing and dyeing enterprises in taizihe watershed. *Chin. J. Environ. Eng.* 9 (4), 2007–2013.

Zhou, l. J., Zhang, Q., and Shi, L. L. (2019). The formulation methods of priority water pollutants and environmental quality standards in the Eu and their reference significance to China. *Environ. Monit. Forewarning* 11 (1), 1–9.

Zhu, F. F., Qin, P. F., Zhang, J., Yan, Z. G., Hou, H., and Li, F. S. (2013). Screening of priority organic pollutants in groundwater of China. *J. Environ. Eng. Technol.* 3 (5), 443–450.

frontiers | Frontiers in Environmental Science

TYPE Mini Review
PUBLISHED 16 December 2022
DOI 10.3389/fenvs.2022.1077974

OPEN ACCESS

EDITED BY
Xiaohu Wen,
Northwest Institute of Eco-Environment and Resources (CAS), China

REVIEWED BY
Miguel Machado Santos,
University of Porto, Portugal
Haile Kassahun,
Wollo University, Ethiopia

*CORRESPONDENCE
Milica Paut Kusturica,
milica.paut-kusturica@mf.uns.ac.rs

SPECIALTY SECTION
This article was submitted to Toxicology, Pollution and the Environment, a section of the journal Frontiers in Environmental Science

RECEIVED 23 October 2022
ACCEPTED 08 December 2022
PUBLISHED 16 December 2022

CITATION
Paut Kusturica M, Jevtic M and Ristovski JT (2022), Minimizing the environmental impact of unused pharmaceuticals: Review focused on prevention.
Front. Environ. Sci. 10:1077974.
doi: 10.3389/fenvs.2022.1077974

Minimizing the environmental impact of unused pharmaceuticals: Review focused on prevention

Milica Paut Kusturica[1]*, Marija Jevtic[1,2] and Jovana Trifunovic Ristovski[1]

[1]Faculty of Medicine, University of Novi Sad, Novi Sad, Serbia, [2]School of Public Health, Research Center on Environmental Health and Occupational Health, Université libre de Bruxelles (ULB), Bruxells, Belgium

Pharmaceuticals are essential for human health, but they become an environmental concern when entering the environment which occurs when residues are excreted after consumption or when unused pharmaceuticals are discarded improperly. Although there are no developed detection methods for all pharmaceuticals that reach the ecosystem, certain groups have been proven to cause adverse effects on ecosystems, including increased mortality in aquatic species and changes in physiology, behavior, or reproduction. Particular attention is devoted to these groups of pharmaceuticals and their environmental impact. In this review, the authors suggest measures for the reduction of unused pharmaceuticals in the environment, with a strong emphasis on prevention. Various policy interventions are recommended across the lifecycle including source-directed, user-orientated, and waste management measures, to prevent the creation of household pharmaceutical waste and to ensure environmentally friendly ways of pharmaceutical household waste disposal. Preventive measures include rational pharmaceutical consumption, prescribing greener drugs, or designing pharmaceuticals that are benign and easily biodegradable, improved disease prevention, personalized medicine, enhanced dimensioning of pack sizes, and marketplaces for redistribution of unused pharmaceuticals. The next step is to prevent unavoidable waste to reach the environment, so proper collection and disposal of unused pharmaceuticals is of utmost importance. Finally, educating health professionals and the public and partnership between environmental and healthcare scientists are of vital significance in all stages of the pharmaceuticals' lifecycle. Minimalization of the level of pharmaceuticals in the environment will benefit human life.

KEYWORDS

unused pharmaceuticals, environmental impact, waste prevention, waste reduction, pharmaceutical waste disposal

1 Introduction

Demographic, epidemiological and lifestyle changes such as aging population, the increase of chronic diseases, the availability of inexpensive generic treatments and ease of access to vast amounts of over-the-counter drugs have been key drivers for increased pharmaceutical consumption (González Pena et al., 2021; European Commission, 2019). The global increase in pharmaceutical consumption has led to an enhanced international awareness of the issue of unused pharmaceuticals (UPs) in households and the harmful environmental and health effects of their improper disposal (Paut Kusturica et al., 2016; Mitkidis et al., 2022). Pharmaceuticals in the environment are a challenge to manage as they are designed to interact with a living system and produce a pharmacological response at low doses, which makes them of environmental concern even at low concentrations. Secondly, pharmaceuticals are designed to be stable in order to reach and interact with target molecules, meaning that either they are very slow to degrade or their constant use leads to continuous release into the environment at rates above degradation rates. Also, conventional wastewater treatment plants are not designed to fully remove pharmaceuticals from wastewater (OECD, 2019).

There are two main ways by which pharmaceuticals enter the environment: excretion and improper disposal (OECD, 2022). In both cases, pharmaceuticals end up in sewage treatment plants that are generally not designed to remove such pollutants from wastewater (Thomas,Felicity and WHO, 2017). Pharmaceuticals have been detected primarily in surface waters, but also in groundwater, soil, manure and even drinking water. The presence of pharmaceuticals in freshwater and terrestrial ecosystems can result in the uptake of pharmaceuticals into wildlife with the potential to bioaccumulate (Zenker et al., 2014). Humans are subsequently exposed to pharmaceuticals *via* drinking water, and ingestion of its residues in plant crops, fish, dairy products and meat. The consequences of pharmaceuticals in the aquatic environment are an issue of rising concern, with impacts that can range from molecular alterations to effects at the population level (Queirós et al., 2021). Given that this is a growing environmental and health concern globally, this review pursues to answer the following questions: 1) which pharmaceuticals have been proven to cause detrimental effects on the environment 2) what are the options to reduce detrimental environmental impact of UPs before they reach the environment.

2 Effect of pharmaceuticals on the environment and human health

Human pharmaceuticals are listed as emerging contaminants by UNESCO. Their detection and elimination represent the crucial step according to the "2030 Agenda for Sustainable Development" Goal Targets (UNESCO 2020). The concentrations of drugs found in the environment are under therapeutic levels. In water surfaces that receive treated wastewater, pharmaceuticals are detected in concentrations less than 100 ng/L (Vumazonke et al., 2020; Björklund and Svahn, 2021; Li et al., 2021). These low concentrations are the reason for the difficult assessment of their toxic effects on the ecosystem and human health. The vast majority of pharmaceuticals have not been sufficiently explored for their long-term toxic effects, presence and fate in the environment (aus der Beek et al., 2016). However, certain pharmaceutical groups such as beta-blockers, antibiotics, anticancer drugs and endocrine disruptors (Nie et al., 2013; Kovács et al., 2015; Godlewska et al., 2021; Ortuzar et al., 2022) have been shown to cause devastating effects on the ecosystem including increased mortality, and impairment of the physiological and reproductive functions of aquatic species. Also, devastating effects are reflected on human health because it is impossible to separate humans from nature. Still, the scale of the problem remains highly unknown, due to the huge number of pharmaceuticals and the challenges of evaluating risks related to multi-compound exposure at low doses and over long periods of time (Kümmerer, 2019). The German Environment Agency (UBA) announced that 10% of medicines on the market represent potential environmental risk. Even though there are no developed detection methods for all pharmaceutics that reach the ecosystem some of them are predominantly present and proven to cause negative adverse effects on ecosystems (Küster et al., 2010). These groups include hormones, antibiotics, antidepressants, anti-inflammatories and analgesics, beta-blockers and anticancer pharmaceuticals (Monteiro and Boxall, 2010).

The presence of estrogens in the environment represents a serious contamination problem (Bilal and Igbal, 2019). The world's human population discharges approximately 30,000 kg/yr of natural steroidal estrogens and an additional 700 kg/yr of synthetic estrogens only from birth control pill practices. However, the abundance of these hormones in the environment mostly originates from the livestock industry due to the wide usage of a variety of growth-regulating steroids to enhance the production rate of meat. Undoubtedly, estrogens are essential for normal human physiology but can have serious adverse effects if accumulate in the environment and enter the human food chain (Adeel et al., 2017). These types of hormones are capable to perturb human and animal physiology and affect normal reproduction. Estrogens as pollutants are also linked with a higher incidence of breast cancer in women and prostate cancer in men (Nelles et al., 2011; Trevino et al., 2015).

Antimicrobial resistance represents a global public health issue, especially considering the increased use of antibiotics during the COVID-19 pandemic which led to the depletion of the last line of antibiotics (Lai et al., 2021). It has been noted that

the application of antibiotics in human medicine, veterinary medicine and agriculture is related to the contamination of the different parts of the environment which contributed to an increase in antibiotic resistance and the occurrence of ecotoxicological effects (Zainaba et al., 2020). A lack of proper antibiotic disposal practices among patients by discharging them into the sewage systems represents also a growing environmental threat to public health (Anwar et al., 2020). Also, the strong impact of antibiotic pollution after long-term exposure can affect human health, especially in patients with chronic diseases including obesity, diabetes, and asthma (Ianiro et al., 2016).

The worldwide contamination with antidepressants significantly increased during the COVID-19 pandemic (Rabeea et al., 2021). To this day antidepressants have been detected in urban and non-urban water systems. Many different types of aquatic animals bioaccumulate different antidepressants in their tissues which leads to cytotoxicity, genotoxicity, stress response alteration, increase/decrease in weight and length, and liver and kidney damage (Castillo-Zacarías et al., 2021). Considering that the human and animal environments significantly overlap, antidepressant pollution (sertraline, fluoxetine) has also impacted human neurodevelopment and different psychiatric conditions (Abbey-Lee et al., 2018; Li et al., 2020). Although psychopharmaceuticals are generally present in wastewaters at subtherapeutic levels they are capable to induce biological effects at low doses, particularly in an environment is often presents a combination of several psychopharmaceuticals which increases the risk of their toxic effects (Chan et al., 2021).

Large amounts of non-steroidal anti-inflammatory drugs, including acetaminophen, acetylsalicylic acid, ibuprofen, diclofenac and naproxen significantly contribute to the pollution of the environment, particularly as they have been found in nanograms and micrograms in soil, wastewater, surface water, drinking water, groundwater (Tyumina et al., 2020). These drugs have chronic ecotoxic effects as they are very resistant to biological transformation in the environment due to their stable chemical structure. It is known so far that they mostly cause disorders in the organs of invertebrates and vertebrates by inducing oxidative stress and disrupting activity of detoxification enzymes (Hodkovicova et al., 2022). These pharmaceuticals can also cause cardiovascular abnormalities, and hepatotoxicity and disrupt oocyte maturation by an unknown mechanism (Lister and Van Der Kraak, 2009; Xia et al., 2017).

Beta-blockers represent pharmaceutical compounds that show the potential to be highly persistent and toxic in the environment (Kuster et al., 2010). While some data about their environmental adsorption are lacking, it is known that these pharmaceuticals demonstrate moderately high solubility in water and have been detected in surface waters at concentrations of μg/L. These compounds are very resistant to hydrolysis, bioavailable and mobile in the environment. Therefore, their accumulation in the environment can cause unexpected consequences to different living organisms. In accordance with European Union Directive 93/67EEC, metoprolol and propranolol represent adverse compounds to aquatic species. This indicates results from tests performed on green alga (*S. vacuolatus*) (Maszkowska et al., 2014).

Anticancer drugs stop the growth and division of cells and by their release into the environment, these pharmaceuticals affect the ecosystem through disruption of fertility and significant genetic alteration of living organisms. Anticancer drugs are prescribed in lower quantities but their effects even in ng/l concentrations are devastating, including mutagenic, carcinogenic, and teratogenic consequences to aquatic species. Due to their application and inappropriate disposal, cytostatic drugs are often detected in wastewater from pharmaceutical manufactories and hospitals. The detection frequency of anticancer drugs in hospital wastewater is 58% and cisplatin is marked as one of the most hazardous pharmaceuticals (Dan et al., 2021). The presence of cisplatin in waterbodies even at ng/l concentrations can cause toxic effects on aquatic species (Roque-Diaz et al., 2021) The surface water Watch List (WL) includes information about emerging pollutants that can cause a significant risk to aquatic organisms and humans upon consumption of contaminated drinking water. This list contains all the above-mentioned groups of pharmaceuticals (Gomez Cortes et al., 2022).

3 Measures to mitigate environmental impacts of UPs from households

Prior to seeking ways to improve the elimination processes of pharmaceuticals once they reach the environment, it is apparently more rational to act at source(Table 1). Considering that pharmaceuticals provide an unquestionable benefit to the health of humanity, great care must be taken not to restrict access to those pharmaceuticals that are necessary but to prevent their negative environmental impact (Argaluza et al., 2021).

3.1 Prevention of pharmaceutical waste

The findings from a recent study showed that more than one-third of UPs were classified as preventable pharmaceutical waste (Bekker et al., 2018). Given that 'prevention is better than cure' the priority is avoidance of pharmaceutical waste. Prevention of pharmaceutical waste could be performed through various measures such as improved disease prevention, personalized and precision medicine, and improved dimensioning of packaging sizes (Straub, 2016; Klatte et al., 2017; OECD, 2022).

Where the dose of pharmaceuticals must be calculated on a per-patient basis there exists a degree of wastage. The medication that is dosed based on the patient's weight or body size is often

wasted due to the required dose not matching the vial size. Therefore, to encounter medication waste, manufacturers ought to facilitate more variety in package sizes and avoid large packages. Policymakers can urge manufacturers to stimulate a reasonable set of size options by requiring a maximum percentage of waste (Bach et al., 2016). Furthermore, the risk of accumulation of UPs in households can be reduced by reducing packaging sizes, particularly for new drug treatments and starter packs. Also, the appropriate range of pack sizes should be in line with the treatment duration and the posology in the summary of product characteristics (European Commission, 2021; OECD, 2022).

Pharmaceutical waste is only partially preventable, and should therefore be accompanied by other waste-minimizing approaches. Throughout society, recycling programs for the sustainable use of different resources have been implemented. A similar approach could be implemented for pharmaceutical waste, such as the redispensing of UPs that are within the expiration date (Bekker et al., 2018). Bekker et al. estimated that one-fifth of the returned medications were potentially suitable for redispensing. Returned UPs were considered eligible for redispensing if the package was unopened, undamaged and the period between the return and the expiry date was at least 6 months. One of the possible solutions for unused close-to-expiry-date pharmaceuticals is marketplaces that offer better matching of supply and demand. Although redispensing has the potential to contribute to waste minimization and monetary savings, it is still not applied in the practice due to concerns regarding counterfeits, quality assurance, and following legal restraints. However, some initiatives occur. In the Netherlands, there is a platform under the name PharmaSwap that allows certified pharmacists to sell undamaged UPs before their expiration date to other pharmacies, often at reduced prices. Likewise, two US start-ups are founded with the aim to collect and redistribute UPs to patients with low income (OECD, 2022). Redispensing is a promising way of UPs minimization, but requires a thoughtful implementation strategy with comprehensive communication with all stakeholders, paying particular attention to product quality assurance, financial handling, and legal aspects.

3.2 Collection schemes and take-back systems for household pharmaceutical waste

The practice of improper disposal of UPs from households represents a global phenomenon. Thus, effective collection schemes and take-back programs with the main purpose to offer an easy method for disposal of UPs represent an important measure to protect the environment (Paut Kusturica et al., 2016). Separate collection systems help avoid environmental leakage caused by flushing pharmaceuticals *via* drain or by mixing them with solid household waste that is destined for landfills without leachate collection (Masoner et al., 2016). The approaches used for collection differ among countries, but in general, pharmacies play an essential role. One-day collection events or mail-back envelopes are also available in some countries (e.g., United States). Some programs rely only on government funding (e.g., Australia) while others are financed by the pharmaceutical industry or pharmacies that provide support voluntarily or driven by extended producer responsibility (EPR) legislation (OECD, 2022).

Given that financial moment plays a significant role in UPs disposal systems, one of the valuable solutions is an implementation of the EPR laws which require that pharmaceutical manufacturers manage their products in all phases of their life cycle, including end-of-life treatment and waste management. Countries that have pursued an EPR approach shift the financial and organizational burden of UPs collection and disposal from the government to the pharmaceutical industry (Paut Kusturica et al., 2020). As a result, EPR implements the "producer pays principle", moving waste management costs from taxpayers to manufacturers. Companies can incorporate these costs in the price and provide services more cost-efficiently. European waste legislation currently provides a global framework for the implementation of EPR law in Europe and its policies have been designed and implemented in a very heterogeneous manner across Europe (OECD, 2022).

3.3 "Eco-prescription"

"Eco-prescription" or "green prescription" implies that the prescriber should consider the characteristics and environmental behavior of pharmaceuticals when prescribing (Daughton and Ruhoy, 2011). For instance, although oxazepam is considered a good option for the elderly due to its suitable pharmacokinetic profile, it is excreted unchanged *via* urine and accumulates for decades without biodegrading. From an environmental perspective, pharmaceuticals that are metabolized to inactive metabolites prior to elimination are preferable (Daughton, 2014). Incorporating environmental criteria in the use of pharmaceuticals is crucial, and it may represent a true revolution in pharmacology (Lertxundi et al., 2020).

The Stockholm County Council possesses an environmental classification of pharmaceuticals, created from a joint initiative between producers, authorities, and public health professionals. The classification indicates the risk and environmental hazards of pharmaceuticals determined based on the active pharmaceutical ingredient's persistence, bioaccumulation potential and toxicity. The risk refers to the likelihood that a pharmaceutical is toxic to aquatic organisms. Prescribers may incorporate this information when using pharmaceuticals for individual patients and choose

TABLE 1 Measures to mitigate impacts of UPs.

UPs mitigation	Measure	Description
UPs avoidance	Disease prevention	Communication and education activities and policy interventions aimed at reducing the development and severity of chronic diseases and other morbidities can reduce pharmaceutical consumption and UPs creation
	Personalized medicine	Fewer and more effective treatments can be achieved by using pharmaceuticals that are better targeted to patients' needs
	Dimensioning	Reducing packaging sizes for new drug treatments and starter packs can reduce risk of accumulation of UPs in households
	Marketplace for UPs	A marketplace for UFs that are close-to-expiry-date, unopened and undamaged provides better matching of supply and demand
Collection and safe final disposal of UPs	Collection in mixed municipal solid waste and controlled final disposal	Collection in mixed municipal solid waste and incineration in state-of-the-art incinerators
	Drug take-back programs	Take-back programs can prevent improper disposal of UPs from households
	EPR schemes	EPR implements the "producer pays principle", moving waste management costs from tax payers to pharmaceutical industry
"*Eco-prescription*"	Change prescriptions to more environmentally-friendly drugs	The "Wise List" incorporate environmental aspects to recommend drugs in ambulatory care prescribing
"*Green pharmacy*"	Development of more "environmentally friendly" pharmaceuticals	Designing more biodegradable pharmaceuticals that are less harmful for the environment ("benign by design")
Increase awareness and induce behaviour change	Information campaigns	They can be financed and managed by public authorities, the private sector, NGOs or be an accompanying requirement in the design of EPR schemes
	Incentives for returning UPs to pharmacies	Refunds or other rewards to nudge consumers for returning UFs to collection points
	Pharmaceutical ecolabelling	A mandatory information in EU countries
	Environmental classification schemes	Environmental classifications schemes allow doctors to make informed prescription choices

those that are environmentally friendly. To date, the "Wise List" (Kloka Listan) is the only multifaceted approach incorporating environmental aspects to recommend drugs in ambulatory care (Gustafsson et al., 2011).

3.4 New development or redesign of pharmaceuticals

To follow the concept of environmental protection, the pharmaceutical industry should develop promising concepts to minimize the content in excretion while ensuring sufficient pharmacologically active concentrations in the patient. "Green pharmacy" recognizes the potential for designing new more biodegradable pharmaceuticals that are less harmful to the environment (Daughton and Ruhoy, 2011). "Greener drugs" also contribute to the Sustainable Development Goals 6 (Clean Water), 3 (Health), 9 (Sustainable industries), 11 (Sustainable cities) and 12 (Responsible production and consumption) of the United Nations (Kummerer, 2019). There are already some examples of the development of more "environmentally friendly" pharmaceuticals, such as glufosfamide and green drug delivery systems (Dai et al., 2016; Banik, 2020). Scientists are currently developing an effective and environmentally friendly variant of the antibiotic ciprofloxacin which is a very stable pharmaceutical. Through computer modeling, the existing active substance is analyzed and changed theoretically for improved biological degradability and lower toxicological effects. The most promising candidates will be synthesized and tested *in vitro* (Kummerer, 2019).

3.5 Education and information campaigns

The limited consumers' awareness of proper disposal practices weakens their impact on disposal practices in many countries (Paut Kusturica et al., 2016). Information campaigns can increase the awareness and use of environmentally friendly ways of pharmaceutical waste from households. A good example is The #Medsdisposal campaign, a European initiative jointly coordinated by several European supply chain and healthcare organizations and supported by media campaigns in different languages. The initiative aimed to combat the detrimental impacts of mishandled pharmaceuticals on the environment

by educating consumers about proper disposal routes and available take-back systems in different European countries. The German campaign entitled: "No pharmaceuticals down the toilet or sink!" is also considered a cost-efficient and effective educational campaign (OECD, 2022).

Furthermore, awareness and behavioral change can be achieved with special instructions for disposal that appear on the outer packaging or in the information leaflet of the drug, which is mandatory in EU countries. Incentives for returning UPs to collection points, such as various rewards to encourage consumers to adopt proper disposal practices are also useful approaches. For example, in Sweden, most pharmacy chains offer bonus credit points to consumers who return UPs to collection points. Furthermore, eco-labels on the environmental impact of different pharmaceuticals can influence consumer choice and awareness and help doctors make a decision while prescribing medications. The aforementioned environmental classification schemes include about 200 pharmaceuticals that are available online for consumers and prescribers (Stockholm County Council, 2014). The advice on proper drug disposal should also routinely follow drug dispensing. Pharmacists can play a key role in educating their customers on proper medication disposal methods (Paut Kusturica et al., 2016).

4 Conclusion

Environmental pollution with pharmaceuticals is a complex public health challenge that entails scientific doubts and involves a great number of stakeholders with various interests and at different organizational levels: governments, non-governmental organizations, scientific institutions, manufacturers, industry and households.

Various policy interventions should be implemented across the pharmaceutical lifecycle including source-directed, user-orientated and waste-management activities. The most valuable solutions should be implemented at source before pharmaceuticals reach the environment. These measures include rational pharmaceutical consumption, prescribing greener drugs, or designing pharmaceuticals that are benign and easily biodegradable. Improved disease prevention, personalized medicine, enhanced dimensioning of packaging sizes, and marketplaces for redistribution of UPs can to some extent prevent pharmaceutical waste creation. The next step is to prevent unavoidable waste to reach the environment, thus appropriate collection and disposal of UPs is essential and needs to be tailored to the national context and local challenges. Finally, educating health professionals and the public and partnership between environmental and healthcare scientists are of crucial importance in all phases of the pharmaceuticals' lifecycle. The heart of all joint efforts should be the "One Health" approach to tackle pharmaceutical waste and enhance human, animal, and environmental health that are strongly interconnected.

Author contributions

MPK: conceptualization. All authors listed have made a substantial, direct and intellectual contribution to the work, and approved it for publication.

Acknowledgments

This work was supported by the Ministry of Education and Science of the Republic of Serbia through the Project of the Faculty of Medicine University of Novi Sad (Science Research Organization 200114) 451-03-68/2022-14/200114.

Conflict of interest

The authors declare that the research was conducted in the absence of any commercial or financial relationships that could be construed as a potential conflict of interest.

Publisher's note

All claims expressed in this article are solely those of the authors and do not necessarily represent those of their affiliated organizations, or those of the publisher, the editors and the reviewers. Any product that may be evaluated in this article, or claim that may be made by its manufacturer, is not guaranteed or endorsed by the publisher.

References

Abbey-Lee, R. N., Uhrig, E. J., Garnham, L., Lundgren, K., Child, S., and Løvlie, H. (2018). Experimental manipulation of monoamine levels alters personality in crickets. *Sci. Rep.* 8, 16211. doi:10.1038/s41598-018-34519-z

Adeel, M., Song, X., Wang, Y., Francis, D., and Yang, Y. (2017). Environmental impact of estrogens on human, animal and plant life: A critical review. *Environ. Int.* 99, 107–119. doi:10.1016/j.envint.2016.12.010

Anwar, M., Iqbal, Q., and Saleem, F. (2020). Improper disposal of unused antibiotics: an often overlooked driver of antimicrobial resistance. *Expert. Rev. anti. Infect. Ther.* 18, 697–699. doi:10.1080/14787210.2020.1754797

Argaluza, J., Domingo-Echaburu, S., Orive, G., Medrano, J., Hernandez, R., and Lertxundi, U. (2021). Environmental pollution with psychiatric drugs. *World. J. Psychiatr.* 11, 791–804. doi:10.5498/wjp.v11.i10.791

aus der Beek, T., Weber, F. A., Bergmann, A., Hickmann, S., Ebert, I., Hein, A., et al. (2016). Pharmaceuticals in the environment—global occurrences and perspectives. *Environ. Toxicol. Chem.* 35, 823–835. doi:10.1002/etc.3339

Bach, P. B., Conti, R. M., Muller, R. J., Schnorr, G. C., and Saltz, L. B. (2016). Overspending driven by oversized single dose vials of cancer drugs. *BMJ* 352, i788. doi:10.1136/bmj.i788

Banik, B. K. (2020). *In advances in green chemistry, green approaches in medicinal chemistry for sustainable drug design*. Netherland: Elsevier.

Bekker, C., van den Bemt, B. J. F., Egberts, A. C. G., Bouvy, M. L., and Gardarsdottir, H. (2018). Patient and medication factors associated with preventable medication waste and possibilities for redispensing. *Int. J. Clin. Pharm.* 40, 704–711. doi:10.1007/s11096-018-0642-8

Bilal, M., and Igbal, H. M. N. (2019). Persistence and impact of steroidal estrogens on the environment and their laccase-assisted removal. *Sci. Total. Environ.* 690, 447–459. doi:10.1016/j.scitotenv.2019.07.025

Björklund, E., and Svahn, O. (2021). Total release of 21 indicator pharmaceuticals listed by the Swedish medical products agency from wastewater treatment plants to surface water bodies in the 1.3 million populated county skåne (scania), Sweden. *Molecules* 27, 77. doi:10.3390/molecules27010077

Castillo-Zacarías, C., Barocio, M. E., Hidalgo-Vázquez, E., Sosa-Hernández, J. E., Parra-Arroyo, L., López-Pacheco, I. Y., et al. (2021). Antidepressant drugs as emerging contaminants: occurrence in urban and non-urban waters and analytical methods for their detection. *Sci. Total. Environ.* 757, 143722. doi:10.1016/j.scitotenv.2020.143722

Chan, S. J., Nutting, V. I., Natterson, T. A., and Horowitz, B. N. (2021). Impacts of psychopharmaceuticals on the neurodevelopment of aquatic wildlife: A call for increased knowledge exchange across disciplines to highlight implications for human health. *Int. J. Environ. Res. Public. Health.* 18, 5094. doi:10.3390/ijerph18105094

Dai, L., Liu, K., Si, C., Wang, L., Liu, J., Heet, J., et al. (2016). Ginsenoside nanoparticle: a new green drug delivery system. *J. Mat. Chem. B* 4, 529–538. doi:10.1039/C5TB02305J

Dan, L., Hongxing, C., Hongsong, L., Schlenkc, D., Mue, J., Lacorte, S., et al. (2021). Anticancer drugs in the aquatic ecosystem: Environmental occurrence, ecotoxicological effect and risk assessment. *Environ. Int.* 153, 106543. doi:10.1016/j.envint.2021.106543

Daughton, C. D., and Ruhoy, I. S. (2011). Green pharmacy and pharmEcovigilance: prescribing and the planet. *Expert. Rev. Clin. Pharmacol.* 4, 211–232. doi:10.1586/ecp.11.6

Daughton, C. G. (2014). Eco-directed sustainable prescribing: feasibility for reducing water contamination by drugs. *Sci. Total. Environ.* 493, 392–404. doi:10.1016/j.scitotenv.2014.06.013

European Comission (2021). Guideline on the packaging information of medicinal products for human use authorised by the Union. Available at: https://health.ec.europa.eu/system/files/2021-04/2018_packaging_guidelines_en_0.pdf

European Commission (2019). *Directorate-general for environment, kümmerer, K., options for a strategic approach to pharmaceuticals in the environment: final report*. Brussels, Belgium: Publications Office.

Godlewska, K., Jakubus, A., Stepnowski, P., and Paszkiewicz, M. (2021). Impact of environmental factors on the sampling rate of β-blockers and sulfonamides from water by a carbon nanotube-passive sampler. *J. Environ. Sci.* 101, 413–427. doi:10.1016/j.jes.2020.08.034

Gomez Cortes, L., Marinov, D., Sanseverino, I., Navarro Cuenca, A., Niegowska Conforti, M., Rodriguez, P., et al. (2022). *Selection of substances for the 4th Watch list under the water framework directive*. Luxembourg: Publications Office of the European Union.

González Peña, O. I., López Zavala, M. Á., and Cabral Ruelas, H. (2021). Pharmaceuticals market, consumption trends and disease incidence are not driving the pharmaceutical research on water and wastewater. *Int. J. Environ. Res. Public. Health.* 18, 2532. doi:10.3390/ijerph18052532

Gustafsson, L. L., Wettermark, B., Godman, B., Andersén-Karlsson, E., Bergman, U., Hasselströmet, J., al., et al. (2011). The 'wise list'- A comprehensive concept to select, communicate and achieve adherence to recommendations of essential drugs in ambulatory care in Stockholm. *Basic. Clin. Pharmacol. Toxicol.* 108, 224–233. doi:10.1111/j.1742-7843.2011.00682.x

Hodkovicova, N., Hollerova, A., Blahova, J., Mikula, P., Crhanova, M., Karasova, D., et al. (2022). Non-steroidal anti-inflammatory drugs caused an outbreak of inflammation and oxidative stress with changes in the gut microbiota in rainbow trout (*Oncorhynchus mykiss*). *Sci. Total. Environ.* 849, 157921. doi:10.1016/j.scitotenv.2022.157921

Ianiro, G., Tilg, H., and Gasbarrini, A. (2016). Antibiotics as deep modulators of gut microbiota: Between good and evil. *Gut* 65, 1906–1915. doi:10.1136/gutjnl-2016-312297

Klatte, S., Schaefer, H. C., and Hempel, M. (2017). Pharmaceuticals in the environment – a short review on options to minimize the exposure of humans, animals and ecosystems. *Sustain. Chem. Pharm.* 5, 61–66. doi:10.1016/j.scp.2016.07.001

Kovács, R., Csenki, Z., Bakos, K., Urbányi, B., Horváth, Á., Garaj-Vrhovac, V., et al. (2015). Assessment of toxicity and genotoxicity of low doses of 5-fluorouracil in zebrafish (*Danio rerio*) two-generation study. *Water. Res.* 77, 201–212. doi:10.1016/j.watres.2015.03.025

Kümmerer, K. (2019). From a problem to a business opportunity-design of pharmaceuticals for environmental biodegradability. *Sustain. Chem. Pharm.* 12, 100136. doi:10.1016/j.scp.2019.100136

Küster, A., Alder, A. C., Escher, B. I., Duis, K., Fenner, K., Garric, J., et al. (2010). Environmental risk assessment of human pharmaceuticals in the European union: A case study with the β-blocker atenolol. *Integr. Environ. Assess. Manag.* 6, 1–523. doi:10.1897/IEAM_2009-050.1

Lai, C. C., Chen, S. Y., Ko, W. C., and Hsueh, P. R. (2021). Increased antimicrobial resistance during the COVID-19 pandemic. *Int. J. Antimicrob. Agents.* 57, 106324. doi:10.1016/j.ijantimicag.2021.106324

Lertxundi, U., Hernández, R., Medrano, J., and Orive, G. (2020). Drug pollution and pharmacotherapy in psychiatry:A "platypus" in the room. *Eur. Psychiatry.* 63, e33. doi:10.1192/j.eurpsy.2020.32

Li, Y., Miao, Y., Zhang, W., Yang, N., Niu, L., Zhang, H., et al. (2020). Sertraline inhibits top-down forces (predation) in microbial food web and promotes nitrification in sediment. *Environ. Pollut.* 267, 115580. doi:10.1016/j.envpol.2020.115580

Li, Z., Yu, X., Yu, F., and Huang, X. (2021). Occurrence, sources and fate of pharmaceuticals and personal care products and artificial sweeteners in groundwater. *Environ. Sci. Pollut. Res. Int.* 28, 20903–20920. doi:10.1007/s11356-021-12721-3

Lister, A. L., and Van Der Kraak, G. J. (2009). Regulation of prostaglandin synthesis in ovaries of sexually-mature zebrafish (*Danio rerio*). *Mol. Reprod. Dev.* 76, 1064–1075. doi:10.1002/mrd.21072

Masoner, J. R., Kolpin, D. W., Furlong, E. T., Cozzarelli, I. M., and Gray, J. L. (2016. Landfill leachate as a mirror of today's disposable society: Pharmaceuticals and other contaminants of emerging concern in final leachate from landfills in the conterminous United States. *Environ. Toxicol. Chem.* 35, 906–918. doi:10.1002/etc.3219

Maszkowska, J., Stolte, S., Kumirska, J., Łukaszewicz, P., Mioduszewska, K., Puckowski, A., et al. (2014). Beta-blockers in the environment: part II. Ecotoxicity study. *Sci. Total. Environ.* 493, 1122–1126. doi:10.1016/j.scitotenv.2014.06.039

Mitkidis, P., Chrysochou, P., Obolevich, V., and Mitkidi, K. (2022). Effectiveness of environmental health and loss framing on household pharmaceutical take-back schemes. *Waste. Manage.* 143, 61–68. doi:10.1016/j.wasman.2022.02.017

Monteiro, S. C., and Boxall, A. B. A. (2010). Occurrence and fate of human pharmaceuticals in the environment. *Rev. Environ. Contam. Toxicol.* 202, 53–154. doi:10.1007/978-1-4419-1157-5_2

Nelles, J. L., Hu, W. Y., and Prins, G. S. (2011). Estrogen action and prostate cancer. *Expert. Rev. Endocrinol. Metab.* 6, 437–451. doi:10.1586/eem.11.20

Nie, X. P., Liu, B. Y., Yu, H. J., Liu, W. Q., and Yang, Y.-F. (2013). Toxic effects of erythromycin, ciprofloxacin and sulfamethoxazole exposure to the antioxidant system in Pseudokirchneriella subcapitata. *Environ. Pollut.* 172, 23–32. doi:10.1016/j.envpol.2012.08.013

OECD (Organisation for Economic Co-operation and Development (2022). *Management of pharmaceutical household waste: Limiting environmental impacts of unused or expired medicine*. Paris, France: OECD Publishing.

OECD (Organisation for Economic Co-operation and Development) (2019). *Pharmaceutical residues in freshwater: Hazards and policy responses, OECD studies on water*. Paris, France: OECD Publishing.

Ortúzar, M., Esterhuizen, M., Olicón-Hernández, D. R., González-López, J., and Aranda, E. (2022). Pharmaceutical pollution in aquatic environments: a concise review of environmental impacts and bioremediation systems. *Front. Microbiol.* 26, 869332. doi:10.3389/fmicb.2022.869332

Paut Kusturica, M., Golocorbin-Kon, S., Ostojic, T., Kresoja, M., Milovic, M., Horvat, O., et al. (2020). Consumer willingness to pay for a pharmaceutical disposal program in Serbia: a double hurdle modeling approach. *Waste. Manag.* 104, 246–253. doi:10.1016/j.wasman.2020.01.029

Paut Kusturica, M., Tomas, A., and Sabo, A. (2016). Disposal of unused drugs: Knowledge and behavior among people around the world. *Rev. Environ. Contam. Toxicol.* 40, 71–104. doi:10.1007/398_2016_3

Queirós, V., Azeiteiro, U. M., Soares, A. M. V. M., and Freitas, R. (2021). The antineoplastic drugs cyclophosphamide and cisplatin in the aquatic environment - Review. *J. Hazard. Mat.* 412, 125028. doi:10.1016/j.jhazmat.2020.125028

Rabeea, S. A., Merchant, H. A., Khan, M. U., Kow, C. S., and Hasan, S. S. (2021). Surging trends in prescriptions and costs of antidepressants in England amid COVID-19. *DARU. J. Pharm. Sci.* 29, 217–221. doi:10.1007/s40199-021-00390-z

Roque-Diaz, Y., Sanadar, M., Han, D., López-Mesas, M., Valiente, M., Tolazzi, M., et al. (2021). The dark side of platinum based cytostatic drugs: From detection to removal. *Processes* 9, 1873. doi:10.3390/pr9111873

Stockholm County Council (2014). *Environmentally classified pharmaceuticals 2014-2015*. Stockholm, Sweden: Stockholm County Council.

Straub, J. O. (2016). Reduction in the environmental exposure of pharmaceuticals through diagnostics, Personalised Healthcare and other approaches. A mini review and discussion paper. *Sustain. Chem. Pharm.* 3, 1–7. doi:10.1016/j.scp.2015.12.001

Thomas, Felicity & WHO (World Health Organization) (2017). *Pharmaceutical waste in the environment: a cultural perspective*. Regional Office for Europe. Available at: https://apps.who.int/iris/handle/10665/254734.

Trevino, L. S., Wang, Q., and Walker, C. L. (2015). Hypothesis: Activation of rapid signaling by environmental estrogens and epigenetic reprogramming in breast cancer. *Reprod. Toxicol.* 54, 136–140. doi:10.1016/j.reprotox.2014.12.014

Tyumina, E. A., Bazhutin, G. A., Cartagena Gómez, A. D., and Ivshina, I. B. (2020). Nonsteroidal anti-inflammatory drugs as emerging contaminants. *Microbiology* 89, 148–163. doi:10.1134/S0026261720020125

UNESCO (United Nations Educational, Scientific and Cultural Organization). 2020. *Emerging pollutants in water and wastewater*. Available at: https://en.unesco.org/emergingpollutantsinwaterandwastewater

Vumazonke, S., Khamanga, S. M., and Ngqwala, N. P. (2020). Detection of pharmaceutical residues in surface waters of the eastern cape province. *Int. J. Environ. Res. Public. Health.* 17, 4067. doi:10.3390/ijerph17114067

Xia, L., Zheng, L., and Zhou, J. L. (2017). Effects of ibuprofen, diclofenac and paracetamol on hatch and motor behavior in developing zebrafish (*Danio rerio*). *Chemosphere* 182, 416–425. doi:10.1016/j.chemosphere.2017.05.054

Zainaba, S. M., Junaidb, M., Xu, N., and Malik, R. N. (2020). Antibiotics and antibiotic resistant genes (ARGs) in groundwater: A global review on dissemination, sources, interactions, environmental and human health risks. *Water. Res.* 187, 116455. doi:10.1016/j.watres.2020.116455

Zenker, A., Cicero, M. R., Prestinaci, F., Bottoni, P., and Carere, M. (2014). Bioaccumulation and biomagnification potential of pharmaceuticals with a focus to the aquatic environment. *J. Environ. Manage.* 133, 378–387. doi:10.1016/j.jenvman.2013.12.017

frontiers | Frontiers in Environmental Science

TYPE Original Research
PUBLISHED 04 January 2023
DOI 10.3389/fenvs.2022.1086753

OPEN ACCESS

EDITED BY
Jun Wu,
Harbin Engineering University, China

REVIEWED BY
Xiaobing Wang,
Yangzhou University, China
Guoyong Huang,
Huazhong Agricultural University, China
Huidan Jiang,
Hunan Academy of Agricultural Sciences (CAAS), China

*CORRESPONDENCE
Changyin Tan,
chytan@hunnu.edu.cn
Chen Tu,
ctu@issas.ac.cn

SPECIALTY SECTION
This article was submitted to Toxicology, Pollution and the Environment,
a section of the journal
Frontiers in Environmental Science

RECEIVED 01 November 2022
ACCEPTED 12 December 2022
PUBLISHED 04 January 2023

CITATION
Xing Q, Cao X, Tan C, Sun L, Deng Y, Yang J and Tu C (2023), Effects of single and combined applications of three root exudates of *Sedum plumbizincicola* on the phytoremediation efficiency of paddy soil contaminated with Cd. *Front. Environ. Sci.* 10:1086753. doi: 10.3389/fenvs.2022.1086753

Effects of single and combined applications of three root exudates of *Sedum plumbizincicola* on the phytoremediation efficiency of paddy soil contaminated with Cd

Qianwen Xing[1,2], Xueying Cao[3], Changyin Tan[1]*, Lijuan Sun[1], Yueqiang Deng[1], Jia Yang[1] and Chen Tu[2]*

[1]School of Geographic Sciences, Hunan Normal University, Changsha, China, [2]CAS Key Laboratory of Soil Environment and Pollution Remediation, Institute of Soil Science, Chinese Academy of Sciences, Nanjing, China, [3]Rural Vitalization Research Institute, Changsha University, Changsha, China

Root exudates are carriers for the transfer of material, energy and information between plant roots and soils. Plants encountering environmental stresses such as heavy metal pollution adapt to the environment by producing and secreting root exudates. In this study, laboratory soil culture experiment and pot experiment with *Sedum plumbizincicola* were used to study the effects of single and combined application of three root exudates, citric acid, glycine, and fructose, on the Cd-activation and phytoremediation of Cd-contaminated paddy soil. Results from the soil culture experiment showed that for the single application of root exudates, all three root exudates significantly activated the Cd in soil as presented by the increased content of diethylenetriamine pentaacetic acid extracted Cd (DTPA-Cd). In Particular, citric acid (SC) at a relatively low concentration (2 mmol/kg) exhibited the best Cd activation efficiency by increasing DTPA-Cd in the soil by 66.12%. For the combined application of root exudates, citric acid in combination with glycine (SC + G, 1:3) had the best activation effect on the Cd in the soil. In the phytoremediation pot experiment, both the single application of citric acid at a low concentrate (1 mmol/kg) and the combined application of citric acid and glycine (1:1) significantly reduced the total Cd and DTPA-Cd in the soil and increased the biomass and the content of Cd in *S. plumbizincicola*; thus, the phytoremediation efficiency of Cd-contaminated soil increased by 42.33% and 35.61%. The results from this study suggest that citric acid plays a crucial role in Cd activation and phytoremediation with single or combined applications with glycine. However, the mechanisms under the synergetic interaction between citric acid and glycine require further investigation.

KEYWORDS

Sedum plumbizincicola, root exudates, citric acid, glycine, fructose

1 Introduction

With the development of modern industry and agriculture, environmental pollution is becoming increasingly serious, among which heavy metal pollution is an important aspect. Cadmium (Cd) is a heavy metal with inherent toxicity, non-degradability, persistence, and frequent detection in different matrices, which directly or indirectly plays a critical role in human health due to its bioaccumulation and biomagnification through the food chain and its carcinogenic effects (Wu et al., 2020). According to the *National Soil Pollution Survey Bulletin of China* issued in 2014, cadmium is one of the most concerning heavy metal pollutants in farmland soil. Thus, green and efficient remediation materials and technologies are urgently needed for the sustainable remediation of Cd-polluted farmland soil.

Sedum plumbizincicola has been recognized as a typical Cd-hyperaccumulating plant since 2006 (Wu et al., 2006). Due to its high Cd uptake ability, large biomass, and suitability for mowing, *S. plumbizincicola* has been confirmed as a promising plant for the phytoremediation of Cd-contaminated soils (Shen et al., 2011). Plants can directly or indirectly change metal availability and promote the uptake of heavy metals through different mechanisms, such as changes in root exudates and rhizosphere pH (Hammer and Keller, 2002). Root exudates are important plant metabolites that are released from plant roots into the rhizosphere soil to facilitate the uptake of nutrients (Jiang et al., 2023). The composition of root exudates is diverse; for example, Sun et al. (2020) identified 155 compounds in the root exudates of *S. plumbizincicola*, i.e., 12 organic acids, 14 amino acids, 10 fatty acids, 10 amines, 17 polyols, 17 lipids, 11 carbohydrates, and 64 other substances. The secretion of low-molecular-weight organic acids plays a crucial role in improving plant growth and development and it also significantly alters the speciation and mobility of heavy metals in the soil, thus affecting the stress resistance and/or the phytoremediation efficiency of plants (Jiang et al., 2023). Citric acid is a type of common but important component of root exudates. It can form chelates with Cd, thereby reducing the pH of plant rhizosphere and improving Cd availability in soil. Activated Cd in rhizosphere soil can adsorb to the surface of root cells and transmembranes in root cells and be transported to the aboveground parts, thus improving the efficiency of phytoremediation (Liu et al., 2022). Amino acids are another type of root exudates that are involved in various activities during plant development, including responses to biotic and abiotic stresses (Galili et al., 2016). Total amino acids (AAs) and free amino acids (FAAs) secreted by plant roots are essential for mitigating the toxicity of heavy metals in crops (Xue et al., 2022). In addition, saccharides can improve the activities of particular soil microorganisms, which can effectively increase the activity of heavy metals in the soil through the secretion of protons and organic matter (Zhu et al., 2003). However, previous studies only focused on the effect of one particular root exudate on soil Cd species; the effect of combined root exudates on the remediation efficiency of *S. plumbizincicola* has rarely been referred.

Therefore, in this study, citric acid, glycine (Gly), and fructose were selected as three typical root exudates to investigate their single and combined effects on Cd activation and phytoremediation efficiency in Cd-contaminated soil. A soil culture experiment, as well as a phytoremediation pot experiment with *S. plumbizincicola*, was conducted to 1) compare the effects of the three root exudates (citric acid, Gly, fructose) on the activation of total and bioavailable Cd in the soil under single addition treatment; 2) explore the optimal combination of the mixed application of different root exudates; and 3) elucidate the effects of different root exudates on the soil Cd removal, biomass and remediation efficiency of *S. plumbizincicola*. The results of this study could help enhance the Cd phytoremediation efficiency of *S. plumbizincicola*, and may provide a theoretical reference for the sustainable remediation of heavy metal-polluted farmland soil.

2 Materials and methods

2.1 Materials

The tested soil was collected from the surface (0–20 cm) of a heavy metal-polluted paddy soil in Xiangtan city, Hunan Province, China. The parent material of the soil was Quaternary red clay. After air drying, the soil was ground and passed through a 2 mm sieve before use. The pH of the soil was 5.12, the organic matter content was 25.2 g/kg, and the contents of total N, total P, and total K were 1.47 g/kg, 0.77 g/kg, and 13.1 g/kg. The total Cd content in the soil was 0.81 mg/kg, which exceeds the national standard for Cd in paddy soil (0.3 mg/kg, GB15618-2018). The available Cd content in the soil was 0.34 mg/kg, which was presented as diethylenetriamine pentaacetic acid extracted Cd (DTPA-Cd). The tested Cd hyperaccumulator was *S. plumbizincicola*, which was also collected from an experimental base in Xiangtan city. Healthy plants of uniform size were cut to about 10 cm for cutting. The average biomass as measured by the dry mass of *S. plumbizincicola* cuttings was 1.03 g/pot, and the total Cd was 41.30 mg/kg. Citric acid, glycine (Gly), and fructose were of analytical pure grade and were purchased from the Shanghai Sinophosphoric Medicine Group.

2.2 Soil culture experimental design

The effects of different components, contents and pairwise combinations of *S. plumbizincicola*'s root exudates on soil pH and DTPA-Cd were studied using laboratory soil culture experiments. It was carried out in a greenhouse at Hunan Normal University for 1 month. Citric acid, Gly and fructose were selected as the target root exudates of *S. plumbizincicola* according to our previous study (Sun et al., 2020). Four concentrations (0, 2, 4, and 8 mmol/kg) were set for each root

TABLE 1 Experimental design of single and in combination addition of citric acid, Gly and fructose at different concentrations.

Treatment	Acronym	Citric acid (mmol/kg)	Gly (mmol/kg)	Fructose (mmol/kg)
Control	SCK	0	0	0
Citric Acid	SC1	2	0	0
	SC2	4	0	0
	SC3	8	0	0
Gly	SG1	0	2	0
	SG2	0	4	0
	SG3	0	8	0
Fructose	SF1	0	0	2
	SF2	0	0	4
	SF3	0	0	8
Citric Acid + Gly	SC + G1	1	3	0
	SC + G2	2	2	0
	SC + G3	3	1	0
Citric Acid + Fructose	SC + F1	1	0	3
	SC + F2	2	0	2
	SC + F3	3	0	1
Gly + Fructose	SG + F1	0	1	3
	SG + F2	0	2	2
	SG + F3	0	3	1

"S" in the acronym stands for soil culture experiment.

exudate in their single application treatment, which was based on both our previous studies (Deng et al., 2020a; Bai et al., 2020; Sun et al., 2020; Liu et al., 2022) and related literature (Wu et al., 2016; Wei, 2017; He et al., 2022). The selected concentrations include the properties of different root exudates and the tolerance of *S. plumbizincicola*. In the combination experiment, the total concentration of different exudates was 4 mmol/kg, but the specific ratio of the two components varied. The specific experimental design is shown in Table 1. Each treatment was replicated three times.

For the soil cultivation experiment, 100 g (dry weight) of prepared soil was added to a 250 ml beaker. The soil was first mixed with 10 ml of deionized water, followed by 10 ml of the prepared *S. plumbizincicola* root exudate. The soil water content was maintained at about 20% during the incubation period.

2.3 Experimental design for pot phytoremediation

A pot experiment was also carried out in a greenhouse at Hunan Normal University for 5 months. It was conducted to study the effects of the single application of citric acid (CA1 = 1 mmol/kg; CA2 = 2 mmol/kg; CA3 = 4 mmol/kg) or the combination with Gly (C + G1 = 1 mmol/kg + 3 mmol/kg; C + G2 = 2 mmol/kg + 2 mmol/kg; C + G3 = 3 mmol/kg + 1 mmol/kg) on the phytoremediation efficiency of *S. plumbizincicola* in Cd-contaminated soil. Seven treatments were designed in this experiment with three replicates per treatment. One kilogram of the prepared soil (dry weight) was added to each pot, and the soil moisture was maintained at about 70% of the field water-holding capacity. Three cuttings of *S. plumbizincicola* were planted in each pot. On days 15 and 30 before the end of the experiment, 10 ml citric acid solution and a mixed citric acid + Gly solution were added to the soil by spraying. The same amount of deionized water was also added by spraying in the control treatment (CK). Water and fertilizer management was performed according to field conditions throughout the experiment.

2.4 Sample collection and determination

2.4.1 Sample collection

For the soil culture experiment with single root exudate treatments, soil samples were collected on the days 1, 3, 7,

14 and 28 after the start of the experiment, and for the soil culture experiment with combined root exudate treatments, soil samples were collected on the days 1, 14, and 28. All soil samples were air-dried, ground, and passed through 10, 20, and 100 mesh nylon sieves before use.

For the pot experiment, the *S. plumbizincicola* samples were harvested at the end of the experiment, washed with tap water to remove soil and rotting leaves, and then washed with deionized water three times. The washed plant samples were deactivated in an oven at 105 °C for 30 min and then dried at 70 °C to constant weight. The dry mass was weighed and recorded as the biomass of whole *S. plumbizincicola* plant. The dried plant samples were pulverized, passed through a 60-mesh sieve, and stored in a sealed bag until analysis. After the plant samples were removed, the soil in each pot was mixed and air dried and then ground and passed through 10, 20, and 100 mesh nylon sieves before analysis.

2.4.2 Analysis of soil pH

Soil pH was determined by the extraction of soil to water at a ratio of 1:2.5 (*m:v*) and measured by a PHS-4CT digital pH meter (Deng et al., 2020b). Five grams of soil samples were collected to determine the soil pH in each treatment.

2.4.3 Analysis of Cd in plants and soil

For the analysis of the total Cd in soil and plant samples, digestion was conducted according to the US EPA3051a standard method. The content of heavy metals in *S. plumbizincicola* was digested by HNO_3 (10 ml), and the total amount of heavy metals in the soil was digested by HNO_3: HCl (3:1, *v/v*) mixed acid solution. Digestion was carried out with a microwave digestion instrument (CEM MARS6, Matthews, NC, USA). Cd concentrations in plants and soils were determined using an atomic absorption spectrometer (PinAAcle 900T, Perkin Elmer, USA). In the process of sample testing, a blank test and national standard substances (soil: GBW07406; plant: GBW07603) were used for quality control (Deng et al., 2020a).

Soil available Cd was extracted with 0.05 mol/L DTPA at a soil-to-liquid ratio of 1:5. A PinAAcle 900T atomic absorption spectrometer was used for determination, and national reference materials (GSS, GBE) were used for quality control (Sun, 2021). Cd species in the soil were analyzed by the four-step BCR sequential extraction of a European reference plant (Liu et al., 2021). The method for determination of Cd was the same as that reported above.

2.5 Data processing and statistical analysis

The remediation efficiency was calculated as the amount of Cd absorbed by the plant (PRE). It was estimated as follows, Eqs. 1, 2 (Cao et al., 2019):

$$Q_p = C_{p2} \times W_{p2} - C_{p1} \times W_{p1} \quad (1)$$

$$PRE = \frac{Q_p}{TC_{before\ remediation} \times W_s} \times 100\% \quad (2)$$

Where Q_p is the amount of Cd absorbed by *S. plumbizincicola*, mg/pot; CP_2 is the Cd content in *S. plumbizincicola* after phytoremediation, mg/kg; WP_2 is the biomass of *S. plumbizincicola* after phytoremediation, kg/pot; CP_1 is the Cd content in *S. plumbizincicola* before phytoremediation, mg/kg; WP_1 is the biomass of *S. plumbizincicola* before phytoremediation, kg/pot; W_S is the quality of soil in each pot, kg; $TC_{before\ remediation}$ is the total Cd content in the soil before remediation, mg/kg.

The remediation efficiency was calculated as the amount of reduced Cd in the soil (SRE). It was calculated by the difference in total Cd concentration (mg/kg) before and after remediation following Eq. 3 (Xue et al., 2022):

$$SRE = \frac{(TC_{before\ remediation} - TC_{after\ remediation})}{TC_{before\ remediation}} \times 100\% \quad (3)$$

Excel 2019 and Origin 2021 were used to process data and draw diagrams, and SPSS 20.0 software was used to check the statistical significance of the data among different treatments.

3 Results and discussion

3.1 Effects of single root exudates on soil pH and DTPA-Cd

All three root exudate fractions reduced the soil pH to some extent, and the decrease was more obvious with the increase in their dosage. Figure 1 shows the changes in soil pH under different fractions and dosages of single citric acid, Gly, and fructose. Compared with the control soil (SCK), single citric acid treatment (SC) significantly reduced the soil pH within 1 week after its application, especially on the first day when the pH decreased markedly by 1 unit. Moreover, the decrease in soil pH was positively dosage dependent. Similarly, the pH of soil treated with Gly (SG) also decreased within 1 week after application, with the most significant decrease in soil pH on the first day, and the soil pH in the SG1, SG2, and SG3 treatments decreased by 0.14, 0.26 and 0.43 units, respectively. However, the Gly treatment had no significant effects on soil pH on days 14 and 28. In contrast to citric acid and Gly, the addition of fructose (SF) significantly reduced the soil pH only on day14, and a dose-dependent effect was not observed.

All three root exudate fractions activated the Cd in the soil and increased the content of available Cd (DTPA-Cd). Figure 2 shows the changes in DTPA-Cd in soil under different fractions and dosages of single citric acid, Gly and fructose. In the citric acid treatment, the content of DTPA-Cd peaked at 0.67 mg/kg on the first day, and the activation efficiency reached 66.12%. Next, DTPA-Cd content continued to decrease until the seventh day.

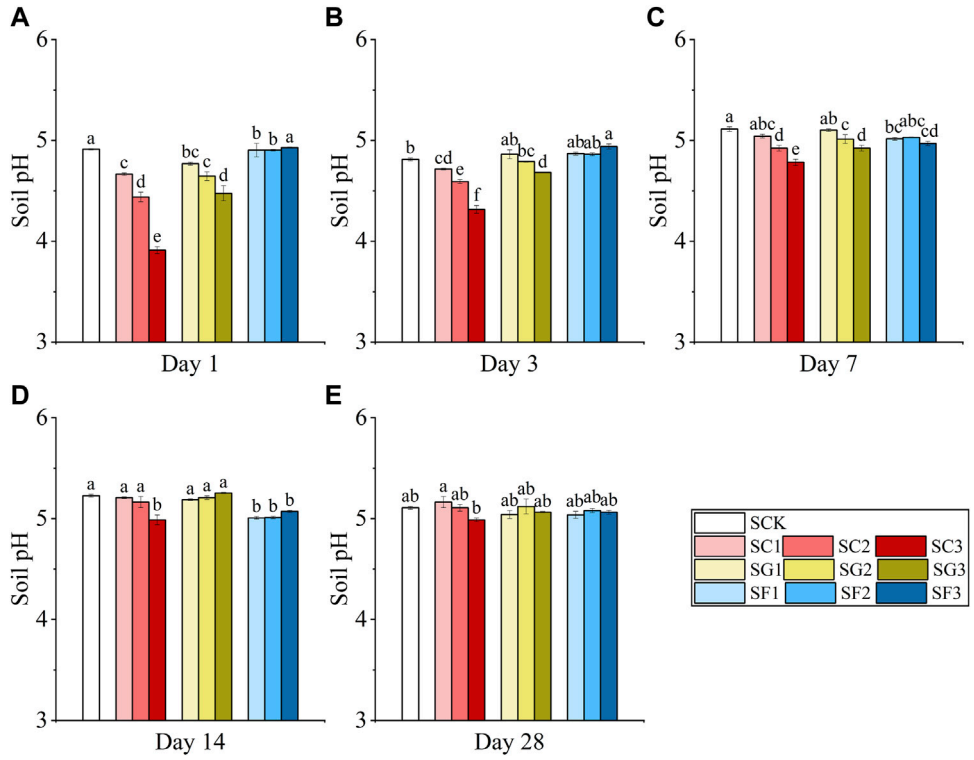

FIGURE 1
Changes in soil pH under different fractions and dosages of single citric acid (SC1, SC2, SC3), Gly (SG1, SG2, SG3), and fructose (SF1, SF2, SF3) application on days 1 **(A)**, 3 **(B)**, 7 **(C)**, 14 **(D)**, and 28 **(E)** (Different letters in each sampling timepoint show significant differences, $p < 0.05$).

On the seventh day, citric acid was even less effective in reactivating Cd in soil than the Gly and fructose treatments. After day 7, the activation efficiency of citric acid increased and reached a stable state. On the 28th day, the activation efficiency of citric acid was 22.35% higher than that of Gly, 24.16% higher than that of fructose, and 31.27% higher than that of SCK. Furthermore, the DTPA-Cd under a low concentration of citric acid application (SC1 and SC2) was higher than that under a high concentration (SC3). Similarly, Gly also effectively increased the DTPA-Cd content in the soil within 1 week after addition, but there were no significant differences among different dosages. The contents of DTPA-Cd in soil increased by 25.66%–27.87%, 12.15%–18.79% and 21.22%–26.47% on the first, third, and seventh days, respectively, compared with SCK. However, the increase in DTPA-Cd in the soil gradually weakened after 1 week. In addition, the activation effect of fructose on Cd increased on days 1 (0.58 mg/kg) and 3 (0.66 mg/kg), then decreased on days 14 (0.42 mg/kg) and was generally higher than that in the SCK group during the whole experimental period. The activation effect of Cd by citric acid was significantly stronger than that of Gly and fructose during the whole incubation, except for the third and seventh days.

Some organic acids, amino acids and other substances in the *S. plumbizincicola* root exudates can change the acidity and alkalinity of the rhizosphere soil. The concentration of H^+ in an aqueous solution was positively correlated with the concentration of organic acids and amino acids. The release of more H^+ in the aqueous solution reduces the electronegativity of the soil surface, weakens the adsorption capacity of soil for heavy metals, and thus promotes the desorption of heavy metals (Tang et al., 2022). In this experiment, different concentrations of citric acid and Gly rapidly decreased the pH of the soil in a short period, and with the increase in the applied concentration, the soil pH decreased accordingly. However, with the extension of the culture time, the soil pH gradually increased in all treatments, and finally reached a new stable state. This is consistent with the findings of Chen et al. (2003) and Jiang et al. (2023), which may be due to the degradation of citric acid by microorganisms in the soil and the adsorption and deposition of citric acid by soil particles.

A lower soil pH range is more conducive to the desorption of heavy metals. Among the three additives, citric acid is a low molecular organic acid with stronger acidity, which can effectively reduce the pH and electronegativity of the surface soil and thus can active heavy metals in the soil. However, the

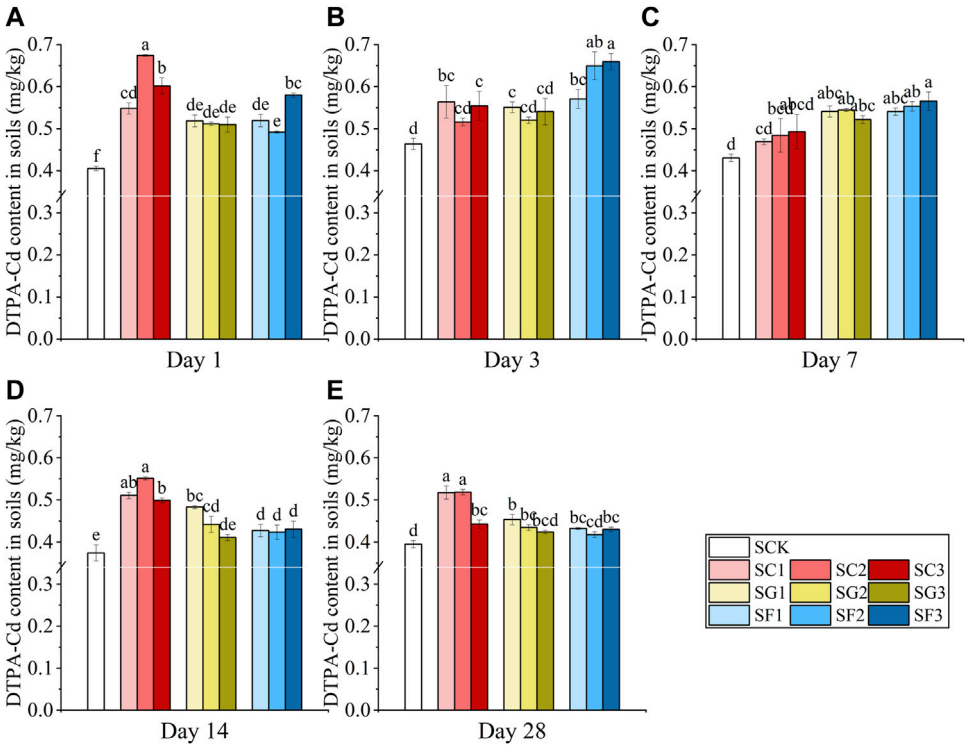

FIGURE 2
Changes in DTPA-Cd in soil under different fractions and dosages of single citric acid (SC1, SC2, SC3), Gly (SG1, SG2, SG3), and fructose (SF1, SF2, SF3) application on days 1 **(A)**, 3 **(B)**, 7 **(C)**, 14 **(D)**, and 28 **(E)** (Different letters in each sampling timepoint show significant differences, $p < 0.05$).

activation of heavy metals by citric acid mainly relies on chelation to form relatively stable ring structures rather than a decrease in soil pH only (Wu et al., 2016). Wei (2017) also found that the chelation contribution of citric acid accounted for 72.79% while that of oxalate accounted for only 1.42% when using various rhizosphere organic acids to activate cadmium carbonate, and the ability of citric acid to activate cadmium carbonate was much greater than that of oxalate. Therefore, although the content of DTPA-Cd under citric acid treatment was slightly lower than that under the Gly and fructose treatments on days 3 and 7, the advantage of citric acid application was gradually increased with the increase in the culture time (28 days), and the content of DTPA-Cd in the soil was significantly higher than that of other treatments.

Furthermore, our study also found that higher a concentration of citric acid (SC3) resulted in less Cd activation, than the lower concentration ones (SC1 and SC2). This is because when the concentration of organic acid is lower, the pH and negative charges are significantly reduced, which promotes the desorption of heavy metals. However, with the increase of organic acid concentration, organic acids, Cd and Mn form ternary surface complexes on the soil surface, which promote adsorption and inhibit desorption (Xu et al., 2005). Under the fructose treatment, different dosages of fructose did not significantly reduce the soil pH, but the activation of heavy metals still had a positive effect on the first, third and seventh days. On the one hand, fructose is a reducing sugar with reducing groups (C = O), which mainly changes the speciation and availability of heavy metals through the oxidation-reduction redox rather than the soil pH (Wang et al., 2022). On the other hand, the addition of fructose to soil may affect the activity of soil microorganisms and the production of their metabolites, thus effectively enhancing the activation of heavy metals in the soil. Fructose supplementation promoted carbohydrate metabolism (1.13-fold increase in isomaltose). Although fructose application decreased the alpha diversity of bacterial species in rhizosphere soil by 12.95%, it increased the relative abundance of actinomycetes in rhizosphere soil by 94.60%. Actinomycetes can secrete protons, organic matter and other substances, thus effectively enhancing the activation of heavy metals (Jiang, 2021).

3.2 Effects of combined root exudates on soil pH and DTPA-Cd

The variation in soil pH under the three different combinations is shown in Figure 3. The combination of citric acid + Gly and citric

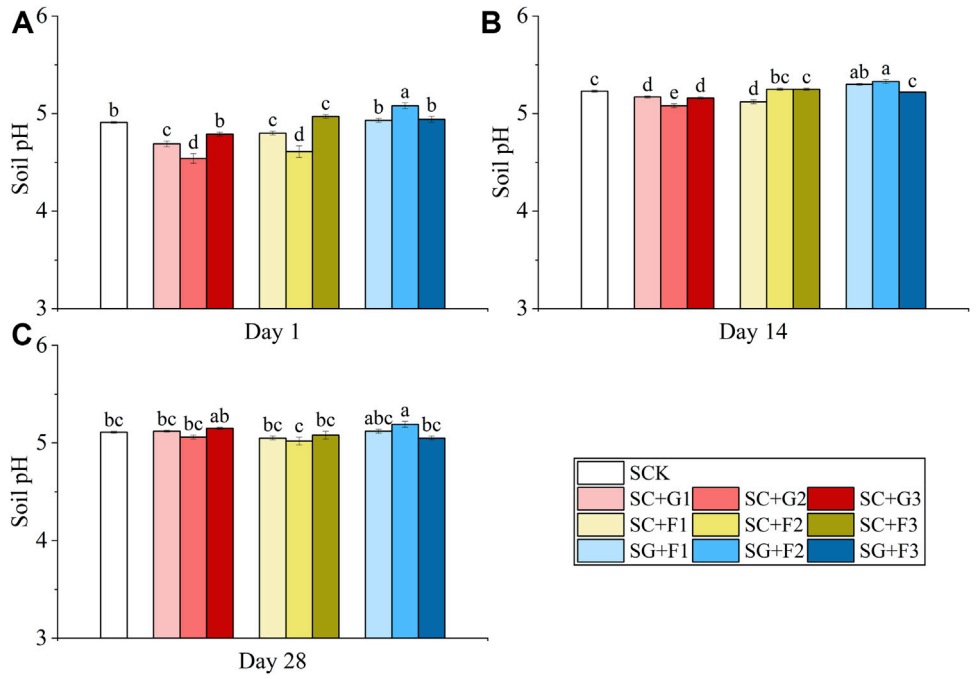

FIGURE 3
Changes in soil pH under the combined treatment of citric acid, Gly and fructose on days 1 **(A)**, 14 **(B)**, and 28 **(C)**. The combination of citric acid + Gly: SC + G1, SC + G2, SC + G3; the combination of citric acid + fructose: SC + F1, SC + F2, SC + F3; the combination of Gly + fructose: SG + F1, SG + F2, SG + F3 (Different letters in each sampling time point show significant differences, $p < 0.05$).

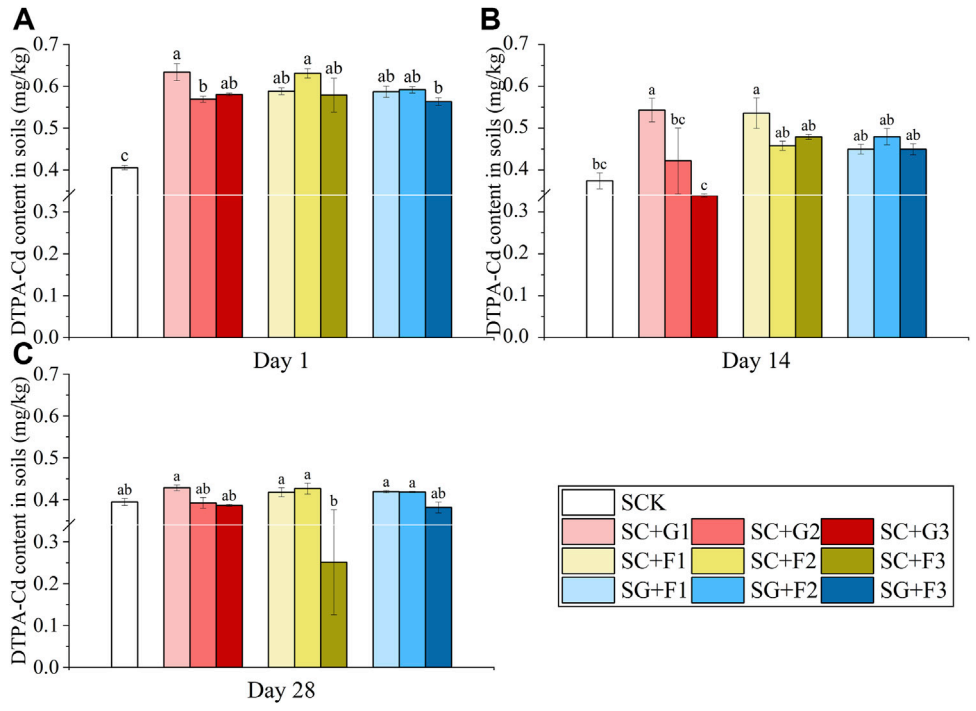

FIGURE 4
Changes in DTPA-Cd in soil under the combined treatment of citric acid, Gly and fructose on days 1 **(A)**, 14 **(B)**, and 28 **(C)**. The combination of citric acid + Gly: SC + G1, SC + G2, SC + G2; the combination of citric acid + fructose: SC + F1, SC + F2, SC + F3; the combination of Gly + fructose: SG + F1, SG + F2, SG + F3 (Different letters in each sampling timepoint show significant differences, $p < 0.05$).

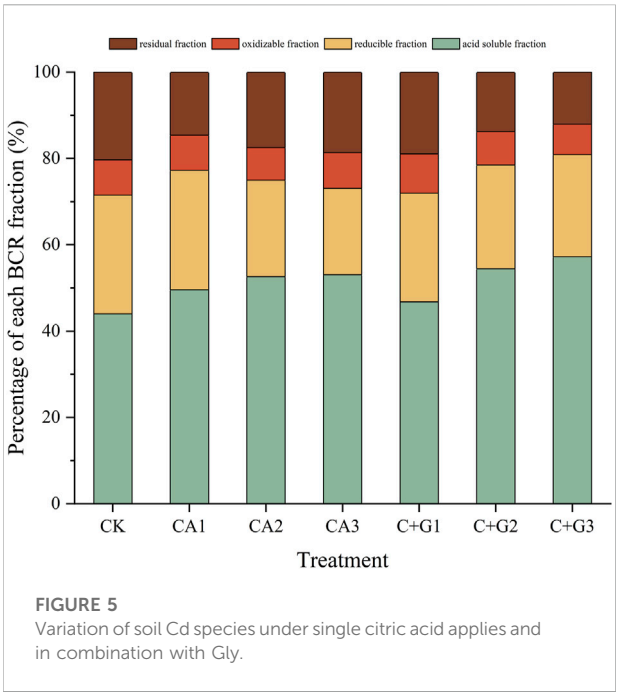

FIGURE 5
Variation of soil Cd species under single citric acid applies and in combination with Gly.

acid + fructose significantly reduced soil pH on the first day, especially the combination of 2 mmol/kg citric acid +2 mmol/kg Gly (SC + G2) and 2 mmol/kg citric acid +2 mmol/kg fructose (SC + F2). However, the combination of Gly + fructose increased the soil pH. With the increase in the culture time, all three combinations increased the soil pH, and there was no significant difference in the pH value compared with SCK.

Figure 4 shows the changes in DTPA-Cd in soil under different dosages of combinations of citric acid, Gly and fructose. Except for SC + G3, all other combinations effectively activated Cd in soil and increased the content of DTPA-Cd during the first 14 days. Among all combinations, the SC + G1 had the best Cd-activation rate, which reached 56.18%. The content of DTPA-Cd in soil under the three combinations showed a downward trend during the experiment.

The synergistic effect of various chelators effectively increased the DTPA-Cd content in the soil in a short time. First, the combination of two chelators increased the solubility of metals by lowering the pH of the soil. Second, in the process of the interaction between metals and different chelators, one metal reacts with one chelator, and its solubility is increased by the addition of another chelator. This is because it can reduce the solubility of another metal in the soil and its competitiveness effects between these matters (Zheng and Zhu, 2009). The significant increase in the DTPA-Cd content on the first day of the experiment was due to a large extent to the added compound solution that effectively reduced the soil pH and reduced the electronegativity of the soil surface, thus promoting the desorption of heavy metals. In the combination experiment, we also found that instead of lowering the soil pH, the combination of Gly + fructose slightly increased it. Nonetheless, the combination of Gly + fructose still significantly increased soil DTPA-Cd in the short term, and the effect was not different from that of the other two combination modes. This indicates that the removal effect of citric acid on heavy metals is related to its acidity to a certain extent, but it mainly depends on the complexation ability of the acid radical, and the activation process can be carried out under mild acidic conditions (Chen, 2011). When SG1 was compared with SC + G2 and SF1 was compared with SC + F2, it was found that the activation efficiency of heavy metals by adding 2 mmol/kg citric acid based on 2 mmol/kg Gly or 2 mmol/kg fructose was further increased by 12.34% and 27.36%, respectively. This may be because the addition of Gly and fructose reduces the competitive cations for citric acid to capture trace metals, such as soil-soluble Ca, thus increasing the solubility of Cd in soil (Tandy et al., 2004; Yuan, 2021).

3.3 *Sedum plumbizincicola* root exudates enhance the efficiency of phytoremediation in Cd-contaminated soil

3.3.1 *Sedum plumbizincicola* root exudates enhance the reduction of soil Cd

In the soil culture experiment, single citric acid application and its combination with Gly (SC + G) exhibited the best Cd activation efficiency in the soil. To further verify their effects on phytoremediation, a pot experiment was conducted with *S. plumbizincicola*. The changes in soil Cd species under single citric acid treatment and the combination of citric acid and Gly are shown in Figure 5. The percentage of the acid soluble Cd fraction in CA1, CA2, and CA3 increased by 5.63%, 8.68%, and 9.14% when compared with CK, which was positively related to the citric acid concentration. Whilst the percentage of the residual fraction decreased in all CA treatments (1.69%–5.71%). Similarly, for the combined application of citric acid and Gly, with the increasing ratio of the citric acid proportion, the percentage of the acid soluble fraction increased, and the residual fraction decreased accordingly when compared with CK. However, when compared with the single application of citric acid at the same dosage (CA3, 4 mmol/kg), only the C + G2 and C + G3 treatments resulted in increased acid soluble fraction and a decreased residual fraction. This indicated that the higher ratio of citric acid proportion in the combined application of citric acid and Gly was helpful in transforming the residual fraction into the acid soluble fraction and reducible fraction in the soil with higher bioavailability.

The contents of total Cd and DTPA-Cd in soil were determined after 30 days of incubation in all treatments (Figure 6). For the single citric acid addition (CA), the total amount of Cd in CA1 treated soil was the lowest (0.44 mg/kg), which was 46.16% lower than that in the original soil

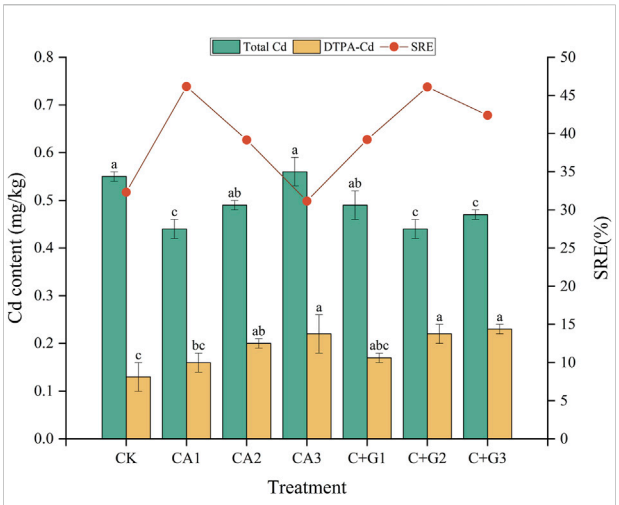

FIGURE 6
Changes in total Cd and DTPA-Cd in soils under different fractions and dosages of single citric acid application and its combination with Gly. The remediation efficiency of Cd was evaluated by calculating the removal rate of Cd in the soil (Different letters indicate significant differences, $p < 0.05$).

(0.81 mg/kg). With the increase in the citric acid concentration, the total Cd content in the soil gradually increased. A similar trend was observed for the content of DTPA-Cd with the increasing concentration of citric acid, the concentration of DTPA-Cd in the CA2 and CA3 treatments was significantly higher than that of CK, by 53.85% and 69.23%, respectively. For the combination of citric acid and Gly treatment (C + G), all treatments could significantly reduce the total soil Cd content, among which the C + G2 treatment (2 mmol/kg citric acid +2 mmol/kg Gly) showed the best effect. The total Cd concentration was significantly reduced by 46.11% compared with the original soil (0.81 mg/kg) (Figure 6). Similar to the addition of single citric acid, there was also a positive correlation between soil DTPA-Cd and the citric acid concentration in the C + G combination treatment. These results indicated that citric acid played a dose-dependent facilitation effect on the activation of Cd in the soil, and Gly played a synergistic role in the activation.

SRE was used to evaluate the remediation efficiency of Cd by calculating the removal rate of Cd in the soil. Except for CA3, all treatments showed a higher SRE than CK, among which CA1 and C + G2 showed the highest remediation efficiency (Figure 6).

Low-molecular-weight organic acids in root exudates, such as citric acid, carboxylic acid, amino acid and phenolic acid, can promote the activation of heavy metals in the soil by reducing the soil pH, changing the soil redox potential and complexing with heavy metals, thus affecting the bioavailability and uptake of heavy metals by plants (Guo, 2017). The H^+ released by organic acids can destroy the bonding forms of heavy metals in the soil and, thus promote the conversion of the heavy metals from the reduced state to the acid-soluble state (Jelusic et al., 2014). In this study, a higher concentration of citric acid in both the single and combined treatments induced the conversion of stable Cd (residual Cd) into exchangeable Cd (acid soluble Cd) in the soil, resulting in an increase in the concentration of bioavailable Cd (DTPA-Cd) in the soil. This is in consist with the results reported by Qian and Liu (2012). Perez-Esteban et al. (2013) also found that higher concentrations of citric acid and tartaric acid significantly decreased soil pH, thus promoting the dissolution of iron and manganese oxide bonded copper and zinc in the soil and increasing the desorption of heavy metals in the soil in a mining area.

For the Cd removal efficiency among different treatments, CA1 and C + G2 had the best effect. This likely indicated that although a higher concentration of citric acid may increase the availability of Cd in the soil, the activated Cd could not be taken up and removed by the plants effectively. In addition, Gly may also play an important role in regulating the Cd removal efficiency, especially in an equal proportion with CA. The potential reason for these results will be explained in detail in the next section.

3.3.2 *Sedum plumbizincicola* root exudates enhance Cd uptake by plants

The biomass and concentration of Cd in *S. plumbizincicola* were determined after 30 days of incubation under the addition of different doses of single citric acid (CA) and its combination with Gly (C + G) (Figure 7). For the single citric acid addition (CA), the CA1 treatment resulted in the greatest biomass (Figure 7A) and the highest Cd concentration in *S. plumbizincicola* (Figure 7B), so the phytoremediation efficiency was the highest (42.33%) (Figure 7B). But in the CA3 treatment with the highest concentration of citric acid, the Cd concentration in *S. plumbizincicola* decreased significantly, which lead to a marked decrease in the phytoremediation efficiency (25.74%) compared with that of CA1. For the combined treatment (C + G), C + G1 had the highest plant biomass (Figure 7A), while C + G2 had the best phytoremediation efficiency (35.61%) (Figure 7B), despite its biomass was lower than that of C + G1. Moreover, C + G3 treatment with the highest concentration of citric acid had the lowest phytoremediation efficiency (29.43%).

A low concentration of citric acid significantly increased the biomass of *S. plumbizincicola* and thus promoted the uptake and transport of heavy metals by the plant *via* the "biological dilution effect" (Zhang et al., 2015). Hence, the lowest dosage of citric acid used in this study (C1 and C + G1 treatments) resulted in the increased phytoremediation efficiency of Cd by *S. plumbizincicola*. When the concentration of citric acid increases (CA3 and C + G3), it may cause growth inhibition or even damaged to the plant tissues, thus decreasing the plant biomass and the absorption of Cd by plant roots, and finally affecting the phytoremediation efficiency (Qiao, 2010). In addition to the biological dilution effect, it is possible that Gly also plays a synergetic role in Cd phytoremediation *via* two pathways. On the one hand, under Cd stress, plants can synthesize

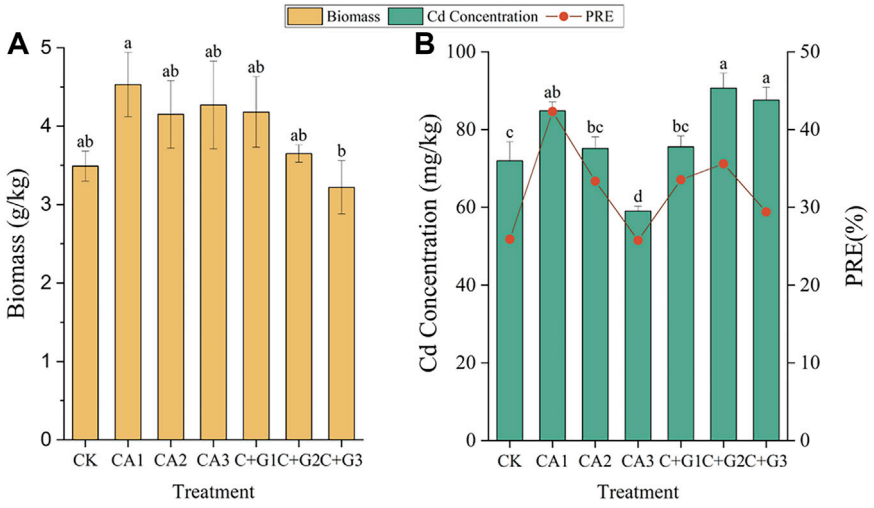

FIGURE 7
Changes in the biomass **(A)** and Cd concentration in *S. plumbizincicola* **(B)** under different fractions and dosages of single citric acid application and its combination with Gly. The remediation efficiency of Cd was evaluated by calculating the absorption rate of Cd in *S. plumbizincicola* **(B)** (Different letters indicate significant differences. Biomass: $p < 0.1$; Cd concentration: $p < 0.05$).

and secrete a series of nitrogenous metabolites, such as amino acids, plant chelates, and glutathione, to help plants cope with environmental stress and alleviate the toxic effects (Ma, 2019). On the other hand, exogenous addition of Gly may provide beneficial nutrient elements for the rhizosphere microorganisms, thus regulating the microbial community structure and function and indirectly affecting the phytoremediation efficiency (Wang et al., 2022). Therefore, in the combined application of citric acid and Gly, when citric acid and Gly were in equal proportions (C + G2), both SRE (46.11%) and PRE (35.61%) had the highest efficiency, which verified the importance of glycine in promoting the Cd phytoremediation effect of *S. plumbizincicola*.

4 Conclusion

In this study, the effects of *S. plumbizincicola*'s root exudates and their combination patterns on the activation and remediation of Cd-contaminated soils were evaluated. The results showed that, compared with the single application of Gly and fructose, citric acid had the best effect on Cd activation by increasing the DTPA extracted Cd in the soil. Lower concentration of citric acid application resulted in a significantly higher content of DTPA-Cd than the higher one. Furthermore, the combined application of citric acid and Gly, especially at the ratio of 1: 3, had the best activation effect on the Cd in the soil. In addition, the single application of citric acid at lower concentration could significantly reduce the total Cd and DTPA-Cd in the soil and enhance the biomass and the content of Cd in *S. plumbizincicola*, thus increase the phytoremediation efficiency of Cd-contaminated soil. While for the combined treatment, citric acid and Gly had the best effects of Cd removal and the phytoremediation efficiency. In conclusion, citric acid plays a crucial role in the phytoremediation of Cd by the activation of Cd in the soil, as well as the accumulation of Cd in *S. plumbizincicola*. Gly was also synergistically involved in relieving the environmental stress on *S. plumbizincicola* growth and enhancing the uptake of Cd. The detailed mechanisms of the synergetic interaction between citric acid and Gly need further investigation in the future.

Data availability statement

The original contributions presented in the study are included in the article/supplementary material, further inquiries can be directed to the corresponding authors.

Author contributions

QX and LS are responsible for the conduct of the experiment and the writing of the manuscript. XC, YD and JY also contributed partially in designing and conducting of the experiment. CTa and CTu have made contributions to the revision of the logic and language of the manuscript.

Funding

This research was financially supported by the National Natural Science Foundation of China (42107018), the Hunan Innovative Province Construction Special Fund (2020NK 2001), the Natural Science Foundation of Hunan Province

(2021JJ40630), and the Independent Project of Institute of Soil Science, Chinese Academy of Sciences (ISSASIP2204).

Conflict of interest

The authors declare that the research was conducted in the absence of any commercial or financial relationships that could be construed as a potential conflict of interest.

Publisher's note

All claims expressed in this article are solely those of the authors and do not necessarily represent those of their affiliated organizations, or those of the publisher, the editors and the reviewers. Any product that may be evaluated in this article, or claim that may be made by its manufacturer, is not guaranteed or endorsed by the publisher.

References

Bai, J., Tan, C. Y., Cao, X. Y., Zhou, Q., Huang, S. P., Peng, X., et al. (2020). Effect of three organic acids on the remediation efficiency of *Sedum plumbizincicola* and soil microbial quantity. *J. Soil Water Conservation* 34, 318–324. doi:10.13870/j.cnki.stbcxb.2020.02.045

Cao, X. Y., Tan, C. Y., Xie, Y., Dai, B., Zhu, S., and Wang, Y. (2019). Effect of soil pH and total cadmium concentration of soil on the remediation efficiency of *Sedum plumbizincicola*. *Res. Environ. Sci.* 32, 1604–1612. doi:10.13198/j.issn.1001-6929.2019.05.08

Chen, J. J. (2011). *Eeffects of added maize straw and citric acid on Cu and Cd availability in soil*. Zhengzhou: Henan Agricultural University.

Chen, Y. X., Lin, Q., Luo, Y. M., He, Y. F., Zhen, S. J., Yu, Y. L., et al. (2003). The role of citric acid on the phytoremediation of heavy metal contaminated soil. *Chemosphere* 50, 807–811. doi:10.1016/S0045-6535(02)00223-0

Deng, Y. Q., Cao, X., Tan, C., Sun, L., Peng, X., Bai, J., et al. (2020a). Effect of organic materials on phytoremediation efficiency of Cd-contaminated acid soil by *Sedum plumbizincicola*. *J. Agro-Environment Sci.* 39, 2762–2770. doi:10.11654/jaes.2020-0605

Deng, Y. Q., Cao, X., Tan, C., Sun, L., Peng, X., Bai, J., et al. (2020b). Strengthening the effect of Bacillus megaterium on remediation of Cd-contaminated farmland soil by *Sedum plumbizincicola*. *Chin. J. Appl. Ecol.* 31, 3111–3118. doi:10.13287/j.1001-9332.202009.036

Galili, G., Amir, R., and Fernie, A. R. (2016). The regulation of essential amino acid synthesis and accumulation in plants. *Annu. Rev. Plant Biol.* 67, 153–178. doi:10.1146/annurev-arplant-043015-112213

Guo, S. H. (2017). *Effect of salt stress on soil Cd mobility and Cd uptake by edible amaranth (Amaranthus mangostanus L.) cultivar*. Guangzhou: Jinan University.

Hammer, D., and Keller, C. (2002). Changes in the rhizosphere of metal-accumulating plants evidenced by chemical extractants. *J. Environ. Qual.* 31, 1561–1569. doi:10.2134/jeq2002.1561

He, M. F., Li, Z. B., Chen, C., and Mei, P. (2022). Activation and remediation of Cu^{2+} and Cd^{2+} in soil by root exudates and plants. *Environ. Sci. Technol.* 45, 198–205. doi:10.19672/j.cnki.1003-6504.0039.22.338

Jelusic, M., Vodnik, D., and Lestan, D. (2014). Revitalization of EDTA-remediated soil by fertilization and soil amendments. *Ecol. Eng.* 73, 429–438. doi:10.1016/j.ecoleng.2014.09.068

Jiang, O. Y., Li, L. Y., Duan, G. L., Gustave, W., Zhai, W. W., Zou, L. N., et al. (2023). Root exudates increased arsenic mobility and altered microbial community in paddy soils. *J. Environ. Sci.* 127, 410–420. doi:10.1016/j.jes.2022.05.036

Jiang, Y. Y. (2021). *Effect of cadmium stress on symbiont combined with AM fungi and medicago truncatula and the effect of additional fructose*. Chongqing: Southwest University of Science and Technology. doi:10.27415/d.cnki.gxngc.2021.000933

Liu, L. L., Tan, C. Y., Cao, X. Y., Peng, X., Bai, J., Cheng, X. Q., et al. (2022). Remediation effects of citric acid activation combined with *Sedum plumbizincicola* intercropped with maize on slightly Cd-contaminated soil. *Trans. Chin. Soc. Agric. Eng.* 38, 257–263. doi:10.1016/j.jes.2022.05.036

Liu, S. H., Chen, H. Y., Ji, X. H., Liu, S. B., and Xie, Y. H. (2021). Remediation potential of rice with high cadmium accumulation to cadmium contaminated farmland. *Trans. Chin. Soc. Agric. Eng. Trans. CSAE)* 37, 175–181. doi:10.11975/j.issn.1002-6819.2021.10.021

Ma, Q. X. (2019). *The uptake of amino acids and the effects of pH and Cd stress on plants absorption*. Hangzhou: Zhejiang University.

Perez-Esteban, J., Escolastico, C., Moliner, A., and Masaguer, A. (2013). Chemical speciation and mobilization of copper and zinc in naturally contaminated mine soils with citric and tartaric acids. *Chemosphere* 90, 276–283. doi:10.1016/j.chemosphere.2012.06.065

Qian, L., and Liu, Y. (2012). Effects of single and combined organic acids on form of Cd in soil. *Chin. J. Soil Sci.* 43, 186–189. doi:10.19336/j.cnki.trtb.2012.01.036

Qiao, D. M. (2010). *Phytoremediation mechanism of lead pollution base on organic acid exudation from ryegrass root*. Beijing: Chinese Academy of Agricultural Sciences.

Shen, L. B., Wu, L. H., Han, X. R., Tan, W. N., Huang, Y. J., Luo, Y. M., et al. (2011). Effects of nutrient regulation and control on plant growth and Zn/Cd uptack by hyperaccmulator *Sedum plumbizincicola*. *Soils* 43, 221–225. doi:10.13758/j.cnki.tr.2011.02.009

Sun, L. J., Cao, X. Y., Tan, C. Y., Deng, Y. Q., Cai, R. Z., Peng, X., et al. (2020). Analysis of the effect of cadmium stress on root exudates of *Sedum plumbizincicola* based on metabolomics. *Ecotoxicol. Environ. Saf.* 205, 111152. doi:10.1016/j.ecoenv.2020.111152

Sun, L. J. (2021). *Effects of Sedum plumbizincicola root exudates and its components in Cd-contaminated soil remediation*. Changsha: Hunan Normal University. doi:10.27137/d.cnki.ghusu.2021.002504

Tandy, S., Bossart, K., Mueller, R., Ritschel, J., Hauser, L., Schulin, R., et al. (2004). Extraction of heavy metals from soils using biodegradable chelating agents. *Environ. Sci. Technol.* 38, 937–944. doi:10.1021/es0348750

Tang, D. Y., Xiang, Q., Lei, W. D., and Sun, J. (2022). Effects of organic acids on the desorption of Cd, Cr and Mn ions in heavy metal contaminated soil. *J. South-Central Univ. Natl. Nat. Sci. Ed.* 41, 44–50. doi:10.12130/znmdzk.20220108

Wang, Y., Feng, F. Y., Ge, J., Li, Y., and Yu, X. Y. (2022). Effects and mechanisms of plant root exudates on soil remediation. *Acta Ecol. Sin.* 42, 829–842. doi:10.5846/stxb202101030011

Wei, J. (2017). *A comparative study on insoluble cadmium mobilized by various rhizosphere organic acids*. Guangzhou: Jinan University.

Wu, J., Lu, J., Zhang, C., Zhang, Y. X., Lin, Y. C., and Xu, J. (2020). Pollution, sources, and risks of heavy metals in coastal waters of China. *Hum. Ecol. Risk Assess. Int. J.* 26, 2011–2026. doi:10.1080/10807039.2019.1634466

Wu, L. H., Zhou, S. B., Bi, D., Guo, X. H., Qin, W. H., Wang, H., et al. (2006). *Sedum plumbizincicola*, A new species of the crassulaceae from zhejiang, China. *Soils*. Thesis. Beijing 38, 632–633. doi:10.13758/j.cnki.tr.2006.05.022

Wu, L. S., Xian, S. Y., Kong, D., C Ou, M. Y., and Deng, Q. G. (2016). Remediation of Cd polluted soil by Co-leaching of tannic acid and citric acid. *Environ. Eng.* 34, 178–181+165. doi:10.13205/j.hjgc.201608037

Xu, R. K., Xiao, S. C., and Ji, G. L. (2005). Mechanisms of low molecular weight organic acids affecting Cu adsorption by variable charge soils. *China Environ. Sci.* 25, 334–338.

Xue, W., Zhang, C., Huang, Y., Wang, C., Zhang, X., and Liu, Z. (2022). Rice organs concentrate cadmium by chelation of amino acids containing dicarboxyl groups and enhance risks to human and environmental health in Cd-contaminated areas. *J. Hazard Mater* 426, 128130. doi:10.1016/j.jhazmat.2021.128130

Yuan, K. (2021). Effects of amino acids and calcium magnesium phosphate fertilizer on characteristic of cadmium accumulation in rice and their mechanism thesis. Beijing: Chinese Academy of Agricultural Sciences.

Zhang, X., Chen, B. D., and Ohtomo, R. (2015). Mycorrhizal effects on growth, P uptake and Cd tolerance of the host plant vary among different AM fungal species. *Soil Sci. Plant Nutr.* 61, 359–368. doi:10.1080/00380768.2014.985578

Zheng, X. L., and Zhu, K. (2009). The application of chelating agents in the phytoremediation of heavy mental contaminated soils. *Environ. Sci. Manag.* 34, 106–109. doi:10.13292/j.1000-4890.2009.0317

Zhu, L. X., Zhang, J. E., and Liu, W. G. (2003). Review of studies on interactions between root exudates and rhizopheric microorganisms. *Ecol. Environ.* 12, 102–105. doi:10.16258/j.cnki.1674-5906.2003.01.025

frontiers | Frontiers in Environmental Science

TYPE Original Research
PUBLISHED 04 January 2023
DOI 10.3389/fenvs.2022.1048345

OPEN ACCESS

EDITED BY
Jun Wu,
Harbin Engineering University, China

REVIEWED BY
Wenjie Ren,
Institute of Soil Science (CAS), China
Omowunmi H. Fred-Ahmadu,
Covenant University, Nigeria

*CORRESPONDENCE
Zhen Zhang,
zhangzhen-911@163.com

SPECIALTY SECTION
This article was submitted to Toxicology, Pollution and the Environment, a section of the journal Frontiers in Environmental Science

RECEIVED 19 September 2022
ACCEPTED 08 December 2022
PUBLISHED 04 January 2023

CITATION
Zhang Z, Chen LH, Tao ML, Zhou DD, Zhang Y, Yao J, Kong QN and Guo BB (2023), Occurrence and distribution characteristics of PCBs and PBDEs in farmland soils adjacent to electronic circuit board dismantling ruins. *Front. Environ. Sci.* 10:1048345. doi: 10.3389/fenvs.2022.1048345

Occurrence and distribution characteristics of PCBs and PBDEs in farmland soils adjacent to electronic circuit board dismantling ruins

Zhen Zhang[1]*, Lin Hua Chen[2], Min Long Tao[2], Dan Dan Zhou[2], Yuan Zhang[2], Jun Yao[1], Qing Na Kong[1] and Bin Bin Guo[2]

[1]Zhejiang Provincial Key Laboratory of Plant Evolutionary Ecology and Conservation, Taizhou University, Taizhou, China, [2]Taizhou Pollution Prevention and Control Engineering Center, Taizhou University, Taizhou, China

The Nanwan village, a green ecological village in Taizhou city, is used as a recycling area (recycling for heavy metal) for electronic circuit boards and as crushing and stacking sites of waste circuit boards for nearly 20 years from 1980s to 2000s. At present, although the e-waste recycling activities in Taizhou city have been effectively controlled, and many areas polluted by the e-dismantling activities have been gradually remediated except Nanwan village. Nanwan village seems to have been forgotten for its special geographical location, which has attracted our attention because of its ecological and food safety issues. Accordingly, the content of polychlorinated biphenyls (PCBs) and polybrominated diphenyl ethers (PBDEs) in the surface soil around the ruins and four edible agricultural crops were investigated. The main conclusions are as follows: among the four dismantling ruins and surrounding soil samples investigated, the content of Σ_{20}PCBs in vegetable field topsoil of 2(20) is 1,321.3 $\pm$ 132.1 μg kg^{-1}; the content of Σ_8PBDEs in the paddy soil of 3(1S) is 7,216.9 $\pm$ 232.0 μg kg^{-1}; biological toxicity events are likely to occur frequently in 2(20) and 3(1S). PCBs and PBDEs have both horizontal diffusion in distance and vertical diffusion in depth. The lifetime carcinogenic and non-carcinogenic risks of PCBs and PBDEs are at a low risk level, except for the non-carcinogenic risk of PCBs for children in 3(1S). The lifetime carcinogenic and non-carcinogenic risks of PCBs and PBDEs in the edible parts of garlic, ginger, mung beans, and oranges were all at acceptable or negligible levels.

KEYWORDS

electronic circuit board, soil pollution, PCB, PBDEs, health risk

1 Introduction

The disassembly activities of electronic products in Taizhou City, Zhejiang Province, began in the 1970s. The initial family workshop until today's metal recycling industry base spanned for 40 years (Fu et al., 2012). In Taizhou, people once used e-waste to recycle useful metals for profit, and then threw the garbage to the land and rivers under their feet. The electronic products in Taizhou are mainly disassembled in Fengjiang and Jinqing town in Luqiao District, and in Zeguo and Wenqiao town in Wenling City. Nanwan village is a small village located south of Qingyu village in Wenqiao Town near the seaside of Yueqing Bay. It is surrounded by mountains on three sides and faces the sea on the other side. Its special geographical location leads to the inconvenient transportation, and it is used as a recycling area for electronic circuit boards and as crushing and stacking sites of waste circuit boards. The disassembly of electronic circuit boards in Nanwan village began in the early of 1980s. At first, people directly stacked the waste electronic circuit boards after recycling useful metals in open air. As the time passed, the stacking of waste circuit boards occupied a large area of the farmland, and then the waste electronic circuit boards were crushed and stacked in open air. The plastic powder of waste electronic circuit boards once produced in Nanwan village can be stacked into several "white hills" each year, where the plastic electronic circuit boards turn white after crushing. With the strict control of local government in the early 2000s, e-waste dismantling activities in Nanwan village were banned gradually, only the stacked electronic circuit boards and powders left, and told people what happened ever.

Generally, the dismantling of waste electronic circuit boards causes serious combined pollution problems of polychlorinated biphenyls (PCBs), polybrominated diphenyl ethers (PBDEs), heavy metal ions, and so on (Fu et al., 2012; Das et al., 2020; Liu et al., 2021). The direct stacking of electronic circuit boards and the powder without any treatment of the stacking sites have increased PCBs and PBDEs pollution in the groundwater and soil. According to a survey by Zhejiang Environmental Science Design and Research Institute, the soils in Fengjiang Town, Luqiao District, Taizhou City, Wenqiao and Zeguo town in Wenling City have been jointly polluted by PCBs and PBDEs to varying degrees, thus affecting the land quality and causing significant environmental safety problems.

Although the industrial use of PCBs and PBDEs has been banned (Li et al., 2020), considering that PBDEs and PCBs are quite stable in the environment and difficult to degrade. At the same time, these compounds are insoluble in water and soluble in fat, easy to be absorbed by animals, and gradually enriched in the food chain, thus endangering human health. In 2006, to chase for "green ecological village", local people in Nanwan village removed the "white hills" to deep pits behind the village or at the foot of the mountain, directly buried the waste circuit boards and their plastic powder, and then covered them with sea mud. The extensive landfill without leakage prevention and anti-seepage treatment will cause unpredictable pollution to the groundwater and soil after long-term atmospheric settlement, surface overflow, underground runoff, and vertical infiltration. In 2011, the plastic powder in Nanwan village had new utilization value as an adhesive to make sintered bricks. The "white hill" was dug up and sold to brick kiln factories far away. After 2014, the sale of waste electronic circuit boards plastic powder was basically completed, and the ruins were left empty. Some areas were covered with a layer of sea mud, while some areas were directly exposed. A few years later, some ruins remained barren with little plant growth. This phenomenon occurred, mainly because the waste electronic circuit boards and their plastic powder had been stacked for a long time (even more than 20 years), and pollutants such as PBDEs, PCBs, and heavy metal ions have already penetrated the ruins and the surrounding soils or groundwater, which seriously threatened the food safety of the ruins, the surrounding farmland, and vineyards, and as well as threatened the health of the surrounding residents. Today, local agricultural and sideline products are labeled "green" or "organic" and sold all over the country, and their ecology and food safety are worrying.

At present, although the e-waste recycling activities in Taizhou city have been effectively controlled, and the areas polluted by the e-dismantling activities in Fengjiang town of Luqiao District and in Zeguo and Wenqiao town of Wenling City, have been gradually remediated. So far, many studies have focused on PCBs and PBDEs in soils, sediments, house dusts, plants in the well-known e-waste dismantling sites such as Guiyu and Longtang in Guangdong Province, Wenqiao and Fengjiang in Taizhou city, Zhejiang Province (Yang Z Z, 2009; Yu, et al., 2018; Li et al., 2019; Liu et al., 2019; Shi et al., 2019; Mao et al., 2021; Zhou et al., 2021). Few studies focus on the soil pollution and food safety issues caused by the dismantling and accumulation of waste circuit boards and their plastic powder in Nanwan Village, let alone the remediation of contaminated soil in Nanwan Village. Accordingly, four stacking ruins of electronic circuit boards and their plastic powder in Nanwan village, Wenqiao Town, Wenling City, Taizhou City were selected as the research areas, and the compound pollution of PCBs and PBDEs in the ruins, surrounding soils, and around the four crops were investigated to assess its ecological and food safety, also provide a theoretical basis for the subsequent remediation of contaminated soil in Nanwan Village.

2 Study sites

After the investigation, four dismantling ruins, namely, No. 1, No. 2, No. 3, and No. 4 were selected as the dismantling or stacking ruins, which were stacked with the electronic circuit board or its plastic powder for more than 10 years Figures 1, 2 show the geographical locations and current situation of the sampling points.

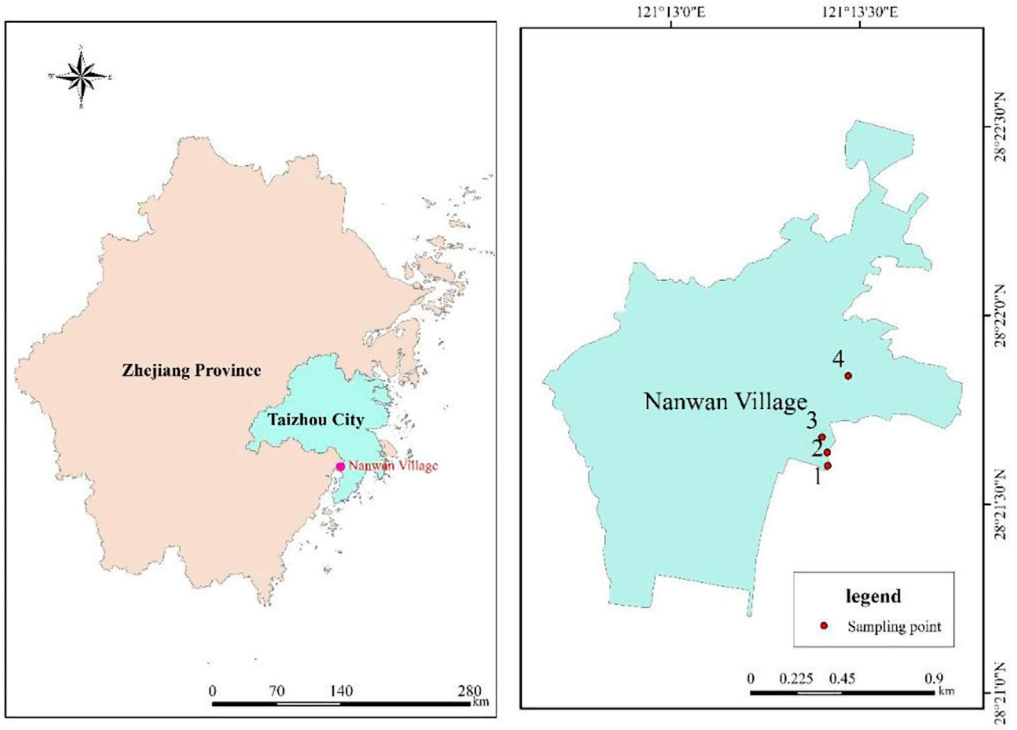

FIGURE 1
Location and sampling sites in the study area.

FIGURE 2
Situation of sampling points.

The No. 1 sampling point is located on the hillside in the east of Nanwan village, where the plastic powder of electronic circuit boards has the longest stacking history and the largest scale. The plastic circuit board powder was cleaned up and sold in 2011–2012. At present, it is filled with a thick layer of sea mud, exposed, and without plant growth. The sampling point is located in 5 m away from No. 1 ruins [1(5)] at the foot of the hillside (now abandoned). Vineyards, orange orchards, and paddy fields lie at the foot of No. 1 ruins.

The No. 2 sampling point is on the hillside to the north of No. 1 ruins. Initially, waste electronic circuit boards were stacked after copper recycling (more than 20 years), and then a large number of circuit boards plastic powder was covered on the waste circuit board. The electronic circuit board powder was cleaned and sold in 2011–2014, and the waste electronic circuit board was removed in 2019. Currently, it is covered with a layer of soil. At No. 2 ruins, many electronic circuit boards and their

plastic powder are directly exposed because of long-term rain erosion. During sampling, a 30–40 cm-thick circuit board powder is present on the surface, and the bottom soil (>40 cm) under the circuit board powder [2(0)] was collected after removing the surface plastic powder. Then, the vegetable field topsoil at 20 and 30 m around [2(20) and 2(30)]were collected. The topsoil at 2(20) contains a large amount of circuit board powder, circuit boards, and topsoil washed from No. 2 ruins, and the bottom layer contains circuit boards and their powder that cannot be sampled. Pumpkin and other vegetables were planted in this area. The vegetable field at 2(30) is a slightly higher than the vegetable field at 2(20).

The No. 3 ruins are located at the foot of the mountain at the east of Nanwan village adjacent to No. 2 ruins. The electronic circuit board powder stacked in there has been cleaned and sold from 2011 to 2014, and the surface is covered with a layer of sea mud. At present, a few citrus trees are planted in the sample plot, but the survival rate is very low, and weeds are rarely grown. The east and north areas of No. 3 ruins are hillsides. The south of No. 3 ruins is a paddy field, which is approximately 40 cm lower than the No. 3 ruins. A vegetable field is located at the west of No. 3 ruins, and this field is as high as the No. 3 ruins. The 1 m vegetable field soil to the west and 1 m paddy soil to the south of No. 3 ruins [3(1W) and 3(1S)] were sampled.

The No. 4 ruins are located at the foot of the mountain in the northeast of Nanwan village, where electronic circuit board powder has been stacked till today. In 2006, to chase for the "green ecological village", the "white hill" near the roads were removed to No. 4 ruins. The villagers dug a deep pit at the foot of the mountain, filled in the plastic powder, and covered it with a thick layer of sea mud. The No. 4 ruins is a sloping land with a slope of approximately 25°. Ginger was planted in No. 4 ruins during sampling, and the soil samples at 1 and 20 m away (low terrain direction) from No. 4 ruins [4(1) and 4(20)], as well as the ginger were collected.

No. 1, No. 2, and No. 3 ruins are relatively close and located on the hillside or foot of the same mountain. To investigate the attenuation of PCBs and PBDEs with distance, the ruins of the accumulation area as the center at 100 and 200 m (100 and 200) paddy soil away from No. 1, No. 2, and No. 3 ruins in the low terrain direction near the coast around the electronic circuit board powder stacking ruins were sampled.

Three different soil samples were collected in each location, wrapped with Aluminum foil and took to the lab, natural air drying, then grinding and screening, equal mixing of different samples at the same location, put in the dryer before use (no more than 30 days). Oranges from the orchard 100 m away from No. 1, mung beans 2 m away, and garlic 5 m away from the vegetable field to the west of No. 3, and ginger planted on the coastal mud of No. 4 ruins were collected to investigate the contents of PCBs and PBDEs in the edible parts of the 4 crops. No. 4 ruins is located at the foot of the mountain behind Nanwan village, and this area is less than 50 m away from the villagers' gathering area. In addition, the paddy fields 100 and 200 m away from No. 1, No. 2, and No. 3 ruins, the orchard 100 m away from No. 1, and the 3(1S) paddy field are at the same altitude. The vegetable fields soils at 2 and 5 m to the west of No. 3 ruins (3(2) and 3(5)) and 2(20) are at the same height. The 2(30) vegetable field is slightly higher than 2(20), and the altitudes of No. 1 and No.2 ruins are the highest with values that are at least 10 m higher than the paddy field. Table 1 shows the detail information of the soil samples.

3 Materials and methods

3.1 Chemicals

Chemical reagents such as dichloromethane (ACS), n-hexane, neutral silica gel, neutral alumina, and anhydrous sodium sulfate (superior pure) were used directly without special treatments. n-Hexane (HPLC), eight-component PBDE mixed standard (batch No.214061106), and 20-component PCBs mixed standard (batch No.212071226) were obtained from J&K Scientific Ltd. (Shanghai). Neutral silica gel was placed on aluminum foil, baked at 550°C in muffle furnace for at least 12 h, and then cooled to 180°C for 1 h for activation. After cooling in dryer, the sample was transferred into a flask. Ultrapure water with mass ratio of 5% was added dropwise, and the mixture was shaken violently to prevent the silica gel from caking. The activated silica gel was inactivated, and then placed in the dryer for standby. Alumina was packed in the flask (no more than half of the volume). The bottle was loosely covered with aluminum foil, baked at 130°C for at least 12 h, plugged and sealed after cooling, and placed in the dryer for standby. Anhydrous Na_2SO_4 was calcined in a muffle furnace at 660°C for at least 6 h before use.

3.2 Methods

The sample extraction, cleanup, and chemical analysis of the PCBs and PBDEs were conducted using established methods (Li et al., 2018). In total, 10 ± 0.0005 g soil samples were spiked with 10 ng chemical surrogates (PCB209 and 2, 4, 5, 6-tetrachloro-m-xylene) and extracted *via* accelerated solvent extraction with mixed solvent (hexane/dichloromethane (DCM), 1:1, *v*/*v*). The cleaned extracts were passed through a silica gel/Florisil packed column for cleanup. The column was packed with 5 cm deactivated Florisil, 15 cm deactivated silica gel, 5 cm neutral alumina, and 5 cm anhydrous sodium sulfate from bottom to top. Elution was subsequently conducted using 20 ml of hexane, followed by 20 ml of DCM. The elute was concentrated to 0.5 ml by rotary evaporation, and then transferred to a nitrogen blowing pipe to blow nitrogen to 1 ml. The sample was passed through a 0.22-μm organic filter membrane, bottled, and placed in refrigerator at −4°C before GC-MS analysis.

TABLE 1 Soil samples number detail information.

Label	Sampling point	Sampling depth, cm
1(5)	5 m away from No. 1 ruins (low terrain direction)	0–20
2(0)	No. 2 ruins (wastelands)	>40
2(20)	20 m away from No.2 ruins (low terrain direction)	0–10
2(30)	30 m away from No.2 ruins (low terrain direction)	0–20
3(1S)	1 m away to the south of No.3 ruins	0–20
3(1W)	1 m away to the west of No.3 ruins	0–20
4(1)	1 m away from No.4 ruins (low terrain direction)	0–20
4(20)	20 m away from No.4 ruins (low terrain direction)	0–20
100	100 m away from No.1, No.2 and No.3 ruins (low terrain direction)	0–20
200	200 m away from No.1, No.2 and No.3 ruins (low terrain direction)	0–20

Twenty PCB congeners (PCB 8, PCB 18, PCB 28, PCB 44, PCB 52, PCB 66, PCB 77, PCB 101, PCB 105, PCB 118, PCB 126, PCB 128, PCB 138, PCB 153, PCB 170, PCB 180, PCB 187, PCB 195, PCB 206, and PCB 209) and eight PBDE congeners (BDE 28, BDE 47, BED 99, BDE 100, DBE 153, BDE 154, BDE 181, and BDE 209) were determined using the Agilent (6890) gas chromatography/mass spectrometry (5975inert MSD, GC/MS) instrument. DP-5MS column was used, and the device was operated in electron impact (EI) ionization mode. The temperatures of the injector and detector were set to 260°C and 280°C, respectively. In total, 1 μl of the extracts was injected in the pulsed splitless mode. The carrier gas was nitrogen (99.99% purity), and the ion source and quadrupole temperatures were set at 230°C and 150°C. For PCBs, 30 m × 250 μm×0.25 μm DP-5MS column was used, the carrier flow rate was 1 ml min^{-1}, and the oven program was started at 100°C. This temperature was then increased at a rate of 20°C min^{-1} to 230°C, then at 5°C min^{-1} to 240°C, kept at 3 min, increased at a rate of 20°C min^{-1} to 300°C, and finally kept for 5 min. For PBDEs, 15 m × 250 μm × 0.25 μm DP-5MS column was used. The carrier flow rate was 1.8 ml min^{-1}, and the oven program was started at 120°C, which was then increased at a rate of 20°C min^{-1} to 325°C, and then kept for 6 min.

3.3 Risk assessment

3.3.1 Ecological risk assessment

At present, no clear method has been established for the ecological risk assessment of PCBs in farmland soil at home or abroad. The ecological risk analysis of PCBs in farmland soil in Nanwan village was carried out by using the Environmental Quality Standard for sediments proposed by Long et al. (Long et al., 1995; Yao, 2019), and this guide is used as the national standard of the United States by the USEPA, as well as in related research (Yao, 2019). The standard proposed that organic matter in sediments can be divided into two boundaries, namely, low toxic effects (ERL) and toxic effects in value (ERM), and the thresholds of ERL and ERM were 22.7 and 180 μg kg^{-1}, respectively. When the target pollutant concentration is less than ERL, it represents a minimal-effects range, in which effects are rarely observed. When the targe contaminant concentration is greater than ERM, the probability of biological effects is greater than 50% (Long et al., 1995; Wang et al., 2018).

3.3.2 Health risk assessment

For PCBs and PBDEs in soils and crops, USEPA exposure calculation model was used to calculate the human health risk assessment. The exposure to non-carcinogenic and carcinogenic risks of human population to PCBs and PBDEs in soils was estimated with the reference to the Regional Screening Levels (RSL) (Wu et al., 2019; Chen et al., 2021; Sun et al., 2021). Three routes that cover soil ingestion, soil dermal contact, and soil inhalation were considered to count the average daily dose (ADD, mg kg^{-1} day^{-1}) of soil. ADD of PCBs and PBDEs congeners through soil were calculated as follows:

$$ADD_{ing} = \frac{C_s \times EF \times ED \times IRs}{AT \times BW} \quad (1)$$

$$\mathrm{ADD}_{der} = \frac{C_s \times EF \times ED \times SA \times AF \times ABS}{AT \times BW} \quad (2)$$

$$ADD_{inh} = \frac{C_s \times EF \times ED \times HRs}{PEF \times AT \times BW} \quad (3)$$

$$ADD = \sum \mathrm{ADD}_i \quad (4)$$

where ADD_{ing}, ADD_{der} and ADD_{inh} were cancer risk *via* ingestion, dermal contact, and inhalation of soil; C_s represents concentration of pollutant in soil.

Only intake was considered to count the ADD of the crops (*ADDp*). *ADDp* of PCBs and PBDEs congeners through food intake were calculated as follows:

TABLE 2 Associated parameters used for the risk assessment.

Parameters	Implications		Parameter values	
			Adults	Children
EF	Exposure frequency, d a^{-1}		350	
ED	Exposure duration time, a	Non-carcinogenic risks	26	6
		Carcinogenic risks	70	
BW	Average bodyweight, kg		70	15
AT	Average exposure time, d	Non-carcinogenic risks	9,490	2,190
		Carcinogenic risks	25550	
IRs	Ingestion rate, mg d^{-1}		100	200
SA	Exposed skin area, cm^2		6032	2,373
AF	Skin adherence factor, mg cm^{-2}		0.07	0.2
ABS	Dermal absorption factor		0.13	
HRs	Inhalation rate, m^3 d^{-1}		20	
PEF	Particle emission factor, m^3 kg^{-1}		1.36×10^9	
IR_p	Ingestion rate for crops, g d^{-1}	Garlic	5	
		Gingerr	5	
		Mung bean	30	
		Orange	200	
SF	Cancer slope factor		Chemical-specific	
RfD	Reference dose		Chemical-specific	

$$ADD_p = \frac{C_p \times IR_p \times EF \times ED}{BW \times AT} \quad (5)$$

C_p represents concentration of pollutant in the edible parts of the crops. The meaning and value of associated parameters used for the risk assessment are shown in Table 2, which are obtained from the USEPA and the corresponding literature, and listed in Table 2 (USEPA, 2008, USEPA, 2015, USEPA, 2018; Yu et al., 2011; Wu et al., 2018; Wu et al., 2019; Xu et al., 2014; Xu et al., 2019; Yu et al., 2020; Chen et al., 2021; Sun et al., 2021; Chinese Nutrition Society, 2022.).

PCBs and PBDEs are non-carcinogenic to adults and children (USEPA, 2018). PCBs and BDE 209 have carcinogenic risks to human health. The carcinogenic and non-carcinogenic risks associated with exposure to PCBs and PBDEs were evaluated based on the Risk Assessment Guidance for Superfund methodology from the USEPA (USEPA, 2008). As described in the USEPA screening level equations for preliminary remediation goals, the non-carcinogenic child, non-carcinogenic adult, and carcinogenic risk (age adjusted) were counted for soil, while the non-carcinogenic and carcinogenic risks were counted for crops (USEPA, 2018). The risks were calculated based on the estimated daily intake concentrations. For the non-carcinogenic risk (TQ), ADD is divided by the reference dose (RfD) (mg kg^{-1} day^{-1}) (USEPA, 1992), while a TQ < 1 suggests acceptable hazard, while a TQ > 1 indicates potential risk meriting further investigation/remediation (Lim et al., 2014; Yu et al., 2020). For the lifetime carcinogenic risk (TR), ADD is multiplied by the slope factor (SF) (per mg kg^{-1} d^{-1}) (Wu et al., 2019; Chen et al., 2021; Alfaro et al., 2022). According to USEPA, the individual lifetime carcinogenic risk value is 10^{-6}, and the individual lifetime acceptable risk value is limited to 10^{-4} (USEPA, 2015; Yu et al., 2020).

4 Results and discussion

4.1 Distribution characteristics and ecological risk assessment of $\sum_{20}$PCBs and $\sum_{8}$PBDEs in dismantling ruins and surrounding soils

4.1.1 Concentration of $\sum_{20}$PCBs in the dismantling ruins and surrounding soils

The distribution of $\sum_{20}$PCBs in the dismantling ruins and the surrounding soil are shown in Figure 3. The content of $\sum_{20}$PCBs

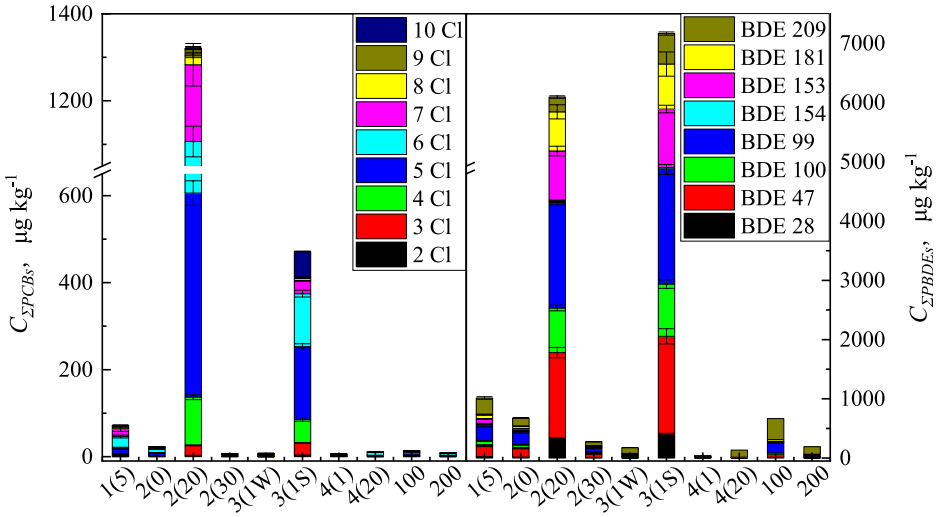

FIGURE 3
Distribution of Σ_{20}PCBs and Σ_8PBDEs in the dismantling ruins and surrounding soils. 1(5): 5 m away from No. 1 ruins; 2(0): No. 2 ruins; 2(20): 20 m away from No.2 ruins; 2(30):30 m away from No.2 ruins; 3(1S):1 m away to the south of No.3 ruins; 3(1W): 1 m away to the west of No.3 ruins; 4(1): 1 m away from No.4 ruins; 4(20): 20 m away from No.4 ruins; 100: 100 m away from No.1, No.2 and No.3 ruins; 200: 200 m away from No.1, No.2 and No.3 ruins.

in 2(20) topsoil was 1,321.3 ± 132.1 μg kg^{-1}, which was the highest value, followed by 471.8 ± 32.8 μg kg^{-1} at the paddy soil of 3(1S). This value reached 72.2 ± 24.2 μg kg^{-1} at the paddy soil of 1(5) and is lower than that at 3(1S). The concentration of $\sum_{20}$PCBs at the farmland soil in 4(1) was 6.4 ± 1.1 μg kg^{-1}, which was the lowest value.

Different content of $\sum_{20}$PCBs in different dismantling ruins and surrounding soils due to the different stacking time of electronic circuit board plastic powder. The pollutant content around the ruins with long stacking time is high, and the pollutant content around the ruins with short stacking time is relatively low. The geographical site of the No. 3 ruins is the most convenient. Thus, the accumulation time of plastic powder in No. 3 dismantling ruins is the longest. Therefore, the concentration of $\sum_{20}$PCBs at the paddy soil in 3(1S) is the highest. The No.4 ruins had the shortest time for the stacking of plastic powder, resulting in the lowest $\sum_{20}$PCB concentration.

Based on the $\sum_{20}$PCBs in the subsoil of 2(0), vegetable field topsoil of 2(20) and 2(30), the $\sum_{20}$PCBs in the topsoil of 2(20) was the highest with the value of 1,321.3 ± 132.1 μg kg^{-1}, followed by 23.1 ± 1.3 μg kg^{-1} in the subsoil in 2(0). The $\sum_{20}$PCBs in 2(30) was the lowest with the value of 7.1 ± 0.9 μg kg^{-1}. Considering that the No. 2 dismantling ruins are on the hillside, the plastic powder and the pollutants have been washed by rain for a long time and gathered at the foot of the mountain under the action of gravity. Consequently, the $\sum_{20}$PCBs of the topsoil in 2(20) is remarkably higher than that in the subsoil in 2(0). The content of $\sum_{20}$PCBs of farmland topsoil in 2(30) is lower than that of the subsoil (>40 cm) in 2(0) and the topsoil in 2(20). The main reason is that the altitude of 2(30) is slightly higher than that of 2(20), it is further away from the No. 2 ruins, and the waste plastic powder and its pollutants were washed from the No. 2 ruins and gathered at 2(20) but not at 2(30).

The content of $\sum_{20}$PCBs of paddy soil in 3(1S) and 3(1W) remarkably differed, and the content of $\sum_{20}$PCBs in 3(1S) reached 471.8 ± 32.8 μg kg^{-1}. Meanwhile, the content in 3(1W) was only 7.7 ± 1.5 μg kg^{-1}, mainly because 3(1W) has the same altitude as the No. 3 ruins, while the paddy field in 3(1S) is approximately 40 cm lower than the No. 3 ruins, and the pollutants preferentially gather and diffuse to a low-lying direction.

The content of $\sum_{20}$PCBs in paddy soil of 100 and 200 m away from No. 1, No. 2, and No. 3 dismantling "ruins" decreased with the increase in radial distance, and it reached 14.2 ± 0.8 μg kg^{-1} at a distance of 100 m away and 9.2 ± 1.4 μg kg^{-1} at a distance of 200 m. The content of $\sum_{20}$PCBs at the 100 m paddy soil is lower than that in 1(5) and 3(1S), and the content of $\sum_{20}$PCBs at the 200 m paddy soil is lower than that at the 100 m paddy soil. With the increase in the distance from the ruins of plastic powder stacking, the content of $\sum_{20}$PCBs in soil gradually decreased as a result of the horizontal diffusion of pollutants. Therefore, the main sources of PCBs in the soil of Nanwan village are the dismantling of electronic circuit boards and the accumulation of waste plastic circuit board powders.

The content of $\sum_{20}$PCBs in paddy soil at 100 m away from No. 1, No. 2, and No. 3 dismantling ruins is slightly higher than that of 2(30), mainly because the 100 and 200 m paddy fields have the same altitude as that of 3(1S) and are lower than the vegetable

field of 2(20). However, the vegetable field of 2(30) is slightly higher than that of 2(20). Pollutant diffusion preferentially spreads from No. 2 ruins to the vegetable field of 2(20), and then to the paddy soil of 100 m. The diffusion of PCBs includes the horizontal diffusion of pollutants and the vertical diffusion caused by groundwater and surface runoff. The diffusion of PCBs from 2(20) to 2(30) mainly involves horizontal diffusion caused by soil and atmosphere.

In addition, the content of $\sum_{20}$PCBs in the vegetable field soil of 4(1) is 6.4 ± 1.1 μg kg^{-1}, which is lower than 11.3 ± 3.5 μg kg^{-1} at 4(20). Considering that the No. 4 ruins is inclined, the content of $\sum_{20}$PCBs in farmland soil of 4(20) is significantly lower than that in 4(1). Considering the downward accumulation of pollutants caused by rainwater scouring, the content of $\sum_{20}$PCBs in the vegetable field soil of 4(1) is lower than that of 4(20).

4.1.2 Characteristics and ecological risk assessment of $\sum_{20}$PCBs in dismantling ruins and surrounding soils

China's Soil Environmental Quality—Risk control Standard for Contamination of Agricultural Land (Trial, GB15618-2018) does not provide corresponding guidance values for PCBs in farmland soil. Different countries and regions abroad provide different regulatory guidance values of ΣPCBs for farmland soil. The Canadian soil quality guide stipulates that ΣPCBs in farmland soil is limited to 0.5 mg kg^{-1}, and the preventive values of ΣPCBs by German soil protection regulations for sensitive use are 0.1 mg kg^{-1} (humus content <8%) and 0.05 mg kg^{-1} (humus content >8%). The soil quality standards of the Netherlands and Czech Republic stipulate that ΣPCBs in farmland soil is limited to 0.02 mg kg^{-1}, while that of the United States stipulates that the screening value of ΣPCBs in soil based on groundwater protection is 0.026 mg kg^{-1}. The content of Σ_{20}PCBs in the topsoil of 2(20) exceeded the screening value or the abovementioned limiting values for farmland soil. The content of Σ_{20}PCBs in the paddy soil of 3(1S) is only lower than the limit of ΣPCBs in the farmland soil specified by the Canadian soil quality guide, indicating the presence of ecological risks in the No. 2 and No. 3 ruins and the surrounding farmland soils, and this area is not suitable for agricultural use any more.

Other studies on PCBs in farmland soil carried out in the adjacent areas of this study pointed out that the average concentration of ΣPCBs was 0.509 mg kg^{-1}, the maximum concentration was 7.914 mg kg^{-1}, and the minimum concentration was 0.027 mg kg^{-1} in Wenqiao Town, Wenling City in 2007. According to the detailed investigation of soil pollution in 2013, the Wenqiao town has 42 sites, the average concentration of ΣPCBs was 0.206 mg kg^{-1}, the maximum and minimum concentrations were 2.994 and 0.023 mg kg^{-1}, and the over standard rate of ΣPCBs was 40.48%. In the present study, the average content of Σ_{20}PCBs in all soil samples was 0.142 mg kg^{-1}, the maximum concentration was 1.321 mg kg^{-1}, and the minimum concentration was 0.006 mg kg^{-1}. Evidently, the pollution degree of PCBs in the study area has improved with the passage of time, because the dismantling activities of electronic products had stopped as early as around 2006, the input of large number of exogenous PCBs has stopped, and the original PCBs in the soil gradually migrated and transformed, resulting in a decreasing trend of PCBs content in the study area.

In comparison with the ΣPCBs in the soils of other regions, which are also the dismantling places of e-waste in this study, the average content of Σ_{39}PCBs in the soil of an electronic waste recycling plant in Guanzhong area of China was 18.95 μg kg^{-1}, which reached 20.31 μg kg^{-1} in the soil of Jiangcungou landfill, and then reached 33.89 μg kg^{-1} in the soil of waste compression station and waste recovery point (Liu et al., 2021). The content of ΣPCBs in an electronic waste recycling town soil of northern Vietnam is in the range of 2.0–7,200 μg kg^{-1} (Fujimori et al., 2018). The highest content of Σ_{26}PCBs in the topsoil of e-waste recycling sites and nearby open-air waste sites near New Delhi (North), Kolkata (East), Mumbai (West), and Chennai (South) was 437 μg kg^{-1} in Chennai, followed by 102 μg kg^{-1} in Mumbai (Chakraborty et al., 2018). The average content of Σ_{19}PCBs in the soil of Fengjiang Town (another town for e-waste disassembly and recycling), Luqiao District, Taizhou city, is 431 (11.7–2.61 × 10^3) μg kg^{-1}, while that in Luqiao coastal metal resources regeneration industrial base was 15.5 (0.350–50.8) μg kg^{-1} (Liu et al., 2019). The contents of ΣPCBs in the soil of Guanzhong electronic waste resource recycling plant, Jiangcungou landfill, Luqiao waste compression station, and Luqiao Binhai waste recycling metal resource regeneration industrial base were considerably lower than that in the study area, and while those in the soil of Fengjiang Town, Luqiao District, northern Vietnam, and southern India (Chennai) were much higher than that in the study area. This finding was obtained, because the types and concentrations of pollutants differ because of the different types of electronic products disassembled in different electronic product disassembly sites and different service times.

The content of ΣPCBs was 3.25 (2.92–3.38) μg kg^{-1} in the organic farmland soil in Hong Kong, China and 5.96 (2.67–16.5) μg kg^{-1} in the ordinary farmland soil (Yu et al., 2011). The average concentration of Σ_7PCBs in the farmland topsoil in the Yellow River irrigation area is 11.18 μg kg^{-1} (Yao, 2019). The concentration of Σ_{209}PCBs in soils across China was in the range of 64.3–4,358 pg g^{-1} (Mao et al., 2021). The concentrations of Σ_{26}PCBs is 0.256–2.140 μg kg^{-1} on dry weight basis in surface soils (Wang et al., 2010). The content of Σ_7PCBs in farmland soil in the southwest of Buenos Aires Province, Argentina is 0.04–1.67 μg kg^{-1} (Tombesi et al., 2017). The levels of PCBs ranged from 10.46 ng g^{-1} for PCB 105 to 89.46 ng g^{-1} for PCB180, with an average PCB value of 25.47 ± 1.26 ng g^{-1}, in the banks of the Umgeni River soil, KwaZulu-Natal, South Africa (Gakuba et al., 2019). The content of ∑PCBs was <0.003–0.807 ng g^{-1}, and congener Nos. 114, 138, and

187 were the most abundant in Victoria Land, East Antarctica (Corsolini et al., 2019). The content of Σ_{18}PCBs in 25 soil sampling sites within a radius of 6 km around an e-waste treatment site in Hangzhou was 0.051–1.835 μg kg^{-1}(Zhou et al., 2020). In comparison with the content of ΣPCBs in farmland soil, the content of $\sum_{20}$PCBs in the study area is significantly higher, except for the riverbank soil in South Africa, which is obviously affected by the disassembly of electronic circuit boards and the accumulation of plastic powder of waste circuit boards.

By comparing the detection results of Σ_{20}PCBs in the soils of different electronic circuit board plastic powder dismantling ruins with the Environmental Quality Standard for sediments proposed by Long et al., the content of Σ_{20}PCBs in the topsoil of 2(20) and the paddy soil of 3(1S) exceeds the ERM value, indicating that the probability of biological toxicity events would frequently occur, and PCBs could be toxic to the organisms in the study area. The contents of Σ_{20}PCBs in the subsoil (>40 cm) of 2(0) and the topsoil of 1(5) are between the ERL and ERM value, indicating that the probability of biological toxicity events may occur, and PCBs may have toxic effects on organisms in the study area. However, the content of Σ_{20}PCBs in other soil samples is lower than ERL value, indicating that the probability of biological toxicity effect would be rarely observed.

Based on the distribution characteristics of PCBs, among the 20 PCBs investigated, the contents of PCB 101, PCB 138, and PCB 153 in the topsoil of 2(20) are higher than the ERM value, and the contents of PCB 44, PCB 66, PCB 105, PCB 118, PCB 128, PCB 170, PCB 180, and PCB 187 in the topsoil of 2(20) and those of PCB 101, PCB 118, PCB 126, PCB 138, PCB 153, and PCB 209 in the paddy soil of 3(1S) are between the ERL and ERM value. Whether from the total amount of PCBs or the content of individual PCBs, certain ecological risks are present in the ruins of waste electronic circuit board plastic powder accumulation in Nanwan village and the surrounding farmland soil, and some areas are not suitable for use as farmland. The composition of PCBs in the topsoil of 2(20) and the paddy soil of 3(1S) is similar, indicating that the content of PCBs containing four chlorine atoms (4Cl), five chlorine atoms (5CL), six chlorine atoms (6Cl), seven chlorine atoms (7Cl), and 10 chlorine protons (10Cl) are higher, while the content of PCBs containing two chlorine atoms (2Cl), three chlorine atoms (3Cl), eight chlorine atoms (8Cl), and nine chlorine atoms (9Cl) are low.

4.1.3 Concentration of $\sum_8$PBDEs in the dismantling ruins and surrounding soils

The distribution of Σ_8PBDEs content in the waste electronic circuit board plastic powder stacking ruins and surrounding soil is shown in Figure 3. The content of Σ_8PBDEs in the dismantling ruins and surrounding soils is similar to that of $\sum_{20}$PCBs. The contents of Σ_8PBDEs in the vegetable field soil of 2(20) and paddy soil of 3(1S) are significantly higher than that in other points. The highest value of Σ_8PBDEs in the dismantling ruins and surrounding soils was recorded in the paddy soil of 3(1S) with a value of 7,216.9 ± 232.0 μg kg^{-1}, followed by 6,094.3 ± 389.2 μg kg^{-1} in the vegetable field soil of 2(20), and these values slightly differ from the content of $\sum_{20}$PCBs. The content of Σ_8PBDEs was 1,010.8 ± 36.2 μg kg^{-1} in the paddy soil of 1(5) and 40.3 ± 1.4 μg kg^{-1} in the vegetable field of 4(1).

Considering the combined action of horizontal and vertical diffusion of pollutants, the content of Σ_8PBDEs in the topsoil (0-10 cm) of 2(20) is higher than that in the subsoil (>40 cm) of 2(0) (677.8 ± 35.7 μg kg^{-1}), and the lowest value of 276.1 ± 22.2 μg kg^{-1} was obtained in the vegetable field soil of 2(30). The content of Σ_8PBDEs in the paddy soil of 3(1S) and vegetable field soil of 3(1W) remarkably differ with the value of 7,216.9 ± 232.0 μg kg^{-1} in the paddy soil of 3(1S), which is far higher than 177.6 ± 2.3 μg kg^{-1} in the vegetable field soil of 3(1W). In addition, the content of Σ_8PBDEs in the vegetable field soil of 4(1) is 40.3 ± 1.4 μg kg^{-1}, which is also lower than 135.3 ± 6.4 μg kg^{-1} in 4(20), mainly because the ruins of No. 4 is sloped with a certain inclination, and the combined action of horizontal and vertical diffusion increased the content of Σ_8PBDEs in the vegetable field soil of 4(20).

In the paddy soils 100 and 200 m away from the ruins of No. 1, No. 2, and No. 3, the content of Σ_8PBDEs decreased with the increase in radial distance with values of 667.3 ± 26.2 μg kg^{-1} at 100 m and 191.5 ± 12.5 μg kg^{-1} at 200 m. The content of Σ_8PBDEs in paddy soil of 100 m is lower than those in the paddy soil of 1(5), vegetable field soil of 2(20), and paddy soil of 3(1S), but it is higher than that in the vegetable field soil 2(30) (276.1 ± 22.2 μg kg^{-1}) and that in the vegetable field soil of 3(1W) (177.6 ± 2.3 μg kg^{-1}). This phenomenon is also the result of the joint action of horizontal diffusion and vertical diffusion.

4.1.4 Characteristics of $\sum_8$PBDEs in dismantling ruins and surrounding soils

Eight PBDEs were all detected in the dismantling ruins and all surrounding soil samples, and the content of BDE 209 was notably high. Among all the PBDEs investigated, the percentage content of BDE 209 exceeded 20% in most soil samples, except that in the vegetable field soil of 2(20) and the paddy soil of 3(1S). The percentage content of BDE 209 was 53.2% in the paddy soil 100 m away from No. 1, No. 2, and No. 3 ruins, 55.9% in paddy soil of 3(1W), and 65.7% in the paddy soil 200 m away from No. 1, No. 2, and No. 3 ruins. The highest percentage content of BDE 209 was 88.3% in the vegetable field soil of 4(20).

Zhongzhi Yang inspected the contents of $\sum_{39}$PBDEs in soil samples of Nanwan village in 2006 and found that the content of BDE 209 accounted for 72.4% of the detected Σ_{39}PBDEs. Moreover, PBDEs in soil samples in Nanwan village had a degradation trend (Yang, 2009). This result was consistent with the findings of Zhongzhi Yang's research, except for the high percentage content of BDE 209 in the vegetable field soil of 4(20), in which the percentage content of BDE 209 in other samples is significantly lower than Zhongzhi Yang's research

results. This finding was obtained, because the dismantling activities of electronic circuit boards in Nanwan village had stopped around 2006, and the accumulated plastic circuit board powder was gradually cleaned up after that. Without the input of exogenous PBDEs, the highly brominated PBDEs existing in the environment were gradually degraded to low brominated PBDEs, thus decreasing the percentage content of BDE 209. The percentage content of BDE 209 in the vegetable field soil of 4(20) is high, mainly because the stacking time of PBDEs is short, and the accumulated plastic powder of electronic circuit board has not been cleaned up because of inconvenient transportation. In addition, the percentage contents of BDE 47, BDE 99, and BDE 209 in the study area were high, which is consistent with the research results of Zhongzhi Yang. Therefore, the PBDEs in the study area were obtained from the dismantling activities of electronic products and the accumulation of dismantling waste.

Although the human intake of PBDEs through food would lead to liver enlargement, affect the development of brain, reproductive organs, neurobehavior, and interfere with the level of thyroxine, a soil environmental quality standard for farmland soil on PBDEs has not been formulated at home or abroad. Moreover, neither farmland soil nor construction land in China has not been provided with guidance or control value to PBDEs. The general soil screening value of USEPA sets the soil screening value based on groundwater protection as follows: 97 μg kg^{-1} for BDE 47, 160 μg kg^{-1} for BDE 99, and 53 mg kg^{-1} for BDE 209. In comparison with the results for the soil screening value based on groundwater protection provided by the USEPA, the values for BDE 47 in the paddy soil of 1(5), the subsoil of 2(0), the vegetable field soil of 2(20), and the paddy soil of 3(1S) were all exceeded, and the exceeding rate was 40%. The BDE 47 content in the vegetable field soil of 2(20) and paddy soil of 3(1S) are 15 and 20 times higher than the screening value based on groundwater protection. The BDE 99 content in the paddy soil of 1(5), the subsoil of 2(0), the vegetable field soil of 2(20), the paddy soil of 3(1S), and the 100 m paddy soil all exceeded the screening value based on groundwater protection, and the exceeding rate was 50%. The BDE 99 contents of the vegetable field soil of 2(20) and the paddy soil of 3(1S) were 11 and 12 times higher than the screening value based on groundwater protection. The content of PBDEs in some soil samples at or around the stacking ruins of waste electronic circuit board plastic powder in Nanwan village are higher than the screening value based on groundwater protection in the United States, indicating that the soil in the village may have a certain risk to groundwater caused by the pollution of PBDEs.

The concentrations of BDE 209 were in the range of 0.496–2.040 μg kg^{-1} on dry weight basis in the surface soils of the Tongzhou district, Beijing City, and it accounts for more than 96% of the total PBDEs (Wang et al., 2010). The average concentration of ∑PBDEs in the farmland soil of Longtang-Shijiao town, Guangdong Province, was 19.0 ± 20.1 μg kg^{-1}, which was much lower than that in the roadside soil and in topsoil near the e-waste dismantling sites (Jiao et al., 2016). The concentrations of Σ_8PBDEs were in the range of 29–240 ng kg^{-1} in Jinsha, which is one of the regional background sites in Central China (Zhan et al., 2019). The average $\sum_8$PBDEs in the farmland soil of Baotou city, China, ranged from 1.25 μg kg^{-1}–13.3 μg kg^{-1}, with an average of 3.62 μg kg^{-1}, and a median of 2.91 μg kg^{-1} (Chen et al., 2020). In comparison with this study, the content of ∑PBDEs in farmland soil in the study area was remarkably higher than that in other areas of China, indicating that the farmland soil in Nanwan village was obviously affected by the disassembly activities of electronic circuit board and the stacking of waste plastic powder.

The content of Σ_{25}PBDEs in 66 farmland soil samples collected from an e-waste dismantling area in Taizhou city was 0.13–11.80 μg kg^{-1}, in which the mass concentration of BDE 209 accounted for 50.9%–98.3% (Zhang et al., 2018). The content of PBDEs was 182.5 ± 38.72 μg kg^{-1} in farmland soil near an e-waste dismantling area in Wenling city, China (Zhang et al., 2015). The concentrations of Σ_{12}PBDEs in the farmland soil of e-waste dismantling site in Fengjiang Town and Binhai Town were 21.8–1,310 and 6.19–220 μg kg^{-1}, respectively (Wei et al., 2020). The content of Σ_{13}PBDEs around an e-waste dismantling site in Guiyu, Guangdong Province was 62–76 μg kg^{-1} in rice field soil and 46-58 μg kg^{-1} in vegetable field soil (Li et al., 2018). The total concentration of ΣPBDEs in the surrounding area of an e-waste dismantling park was 11.6–3.60 × 10^4 μg kg^{-1} in Guiyu (Ge et al., 2020). PBDEs were the most abundant at 0.343–69.306 μg kg^{-1} in soils from an e-waste disposal site in Hangzhou (Zhou et al., 2020). The Σ_{13}PBDE concentrations in soils around an open-burning sites in northern Vietnam were 7.6 (1.6 ± 62.0) μg kg^{-1} in 2012, 12.0 (0.1 ± 48.0) μg kg^{-1} in 2013, and 16.0 (2.1 ± 39.0) μg kg^{-1} in 2014. The concentrations were 1,200 (67-9,200) μg kg^{-1} in 2012, 480 (37-3,900) μg kg^{-1} in 2013, and 490 (39-2,900) μg kg^{-1} in 2014 in soils around the electronic waste-processing workshops (Matsukami et al., 2017). Generally, the measured concentrations of PBDEs in the soils analyzed in the present study were higher than or close to those in other areas at home or abroad, which are also the areas of electronic product disassembly.

4.2 Vertical distribution of Σ_{20}PCBs and Σ_8PBDEs in farmland soils around the ruins

The vertical distribution of Σ_{20}PCBs and Σ_8PBDEs in farmland soil around the ruins is shown in Figure 4. When the depth away from the surface soil increased from 0-10, 10-20, 20-30, and 30-40 cm to >40 cm, the content of Σ_{20}PCBs in farmland soils of 1(5) changed from 48.075 ± 5.133, 96.376 ± 43.293, 25.879 ± 2.199, and 7.49 ± 0.737 μg kg^{-1} to 8.625 ± 0.363 μg kg^{-1}, respectively. The disassembly activities of

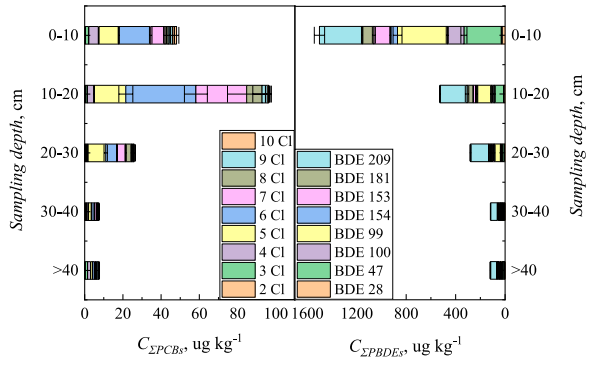

FIGURE 4
Vertical distribution of Σ_{20}PCBs and Σ_8PBDEs in paddy soil around the dismantling ruins.

electronic circuit boards in Nanwan village stopped around 2006, and the stacking electronic circuit board powder had been removed from 2011 to 2014 (except No. 4 ruins). Although the paddy field was deserted at the time of sampling, nearly 10 years had passed, and it is impossible to be barren at that place all the time. With the progress of farming activities, the 0-20 cm topsoil turned up and down coupled with the migration and diffusion of pollutants. As a result, the content of Σ_{20}PCBs in paddy soil with the depth of 10–20 cm is higher than that at 0-10 cm. As shown in Figure 4, with the continuous increase in depth from the surface, the content of Σ_{20}PCBs remarkably decreased because of the vertical diffusion of pollutants. Therefore, the PCBs in the soil were obtained from the disassembly activities and the stacking of electronic circuit boards, and the PCBs in the soil gradually dispersed from the surface to the deep soil until a certain number of PCBs remained detected at the soil depth of >40 cm. The content of Σ_{20}PCBs increased slightly as the depth exceeded 40 cm because of the dual action of surface subsidence and groundwater migration.

The percentage contents of 5Cl, 6Cl, and 7Cl are relatively high, and their total contents accounted for 73%, 77%, 76%, 57%, and 36% of the total amount of Σ_{20}PCBs at the depth of 0–10, 10–20, 20–30, 30–40, and >40 cm soil layer, respectively. Similarly, except for the topsoil, with the increase in soil vertical depth, the percentage contents of PCBs containing 5Cl, 6Cl, and 7Cl decreased gradually, and the percentage contents of PCBs containing 2Cl, 3Cl, and 4Cl increased gradually, indicating that PCBs in the soil tended to degrade gradually from high chlorination to low chlorination.

When the depth away from the surface soil increased from 0–10, 10–20, 20–30, and 30–40 cm to >40 cm, the contents of Σ_8PBDEs in paddy soil at 1(5) changed from 1,501.239 ± 52.965, 520.315 ± 19.425, 279.794 ± 14.974, and 117.457 ± 8.695 μg kg^{-1} to 119.336 ± 10.673 μg kg^{-1}, respectively. The content of Σ_8PBDEs in paddy soil of 1(5) decreased vertically with the increase in depth, indicating that the content of Σ_8PBDEs in soil gradually diffuses vertically from the surface to the deep layer, and a few PBDEs were detected in the soil at a depth higher than 40 cm. The content of Σ_8PBDEs increased slightly at a depth >40 cm as a result of the dual action of surface subsidence and groundwater migration. Zhongzhi Yang (Yang, 2009) sampled in the same study area around 2006 and found that the concentration of PBDEs decreased rapidly with the increase in soil depth, which is consistent with the results of the present study. By contrast, when Zhongzhi Yang obtained the samples, the disassembly activities of electronic circuit board were still in progress, and the vertical change of PBDEs observed was only within the range of 0–20 cm from the surface, while the soil depth investigated in the present study was deeper, and the soil depth range >40 cm from the surface was investigated.

Among the eight PBDEs investigated, BDE 47, BDE 99, and BDE 209 have relatively high percentage contents in the paddy soil of 1(5) because of the large commercial consumption of BDE 47, BDE 99, and BDE 209. The highest percentage content of PBDEs was observed in BDE 209; among all soil samples at the depth of 0 to >40 cm, the lowest percentage content of BDE 209 was 23% at the depth of 0–10cm, while the highest percentage of 53% was observed at the depth of 20–30 cm, and it arrange 42%–47% in other depth's soil. The contents of BDE 99 at the soil depths of 0–10, 10–20, 20–30, 30–40, and >40 cm were 27%, 22%, 18%, 7%, and 9% respectively, showing an obvious downward trend. The percentage contents of BDE 47 at the soil depths of 0–10, 10–20, 20–30, 30–40, and >40 cm were 20%, 15%, 7%, 11%, and 14%, respectively. Among all the eight PBDEs investigated, the lowest percentage contents were obtained for BDE 28 and BDE 154, the values at all soil depths did not exceed 8%.

4.3 Distribution of Σ_{20}PCBs and Σ_8PBDEs in the crops around the ruins

To further investigate the effect of soil organic pollutants on the crops around the ruins, we investigated the contents of Σ_{20}PCBs and Σ_8PBDEs in the directly edible parts of four crops, such as oranges planted in the 100 m orchard away from No. 1 ruins, mung beans and garlic planted in the 2 m and 5 m vegetable field to the west of No. 3 ruins, and ginger in the No. 4 stacking ruins. The results are shown in Figure 5. The contents of Σ_{20}PCBs in the edible parts of garlic, ginger, mung bean, and orange were 8.269 ± 2.735, 30.448 ± 2.287, 6.429 ± 2.065, and 7.458 ± 1.250 μg kg^{-1}, respectively. The percentage contents of PCBs containing 5Cl, 6CL, and 7Cl in the edible part of garlic all exceeded 10%, and the total amount of these three kinds of chlorinated PCBs to Σ_{20}PCBs reached 64%. The percentage contents of PCBs containing 3Cl, 4Cl, 5Cl, and 6Cl

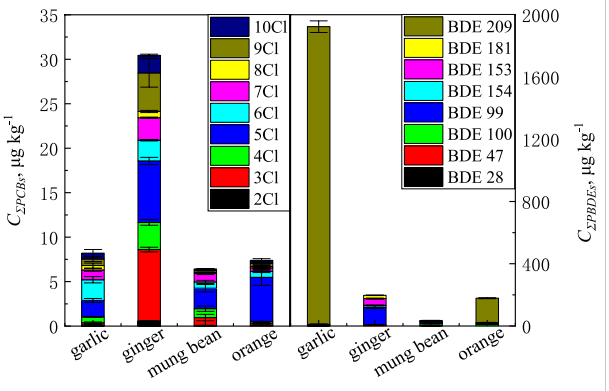

FIGURE 5
Concentration of Σ_{20}PCBs and Σ_8PBDEs in the edible parts of crops.

in edible parts of ginger all exceeded 10%, and the total percentage content of these four kinds of chlorinated PCBs to Σ_{20}PCBs reached 73%. The percentage contents of PCBs containing 3Cl, 4Cl, 5Cl, 6Cl, and 7Cl in the edible parts of mung bean all exceeded 10%, and the total percentage content of these kinds of chlorinated PCBs to Σ_{20}PCBs reached 92%. The percentage content of PCBs containing 5Cl in the edible part of oranges was particularly high, reaching 68%, and the percentage contents of other chlorinated PCBs were all less than 10%. In addition, among the four crops investigated, the content of Σ_{20}PCBs in the edible part of ginger reached 30.448 ± 2.287 μg kg^{-1}, which exceeded the first-class limitation value of construction land set in the National Soil Environmental Quality Standard GB 36620–2018 (Trial, GB 36600-2018). This high content of PCBs in construction land might pose risks to human health, and possible food safety problems should be looked into.

The contents of Σ_8PBDEs in the edible parts of garlic, ginger, mung bean, and orange were 1,923.132 ± 39.545, 197.197 ± 7.050, 35.621 ± 1.461, and 178.77 ± 3.577 μg kg^{-1}, respectively. Among the four crops investigated, the content of Σ_8PBDEs in garlic reached 1,923.123 ± 39.545 μg kg^{-1}. Although no relevant standard data are available, this content is significantly higher than the content of PBDEs in farmland soil at home or abroad,

TABLE 3 Carcinogenic risks and non-carcinogenic risks of PCBs and PBDEs in soils.

Sampling cites and depth	TQ				TR (×10^{-6})	
	∑PBDEs		∑PCBs		BDE 209	∑PCBs
	Children	Adult	Children	Adult		
1(5)	0.0861	0.0110	0.0604	0.0077	0.0011	0.79
2(0) >40 cm	0.0678	0.0086	0.0193	0.0025	0.0005	0.25
2(20) <10 cm	0.6205	0.0787	1.1053	0.1402	0.0010	14.49
2(30)	0.0245	0.0030	0.0059	0.0008	0.0003	0.08
3(1)S	0.6948	0.0881	0.3964	0.0501	0.0020	5.18
3(1)W	0.0092	0.0011	0.0064	0.0008	0.0004	0.08
4(1)	0.0022	0.0002	0.0054	0.0007	0.0001	0.07
4(20)	0.0016	0.0001	0.0094	0.0012	0.0005	0.12
100	0.0399	0.0051	0.0118	0.0015	0.0014	0.16
200	0.0071	0.0008	0.0077	0.0010	0.0005	0.10

TABLE 4 Carcinogenic risks and non-carcinogenic risks of PCBs and PBDEs in crops.

Crops	TQ								TR (×10^{-6})	
	BDE 47	BDE 99	BDE 100	BDE 153	BDE 154	BDE 209	∑PBDEs	∑PCBs	BDE 209	∑PCBs
Garlic	0	0.005	0	0	0	0.019	0.024	0.028	0.733	1.133
Ginger	0.005	0.078	0	0.015	0.004	0	0.102	0.104	0	4.171
Mung bean	0.009	0.054	0.002	0.010	0.002	0	0.077	0.132	0	5.284
Orange	0	0.215	0.013	0.032	0.017	0.007	0.338	0.112	0.263	4.495

which may cause food safety problems that need to be solved. The percentage content of BDE 209 to Σ_8PBDEs in the edible parts of garlic and orange accounted for 99% and 87% respectively, indicating that garlic and orange easily absorb BDE 209. In comparison with other PBDEs, the percentage content of BDE 99 in the edible part of ginger and mung bean was the highest, reaching 58% and 37%, respectively.

Among the four crops investigated, whether Σ_{20}PCBs or Σ_8PBDEs, the content in the edible parts of ginger and garlic are higher than that in the edible parts of oranges and mung beans. The edible parts of ginger and garlic grow in the soil, while the edible parts of mung beans and oranges hang on the branches of plants, indicating that the PCBs and PBDEs in crops were mainly derived from contaminated soil. The contents of 20 PCBs and 8 PBDEs in different crops differed mainly because of the different types of dismantling and stacking waste electronic circuit boards in different dismantling ruins, as well as the different types of pollutants. In addition, the absorption and accumulation of different kinds of PCBs and PBDEs by different crops differed.

4.4 Human health risk assessment of PCBs and PBDEs

Table 3 shows the lifetime carcinogenic risk level and non-carcinogenic level of PCBs and PBDEs in the dismantling ruins and surrounding soils. Among all the soil samples, only Σ_{20}PCBs in the topsoil of 2(20) and the paddy soil of 3(1S) had a TR value that is higher than the individual lifetime carcinogenic risk value (10^{-6}), and both values were lower than the individual lifetime carcinogenic acceptable risk level (10^{-4}), indicating that the lifetime carcinogenic risk level of PCBs and PBDEs in the dismantling ruins and surrounding farmland soil are at acceptable or negligible levels. Among all the soil samples, only the TQ value of PCBs for children in the topsoil of 2(20) is higher than 1, suggesting that the non-carcinogenic risk of PCBs is high among children. All the TQ values of PBDEs for children and adults are lower than 1, indicating that the PBDE level is safe for non-carcinogenic risk.

The crop samples collected in the present study are directly edible parts. Therefore, the food chain is the main exposure route for health risk assessment. According to the average intake of each crop in lifetime, the carcinogenic risk level and non-carcinogenic level of the corresponding crops in lifetime can be calculated. The results are shown in Table 4. As shown in Table 4, the TQ values of PBDEs for the four crops are far less than 1, indicating that the non-carcinogenic risks of PBDEs and PCBs levels are at a safe level. The TR values of BDE 209 in the edible parts of garlic, ginger, mung bean, and orange are all lower than 10^{-6}, indicating the carcinogenic levels caused by BDE 209 in the four crops are at negligible levels. However, the TR values of PCBs in the edible parts of garlic, ginger, mung bean, and orange are all between 10^{-6} and 10^{-4}, indicating that the carcinogenic levels caused by PCBs in the crops are at acceptable levels.

5 Conclusion

Among the four dismantling ruins and surrounding soil samples investigated, the most polluted soil was the vegetable field topsoil of 2(20) and the paddy soil of 3(1S), the content of Σ_{20}PCBs in the vegetable field topsoil of 2(20) was 1,321.3 ± 132.1 μg kg^{-1}, and the content of Σ_8PBDEs in the paddy soil of 3(1S) reached 7,216.9 ± 232.0 μg kg^{-1}. With the increase in soil depth, the content of Σ_{20}PCBs and Σ_8PBDEs remarkably decreased because of the vertical diffusion of pollutants. Therefore, the pollutants in the soil came from the disassembly activities and accumulation of electronic circuit boards, and the pollutants in the soil gradually dispersed from the surface soil to the deep soil, until a certain number of pollutants were still detected at the soil depth above 40 cm. The content of Σ_{20}PCBs and Σ_8PBDEs increased slightly when the depth exceeded 40 cm because of the dual action of surface subsidence and groundwater migration. In comparison with the content of $\sum_{20}$PCBs and $\sum_8$PBDEs in other farmland in this study, the content of $\sum_{20}$PCBs and $\sum_8$PBDEs of the study area was remarkably higher than that at home or abroad as a result of the dismantling activities of electronic circuit boards and the accumulation of plastic powder of waste circuit boards.

Ecological risk assessment showed that the content of Σ_{20}PCBs in the vegetable field topsoil of 2(20) and the paddy soil of 3(1S) exceed the ERM value, indicating that biological toxicity events are likely to occur frequently, and PCBs could be toxic to the organisms in the study area. The contents of Σ_{20}PCBs in the subsoil of 2(0) and topsoil of 1(5) are between ERL and ERM values, indicating that biological toxicity events may occur. Among all the soil samples, the lifetime carcinogenic and non-carcinogenic risks of PBDEs were at a safe level, and only the TQ value of PCBs for children in 2(20) topsoil is higher than 1, suggesting that the non-carcinogenic risk of PCBs is high among children. PCBs and PBDEs in the edible parts of garlic, ginger, mung bean, and orange are at a safe level for non-carcinogenic risk. The carcinogenic risks caused by BDE 209 and $\sum_{20}$PCBs of the crops are at negligible levels or acceptable levels.

Although this study can help in the decision-making process for monitoring soil pollution and food safety in Nanwan village, it also has some limitations. The risk assessment did not consider the synergistic or antagonistic effects between PCBs and PBDEs in soils or crops, or both. Moreover, the risk assessment did not consider the cumulative exposure to other environmental pollutants with a toxicity mechanism, such as Cu^{2+}, Cd^{2+}, and Pd^{2+}. The co-existence of such pollutants will affect the risk assessment of daily exposure. Therefore, systematic studies with larger scale sampling are necessary to expand the database.

Although the human intake of PBDEs through food would lead to some diseases, no soil environmental quality standard has been established for farmland soil on PBDEs has been formulated at home or abroad. Accordingly, appropriate and protective soil standards need to be urgently established to minimize human exposure from food producing animals housed outdoors. Moreover, pollution sources of POPs (e.g., PCBs and PBDEs) in soils need to be eliminated, and contaminated sites and reservoirs need to be controlled, secured, and remediated to reduce exposure and guarantee food safety.

Data availability statement

The original contributions presented in the study are included in the article/Supplementary Material, further inquiries can be directed to the corresponding author.

Author contributions

All authors contributed equally for the conception and writing of the manuscript.

Funding

This work was supported by Zhejiang Province National Science Foundation of China (No.LY20E080013) and Taizhou science and technology planning project by Taizhou Science and Technology Bureau (1902gy17).

Conflict of interest

The authors declare that the research was conducted in the absence of any commercial or financial relationships that could be construed as a potential conflict of interest.

Publisher's note

All claims expressed in this article are solely those of the authors and do not necessarily represent those of their affiliated organizations, or those of the publisher, the editors and the reviewers. Any product that may be evaluated in this article, or claim that may be made by its manufacturer, is not guaranteed or endorsed by the publisher.

References

Alfaro, M. R., Ugarte, O. M., Lima, L. H. V., Silva, J. R., da Silva, F. B. V., da Silva Lins, S. A., et al. (2022). Risk assessment of heavy metals in soils and edible parts of vegetables grown on sites contaminated by an abandoned steel plant in Havana. *Environ. Geochem. Health* 44 (1), 43–56. doi:10.1007/s10653-021-01092-w

Chakraborty, P., Selvaraj, S., Nakamura, M., Prithiviraj, B., Cincinelli, A., and Bang, J. J. (2018). PCBs and PCDD/Fs in soil from informal e-waste recycling sites and open dumpsites in India: Levels, congener profiles and health risk assessment. *Sci. Total Environ.* 621, 930–938. doi:10.1016/j.scitotenv.2017.11.083

Chen, Y. P., Zhao, Y., Zhao, M. M., Wu, J. H., and Wang, K. B. (2021). Potential health risk assessment of HFRs, PCBs, and OCPs in the Yellow River basin. *Environ. Pollut.* 275, 116648. doi:10.1016/j.envpol.2021.116648

Chen, Y., Zhang, A., Li, H., Peng, Y., Jun, J., Liu, M., et al. (2020). Concentrations and distributions of polybrominated diphenyl ethers (PBDEs) in surface soils and tree bark in Inner Mongolia, northern China, and the risks posed to humans. *Chemosphere* 247, 125950. doi:10.1016/j.chemosphere.2020.125950

Chinese Nutrition Society (2022). Dietary guidelines for Chinese residents. Available at: https://www.jandonline.org/article/S0002-8223(00)00257-1/fulltext#relatedArticles.

Corsolini, S., Baroni, D., Martellini, T., Pala, N., and Cincinelli, A. (2019). PBDEs and PCBs in terrestrial ecosystems of the Victoria Land, Antarctica. *Chemosphere* 231, 233–239. doi:10.1016/j.chemosphere.2019.05.126

Das, P., Gabriel, J. C. P., Tay, C. Y., and Lee, J. M. (2020). Value-added products from thermochemical treatments of contaminated e-waste plastics. *Chemosphere* 269, 129409. doi:10.1016/j.chemosphere.2020.129409

Fu, J., Wang, T., Wang, P., Qu, G., Wang, Y., Zhang, Q., et al. (2012). Temporal trends (2005-2009) of PCDD/Fs, PCBs, PBDEs in rice hulls from an e-waste dismantling area after stricter environmental regulations. *Chemosphere* 88 (3), 330–335. doi:10.1016/j.chemosphere.2012.03.006

Fujimori, T., Takigami, H., Agusa, T., Takaoka, M., Suzuki, G., Tue, N. M., et al. (2018). Soil pollution by chlorobenzenes and polychlorinated biphenyls from an electronic waste recycling area in Northern Vietnam. *Int. J. Environ. Pollut.* 63 (4), 283–297. doi:10.1504/ijep.2018.10019177

Gakuba, E., Moodley, B., Ndungu, P., and Birungi, G. (2019). Evaluation of persistent organochlorine pesticides and polychlorinated biphenyls in Umgeni River bank soil, KwaZulu-Natal, South Africa. *Water sa.* 45, 592–607. doi:10.17159/wsa/2019.v45.i4.7540

Gb36600 (2018). National standards of the people's republic of China. *Soil Environ. Qual. - Risk control Stand. Contam. Dev. land (Trial).*

Ge, X., Ma, S. T., Zhang, X. L., Yang, Y., Li, G. Y., and Yu, Y. X. (2020). Halogenated and organophosphorous flame retardants in surface soils from an e-waste dismantling park and its surrounding area: Distributions, sources, and human health risks. *Environ. Int.* 139, 105741. doi:10.1016/j.envint.2020.105741

Jiao, X., Chen, S., Deng, Y. J., and Wang, Y. X. (2016). PBDEs dynamic in farmland soils from an E-waste dismantling area in China (in Chinese). *Acta Sci. Circumstantiae* 36 (12), 4472–4481.

Li, H., Guardia, M. J. L., Liu, H., Hale, R. C., Mainor, T. M., Harvey, E., et al. (2019). Brominated and organophosphate flame retardants along a sediment transect encompassing the Guiyu, China e-waste recycling zone. *Sci. Total Environ.* 646, 58–67. doi:10.1016/j.scitotenv.2018.07.276

Li N, N., Chen, X. W., Deng, W. J., Giesy, J. P., and Zheng, H. L. (2018). PBDEs and dechlorane plus in the environment of Guiyu, southeast China: A historical location for E-waste recycling (2004, 2014). *Chemosphere* 199, 603–611. doi:10.1016/j.chemosphere.2018.02.041

Li Q, Q., Lu, Y., Wang, P., Wang, T., Zhang, Y., Suriyanarayanan, S., et al. (2018). Distribution, source, and risk of organochlorine pesticides (OCPs) and polychlorinated biphenyls (PCBs) in urban and rural soils around the Yellow and Bohai Seas, China. *Environ. Pollut.* 239, 233–241. doi:10.1016/j.envpol.2018.03.055

Li, Y., Chang, Q. M., Luo, Z., Zhang, J., Liu, Y. C., Duan, H. B., et al. (2020). Transfer of POP-BFRs within e-waste plastics in recycling streams in China. *Sci. Total Environ.* 717, 135003. doi:10.1016/j.scitotenv.2019.135003

Lim, Y. W., Kim, H. H., Lee, C. S., Shin, D. C., Chang, Y. S., and Yang, J. Y. (2014). Exposure assessment and health risk of poly-brominated diphenyl ether (PBDE) flame retardants in the indoor environment of elementary school students in Korea. *Sci. Total Environ.* 470-471, 1376–1389. doi:10.1016/j.scitotenv.2013.09.013

Liu, C., Wei, B. K., Bao, J. S., Wang, Y., Jin, J., Tang, Y. E., et al. (2019). Polychlorinated biphenyls in the soil–crop–atmosphere system in e-waste dismantling areas in Taizhou: Concentrations, congener profiles, uptake, and translocation. *Environ. Pollut.* 257, 113622. doi:10.1016/j.envpol.2019.113622

Liu, W., Yuan, Q., and Wang, S. (2021). Distribution characteristics of PCBs in typical soil and sludge in Guanzhong area. *J. Northwest Univ. (Nat. Sci. Ed.* 51 (1), 33–42.

Long, E. R., MacDonald, D. D., Smith, S. L., and Calder, F. D. (1995). Incidence of adverse biological effects within ranges of chemical concentrations in marine and estuarine sediments. *Environ. Manag.* 19 (1), 81–97. doi:10.1007/bf02472006

Mao, S., Liu, S., Zhou, Y., An, Q., Zhou, X., Mao, Z., et al. (2021). The occurrence and sources of polychlorinated biphenyls (PCBs) in agricultural soils across China with an emphasis on unintentionally produced PCBs. *Environ. Pollut.* 271, 116171. doi:10.1016/j.envpol.2020.116171

Matsukami, H., Suzuki, G., Someya, M., Uchida, N., Tue, N. M., Tuyen, L. H., et al. (2017). Concentrations of polybrominated diphenyl ethers and alternative flame retardants in surface soils and river sediments from an electronic waste-processing area in northern Vietnam, 2012–2014. *Chemosphere* 167, 291–299. doi:10.1016/j.chemosphere.2016.09.147

Shi, J., Xiang, L., Luan, H., Wei, Y., Ren, H., and Chen, P. (2019). The health concern of polychlorinated biphenyls (PCBs) in a notorious e-waste recycling site. *Ecotoxicol. Environ. Saf.* 186, 109817. doi:10.1016/j.ecoenv.2019.109817

Sun, J., Hang, T. J., Cao, L., Fan, X. L., Feng, Y. L., Li, T., et al. (2021). Assessment of polybrominated diphenyl ethers and emerging brominated flame retardants in Pheretima (a Traditional Chinese Medicine): Occurrence, residue profiles, and potential health risks. *Environ. Pollut.* 276, 116680. doi:10.1016/j.envpol.2021.116680

Tombesi, N., Pozo, K., Alvarez, M., Pribylova, P., Kukucka, P., Audy, O., et al. (2017). Tracking polychlorinated biphenyls (PCBs) and polybrominated diphenyl ethers (PBDEs) in sediments and soils from the southwest of Buenos Aires Province, Argentina (South eastern part of the GRULAC region). *Sci. Total Environ.* 575, 1470–1476. doi:10.1016/j.scitotenv.2016.10.013

USEPA (2008). *Regional screening levels for chemical contaminants at superfund sites.* Arlington, VA, USA: Chem. Specif. Param.

USEPA (2015). Regional screening levels for chemical contaminants at Superfund sites. Available at: https://www.epa.gov/risk/regional-screening-levels-rsls.

USEPA (2018). Regional screening levels (RSLs)-User's guide. Natl. Cent. Environ. Assess. c/o-Risk Website. Available at: https://www.epa.gov/risk/regional-screening-levels-rsls-usersguide.

Wang, D., Wang, Y., Singh, V. P., Zhu, J., Jiang, L., Zeng, D., et al. (2018). Ecological and health risk assessment of PAHs, OCPs, and PCBs in Taihu Lake basin. *Ecol. Indic.* 92, 171–180. doi:10.1016/j.ecolind.2017.06.038

Wang, T., Wang, Y. W., Fu, J. J., Wang, P., Li, Y. M., Zhang, Q. H., et al. (2010). Characteristic accumulation and soil penetration of polychlorinated biphenyls and polybrominated diphenyl ethers in wastewater irrigated farmlands. *Chemosphere* 81 (8), 1045–1051. doi:10.1016/j.chemosphere.2010.07.045

Wei, B. K., Liu, C., Wang, Y., and Jin, J. (2020). Polybrominated diphenyl ether in E-waste dismantling sites in Taizhou city, zhejiang province: Concentration, distribution, and migration trend. *Environ. Sci.* 41 (10), 4740–4748. doi:10.13227/j.hjkx.202003188

Wu, J., Hu, J. C., Wang, S. J., Jin, J. X., Wang, R., Wang, Y., et al. (2018). Levels, sources, and potential human health risks of pcns, pcdd/fs, and pcbs in an industrial area of shandong province, China. *Chemosphere* 199, 382–389. doi:10.1016/j.chemosphere.2018.02.039

Wu, Q., Leung, J. Y. S., Du, Y., Kong, D., Shi, Y., Wang, Y., et al. (2019). Trace metals in e-waste lead to serious health risk through consumption of rice growing near an abandoned e-waste recycling site: Comparisons with PBDEs and AHFRs. *Environ. Pollut.* 247, 46–54. doi:10.1016/j.envpol.2018.12.051

Xu, C., Niu, L., Zou, D., Zhu, S., and Liu, W. (2019). Congener-specific composition of polychlorinated biphenyls (PCBs) in soil-air partitioning and the associated health risks. *Sci. Total Environ.* 684, 486–495. doi:10.1016/j.scitotenv.2019.05.334

Xu, P., Lou, X., Ding, G., Shen, H., Wu, L., Chen, Z., et al. (2014). Association of pcb, pbde and pcdd/f body burdens with hormone levels for children in an e-waste dismantling area of zhejiang province, China. *Sci. Total Environ.* 499, 55–61. doi:10.1016/j.scitotenv.2014.08.057

Yang, Z. Z. (2009). *Study on the environmental behavior of polybrominated diphenyl ethers in contaminated areas, China*. BeiJing, China: Research Center for Eco-environmental Science, Chinese Academy of Science.

Yao, Y. T. (2019). *Vertical distribution characteristics and influence factors—taking the area of jie fang zha as an example*. Nei Meng Gu, China: Inner Mongolia Agricultural University.

Yu, B. M., Brenda, L. N., Wang, H. S., Leung, A. O. W., Chow, K. L., and Wong, M. H. (2011). Cancer risk assessment of polybrominated diphenyl ethers (PBDEs) and polychlorinated biphenyls (PCBs) in former agricultural soils of Hong Kong. *J. Hazard. Mater.* 195, 92–99. doi:10.1016/j.jhazmat.2011.08.010

Yu, H. Y., Liu, Y. F., Shu, X. Q., Ma, L. M., and Pan, Y. W. (2020). Assessment of the spatial distribution of organochlorine pesticides (OCPs) and polychlorinated biphenyls (PCBs) in urban soil of China. *Chemosphere* 243, 125392. doi:10.1016/j.chemosphere.2019.125392

Yu, Y., Lin, B., Liang, W., Li, L., Hong, Y., Chen, X., et al. (2018). Associations between PBDEs exposure from house dust and human semen quality at an e-waste areas in South China-A pilot study. *Chemosphere* 198, 266–273. doi:10.1016/j.chemosphere.2018.01.150

Zhan, L. X., Lin, T., Cheng, H. R., Wang, Z. W., Cheng, Z. N., Zhou, D., et al. (2019). Atmospheric deposition and air–soil exchange of polybrominated diphenyl ethers (PBDEs) in a background site in Central China. *Environ. Sci. Pollut. Res.* 26 (31), 31934–31944. doi:10.1007/s11356-019-06312-6

Zhang, L., Wang, J. X., Xu, F., Zhang, G., Wang, Y. J., Zhang, W., et al. (2015). Distribution and source apportionment of polybrominated diphenyl ethers(PBDEs) in soils and dusts in E waste recycling and aurrounding areas. *J. Agro-Environment Sci.* 34 (009), 1730–1736.

Zhang, S. J., Zhou, X., Li, M. L., and Zhu, G. H. (2018). Pollution characteristic and environmental transport behavior of PBDEs in agriculture soil around an electric waste dismantling venue. *Environ. Pollut. Control* 40 (7), 819–823.

Zhou, Y., Sun, J., Wang, L., Zhu, G., Li, M., Liu, J., et al. (2021). Multiple classes of chemical contaminants in soil from an e-waste disposal site in China: Occurrence and spatial distribution. *Sci. Total Environ.* 752, 141924. doi:10.1016/j.scitotenv.2020.141924

frontiers | Frontiers in Environmental Science

TYPE Original Research
PUBLISHED 05 January 2023
DOI 10.3389/fenvs.2022.1095731

OPEN ACCESS

EDITED BY
Xiaohu Wen,
Northwest Institute of Eco-Environment and Resources (CAS), China

REVIEWED BY
Chengkai Qu,
China University of Geosciences Wuhan, China
Subramani T,
Anna University, India
Anupma Kumari,
Patna University, India

*CORRESPONDENCE
Xiying Zhang,
xyzhchina@isl.ac.cn

SPECIALTY SECTION
This article was submitted to Toxicology, Pollution and the Environment, a section of the journal Frontiers in Environmental Science

RECEIVED 11 November 2022
ACCEPTED 19 December 2022
PUBLISHED 05 January 2023

CITATION
Cai N, Li L, Zhu H, Chen L, Li S, Meng F and Zhang X (2023), Multiple evaluations, risk assessment, and source identification of heavy metals in surface water and sediment of the Golmud River, northeastern Qinghai-Tibet Plateau, China.
Front. Environ. Sci. 10:1095731.
doi: 10.3389/fenvs.2022.1095731

Multiple evaluations, risk assessment, and source identification of heavy metals in surface water and sediment of the Golmud River, northeastern Qinghai-Tibet Plateau, China

Na Cai[1,2,3], Leiming Li[1], Haixia Zhu[1,2], Liang Chen[1,2], Shanping Li[4], Fanwei Meng[5] and Xiying Zhang[1,2]*

[1]Key Laboratory of Comprehensive and Highly Efficient Utilization of Salt Lake Resources, Qinghai Institute of Salt Lakes, Chinese Academy of Sciences, Xining, China, [2]Qinghai Provincial Key Laboratory of Geology and Environment of Salt Lake, Xining, China, [3]University of Chinese Academy of Sciences, Beijing, China, [4]Qinghai Geological Survey Institute, Xining, China, [5]School of Resources and Geosciences, China University of Mining and Technology, Xuzhou, China

The water quality of the Golmud River is essential for environmental preservation and economic growth of Golmud city and Qarhan Salt Lake in China. Thirty-four samples of surface water and sediment from seventeen places in the Golmud River and thirty-two dustfall samples in the Qaidam Basin were collected. The concentrations of heavy metals (HMs) were measured; water quality, risk assessment, and multiple source analysis were applied. Concentrations of HMs in water were Zn > Cu > Ni > As > Pb > Cd > Hg, and in sediment were Ni > Zn > Pb > As > Cu > Cd > Hg. In water, the Nemerow pollution index (NP) values indicated that most of the sampling points seemly were seriously polluted; other water quality assessment results suggested no pollution. In sediment, the concentrations of 27% HMs exceeded the background values of soil in Qinghai; 48% exceeded the Earth crust background values, which were As, Hg, and Cd. The single factor index method (Pi), geological accumulation index (Igeo), and contamination factor (CF) revealed that As pollution is serious, followed by Hg and Cd; the pollution load index (PLI) and modified pollution index (mCd) values indicated that 64% and 57% of samples were polluted. NP values are shown serious pollution. The ecological risk results demonstrated a low risk in water and a medium risk in sediment. The average total hazard quotient values in sediment and water for adults and children revealed low non-carcinogenic risks. Carcinogenic risk indicated Ni in water and sediment, and As in sediment may be involved in cancer risk. Multivariate statistics showed that the HMs mainly came from nature, and human activities will also impact them. The upper continental crust values indicated that As and Hg have high background values. The saline dust storm was one of the essential sources of HMs, especially Hg. Various provenances constituted the material cycling of HMs in the surface environment.

KEYWORDS

Golmud River, water quality, surface water and sediment, heavy metals, risk assessment, source

1 Introduction

In recent years, HM pollution has become an important environmental hazard and has significantly increased (Ahmed et al., 2015; Vu et al., 2017; Li et al., 2020a). Moreover, it has drawn much attention due to its heavy toxicity and endurance (Zahra et al., 2014; Wei et al., 2016; Lanzerstorfer, 2018; Liu et al., 2018a; Chen et al., 2019). Under natural environmental conditions, the content of HMs in rivers is usually very low, but through unreasonable human actions, such as the emission of agricultural, industrial, domestic wastewater, waste residue, and exhaust gas, excessive HMs are supplied to rivers, lakes, and other surface waters (Tchounwou et al., 2012; Deng et al., 2016; Goher et al., 2019; Bashir et al., 2020; Gopinathan et al., 2022a; Gopinathan et al., 2022b); surface and underground runoff, polluted river sediment, and atmospheric sedimentation can also release HMs, thus resulting in a grave threat to the aquatic environment (Saleem et al., 2015; Harikrishnan et al., 2017; Benson et al., 2018; Sun et al., 2018). In addition, it has been demonstrated that exposure to HM can result in a variety of health problems (Sharma and Agrawal, 2005; Tchounwou et al., 2012; Jaishankar et al., 2014), including harm to the kidneys (Tchounwou et al., 2012) and the development of neuroscience (Jaishankar et al., 2014). Cd, Hg, As, and Pb are toxic heavy metals (Clemens and Ma, 2016); these HMs tend to accumulate in different tissues of the human body and are highly toxic even at low concentrations (Sharafi et al., 2019). Among them, Cd and As are carcinogenic heavy metals, which are widely distributed in the crust (Mehdi et al., 2019). Cu and Zn are essential elements for human metabolism and various biological molecules (Meghdad et al., 2016). However, if their concentrations exceed certain limits, they may endanger human health (Ali et al., 2013).

For the transport and transformation of HMs, water and sediment are essential transporters and storage mediums (Chen et al., 2022). Sediments serve as a supply and a sink for HMs (Liu et al., 2012). Adsorption, hydrolysis, and coprecipitation reactions can all cause the deposition of HMs in sediment (Singh et al., 2005). As it continues to increase, the presence of HMs in the surface sediment is becoming an important issue of global concern. HMs can harm ecological systems and human health since they are durable in river silt and are not easily broken down by bacteria (João et al., 2019). At present, there are many assessment methods for HM pollution in water bodies and sediment, but they all have certain limitations. To compensate for the shortcomings of different methods, a variety of HM pollution assessment methods should be jointly used for comprehensive analysis and evaluation. In recent years, a number of indicators, such as Igeo, CF, and PLI, have been established to determine the level of HM pollution in sediments (Wang et al., 2018; Withanachchi et al., 2018; Zhang et al., 2018), and numerous techniques, including multivariate statistical methods (e.g., principal component analysis, factor analysis, and cluster analysis) (Bodrud-Doza et al., 2016; Gulgundi and Shetty, 2018), have been created to assess water quality.

The Qinghai-Tibet Plateau is frequently referred to as the Third Pole and the Roof of the World (Li D. et al., 2022). It is distinguished by having the most high-altitude rivers in the world, a small number of residents, and few anthropogenic activities (Liu et al., 2021). The main water supply for industrial production, agricultural irrigation, and routine activities in Golmud city is the Golmud River, the second-largest inland river in the Qaidam Basin. At the same time, it is an important source of salt-forming substances for Qarhan Salt Lake. Therefore, the water quality of the Golmud River is vital for regional socioeconomic development and environmental protection. Unfortunately, there is still a shortage of comprehensive analyses and studies on water and sediment quality assessments, ecological-health risk assessments, and source identification of HMs in the Golmud River. Therefore, carrying out this research is crucial. Thirty-four surface water and sediment samples from 17 sites in the Golmud River were collected to thoroughly understand the current distribution of HMs in the surface water and sediment of the Golmud River; seven HM (As, Hg, Pb, Cd, Cu, Ni, and Zn) and eight constant ion (CO_3^{2-}, HCO_3^-, SO_4^{2-}, Cl^-, K^+, Ca^{2+}, Na^+, and Mg^{2+}) concentrations were measured. Meanwhile, to determine the secondary source of HMs, thirty-two dustfall samples from the Qaidam Basin were collected, and HMs were also tested. The evaluation of water and sediment quality, the risk to public health, and the recognition of HM sources in the Golmud River can all be provided in this research.

2 Materials and methods

2.1 Study area, sampling, and analysis

With a length of 468 km, the Golmud River is located at the southern edge of the Qaidam Basin in the north of the Qinghai Tibet Plateau, with a drainage area of 35°49′46″–37°5′19″N and 94°21′13″–95°12′46″E, its main stream length is 325 km and has a basin area of 18,648 km^2 (Wang, 2014a). The terrain in the area is generally high in the South and low in the North, with the Kunlun Mountains in the South and Qaidam Basin in the North. The upstream of the Golmud River is divided into two branches: the Kunlun River and the Xueshui River. Both branches are mainly supplied by the melting water of ice and snow and atmospheric precipitation in the Kunlun Mountains. After converging in the mountains, the runoff flows from South to North and flows into the Qaidam Basin through the southern mountain pass. The Golmud River Basin has a dry climate with little precipitation. The annual evaporation is high, reaching 3,066 mm/a. According to earlier research, except for the eastern reach of the alluvial fan sector (a groundwater recharge river), the entire area is dominated by river recharge to groundwater. The arid climatic conditions of the inland basin formed a typical desertification landscape. Considering Golmud city as the boundary, the southern part is dominated by desertification, and the northern part is dominated by salinization. The landforms of the Golmud River Basin can be divided into five units from South to North: the Gobi, alluvial fans, flood alluvial plain, lacustrine plain, and salt lake.

Thirty-four samples of surface water (W1–W17) and sediment (S1–S17) were collected from seventeen sampling stations in December 2021 (Figure 1). The studied sites were divided into freshwater (1–14) and saline (15–17) groups. Sampling was conducted every 20 km from the Golmud River to Dabuxun Salt Lake. Surface water samples were obtained from the top layer (0–50 cm) of the river at every sampling location used a plastic spoon. The samples were then put into 500 ml polypropylene bottles after being conditioned with nitric acid (HNO_3) to a

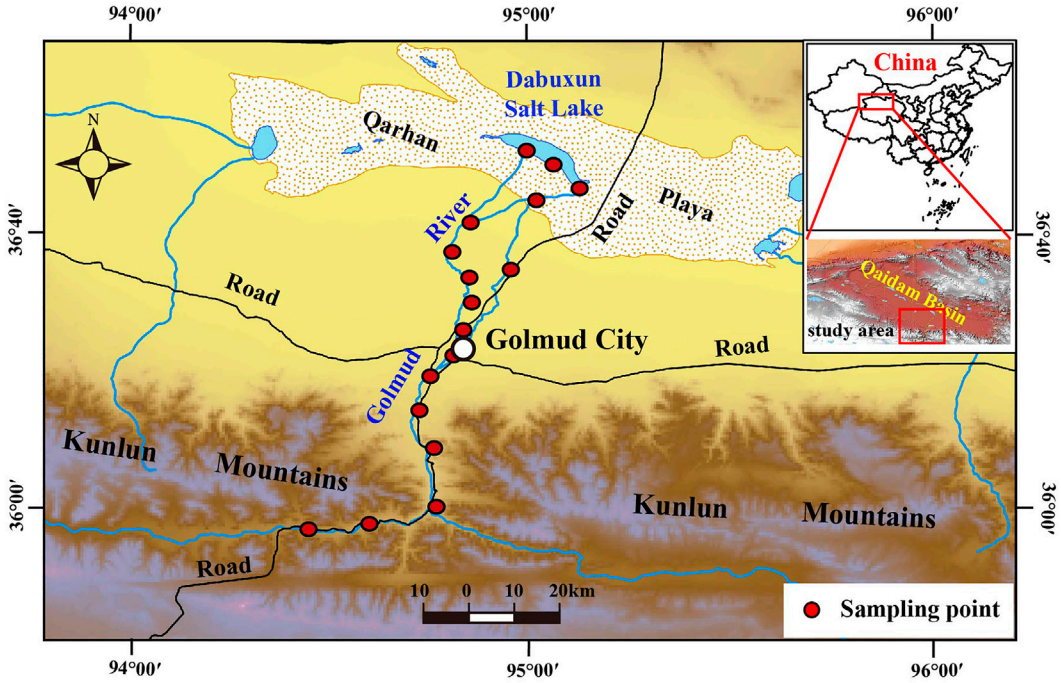

FIGURE 1
Location map of the study area and the surfacewater and sediment sampling locations.

pH of under two. With the aid of a shovel, surface sediment samples were obtained and kept in disposable polypropylene bags. The obtained water and sediment samples were immediately sent to the laboratory for additional analysis after being stored in a cooler at 4°C. In addition, thirty-two dustfall samples in the Qaidam Basin were collected to analyze the source of HMs, and the collection method of dustfall samples refers to Gen Jun's paper (Gen, 2021).

According to previous analysis data (Xiang, 2020), an ICAP Q_C inductively coupled plasma mass spectrometer (ICP-MS) was utilized to identify HM concentrations, and its detection thresholds were as follows: .015 [Pb] and [As], .001 [Hg], .0160 [Ni], .133 [Cu], .470 [Zn], and .035 μg/L [Cd]. While measuring HMs in saline using ICP-MS, the mineralization should be below 2 g/L. Excessively high mineralization will cause the salt to block the sampling cone (Song et al., 2014). Using a NexION 2000 inductively coupled plasma optical emission spectrometer (ICP-OES), Na^+, K^+, Mg^{2+}, Ca^{2+}, and SO_4^{2-} were detected, and HCO_3^- and Cl^- were titrated by chemical titration (allowable error 3‰). To avoid contamination during testing, all glassware was soaked in HNO_3 at a concentration of 5% for 24 h before use and then washed and dried. The testing and analysis employed only the purest reagents. For this quality control analysis, spiked blanks, duplicate method blanks, and spiked samples were utilized to test the reliability of the results.

2.2 Pollution level of heavy metals in surface water and sediment

Various environmental and statistical methods have been used to analyze the impact of human disturbance and contamination (Yao et al., 2006; Suresh et al., 2012; Tang et al., 2014; Wang et al., 2014b; Xiao et al., 2014; Gopal et al., 2016; Iqbal et al., 2016). In this paper, to quantitatively evaluate HM pollution in the Golmud River, Pi, CF (Hakanson, 1980), NP (Li et al., 2018), HPI (Qiao et al., 2020; Karunanidhi et al., 2021a), mCd (Abrahim and Parker, 2008), and HEI (Edet and Offiong, 2002) were chosen to assess water quality. PLI (Tomlinson et al., 1980), Igeo (Taylor and McLennan, 1985; Nethaji et al., 2017), Pi, NP, mCd, and CF were applied to assess the pollution of HMs in sediment.

2.3 Water quality index (WQI) of surface water

A useful instrument for obtaining a complete picture of lake or river water quality is the water quality index (WQI) (Tiwari and Mishra, 1985; Carvalho et al., 2021). The index condenses many water quality parameters from a significant amount of data to a solo value (Ravindra et al., 2019; Ustaoglu et al., 2020). Supplementary Table S1 displayed the relative weights (w_i) for each parameter. The water quality index (WQI):

$$WQI = \sum \left[W_i \times \left(\frac{C_i}{S_i} \right) \right] \times 100$$

where relative weight $W_i = w_i / \sum w_i$. Each parameter's weight, w_i, is determined by its importance for human health and drinking purposes (Sener et al., 2017). $\sum w_i$ is the sum of the w_i. In this study, $\sum w_i$ is 24. C_i is the heavy metal concentration of water samples, and S_i is Chinese drinking water standard value (Ministry of Health, 2006). According to the WQI values, there are five classifications: WQI < 50 indicates excellent, 50 ≤ WQI < 100 suggests good, 100 ≤ WQI < 200 shows bad, 200 ≤ WQI < 300

indicates very poor, and 300 ≤ WQI indicates unfit for drinking (Xiao et al., 2019).

2.4 Risk assessment of surface water and sediment

2.4.1 Ecological risk

The potential risk of one or more HMs on the ecological impact value is assessed by the potential ecological risk index (PERI), which was first presented by the Swedish researcher Hakanson and later widely used to assess the ecological risk of pollutants in sediment and soil (Liu et al., 2017). It has been used recently to assess the ecological risk value of water (Liu et al., 2018b). The PERI was utilized to assess HM pollution in water and sediment.

$$\mathrm{PERI} = \sum_{i=1}^{n} T_m^i \times \frac{C_m^i}{C_b^i}$$

T_m^i, which has values of 10, 40, 5, 30, 5, 5, and 1 for As, Hg, Pb, Cd, Cu, Ni, and Zn, respectively, is the toxic response factor for heavy metals i (Zhang and Liu, 2014). Using the Class Ⅳ standard value in the Surface Water Environmental Quality Standard (GB3838-2002) or UCC values, C_b^i represents the background value of HMs in the water or sediments, and C_m^i is the concentration of HMs at the sampling location. PERI < 150, low; 150 ≤ PERI < 300, medium; 300 ≤ PERI < 600, high; 600 ≤ PERI, very high (Azhari et al., 2017).

2.4.2 Health risk

Hazard quotients (HQs) are frequently used to measure the toxicity produced by HMs (Özgür et al., 2020; Githaiga et al., 2021; Lu et al., 2021), and the hazard index (HI) is used to estimate the total possible non-carcinogenic risks deriving from various approaches (USEPA, 2004). Only HMs with carcinogenic slope factors (CSFs) are evaluated for carcinogenic risks (CRs) (Özgür et al., 2020). Surface water and sediment health risks were calculated independently in this study. The formula is provided in Supplementary Material S1–S14 for surface water and Supplementary Material S15–S18 for sediment.

The HI evaluates the total potential non-carcinogenic risks of each HM. The total hazard index (THI) was computed using Supplementary Material S19, S20 for water and Supplementary Material S21 for sediment. Carcinogenic risks (CRs) were used to compute the total carcinogenic risk (TCR) and were calculated using Supplementary Material S22, S23. Supplementary Table S2 displayed all specific definitions, units, and relevant equation values; Supplementary Table S1 provided the figures for the oral reference dosage (RfDo), oral slope factor (CSFo), gastrointestinal absorption (GIABS), and dermal permeability constant (Kp).

2.5 Source identification methods

Surface water contains a variety of HMs, each of which can have several sources. This study used principal component analysis (PCA) and pearson correlation analysis (Singh et al., 2014; Lu, et al., 2022a; Lu, et al., 2022b) to explore the correlations among the seven HMs in surface water and sediment.

3 Results and discussion

3.1 Heavy metals in surface water and sediment

Supplementary Table S3 shows the content of HMs in water and sediment samples from all locations. Figures 2A, B depict the concentrations of seven HMs in the surface water and sediment of the different sampling sites. In surface water, the average TDS content was 1,757 mg/L, with a range of 473–15,042 mg/L. The cation was Na^+ (329.87 mg/L), followed by Mg^{2+} (122.20 mg/L), Ca^{2+} (59.61 mg/L), and K^+ (17.24 mg/L). The anion was Cl^- (801.68 mg/L), followed by HCO_3^- (230.60 mg/L), SO_4^{2-} (161.00 mg/L), and CO_3^{2-} (71.48 mg/L). In freshwater samples, the average of As was 1.37 μg/L, while concentration values varied from .40 to 4.67 μg/L, Hg had a maximum value of .10 and an average of .04 μg/L, Pb varied from .44 to 2.37 and had an average of 1.47 μg/L, Cd varied from .01 to .16 and had an average of .05 μg/L, Cu varied from 1.24 to 13.48 and had an average of 4.52 μg/L, Ni varied from .88 to 24.64 and had an average of 7.90 μg/L, Zn varied from 3.72 to 23.66 with a mean value of 9.38 μg/L. HMs can be distinguished into two types depending on concentration, Hg and Cd were <1 μg/L and were categorized as low abundance elements; As, Pb, Cu, Ni, and Zn ranged from 1 to 100 μg/L and were deemed moderately abundant elements. Cu, Ni, and Zn were the main HMs, accounting for 18%, 32%, and 38% of the total HM elements, respectively. Hg and Cd had the lowest contents at all sampling locations. The concentration of HMs at site W14 was higher than that at other locations due to its proximity to Qarhan Salt Lake, which has a high Cl^- concentration, and Cl^- can form soluble complexes with HMs, and these HM complexes have a strong migration ability (Wang et al., 2013). The concentration of soluble HM complexes on the shore was high, resulting in a significant concentration of HMs at the mouth of the Golmud River. In addition, the hydrodynamic effect was significantly weakened near the salt lake, resulting in the accumulation of HMs. Combined with the Surface Water Environmental Quality (GB3838-2002), all the HMs in freshwater were suitable for Class I Standard. The water was of great quality and fit for drinking.

In sediments, the HM concentration ranges were as follows: 9.10–16.08 for As, .05–.15 for Hg, 12.84–31.34 for Pb, .09–.21 for Cd, 7.39–10.72 for Cu, 17.39–24.52 for Ni, and 16.26–23.46 mg/kg for Zn. Pb, Ni and Zn were generally more abundant than the other elements. 27% HM concentrations were above the background levels of the soil in Qinghai, especially Hg and Cd. 48% of HMs exceeded the Earth's crustal background values, which were As, Hg, and Cd. Therefore, Hg and Cd are the primary contaminants, and As has a high background value in the Qinghai-Tibet Plateau (Yang et al., 2020). Compared to the results of Xiang, 2020, the current investigation of Cu and Zn concentrations was much lower, and other elements were quite similar. Overall, the sediment contained the highest concentration of HMs, which had higher quantities than the water. In contrast, the lowest mean values occurred in freshwater. The concentrations of HMs are often higher in sediment than in water due to their limited solubility; they can bond to particles and accumulate in the sediment (Wang et al., 2015). Comparing saline samples to freshwater samples revealed greater HM content. Generally, the HM content at each sampling point was basically consistent. The As, Pb, Cu, Ni, and Zn concentrations in saline ranged from 1 to 100 μg/L; these were moderately abundant

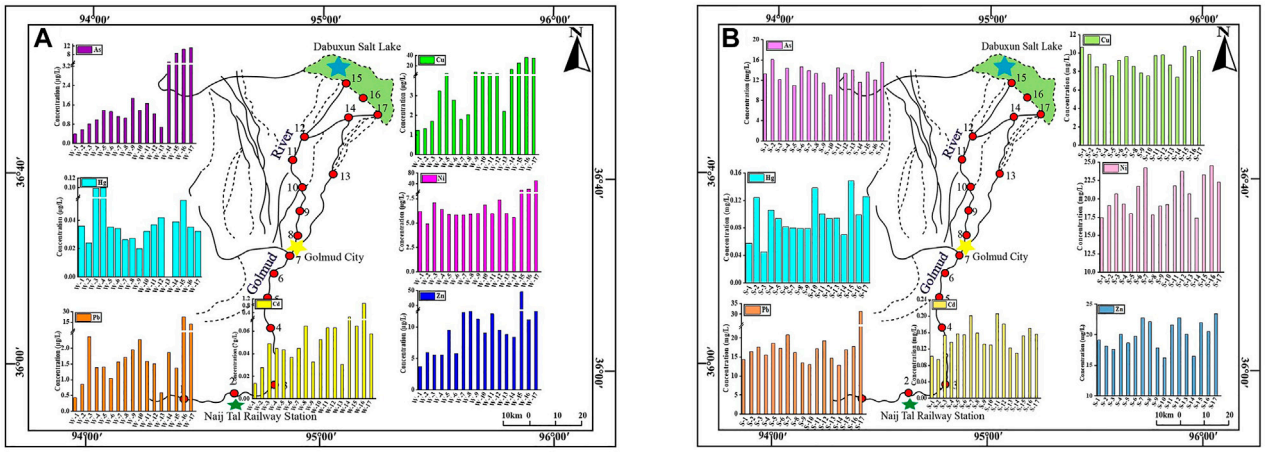

FIGURE 2
Heavy metal spatial distributions in the surface water **(A)** and sediment **(B)** of the Golmud River (μg/L).

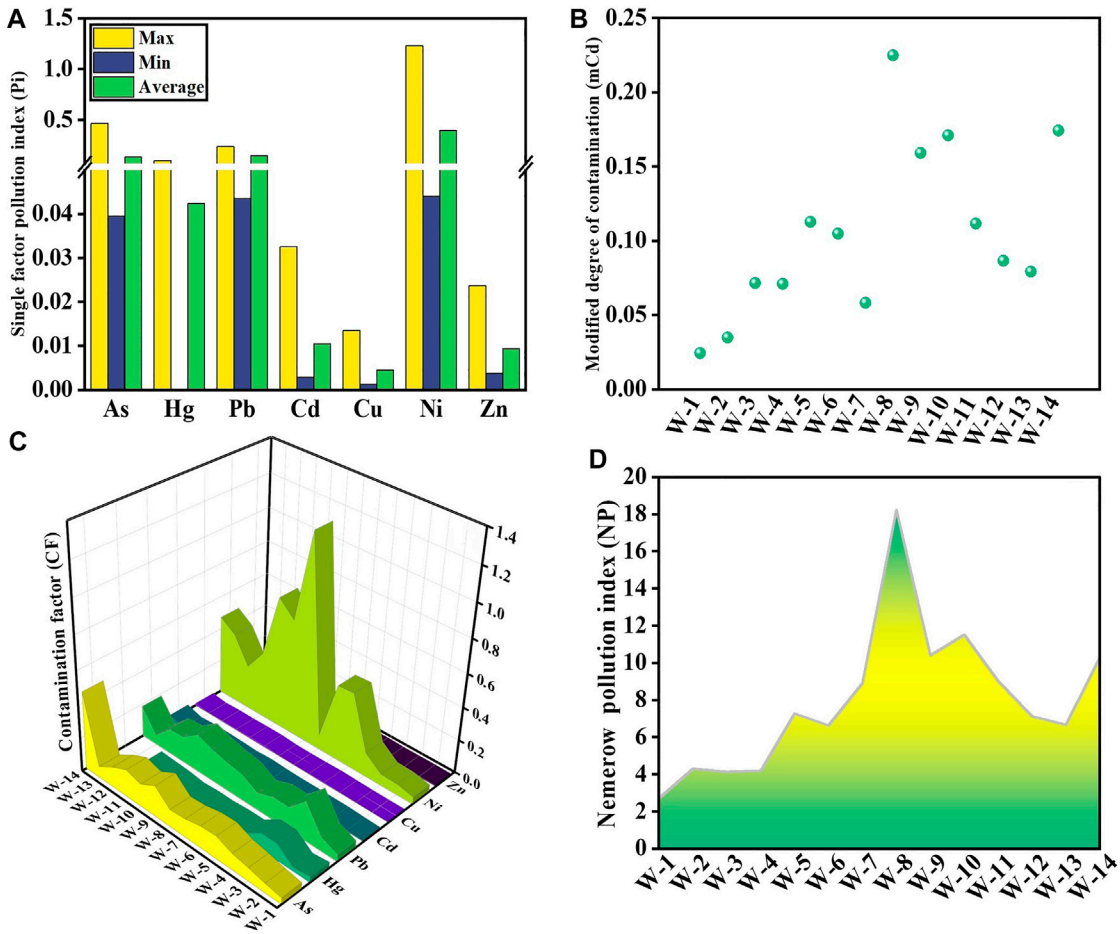

FIGURE 3
Pi **(A)**, mCd **(B)**, CF **(C)**, and NP **(D)** in the surface water of the Golmud River.

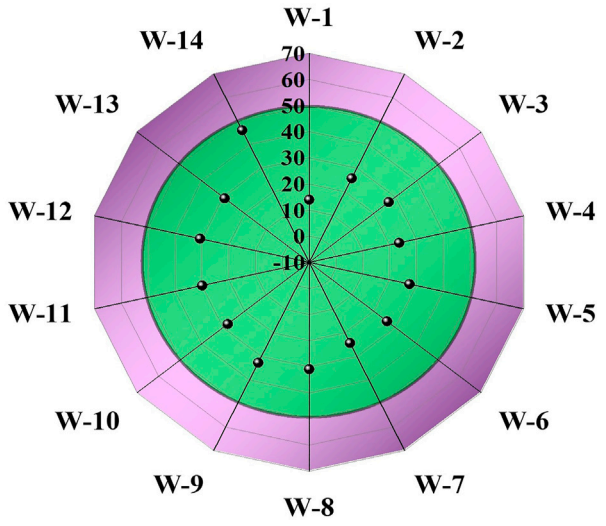

FIGURE 4
The Radar of water quality index for freshwater samples.

elements. Low abundance elements Hg and Cd were present at <1 μg/L. This is consistent with the classification of freshwater. The concentration of HMs in the freshwater changed little, and in saline, they were relatively high, which was consistent with Li D. et al. (2022) conclusion. Due to the enrichment of HMs in the salt lake, the average levels of HMs were greater.

3.2 Pollution and quality indices

3.2.1 Surface water

Brine is a resource for element obtaining rather than drinking. Thus, it was impossible to determine the water quality of brine (Li L. M. et al., 2022). Figure 3 shows the Pi values of surface water and the mCd, CF and NP values. The average Pi for all HMs was less than .7, indicating that the studied region was clean (Figure 3A). All sites had clean levels of mCd, which ranged from .02 to .23; the WQI values had a mean of .11 (Figure 3B). The CF mean values of the sampling were all less than 1 (Figure 3C), indicating low pollution. Accordingly, 100% of the sampling sites demonstrated that the surface water of the Golmud River was not contaminated using the ranking criteria of Pi, mCd, and CF. The max Pi and CF have the same value of 1.23. However, Pi and CF evaluated the total pollution degree. These two HM pollution indices in surface water indicated that most test locations were not polluted, except for one site where Ni made the most dominant contribution. The range of NP values in water was 2.72–18.23, with an average of 7.96 (Figure 3D); there was heavy pollution. NP values consider the average and maximum values of each HM, and severe contaminants have a significant influence on them (Li et al., 2018; Mahmudul et al., 2022). Using NP amplifies the effects of higher concentrations of HMs such as Ni and Zn.

The HEI values had a mean of .11 and a range of .00–.40 (Supplementary Table S3). The results indicated that the HEI for each sample was less than 1. All locations had low pollution levels. The mean HPI value was 10.65, ranged from .45 to 39.52 (Supplementary Table S3); all sites were at a low pollution level and showed similar results with HEI. There was moderate pollution (30–100) of HPI with Ni, which showed similar trends with Pi and CF.

A useful method for keeping track of surface water is the WQI. It condenses several water quality characteristics from a considerable amount of data into one number (Tiwari and Mishra, 1985). In the research area, the WQI value of freshwater samples changed from 13.95 to 46.11, with a mean value of 28.25 (Figure 4). 100% of the water samples fell into the “good” category.

3.2.2 Sediment

The mean Pi value of As was 8.69, belonged to heavy pollution; the mean Pi values of Hg and Cd were 1.59 and 1.49, belonged to low pollution; and the other HMs had clean levels (Figure 5A). PLI was calculated depending on the measured contamination factors (Anbazhagan et al., 2022). Figure 5B shows the PLI results. The PLI values of 36% of the sampling points were below 1, indicated no contamination, while the others were polluted. The Igeo was employed to quantitatively measure an individual HM in the sediment samples (Hong et al., 2020). Figure 5C shows the Igeo values of the HMs. The averaged Igeo results showed the following order of contamination: As > Hg > Cd > Ni > Pb > Cu > Zn. Depending on the criteria of pollution degree, the mean Igeo values of HMs showed no contamination in surface sediment other than As and Hg. The Igeo values of As at all sampling locations showed moderate contamination, and Hg was at different contamination levels. 50% of the sampling sites indicated no pollution, and the other half indicated low pollution. The most notable elements were Ni and Zn because their considerably higher concentrations resulted in the NP values of all sites reached heavy pollution (Figure 5D). In Figure 5E, the CF values for Pb, Cu, Ni, and Zn were .81, .35, 1.00, and .28, respectively, showed low pollution. In contrast, the CF value of As was 8.69, showed high pollution, and the CF values of Hg and Cd were 1.59 and 1.49, indicated moderate pollution. The order of As > Hg > Cd > Ni > Pb > Cu > Zn was the mean CF for all HMs. The mCd values varied from 1.71 to 2.33, with a mean value of 2.03; 43% of sampling sites were low pollution, and 57% showed moderate pollution (Figure 5F). This indicated that the accumulation of HM in the sediment was more severe than in the surface water. As, Hg, and Cd were the major HMs threatened the sediment.

3.3 Risk assessment

3.3.1 Ecological risk of surface water and sediment

Seven HMs are divided by their respective elemental concentrations to determine their PERI values in surface water and sediment (Figure 6). In surface water, the PERI value was 4.18, indicated a low risk (Figure 6A). The PERI values of As varied from .04 to .47 with a mean value of .14; the PERI values of Hg varied from .00 to 4.00 with an average of 1.57; the PERI values of Pb varied from .04 to .24 with an average of .15; the PERI values of Cd ranged from .08 to .98 with an average of .31; the PERI values of Cu varied from .01 to .07 with a mean value .02; Ni varied from .22 to 6.16 with an average of 1.98, and Zn varied from .00 to .01 with an average of .00. In sediment, the PERI value was 206.01, indicated medium risk (Figure 6B); the result was the same as that of Yang et al. (2020). As ranged from 60.64 to 107.19 with an average value of 86.93; Hg ranged from 32.28 to 98.71 with an average value of 63.43. Pb ranged from 3.21 to 5.20 with an average value of 4.06; Cd varied from

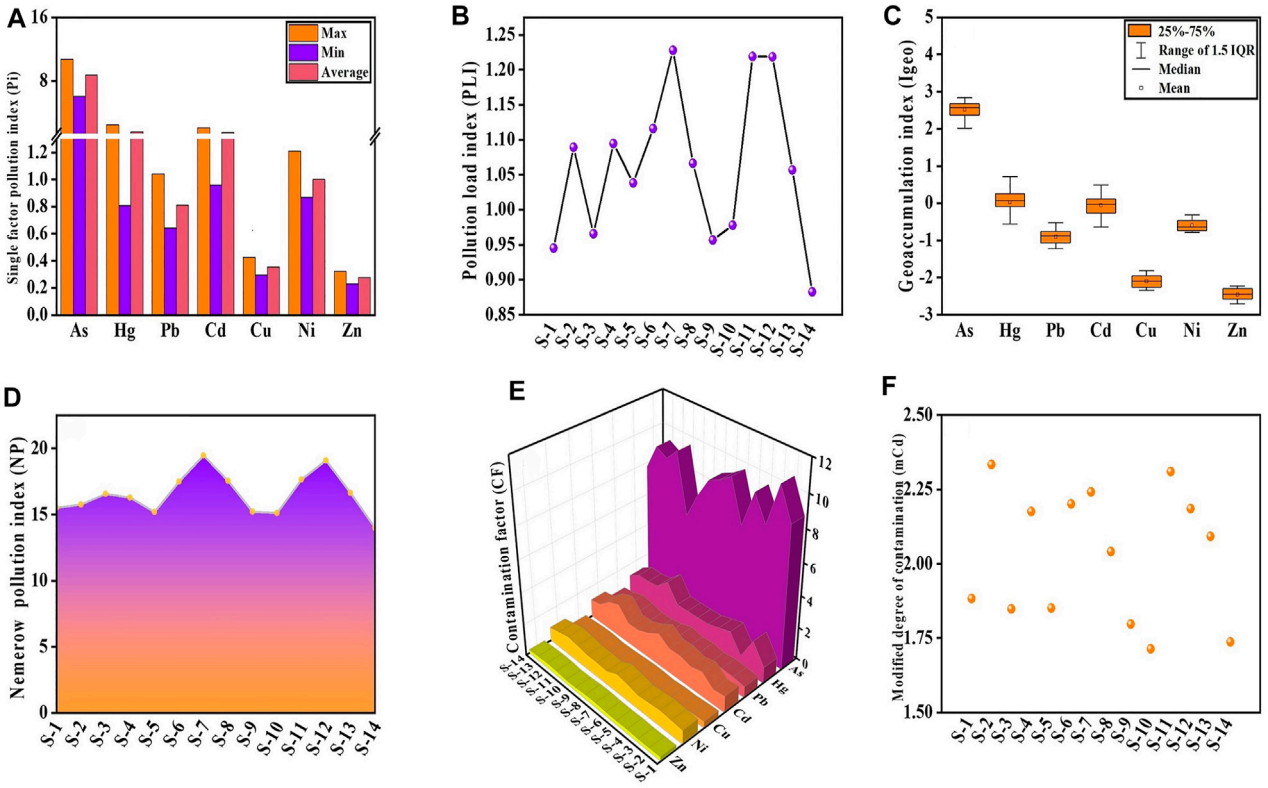

FIGURE 5
Pi **(A)**, PLI **(B)**, Igeo **(C)**, NP **(D)**, CF **(E)**, and mCd **(F)** in the sediment of the Golmud River.

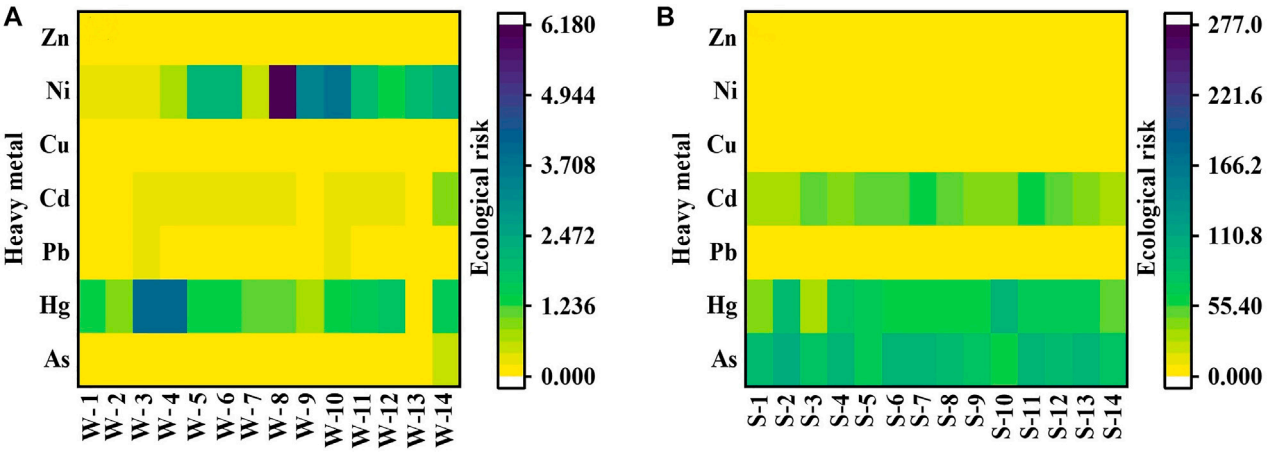

FIGURE 6
Heatmaps of the potential ecological risk index for heavy metals in water **(A)** and sediment **(B)** samples.

28.83 to 62.99 with a mean value of 44.55; Cu varied from 1.48 to 2.13 with a mean value of 1.77; Ni had PERI values between 4.35 and 6.05, with a mean value of 5.00; and Zn had PERI values between .23 and .32, with a mean value of .28. The ecological risk in the water was below that in sediment, especially As, Hg, and Cd; more attention should be given.

3.3.2 Non-carcinogenic and carcinogenic risks in surface water

The USEPA developed the total hazard quotient (THQ) approach, which is frequently used in risk assessment (USEPA, 2004). The THQs of HMs for residential adults and children were between .01–.48 and .04–.93, with an average of .17 and .34, respectively (Figure 7A). The

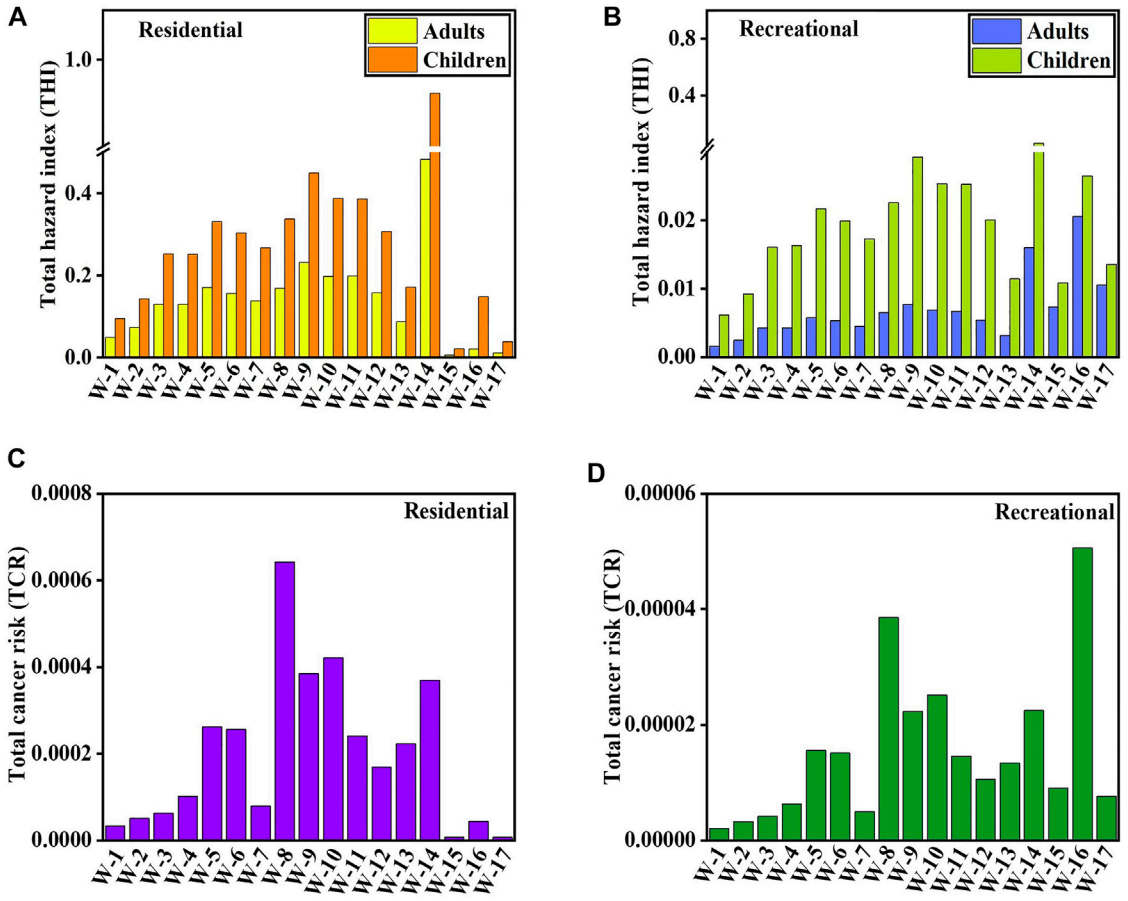

FIGURE 7
Total hazard index (THI) and total carcinogenic risk (TCR) for residential **(A,C)** and recreational **(B,D)** receptors from heavy metals in surface water.

average THQs for adults and children were below 1.0, indicated that neither group faced high non-carcinogenic risks. With average values of .007 and .021, the THQs of HMs for recreational adults and children were between .002–.021 and .006–.062, respectively (Figure 7B). Humans are most commonly exposed by ingestion, inhalation, and dermal absorption (Karunanidhi et al., 2021b; Karunanidhi et al., 2022). The non-carcinogenic risks for water ingestion were .167 and .317 for residential adults and children, respectively, and .002 and .013 for dermal contact in the water of the Golmud River. At the same time, for recreational adults and children, the non-carcinogenic risks for water ingestion were .004 and .019, respectively, and for dermal contact, they were .002 and .003, respectively (Supplementary Table S4). For residential adults and children, the non-carcinogenic risks in saline were .0123 and .0689 by dermal contact, respectively. For dermal contact, the non-carcinogenic risks for recreational adults and children were .0128 and .017, respectively (Supplementary Table S4). These findings demonstrated that inhabitants were more susceptible than recreational receptors to water ingestion. In addition, the water ingestion way had a more detrimental impact on residents' health than dermal contact. Notably, the non-carcinogenic risks for dermal contact and ingestion were lower in residential and recreational adults than in children. This suggested that adults were less susceptible than children when subjected to HMs in water, which was in line with the conclusions of earlier investigations (Xiao et al., 2019; Li et al., 2020b; Aravinthasamy et al., 2021; Karunanidhi et al., 2021c; Karunanidhi et al., 2021d; Li D. et al., 2022). Saline, however, was unfit for drinking, so the health risk from ingestion was not calculated.

Figures 7C, D depict the total carcinogenic risk (TCR) results for all sample locations in the research area. As, Pb, Cd, and Ni were used for CR assessment in this paper because they have carcinogenic slope factors. For residential and recreational receptors, the TCRs of As, Pb, Cd, and Ni were 6.61×10^{-6}–6.42×10^{-4} (Figure 7C) and 2.03×10^{-6}–5.06×10^{-5} (Figure 7D), respectively. Correspondingly, all locations pose acceptable hazards to both residential and recreational people. The CR values of residents for Ni by the ingestion contact exceeded the threshold risk of 1×10^{-4} in freshwater. However, the CR values of residents for dermal contact were lower than that. For residents, the levels of Cd by dermal and ingestion contact were lower than 1×10^{-4}, and the values of Pb were lower than 1×10^{-6} (Supplementary Table S4). As values of residents by dermal contact ways were less than 1×10^{-6}, and those by ingestion contact were less than 1×10^{-4}. For recreators, the CR values of As and Pb by ingestion and dermal contact were lower than 1×10^{-6}, and the CR values of Cd by ingestion contact were lower than those in freshwater. The CR values for Ni by ingestion and dermal contact for recreators were lower than 1×10^{-4}, and the dermal contact value of Cd for recreators was lower than that in freshwater (Supplementary

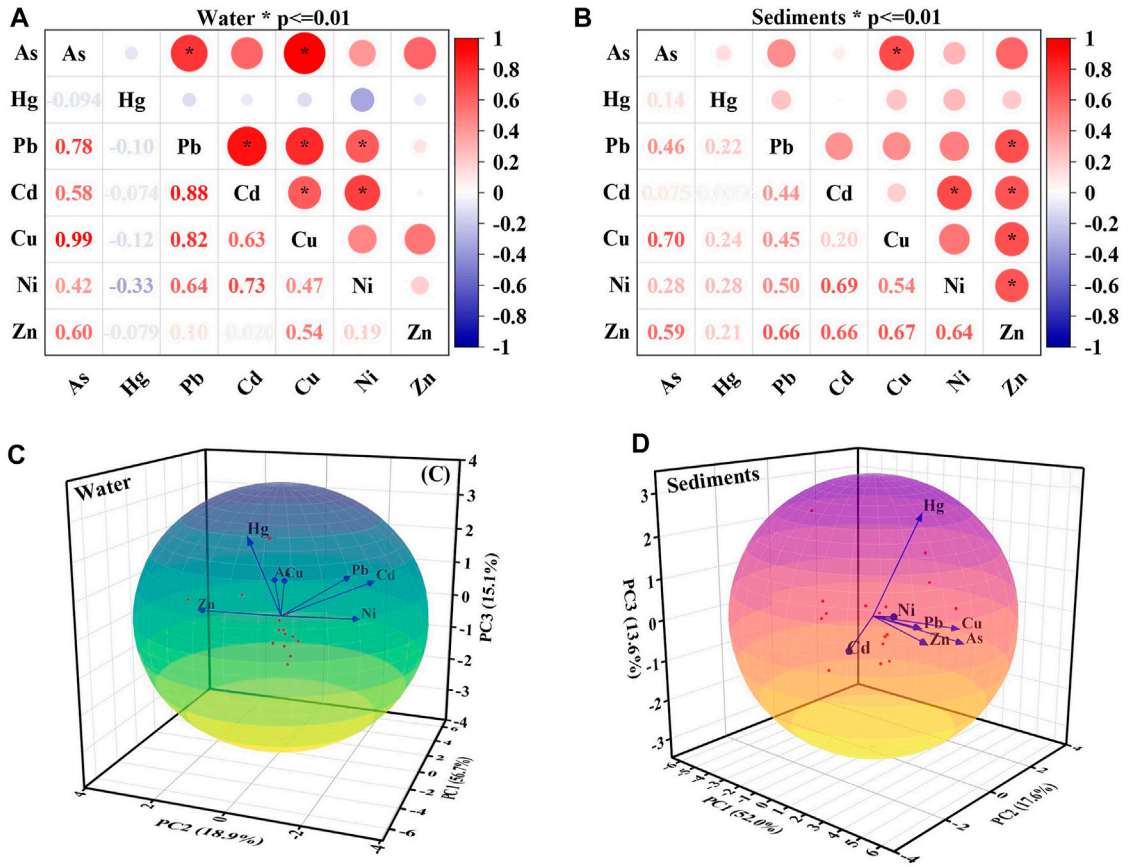

FIGURE 8
Pearson correlation **(A,B)** and principal component analysis (PCA) **(C,D)** of HMs in surface water and sediment samples.

Table S4). Residents had lower CR values of As, Pb, Cd, and Ni in saline for dermal contact than recreationists. As, Pb, Cd, and Ni in saline had CR values that were less than the target risk. By ingestion and dermal contact, Ni was the main contributor to the total CR for residents and recreators. Additionally, all the CR values for Ni in saline fell between 1×10^{-4} and 1×10^{-6}. The findings showed that As, Pb, and Cd would not present a carcinogenic risk for freshwater inhabitants and recreators, whereas people may be at risk for cancer from Ni. All HMs would not put inhabitants and recreators in saline at carcinogenic risk.

3.3.3 Non-carcinogenic and carcinogenic risk in sediment

The sediment in the Golmud River has revealed elevated concentrations of HMs, especially As, Hg, and Cd. Supplementary Table S5 displayed the THI and TCR values of HMs for sediment samples taken from the study area. The THI of HMs ranged from .06–.38 for adults and .07–.87 for children, with averages of .28 and .62, respectively. The THI mean values for adults and children were less than 1.0, indicated that neither group faced high non-carcinogenic hazards. In general, the THI for children and adults followed the order As > Pb > Ni > Cd > Hg > Cu > Zn. Adults and children had non-carcinogenic risks of .311 and .727 for sediment ingestion and .0124 and .0145 for dermal contact, respectively. Adults' and children's non-carcinogenic risks in salt lake sediment were .0668 and .0779 dermal contacts, respectively. This finding was consistent with the surface water results, THI values were higher for children than adults at all sampling locations. Meanwhile, skin contact had less of a negative impact on health than oral ingestion.

The TCR values of As and Ni for adults and children were above 1×10^{-4} in sediment, whereas Cd was higher than 1×10^{-6}. Meanwhile, Pb values for children exceeded 1×10^{-6}, whereas those for adults fell below 1×10^{-6}. The CR values of As and Ni in saline for adults and children were between 1×10^{-6} and 1×10^{-4}. The CR values of Pb and Cd were below 1×10^{-6}). The main contributors to the TCR were As and Ni. The findings suggested that As and Ni might be carcinogenic risks in sediment, while Pb and Cd would not. In saline, none of the HMs would present a carcinogenic risk.

3.4 Sources of heavy metals in the Golmud River

3.4.1 Surface water

The correlation analysis results indicated that Pb-As (.78), Cd-Pb (.88), Cu-As (.99), Cu-Pb (.82), Cu-Cd (.63), Ni-Pb (.64), and Ni-Cd (.73) were significantly positively correlated; Cd-As (.58), Zn-As (.60) and Zn-Cu (.54) were positively correlated; and Hg and other HMs revealed insignificantly positive correlations (Figure 8A). The data were shown to be fit for PCA by the KMO = .653 and Bartlett's

sphericity tests (<.001). Three major components were identified by removing eigenvalues >1, accounting for 90.579% of the overall variability. As, Pb, Cd, Cu, and Ni were the elements that were grouped into the first principal component (PC1) and contributed 56.7% of the variation, this was further confirmed by the significant correlation between these elements, which suggested that their sources were similar; the contribution rate of the second principal component (PC2) was 18.9%, and the positive load on Zn was relatively high. As and Cu were weakly correlated with Zn; the contribution rate of the third principal component (PC3) was 15.1% (Figure 8C). The positive load on Hg was relatively high, indicated that Hg has an independent source and was consistent with the results in Figure 8A.

Human activities are important factors that affect natural processes and the migration and accumulation of HMs: 1) Point-source pollution of HMs from human activities: Golmud is the major industrial city in the Qaidam Basin. The typical components of industry include Ni, As, Pb, Cd, and Cu (Cheng and Hu, 2010; Pourkhabbaz and Pourkhabbaz, 2012; Yuen et al., 2012; McComb et al., 2015; Chen et al., 2016). Previous studies revealed that untreated industrial wastewater and sewage discharge might be the source of Ni, Cd, Pb, and Cu (Shamuyarira and Gumbo, 2014; Rzetala, 2016; Gopinathan et al., 2022c). With social and economic development, wastewater and industrial fuel combustion containing HMs discharged from human activities in Golmud city and Qarhan Salt Lake directly impact the Golmud River. Moreover, brine has many HMs, it is a source of element extraction. 2) Line source pollution of HMs from human activities: Golmud city is the hub of essential transportation lines such as the Qinghai-Tibet Highway and Qinghai-Tibet Railway. These transportation lines parallel the Golmud River (Xiang, 2020). Pb, Zn, Cu, and As are the main elements in traffic exhaust and dust (Lough et al., 2005; Cheng and Hu, 2010; Li et al., 2012; Pourkhabbaz and Pourkhabbaz, 2012; Yuen et al., 2012; McComb et al., 2015; Zhao et al., 2019). Therefore, transportation emissions directly caused linear pollution in the Golmud River. 3) Non-point source pollution of HMs from human activities: Oasis agriculture has developed in the surrounding areas of Golmud city. The misuse of phosphate fertilizer in agriculture may cause Zn contamination (Luo et al., 2007; Ke et al., 2017); essential parts of insecticides, herbicides, and fertilizers include As (Chen et al., 2020). The primary source of Cu is typically agriculture, which is frequently obtained *via* pesticides and fertilizers. As a result, the Cu concentration of farmland has significantly increased (Qu et al., 2018).

Except for the anthropogenic sources mentioned above, the river water chemistry characteristics are closely related to the regional bedrock geochemical background and weathering (Karim and Veizer, 2000). Thus, understanding the geochemical background of the bedrock distribution areas is vital to determine the sources of HMs. We used UCC standardized diagrams (Taylor and Mclennan, 1985) for comparison. That is, the mean value of HMs in the Kunlun River bedrock was compared with the average UCC value. The analysis revealed that Hg and As were significantly enriched after UCC standardization (Supplementary Table S6). This conclusion was in accordance with the result that the As background of the Qinghai-Tibet Plateau is high (Yang et al., 2020). This showed that human activities had a minimal impact on the presence of As and Hg in this basin and was mainly influenced by the weathering of the local parent rock. In contrast, the other five elements did not change significantly; in the bedrock area rocks, the influence of the geochemical background of HMs, such as As, Hg, and other HMs with high contents on the river, was unquestionable.

3.4.2 Sediment

A significant source of HM pollution is sediment, and it has more stable HM concentrations than water (Ustaoglu et al., 2020). When the river environment changes, HMs may be liberated from sediment, resulting in secondary contamination. The sediment of the Golmud River was also polluted with Hg and Cd. The conclusions of correlation analysis indicated that Cu-As (.70), Ni-Cd (.69), Zn-Pb (.66), Zn-Cd (.66), Zn-Cu (.67), and Zn-Ni (.64) were significantly positively correlated; Ni-Pb (.50), Ni-Cu (.54) and Zn-As (.59) were positively correlated (Figure 8B). The data were shown to be fit for PCA by the KMO = .686 and Bartlett's sphericity tests (<.001). Three principal components were found to account for 83.325% of the overall variability by extracting eigenvalues >1, as shown in Figure 8D. A total of 52.0% of the variation was contributed by PC1. The dominant elements changed to Zn (.92), Ni (.80), Cu (.78), Pb (.76), As (.67), and Cd (.65), implied a more complicated source. PC2 demonstrated a positive loading for Cu (.47) and As (.62), which explained 17.6% of the overall variation. PC3 had a significant positive loading for Hg (.95) and 13.6% of the total variance. There were parallels between the sources of HMs in sediment and those in water. Hg was also the single dominant metal for PC3, while As and Cu represent PC2.

The Qaidam Basin is one of the vital places of dust storm disasters in China (Gen, 2021), so saline dust storms are a source of HMs that cannot be ignored. Sheng (2015) studied the chemical composition of the Golmud dust storm and revealed that Pb, Zn, Ni, and Cu were gathered in dust aerosols, which anthropogenic emissions may have caused. This paper tested the HM components in atmospheric dustfall (thirty-two samples in total were gathered) in the Qaidam Basin to understand the enrichment and impact of salt-laden dustfall on HMs. The results indicated that the average HMs in dustfall were 15.94 mg/kg for As, .30 mg/kg for Hg, 43.71 mg/kg for Pb, .92 mg/kg for Cd, 16.35 mg/kg for Cu, 19.94 mg/kg for Ni, and 46.32 mg/kg for Zn (Supplementary Table S6). The content of the element was in the order of Zn > Pb > Ni > Cu > As > Cd > Hg. Compared with the background values of soil in Qinghai, China, and the World (Wei et al., 1990). The average As, Hg, Pb, and Cd contents were higher, and the Cu, Ni, and Zn contents were lower. These findings indicated that the content of these four HMs (As, Hg, Pb, and Cd) in the dustfall was relatively high, especially the Hg content in the dustfall, which was fifteen times as much as the background values of the soil in Qinghai. Therefore, dustfall was one of the essential sources of HMs, especially Hg. HMs in dustfall are neither different from those due to natural sources, such as rock weathering, nor human activities, such as pollutant emissions. It has both natural and artificial sources and is a secondary mixture source in a unique climatic environment. There is still a lack of comprehensive research on the impact of heavy-metal-containing dust on the river environment.

Based on the sources of HMs discussed above, we proposed a new model: the cycling model of HMs in the surface environment (Figure 9). The process from source to sink is the primary line of migration and enrichment of HMs. Undoubtedly, the bedrock area of the Kunlun Mountains has a high HM geochemical background and is the important source of HMs in the Golmud River. After the rock is weathered and leached, many ions, including HMs, are released into

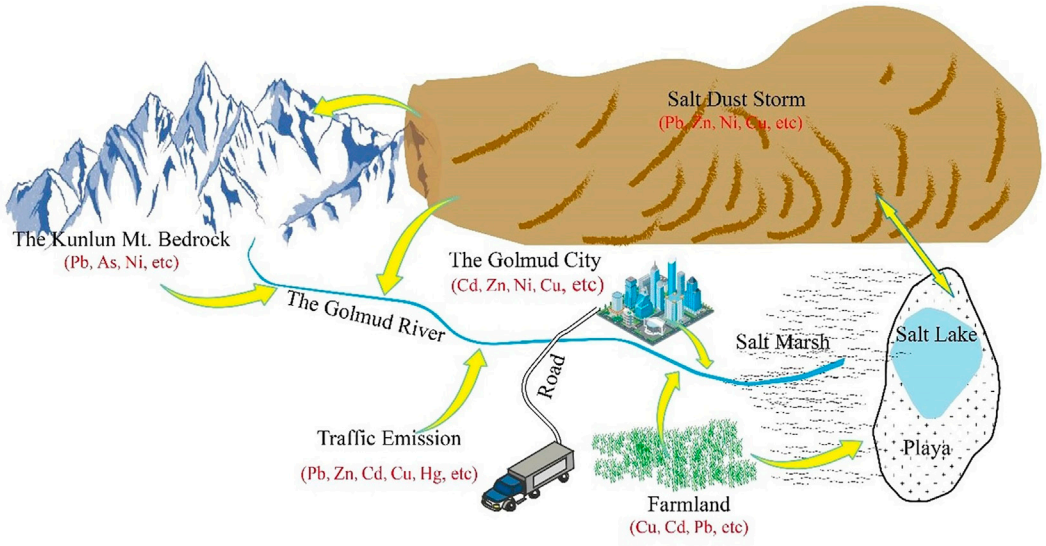

FIGURE 9
Cycling model of heavy metals in the surface environment.

the river, which flows downstream to the basin. From the mountainous watershed of the river to the terminal salt lake, the arid climate causes the continuous salinization of the river and constant enrichment of HMs, which are highly enriched in the salt lake and salt deposits (including playa). In summary, the analysis above considers common natural processes and human actions; however, the source of HMs in the Golmud River is comprehensive and complex. HMs continue to undergo complex migration, enrichment, and transformation with various carriers in atmospheric, soil, and water environments. Under the natural geological and geographical conditions of the Qaidam Basin, various provenances in different environments constitute the material cycle of HM elements in the regional surface environment.

4 Conclusion

In this research, the decreasing trends of HM concentrations in both water and sediment were noted as Zn > Cu > Ni > As > Pb > Cd > Hg and Ni > Zn > Pb > As > Cu > Cd > Hg. The HM contents in water were low but relatively high in sediment. Brine is a particular water type, and existing water quality standards are unsuitable for measuring whether HMs pollute it. Pi, mCd, CF, HPI, HEI, and WQI revealed no risk to the water of the Golmud River, and it was clean. The NP values of HMs in water and sediment were primarily influenced by high concentrations of Ni and Zn. In sediment, the concentrations of 27% HMs exceeded the background values of soil in Qinghai; 48% exceeded the Earth's crust background values, and six water quality evaluation methods showed that As, Hg, and Cd were the major pollutants. The ecological risk values of HMs showed a low risk in water and a medium risk of Hg in sediment. The average THQ values for adults and children suggested that the non-carcinogenic risks were low. According to the carcinogenic risk, Ni may be carcinogenic in freshwater; As and Ni may be carcinogenic in sediment. Multivariate statistical analysis showed that the HMs mainly came from nature, and human activities will also have a certain impact on them. As and Hg had high background values, saline dust storms were one of the critical sources of HMs, especially Hg. The influence of the natural background, human activities, and various provenances in different environments constitutes the material cycling of HM elements in the regional surface environment.

Data availability statement

The original contributions presented in the study are included in the article/Supplementary Material, further inquiries can be directed to the corresponding author.

Author contributions

NC: Sample collection, data analysis, writing of the original draft. LL: Reviewing and editing. HZ: Conducted fieldwork and revised the initial draft. LC: Drew figures. SL: Sample collection, investigation. FM: Article language modification. XZ: Supervision, modify the article, funding acquisition. All authors agree to be accountable for the content of the work.

Funding

This work was financially supported by the Second Tibetan Plateau Scientific Expedition and Research (STEP) (2019QZKK0805), the Science and Technology Plan of Qinghai Province of China (2021-ZJ-T07), the National Natural Science Foundation of China (grant no. 41561144009) and the Basic Frontier Scientific Research Program of the Chinese Academy of Sciences (grant no. ZDBS-LY-DQC021).

Acknowledgments

We thank Donglin Gao for his help in drawing. Xiaolong Yuan, Rongchang Hong, LC, and Zheng Chang for their assistance in the fieldwork and Bo Wang, Haijun Li, Yuan Xue, Yuan Li, Guangqin Zhu, and Xiuzhen Ma for their help with sample pretreatment and analysis.

Conflict of interest

The authors declare that the research was conducted in the absence of any commercial or financial relationships that could be construed as a potential conflict of interest.

Publisher's note

Supplementary material

The Supplementary Material for this article can be found online at: https://www.frontiersin.org/articles/10.3389/fenvs.2022.1095731/full#supplementary-material

References

Abrahim, G., and Parker, R. (2008). Assessment of heavy metal enrichment factors and the degree of contamination in marine sediments from Tamaki Estuary, Auckland, New Zealand. *Environ. Monit. Assess.* 136, 227–238. doi:10.1007/s10661-007-9678-2

Ahmed, M. K., Baki, M. A., Islam, M. S., Kundu, G. K., Habibullah-Al-Mamun, M., Sarkar, S. K., et al. (2015). Human health risk assessment of heavy metals in tropical fish and shellfish collected from the river Buriganga, Bangladesh. *Environ. Sci. Pollut. Res. Int.* 22 (20), 15880–15890. doi:10.1007/s11356-015-4813-z

Ali, H., Khan, E., and Sajad, M. A. (2013). Phytoremediation of heavy metals-concepts and applications. *Chemosphere* 91, 869–881. doi:10.1016/j.chemosphere.2013.01.075

Anbazhagan, V., Partheeban, E. C., and Rajendran, R. (2022). Ecological risk assessment and seasonal variation of heavy metals in water and sediment collected from industrially polluted Cuddalore coast, Southeastern India. *Regional Stud. Mar. Sci.* 49, 102134. doi:10.1016/j.rsma.2021.102134

Aravinthasamy, P., Karunanidhi, D., Shankar, K., Subramani, T., Setia, R., Bhattacharya, P., et al. (2021). COVID-19 lockdown impacts on heavy metals and microbes in shallow groundwater and expected health risks in an industrial city of South India. *Environ. Nanotechnol. Monit. Manag.* 16, 100472. doi:10.1016/j.enmm.2021.100472

Azhari, A. E., Rhoujjati, A., Hachimi, M. L. E., and Ambrosi, J. P. (2017). Pollution and ecological risk assessment of heavy metals in the soil-plant system and the sediment-water column around a former Pb/Zn-mining area in NE Morocco. *Ecotoxicol. Environ. Saf.* 144, 464–474. doi:10.1016/j.ecoenv.2017.06.051

Bashir, I., Lone, F. A., Bhat, R. A., Mir, S. A., Dar, Z. A., and Dar, S. A. (2020). Concerns and threats of contamination on aquatic ecosystems. *Bioremediation Biotechnol.* 27, 1–26. doi:10.1007/978-3-030-35691-0_1

Benson, N. U., Adedapo, A. E., Fred-Ahmadu, O. H., Williams, A. B., Udosen, E. D., Ayejuyo, O. O., et al. (2018). New ecological risk indices for evaluating heavy metals contamination in aquatic sediment: A case study of the gulf of Guinea. *Reg. Stud. Mar. Sci.* 18, 44–56. doi:10.1016/j.Prisma.2018.01.004

Bodrud-Doza, M., Islam, A. R. M. T., Ahmed, F., Das, S., Saha, N., and Rahman, M. S. (2016). Characterization of groundwater quality using water evaluation indices, multivariate statistics and geostatistics in central Bangladesh. *Water Sci.* 30, 19–40. doi:10.1016/j.wsj.2016.05.001

Carvalho, V. S. D., Santos, I. F. D., Almeida, L. C., Souza, C. T. D., Júnior, J. B. D. S., Souza, L. A., et al. (2021). Spatio-temporal assessment, sources and health risks of water pollutants at trace levels in public supply river using multivariate statistical techniques. *Chemosphere* 282, 130942. doi:10.1016/j.chemosphere.2021.130942

Chen, J., Huang, Q., Lin, Y., Fang, Y., Qian, H., Liu, R., et al. (2019). Hydrogeochemical characteristics and quality assessment of groundwater in an irrigated region, Northwest China. *Water* 11, 96. doi:10.3390/w11010096

Chen, J. W., Zhang, H., Xue, J. Z., Yuan, L., Yao, W., and Wu, H. X. (2022). Study on spatial distribution, potential sources and ecological risk of heavy metals in the surface water and sediments at Shanghai Port, China. *Mar. Pollut. Bull.* 181, 113923. doi:10.1016/j.marpolbul.2022.113923

Chen, T., Chang, Q. R., Liu, J., Clevers, J. G. P. W., and Kooistra, L. (2016). Identification of soil heavy metal sources and improvement in spatial mapping based on soil spectral information: A case study in northwest China. *Sci. Total Environ.* 565, 155–164. doi:10.1016/j.scitotenv.2016.04.163

Chen, Y., Liu, Q., Xu, M., and Wang, Z. (2020). Inter-annual variability of heavy metals pollution in surface sediments of jiangsu coastal region, China: Case study of the dafeng port. *Mar. Pollut. Bull.* 150, 110720. doi:10.1016/j.marpolbul.2019.110720

Cheng, H., and Hu, Y. (2010). Lead (Pb) isotopic fingerprinting and its applications in lead pollution studies in China: A review. *Environ. Pollut.* 158 (5), 1134–1146. doi:10.1016/j.envpol.2009.12.028

Clemens, S., and Ma, J. F. (2016). Toxic heavy metal and metalloid accumulation in crop plants and foods. *Annu. Rev. Plant Biol.* 67, 489–512. doi:10.1146/annurev-arplant-043015-112301

Deng, J. C., Wang, Y. S., Liu, X., Hu, W. P., Zhu, J. G., and Zhu, L. (2016). Spatial distribution and risk assessment of heavy metals and as pollution in the sediments of a shallow lake. *Environ. Monit. Assess.* 188, 296. doi:10.1007/s10661-016-5301-8

Edet, A. E., and Offiong, O. E. (2002). Evaluation of water quality pollution indices for heavy metal contamination monitoring. A study case from the Akpabuyo-Odukpani area, Lower Cross River Basin (southeastern Nigeria). *GeoJournal.* 57, 295–304.

Gen, J. (2021). Dissertation. China: University of Chinese Academy of Sciences.Temporal and spatial distribution characteristics and discussion on provenance of soluble salt in atmospheric dustfall in the south of Qaidam Basin.

Githaiga, K. B., Njuguna, S. M., Gituru, R. W., and Yan, X. (2021). Water quality assessment, multivariate analysis and human health risks of heavy metals in eight major lakes in Kenya. *J. Environ. Manag.* 297, 113410. doi:10.1016/j.jenvman.2021.113410

Goher, M. E., Ali, M. H. H., and El-Sayed, S. M. (2019). Heavy metals contents in nasser lake and the nile river, Egypt: An overview. *Egypt. J. Aquatic Res.* 45, 301–312. doi:10.1016/j.ejar.2019.12.002

Gopal, V., Krishnakumar, S., Peter, T. S., Nethaji, S., Kumar, K. S., Jayaprakash, M., et al. (2016). Assessment of trace element accumulation in surface sediments off Chennai coast after a major flood event. *Mar. Poll. Bull.* 114 (02), 1063–1071. doi:10.1016/j.marpolbul.2016.10.019

Gopinathan, P., Ashok, K. S., Pradeep, K. S., and Madhu, J. (2022a). Sulphur in Jharia and Raniganj coalfields: Chemical fractionation and its environmental implications. *Environ. Res.* 204, 112382. doi:10.1016/j.envres.2021.112382

Gopinathan, P., Madhu, J., Ashok, K. S., Mahato, A., Subramani, T., Pradeep, K. S., et al. (2022b). Geochemical characteristics, origin and forms of sulphur distribution in the Talcher coalfield, India. *Fuel* 316, 123376. doi:10.1016/j.fuel.2022.123376

Gopinathan, P., Santosh, M. S., Dileepkumar, V. G., Subramani, T., Roopa, R., Masto, R. E., et al. (2022c). Geochemical, mineralogical and toxicological characteristics of coal fly ash and its environmental impacts. *Chemosphere* 307, 135710. doi:10.1016/j.chemosphere.2022.135710

Gulgundi, M. S., and Shetty, A. (2018). Groundwater quality assessment of urban Bengaluru using multivariate statistical techniques. *Appl. Water Sci.* 8, 43. doi:10.1007/s13201-018-0684-z

Hakanson, L. (1980). An ecological risk index for aquatic pollution control. A sedimentological approach. *Water Res.* 14 (8), 975–1001. doi:10.1016/0043-1354(80)90143-8

Harikrishnan, N., Ravisankar, R., Chandrasekaran, A., Gandhi, M. S., Kanagasabapathy, K. V., Prasad, M. V. R., et al. (2017). Assessment of heavy metal contamination in marine sediments of east coast of Tamil nadu affected by different pollution sources. *Mar. Pollut. Bull.* 121, 418–424. doi:10.1016/j.marpolbul.2017.05.047

Hong, G. H., Chitsan, L., Huu, T. T., Chow, F. C., Xuan, T. B., Nicholas, K. C., et al. (2020). Heavy metal contamination trends in surface water and sediments of a river in a highly industrialized region. *Environ. Technol. Innovation* 20, 101043. doi:10.1016/j.eti.2020.101043

Iqbal, J., Saleem, M., and Shah, M. H. (2016). Spatial distribution, environmental assessment and source identification of metals content in surface sediments of freshwater reservoir, Pakistan. *Geochemistry* 76 (01), 171–177. doi:10.1016/j.chemer.2016.02.002

Jaishankar, M., Tseten, T., Anbalagan, N., Mathew, B. B., and Beeregowda, K. N. (2014). Toxicity, mechanism and health effects of some heavy metals. *Interdiscip. Toxicol.* 7 (2), 60–72. doi:10.2478/intox-2014-0009

João, P. V., Artur, J. M. V., and Luisa, D. (2019). Assessment of heavy metal pollution from anthropogenic activities and remediation strategies: A review. *J. Environ. Manag.* 246, 101–118. doi:10.1016/j.jenvman.2019.05.126

Karim, A., and Veizer, J. (2000). Weathering processes in the Indus River Basin: Implications from riverine carbon, sulfur, oxygen, and strontium isotopes. *Chem. Geol.* 170 (1-4), 153–177. doi:10.1016/S0009-2541(99)00246-6

Karunanidhi, D., Aravinthasamy, P., Subramani, T., and Kumar, M. (2021b). Human health risks associated with multipath exposure of groundwater nitrate and environmental friendly actions for quality improvement and sustainable management: A case study from texvalley (tiruppur region) of India. *Chemosphere* 265, 129083. doi:10.1016/j.chemosphere.2020.129083

Karunanidhi, D., Aravinthasamy, P., Deepali, M., Subramani, T., and Shankar, K. (2021c). Groundwater pollution and human health risks in an industrialized region of southern India: Impacts of the COVID-19 lockdown and the monsoon seasonal cycles. *Arch. Environ. Contam.* 80, 259–276. doi:10.1007/s00244-020-00797-w

Karunanidhi, D., Aravinthasamy, P., Subramani, T., Chandrajith, R., Janardhana Raju, N., and Antunes, I. M. H. R. (2022). Provincial and seasonal influences on heavy metals in the Noyyal River of South India and their human health hazards. *Environ. Res.* 204, 111998. doi:10.1016/j.envres.2021.111998

Karunanidhi, D., Aravinthasamy, P., Subramani, T., Kumar, D., and Venkatesan, G. (2021d). Chromium contamination in groundwater and Sobol sensitivity model based human health risk evaluation from leather tanning industrial region of South India. *Environ. Res.* 199, 111238. doi:10.1016/j.envres.2021.111238

Karunanidhi, D., Aravinthasamy, P., Subramani, T., and Setia, R. (2021a). Effects of COVID-19 pandemic lockdown on microbial and metals contaminations in a part of thirumanimuthar river, south India: A comparative health hazard perspective. *Hazard. Mater.* 416, 125909. doi:10.1016/j.jhazmat.2021.125909

Ke, X., Gui, S., Huang, H., Zhang, H., Wang, C., and Guo, W. (2017). Ecological risk assessment and source identification for heavy metals in surface sediment from the Liaohe River protected area, China. *Chemosphere* 175, 473–481. doi:10.1016/j.chemosphere.2017.02.029

Lanzerstorfer, C. (2018). Heavy metals in the finest size fractions of road deposited sediments. *Environ. Pollut.* 239, 522–531. doi:10.1016/j.envpol.2018.04.063

Li, D., Yu, R., Chen, J., Leng, X., Zhao, D., Jia, H., et al. (2022). Ecological risk of heavy metals in lake sediments of China: A national-scale integrated analysis. *J. Clean. Prod.* 334, 130206. doi:10.1016/j.jclepro.2021.130206

Li, F. L., Liu, C. Q., Yang, Y. G., Bi, X. Y., Liu, T. Z., and Zhao, Z. Q. (2012). Natural and anthropogenic lead in soils and vegetables around guiyang city, southwest China: A Pb isotopic approach. *Sci. Total Environ.* 431, 339–347. doi:10.1016/j.scitotenv.2012.05.040

Li, L. M., Wu, J., Lu, J., Li, K. X., Zhang, X. Y., Min, X. Y., et al. (2022). Water quality evaluation and ecological-health risk assessment on trace elements in surface water of the northeastern Qinghai-Tibet Plateau. *Ecotoxicol. Environ. Saf.* 241, 113775. doi:10.1016/j.ecoenv.2022.113775

Li, L. M., Wu, J., Lu, J., Min, X. Y., Xu, J., and Yang, L. (2018). Distribution, pollution, bioaccumulation, and ecological risks of trace elements in soils of the northeastern Qinghai-Tibet Plateau. *Ecotoxicol. Environ. Saf.* 166, 345–353. doi:10.1016/j.ecoenv.2018.09.110

Li, L., Wu, J., Lu, J., and Xu, J. (2020a). Speciation, risks and isotope-based source apportionment of trace elements in soils of the northeastern Qinghai-Tibet Plateau. *Geochem Explor, Environ. Anal.* 20, 315–322. doi:10.1144/geochem2019-042

Li, L., Wu, J., Lu, J., and Xu, J. (2020b). Trace elements in Gobi soils of the northeastern Qinghai-Tibet Plateau. *Chem. Ecol.* 36 (10), 967–981. doi:10.1080/02757540.2020.1817403

Liu, Q. Q., Wang, F. F., Meng, F. P., Jiang, L., Li, G. J., and Zhou, R. G. (2018a). Assessment of metal contamination in estuarine surface sediments from Dongying City, China: Use of a modified ecological risk index. *Mar. Pollut. Bull.* 126, 293–303. doi:10.1016/j.marpolbul.2017.11.017

Liu, W., Xie, C., Li, R., Liu, G., Wang, W., Liu, H., et al. (2021). Rapid expansion of lakes in the endorheic basin on the Qinghai-Tibet Plateau since 2000 and its potential drivers. *Catena* 197, 104942. doi:10.1016/j.catena.2020.104942

Liu, Y., Cheng, Y., Li, F. X., Zhang, C. P., Liu, J. W., Zhang, L., et al. (2012). Pollution evaluation of vertical sediments in the Yalu River Estuary over the past century. *Res. Environ. Sci.* 25 (5), 489–494.

Liu, Y. F., Huang, H. H., Sun, T., Yuan, Y., Pan, Y., Xie, Y. J., et al. (2018b). Comprehensive risk assessment and source apportionment of heavy metal contamination in the surface sediment of the Yangtze River Anqing section, China. *Environ. Earth Sci.* 77, 493. doi:10.1007/s12665-018-7621-1

Liu, Y. X., Wang, Q., Zhuang, W., Yuan, Y. L., Yuan, Y. N., Jiao, K. Q., et al. (2017). Calculation of thallium's toxicity coefficient in the evaluation of potential ecological risk index: A case study. *Chemosphere* 194, 562–569. doi:10.1016/j.chemosphere.2017.12.002

Lough, G. C., Schauer, J. J., Park, J. S., Shafer, M. M., Deminter, J. T., and Weinstein, J. P. (2005). Emissions of metals associated with motor vehicle roadways. *Environ. Sci. Technol.* 39 (3), 826–836. doi:10.1021/es048715f

Lu, J., Lin, Y., Wu, J., and Zhang, C. (2021). Continental-scale spatial distribution, sources, and health risks of heavy metals in seafood: Challenge for the water-food-energy nexus sustainability in coastal regions. *Environ. Sci. Pollut. Res.* 28, 63815–63828. doi:10.1007/s11356-020-11904-8

Lu, J., Wu, J., and Wang, J. H. (2022a). Metagenomic analysis on resistance genes in water and microplastics from a mariculture system. *Front. Environ. Sci. Eng.* 16, 4. doi:10.1007/s11783-021-1438-y

Lu, J., Zhang, Y. X., Wu, J., and Wang, J. H. (2022b). Intervention of antimicrobial peptide usage on antimicrobial resistance in aquaculture. *J. Hazard Mater* 427, 128154. doi:10.1016/j.jhazmat.2021.128154

Luo, W., Lu, Y., Giesy, J. P., Wang, T., Shi, Y., Wang, G., et al. (2007). Effects of land use on concentrations of metals in surface soils and ecological risk around Guanting Reservoir, China. *Environ. Geochem Health* 29, 459–471. doi:10.1007/s10653-007-9115-z

Mahmudul, H., Mahfujur, R., Alif, A., Md, Atikul, I., and Mahfuzur, R. (2022). Heavy metal pollution and ecological risk assessment in the surface water from a marine protected area, Swatch of No Ground, north-western part of the Bay of Bengal. *Reg. Stud. Mar. Sci.* 52, 102278. doi:10.1016/j.rsma.2022.102278

McComb, J. Q., Han, F. X., Rogers, C., Thomas, C., Arslan, Z., Ardeshir, A., et al. (2015). Trace elements and heavy metals in the grand bay national estuarine reserve in the northern gulf of Mexico. *Mar. Pollut. Bull.* 99, 61–69. doi:10.1016/j.marpolbul.2015.07.062

Meghdad, P., Nazir, F., Kiomars, S., Razieh, K., and Zahra, A. (2016). Essential and toxic heavy metals in cereals and agricultural products marketed in Kermanshah, Iran, and human health risk assessment. *Food Addit. Contam.* Part B 9 (1), 15–20. doi:10.1080/19393210.2015.1099570

Mehdi, Q., Mahmoud, S., Seyed, A. S., Mansoureh, F., Saeed, E., Mahmood, Y., et al. (2019). Cadmium in groundwater consumed in the rural areas of Gonabad and Bajestan, Iran: occurrence and health risk assessment. *Biol. Trace Elem. Res.* 192 (2), 106–115. doi:10.1007/s12011-019-1660-7

Ministry of Health (2006). *Standards for drinking water quality. GB57492006*. Beijing: Ministry of Health of the People's Republic of China.

Nethaji, S., Kalaivanan, R., Arya, V., and Jayaprakash, M. (2017). Geochemical assessment of heavy metals pollution in surface sediments of vellar and coleroon estuaries, southeast coast of India. *Mar. Pollut. Bull.* 115 (1-2), 469–479. doi:10.1016/j.marpolbul.2016.11.045

Özgür, C., Memet, V., Özlem, Ö. O., Kürsad, K. E., and Metin, Ç. (2020). A comparison of trace element concentrations in surface and deep water of the Keban Dam Lake (Turkey) and associated health risk assessment. *Environ. Res.* 190, 110012. doi:10.1016/j.envres.2020.110012

Pourkhabbaz, A., and Pourkhabbaz, H. (2012). Investigation of toxic metals in the tobacco of different Iranian cigarette brands and related health issues. *Iran. J. Basic Med. Sci.* 15, 636–644.

Qiao, J., Zhu, Y., Jia, X., Shao, M., Niu, X., and Liu, J. (2020). Distributions of arsenic and other heavy metals, and health risk assessments for groundwater in the Guanzhong Plain region of China. *Environ. Res.* 181, 108957. doi:10.1016/j.envres.2019.108957

Qu, M., Wang, Y., Huang, B., and Zhao, Y. (2018). Source apportionment of soil heavy metals using robust absolute principal component scores-robust geographically weighted regression (RAPCS-RGWR) receptor model. *Sci. Total Environ.* 626, 203–210. doi:10.1016/j.scitotenv.2018.01.070

Ravindra, K., Thind, P. S., Mor, S., Singh, T., and Mor, S. (2019). Evaluation of groundwater contamination in chandigarh: Source identification and health risk assessment. *Environ. Pollut.* 255, 113062. doi:10.1016/j.envpol.2019.113062

Rzetala, M. A. (2016). Cadmium contamination of sediments in the water reservoirs in Silesian Upland (southern Poland). *J. Soils Sediments* 16, 2458–2470. doi:10.1007/s11368-016-1477-3

Saleem, M., Iqbal, J., and Shah, M. H. (2015). Geochemical speciation, anthropogenic contamination, risk assessment and source identification of selected metals in freshwater sediments a case study from Mangla Lake, Pakistan. *Environ. Nanotechnol. Monit. Manag.* 4, 27–36. doi:10.1016/j.enmm.2015.02.002

Sener, S., Sener, E., and Davraz, A. (2017). Evaluation of water quality using water quality index (WQI) method and GIS in Aksu River (SW-Turkey). *Sci. Total Environ.* 584-585, 131–144. doi:10.1016/j.scitotenv.2017.01.102

Shamuyarira, K. K., and Gumbo, J. R. (2014). Assessment of heavy metals in municipal sewage sludge: A case study of limpopo Province, south Africa. *Int. J. Environ. Res. Public Health* 11, 2569–2579. doi:10.3390/ijerph110302569

Sharafi, K., Nodehi, R. N., Yunesian, M., Mahvi, A. H., Pirsaheb, M., and Nazmara, S. (2019). Human health risk assessment for some toxic metals in widely consumed rice brands (domestic and imported) in tehran, Iran: Uncertainty and sensitivity analysis. *Food Chem.* 277, 145–155. doi:10.1016/j.foodchem.2018.10.090

Sharma, R. K., and Agrawal, M. (2005). Biological effects of heavy metals: An overview. *J. Environ. Biol.* 26, 301–313.

Sheng, Y. (2015). *Physical and chemical characteristics of dust aerosol from Golmud and its source analysis. Master*. China: Nanjing Normal University.

Singh, K. P., Mohan, D., Singh, V. K., and Malik, A. (2005). Studies on distribution and fractionation of heavy metals in Gomti river sediments-A tributary of the Ganges, India. *J. Hydrol.* 312, 14–27. doi:10.1016/j.jhydrol.2005.01.021

Singh, V. B., Ramanathan, A., Pottakkal, J. G., and Kumar, M. (2014). Seasonal variation of the solute and suspended sediment load in Gangotri glacier meltwater, central Himalaya, India. *J. Asian Earth Sci.* 79, 224–234. doi:10.1016/j.jseaes.2013.09.010

Song, W. J., Yang, S. Z., and Mu, B. Z. (2014). Determination methods for rubidium and cesium in salt lake brine. *Inorg. Chem. Ind.* 46 (11), 55–58.

Sun, X., Fan, D., Liu, M., Tian, Y., Pang, Y., and Liao, H. J. (2018). Source identification, geochemical normalization and influence factors of heavy metals in Yangtze River Estuary sediment. *Environ. Pollut.* 241, 938–949. doi:10.1016/j.envpol.2018.05.050

Suresh, G., Sutharsan, P., Ramasamy, V., and Venkatachalapathy, R. (2012). Assessment of spatial distribution and potential ecological risk of the heavy metals in relation to granulometric contents of Veeranam Lake sediments, India. *Ecotoxicol. Environ. Saf.* 84, 117–124. doi:10.1016/j.ecoenv.2012.06.027

Tang, W. Z., Shan, B. Q., Zhang, H., Zhang, W. Q., Zhao, Y., Ding, Y. K., et al. (2014). Heavy metal contamination in the surface sediments of representative limnetic ecosystems in eastern China. *Sci. Rep.* 4 (7152), 7152–7157. doi:10.1038/srep07152

Taylor, S. R., and Mclennan, S. M. (1985). *The continental crust: Its composition and evolution*. London: Blackwell.

Tchounwou, P. B., Yedjou, C. G., Patlolla, A. K., and Sutton, D. J. (2012). Heavy metal toxicity and the environment. *Mol. Clin. Environ. Toxicol.* 101, 133–164. doi:10.1007/978-3-7643-8340-4_6

Tiwari, T. N., and Mishra, M. (1985). A preliminary assignment of water quality index of major Indian rivers. *Indian J. Environ. Prot.* 5 (4), 276–279.

Tomlinson, D. L., Wilson, J. G., Harris, C. R., and Jeffrey, D. W. (1980). Problems in the assessment of heavy-metal levels in estuaries and the formation of a pollution index. *Helgol Meeresunters* 33 (1-4), 566–575. doi:10.1007/bf02414780

USEPA,1991. Human health evaluation manual, supplemental guidance:"Standard default exposure factors". 6–03. OSWER Directive 9285.

USEPA, 2004. Risk assessment guidance for superfund volume I: Human health evaluation manual (Part E, supplemental guidance for dermal risk assessment) final. OSWER 9285.7-02EP, July 2004.

Ustaoglu, F., Tepe, Y., and Tas, B. (2020). Assessment of stream quality and health risk in a subtropical Turkey river system: A combined approach using statistical analysis and water quality index. *Ecol. Indic.* 113, 105815. doi:10.1016/j.ecolind.2019.105815

Vu, C. T., Lin, C., Yeh, G., and Villanueva, M. C. (2017). Bioaccumulation and potential sources of heavy metal contamination in fish species in taiwan: Assessment and possible human health implications. *Environ. Sci. Pollut. Res.* 24 (23), 19422–19434. doi:10.1007/s11356-017-9590-4

Wang, H., Nie, L., Xu, Y., Du, C., Zhang, T., and Wang, Y. (2018). Effects of highway related pollutant on the groundwater quality of turfy swamps in the Changbai Mountain Area. *Int. J. Environ. Res. Public Health.* 15, 1652. doi:10.3390/ijerph15081652

Wang, L., Wang, Y., Zhang, W. Z., Xu, C. X., and An, Z. Y. (2014b). Multivariate statistical techniques for evaluating and identifying the environmental significance of heavy metal contamination in sediments of the Yangtze River, China. *Environ. Earth Sci.* 71 (3), 1183–1193. doi:10.1007/s12665-013-2522-9

Wang, Y. H. (2014a). *Geochemistry evolution and water cycle patterns of groundwater in Golmud River basin*. Dissertation. China: Chang'an University.

Wang, Y. P., Bai, H. J., Xiao, R., Gao, H. F., Huang, L. B., and Huang, C. (2013). Assessment of heavy metal contamination in the soil-plant system of the Suaeda salsa wetland in the Yellow River Estuary. *Acta Ecol. Sin.* 33 (10), 3083–3091. doi:10.5846/stxb201202230246

Wang, Z. H., Feng, J., and Nie, X. P. (2015). Recent environmental changes reflected by metals and biogenic elements in sediments from the Guishan Island, the Pearl River Estuary, China. *Estuar. Coast Shelf Sci.* 164, 493–505. doi:10.1016/j.ecss.2015.08.002

Wei, F. S., Chen, J. S., Wu, Y. Y., Zhen, C. J., Jiang, D. Z., Liu, Z. H., et al. (1990). *Chinese soil element background values*. China: China Environmental Press.

Wei, X., Han, L. F., Gao, B., Zhou, H. D., Lu, J., and Wan, X. H. (2016). Distribution, bioavailability, and potential risk assessment of the metals in tributary sediments of Three Gorges Reservoir: The impact of water impoundment. *Ecol. Indic.* 61, 667–675. doi:10.1016/j.ecolind.2015.10.018

Withanachchi, S., Ghambashidze, G., Kunchulia, I., Urushadze, T., and Ploeger, A. (2018). Water quality in surface water: A preliminary assessment of heavy metal contamination of the mashavera river, Georgia. *Int. J. Environ. Res. Public Health* 15, 621. doi:10.3390/ijerph15040621

Xiang, J. Y. (2020). *Source identification, pollution and potential ecological risk assessment of the potentially toxic elements (PTEs) in the area of the Golmud city-golmud river-dabuxun lake*. Dissertation. China: University of Chinese Academy of Sciences.

Xiao, H. F., Zhang, S. Y., Guan, Y., Liu, S. J., Gao, Y., Sun, Q. Z., et al. (2014). Assessment of potential risks associated with heavy metal contamination in sediment in Aobaopao Lake, China, determined from sediment cores. *Ecotoxicology* 23, 527–537. doi:10.1007/s10646-014-1220-z

Xiao, J., Wang, L., Deng, L., and Jin, Z. (2019). Characteristics, sources, water quality and health risk assessment of trace elements in river water and well water in the Chinese Loess Plateau. *Sci. Total Environ.* 650 (2), 2004–2012. doi:10.1016/j.scitotenv.2018.09.322

Yang, A., Wang, X. X., Xing, W. C., Hu, J., Liu, X. L., and Li, J. (2020). Source and risk evaluation of heavy metals in surface sediments of rivers, lakes and their surrounding soils in Qinghai Province. *J. Tianjin Normal Univ. Nat. Sci. Ed.* 40 (06), 44–53. doi:10.19638/j.issn1671-1114.20200608

Yao, Z. G., Bao, Z. Y., and Gao, P. (2006). Environmental assessments of trace metals in sediments from dong ting lake, central China. *Jour China Univ. Geo Sci.* 17, 310–319. doi:10.1016/S1002-0705(07)60004-1

Yuen, J. Q., Olin, P. H., Lim, H. S., Benner, S. G., Sutherland, R. A., and Ziegler, A. D. (2012). Accumulation of potentially toxic elements in road deposited sediments in residential and light industrial neighborhoods of Singapore. *J. Environ. Manag.* 101, 151–163. doi:10.1016/j.jenvman.2011.11.017

Zahra, A., Hashmi, M. Z., Malik, R. N., and Ahmed, Z. (2014). Enrichment and geo-accumulation of heavy metals and risk assessment of sediments of the kurang nallah—feeding tributary of the rawal lake reservoir, Pakistan. *Sci. Total Environ.* 470-471, 925–933. doi:10.1016/j.scitotenv.2013.10.017

Zhang, L. L., and Liu, J. L. (2014). *In situ* relationships between spatial-temporal variations in potential ecological risk indexes for metals and the short-term effects on periphyton in a macrophyte-dominated lake: A comparison of structural and functional metrics. *Ecotoxicology* 23 (4), 553–566. doi:10.1007/s10646-014-1175-0

Zhang, X., Hu, B., Wang, P., Chen, J., Yang, L., Xiao, K., et al. (2018). Hydrogeochemical evolution and heavy metal contamination in groundwater of a reclaimed land on Zhoushan Island. *Water* 10, 316. doi:10.3390/w10030316

Zhao, R., Guan, Q. Y., Luo, H. P., Lin, J. K., Yang, L. Q., Wang, F. F., et al. (2019). Fuzzy synthetic evaluation and health risk assessment quantification of heavy metals in Zhangye agricultural soil from the perspective of sources. *Sci. Total Environ.* 697 (20), 134126. doi:10.1016/j.scitotenv.2019.134126

frontiers | Frontiers in Environmental Science

TYPE Original Research
PUBLISHED 09 February 2023
DOI 10.3389/fenvs.2023.1071353

OPEN ACCESS

EDITED BY
Jun Wu,
Harbin Engineering University, China

REVIEWED BY
Jian Zhang,
Guizhou University, China
Li Leiming,
Qinghai Institute of Salt Lakes (CAS), China

*CORRESPONDENCE
Ke Liu,
1720906445@qq.com

SPECIALTY SECTION
This article was submitted to Toxicology, Pollution and the Environment, a section of the journal Frontiers in Environmental Science

RECEIVED 16 October 2022
ACCEPTED 27 January 2023
PUBLISHED 09 February 2023

CITATION
Zhang J, Liu K, He X, Li W, Zhang M and Cai Q (2023), Evaluation of heavy metal contamination of soil and the health risks in four potato-producing areas. *Front. Environ. Sci.* 11:1071353. doi: 10.3389/fenvs.2023.1071353

Evaluation of heavy metal contamination of soil and the health risks in four potato-producing areas

Jie Zhang, Ke Liu*, Xue He, Wei Li, Meng Zhang and Quan Cai

College of Agriculture, Guizhou University, Guiyang, Guizhou, China

Areas polluted by heavy metals in soil may pose a major risk to human health and ecological environment safety. In this study, 89 soil samples were collected from four potato producing areas (Libo, Chishui, Panxian and Weining) in Guizhou Province, China, and the concentrations of 9 soil heavy metals were analyzed and measured. The aims of this study was to evaluate the human health risk and pollution index of heavy metals in the soil of some potato-producing areas in Guizhou Province by using the geoaccumulation index method, pollution load index method and health risk assessment method. The results revealed that Igeo<0 in Libo and Chishui, Igeo>0 in Panxian except Pb, The Igeo of As and Sb were less than 0 in Weining, and other elements were polluted to varying degrees. The pollution load index is Panxian (1.47) > Weining (1.39) > Libo (0.67), Chishui (0.67), Libo and Chishui were generally no polluted, soils in Panxian and Weining were polluted. The health risks of potatoes through food ingestion are less than 1. In terms of carcinogenesis, the risk of human in each study area through the ingestion was Cr > As > Cd. Cr and As would be produced certain carcinogenic risk to human through the dermal contact. Cr had a strong carcinogenic risk to adults through the inhalation. In terms of non-carcinogenesis, children in each study area had a strong risk under the each pathways. The risk of carcinogenesis in adults through inhalation pathway is greater than that in children, and the risk of carcinogenesis and non-carcinogenesis in children through Ingestion and dermal contact pathway is greater than adults. The results of this study suggest that attention should be paid to the remediation of heavy metals in contaminated soil to protect human health.

KEYWORDS

soil, heavy metals, potato, pollution evaluation, health risk evaluation

1 Introduction

Soil is the most important natural resource that ensures the safety, quantity and quality of human food and is also an important object of ecological and environmental protection (Ministry of Environmental Protection 2014). The continued acceleration of industrialization in China indicates that the problem of soil environmental pollution has gradually become a major factor that affects the quality of agricultural products and threatens human health (Mohmand et al., 2015). The common heavy metals in soil include Hg, As, Cd, Cr, Cu, Zn, Ni, and Pb, which have strong toxicity (SUN et al., 2008). Human activities will cause the content of heavy metals in soil to be significantly higher than its natural background value, and cause ecological damage and environmental quality deterioration (Jiang 2008).

In recent years, with the intensification of urbanization and the changes in land use, some heavy metal elements caused by the geological background have also been activated, causing the

soil's heavy metals to migrate and become enriched (TUCL et al., 2013). Heavy metals in the soil not only affect and change the ecological function of soil but also directly or indirectly endanger human health through ingestion, dermal contact, and inhalation. When the human body is overloaded with heavy metals, it can damage the function of the nervous system, disrupt the endocrine system, and affect IQ (intelligence quotient) and behavior (US EPA 1994). Heavy metals in soil can combine with proteins, polypeptides, enzymes, and other macromolecular substances in agricultural objects to enrich edible parts, such as potato tubers and carrot roots, and enter the human body through the food chain (Wang et al., 2006). This process poses potential health risks and can have serious carcinogenic and non-carcinogenic hazards. Therefore, the evaluation of the contamination status of soil by heavy metals is a matter of food safety and human health (Yang et al., 2014). For example, the heavy metal Cd will lead to renal dysfunction, lung adenocarcinoma, and prostate hyperplasia, as well as lead to skin cancer, neuropathy, and cardiovascular and cerebrovascular diseases. Excessive intake of Pb will damage human brain cells and cause damage to kidneys, digestion, and the immune system. The toxicity levels of Cu and Ni are relatively small, but excessive intake will also cause damage to human organs (Patlolla et al., 2012; Pascaud et al., 2014; Zhao et al., 2018).

Therefore, it is important to highlight the human health risks brought by heavy metals in the soil so that focus can be given to the study of heavy metal pollution in soil and agricultural areas and the assessment of the harm caused by these heavy metals. The geoaccumulation index, pollution load index, and health risk evaluation methods are usually utilized by researchers to evaluate the heavy metals contamination of soil. The results of such evaluations can accurately reflect the degree of contamination status in a study area. Many studies have focused on this field (Fakhri et al., 2018; Kamani et al., 2018; Rezaei et al., 2018; Yousefi et al., 2018). However, there is no investigation and evaluation of soil heavy metal pollution in many potato-producing areas, and some evaluation methods are too simple. Therefore, the aims of this study were to determine the distribution of soil heavy metal content, pollution situation, and human health risk pollution in some potato-producing areas of Guizhou Province, China.

2 Materials and methods

2.1 Study area description

Guizhou Province in China is between 103° 36′—109° 35′E and 24° 37′—29° 13′N, with an east-west length of approximately 595 km and a north-south distance of approximately 509 km. The total area of the province is 176,167 km^2, accounting for 1.8% of the total area of the country. The geomorphology of the province can be divided into four basic types: plateau, mountain, hill, and basin. The altitude difference is large, with an average altitude of approximately 1100 m. The climate is warm and humid, belonging to the subtropical humid monsoon climate. The annual average temperature is 15–18°C, and the annual average precipitation is 800–1500 mm. The annual average sunshine duration is 1,200–1600 h. There is no excessive heat in summer, the spring is warm, and the autumn is cool. The unique climate and geographical location give rise to diverse ecological types. The soil in Guizhou Province is generally slightly acidic, and the main soil types include yellow soil, lime soil, red soil, yellow-brown soil, purple soil, and paddy soil, which respectively account for 46.51%, 17.55%, 7.22%, 6.21%, 5.59%, and 9.77% of the total soil area in Guizhou Province. Libo and Chishui are both World Natural Heritage Sites, which are protected to a certain extent. Panxian and Weining have been engaged in industrial and mining activities for nearly 60 years; the generated waste residue, smoke and dust pollutes the environment to a certain extent. In addition, local residents apply pesticides and fertilizers to the soil, and the domestic waste is disposed disorderly, resulting in serious heavy metal pollution accumulation. The location of the study area is shown in Figure 1.

2.2 Sampling area distribution and sample collection

The distribution of points in each sampling area is shown in Figure 1. The major counties in Guizhou Province that produce potatoes include Libo (Figure 1A), Chishui (Figure 1B), Panxian (Figure 1C), and Weining (Figure 1D). These counties were selected to serve as the source of 89 soil samples from the upper layer of soil (0–20 cm), including 12 from Libo, 11 from Chishui, 29 from Panxian, and 37 from Weining. The "five-point method" was used to randomly sample five batches of inter-root soil and mix them to generate one soil sample (Brewer R et al., 2017). A total of 1 kg of samples were brought back to the laboratory for processing. A GPS locator was used to precisely position and record the latitude, longitude, elevation, sampling location, and soil type of each sample during the collection process. First, plant residues, gravel, and other debris were removed from the soil samples. These samples were then sieved through 100 mesh after natural air-drying to determine the soil's physical and chemical properties and the contents of heavy metals.

2.3 Sample determination

The soil pH was determined using the $CaCl_2$ leaching method with a pH meter (water:soil = 2.5:1 [v/v]) (Bao 2000). The concentrations of As and Pb were determined by atomic fluorescence spectrometry using the Chinese standard (GB/T 22105.2-2008), (GB/T 22105.3-2008). The concentrations of Mn, Zn, Cu, Ni, and Cr were determined using flame atomic absorption spectrophotometry (HJ 491–2019). The concentration of Cd was determined using graphite furnace atomic absorption spectrophotometry (GB/T 17141-1997). Sb was determined using inductively coupled mass spectrometry (ICP-MS) with microwave digestion, as described by Wang et al. (2022). A blank was used throughout the determination, and the national reference material GB W07428 (GSS-14) was used for quality control (Long and TanJ, 2013). The spiked recoveries of each metal element were in the range of 90%–110%.

2.4 Evaluation methodology

2.4.1 Geoaccumulation index method

The geoaccumulation index method was proposed by the German scientist Muller in 1979 (MÜLLER 1969). The effect of

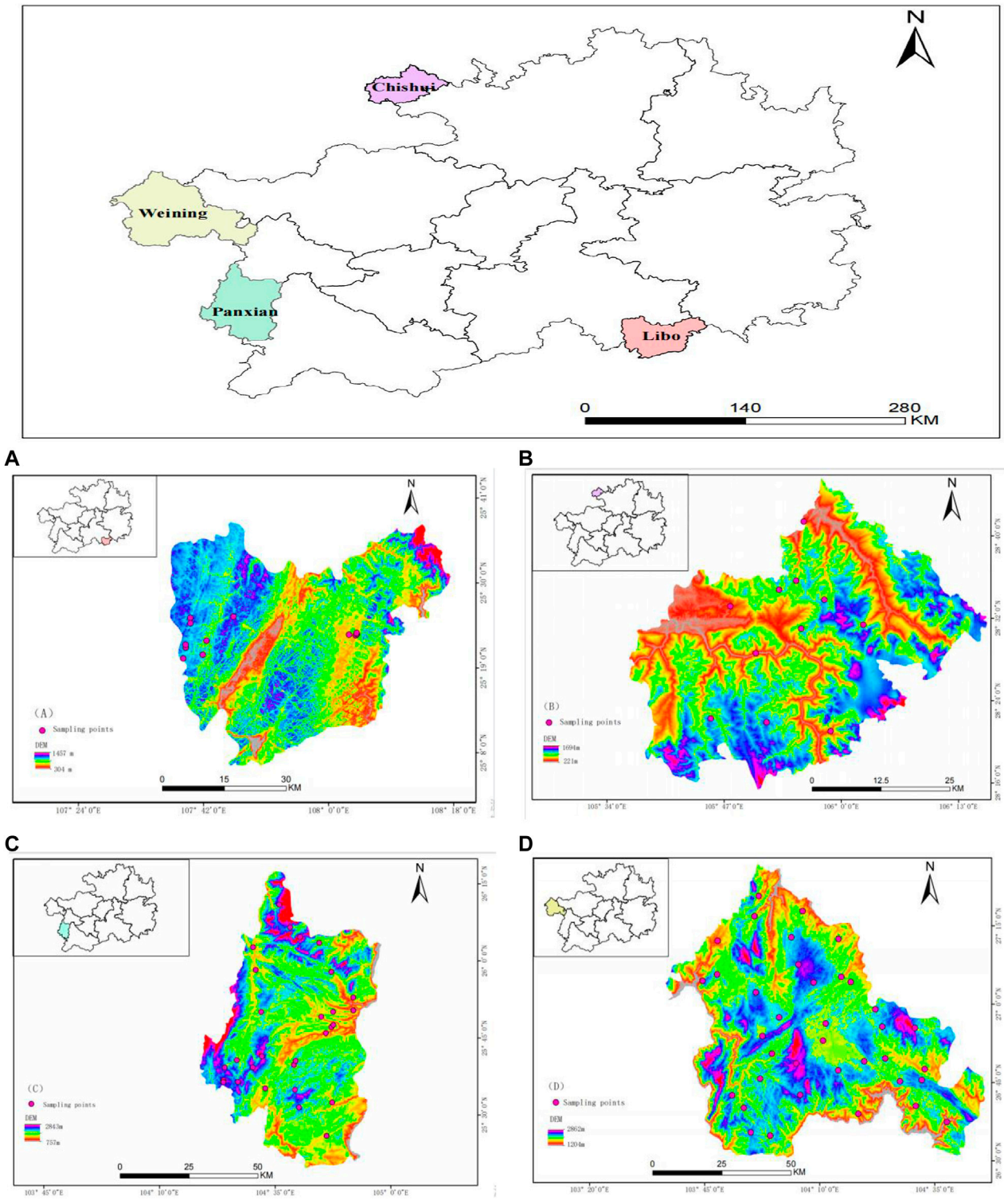

FIGURE 1
Distribution map of sampling points in the study area. Note: **(A–D)** represent Libo, Chishui, Panxian, and Weining in Guizhou Province, China.

diagenesis on the background values of soils is considered and commonly used to quantitatively evaluate the degree of heavy metals contamination in sediments and soils in the aquatic environment and their classification (Ma et al., 2020). The formula is as follows:

$$I_{geo} = \log_2\left(\frac{C_i}{1.5 \times B_i}\right) \quad (1)$$

Where I_{geo} is the geoaccumulation index; C_i is the measured content of element i in the soil sample; B_i is the soil background value for element

i, and 1.5 is the constant term. B_i used the background values of soil elements from Guizhou Province in this study (China General Environmental Monitoring Station 1990), and the evaluation grading criteria are shown in Supplementary Table S1 (Xu et al., 2013; NEYESTANI et al., 2016).

2.4.2 Pollution load index method

The background soil values of heavy metals in Guizhou Province were used as a reference (Yang, 2019), and the pollution load index method proposed by Tomlinson was used to evaluate the heavy metal pollution in soil in the study area. This index can visually reflect the degree of contribution of individual heavy metals to pollution and reflect the trend of heavy metals in time and space (DU et al., 2021). The formula is as follows:

$$CF_i = C_i / C_{0i} \quad (2)$$

$$I_{PL} = \sqrt[n]{CF_1 \times CF_2 \times \cdots \times CF_n} \quad (3)$$

$$I_{PLzone} = \sqrt[m]{I_{PL1} \times I_{PL2} \times \cdots \times I_{PLm}} \quad (4)$$

Where CF_i is the pollution index of heavy metal i; C_i is the measured value of I; C_{0i} is the background value of i; I_{PL} is the pollution load index of a sampling point; n is the number of sampling points; I_{PLzone} is the pollution load index of a sampling area, and m is the number of species of polluting heavy metal i. The evaluation criteria for the pollution load index method are shown in Supplementary Table S1.

2.4.3 Human health risk assessment

Heavy metals in soil enter the human body through exposure routes, such as ingestion, dermal contact, and inhalation, thus affecting human health, as well as posing carcinogenic and non-carcinogenic risks that are generated in this process (LÜ et al., 2017). The health risk evaluation method recommended by the US Environmental Protection Agency (EPA) was used and calculated using the following formulas (US EPA 2001; US EPA 2011):

$$ADD_{Soil-ingestion} = (C_s \times IR_1 \times CF \times EF \times ED) / (BW \times AT) \quad (5)$$

$$ADD_{Soil-dermal\ contact} = (C_s \times CF \times EF \times SA \times AF \times ABS \times ED) \times / (BW \times AT) \quad (6)$$

$$ADD_{Soil-inhalation} = (C_s \times IR_2 \times EF \times ED) / (BW \times PEF \times AT) \quad (7)$$

$$ADD_{vegetable} = (C_v \times IR_v \times EF \times ED) / (BW \times AT) \quad (8)$$

$$HQ_i = ADD_i / RfD \quad (9)$$

$$R = ADD_i \times SF_i \quad (10)$$

$$HI = \sum_{i}^{n} HQ_i \quad (11)$$

Where ADD_i is the long-term average daily exposure dose ($mg.kg^{-1}.d^{-1}$) of heavy metal i; HQ_i is the non-carcinogenic risk entropy of each heavy metal; RfD is the reference dose ($mg.kg^{-1}.d^{-1}$) of heavy metals following different exposure pathways (Ferreira-Baptista and De Miguel, 2005); R is the heavy metal carcinogenic risk index; SF_i is the slope of carcinogenic risk of heavy metal i (US EPA 2002); HI is the non-carcinogenic risk index, and C_S is the content of soil heavy metals ($mg.kg^{-1}$). The US EPA recommended standard parameters that indicate that the non-carcinogenic risk is negligible when the HQ < 1, and there is a non-carcinogenic risk when the HQ > 1. The carcinogenic risk is insignificant when $R < 10^{-6}$. An R of 10^{-6} to 10^{-4} indicates that there is some carcinogenic risk to humans, and when $R > 10^{-4}$, there is a strong carcinogenic risk. The values and significance of the specific parameters are shown in Supplementary Tables S2, S3.

2.5 Data analysis

SPSS 20.0 (IBM, Inc., Armonk, NY, United States) was used for descriptive statistical analyses of heavy metal content in soil, Microsoft Excel 2016 (Redmond, WA, United States) was used for data processing, and Origin 9.2 (OriginLab, Northampton, MA, United States) for graph plotting. ArcGIS 10.2 (ESRI, Redlands, CA, United States) was used to map sample points.

3 Results and analysis

3.1 Characteristics of heavy metal content in soil in the study area

The concentrations of heavy metals in the soils of each sampling area are shown in Table 1. Comparing the average value of heavy metals in the soil with the background value of the soil in Guizhou Province, it can be seen that the Cu element in Panxian is 5.84 times the background value, and there is some pollution; In Weining, Cu and Cd exceeded the standard by 3.87 times and 3.74 times of the background value, respectively. There were significant differences in heavy metal.

Concentrations in soil for different zones in the study area (Figure 2). As a whole, the content of heavy metals in soil in Panxian and Weining was higher than that in Libo and Chishui.

The coefficient of variation can reflect the average variation of each sampling point in the overall sample, and it is influenced by the environment and degree of spatial variation. The coefficient of variation indicates medium variation when it is in the range of 15%–36%, and high variation when it is >36%; a value >50% indicates that there is a possibility of local contamination of the soil (Wilding, 1985). In Libo, the coefficients of variation for Cd, Mn, and Sb were >50%. In Chishui, the coefficients of variation for Cd and As were >50%. Ni in Panxian had medium variability. Other heavy metals were highly variable with the coefficients of variation for Cd, As, Sb, and Cr being >50%. Their sources were complex and subject to human interference. Ni in Weining was <50%, and the coefficients of variation of the remaining eight heavy metal elements were >50%. All were highly variable, indicating that they are primarily influenced by local pollution sources. The coefficient of variation of Ni in Weining was <50%, and the coefficients of variation of the other eight heavy metals were >50%, indicating that they are primarily influenced by local pollution sources and could be attributed to the influence of anthropogenic activities, such as industry, agriculture, and transportation (Pan et al., 2016).

The degree of kurtosis and skewness are primarily used to measure the distribution status of the data (Zhang. 2021). Each heavy metal in Libo and Chishui had a low kurtosis, which belongs to the low peak state, indicating that there were more points with low concentrations. The skewness of nine heavy metals in the soil in Panxian and Weining was >0, which indicates positive skewness. This means that the distribution of heavy metal concentrations in soiul was subject to different degrees of external interference.

3.2 Evaluation of heavy metal pollution in the soil

3.2.1 Evaluation using the geoaccumulation index

The evaluation results of the geoaccumulation index for each heavy metal in the soil in each study area are shown in Figure 3. The

10.3389/fenvs.2023.1071353

TABLE 1 Descriptive statistics of heavy metal content in the soil (Zeng Q Q et al., 2021; China General Environmental Monitoring Station 1990).

Region	Project	Heavy metals in soil (mg.kg^{-1})								
		Cr	Mn	Ni	Cu	Zn	As	Cd	Sb	Pb
Libo	Min	53.55	102.10	13.35	14.63	53.69	5.39	0.12	0.58	23.24
	Max	168.20	856.00	39.69	50.82	161.40	12.68	2.81	3.71	39.00
	Median	104.95	400.75	20.13	25.74	88.15	8.61	0.52	1.50	31.64
	Mean	96.93	451.52	21.48	28.37	96.59	8.76	0.69	1.53	31.32
	Standard deviation (SD)	34.81	268.11	6.76	10.05	29.84	2.52	0.71	0.81	5.05
	Coefficient of variation (CV)/%	36.02	59.38	31.49	35.43	30.89	28.78	103.02	52.53	16.13
	Skewness	0.38	0.25	1.50	1.25	0.84	0.15	2.46	1.61	−0.02
	Kurtosis	−0.49	−1.57	3.59	1.20	0.13	−1.54	6.67	3.56	−1.21
Chishui	Min	58.55	162.10	11.60	21.01	48.28	3.94	0.14	0.53	23.23
	Max	95.82	862.80	45.03	42.93	158.00	23.28	1.65	1.79	52.32
	Median	65.52	683.80	30.19	26.10	106.00	8.43	0.35	0.74	31.72
	Mean	71.37	630.74	31.57	27.61	106.47	9.75	0.48	0.90	34.32
	Standard deviation (SD)	12.77	246.69	8.86	6.20	27.98	4.90	0.42	0.36	8.22
	Coefficient of variation (CV)/%	17.89	39.11	28.08	22.46	26.28	50.23	86.63	40.67	23.96
	Skewness	1.07	−1.06	−0.74	1.54	−0.20	1.93	2.18	1.42	0.85
	Kurtosis	−0.34	−0.17	0.95	2.32	0.79	5.15	5.55	1.88	0.52
Panxian	Min	58.08	135.10	10.49	21.17	43.52	3.18	0.24	0.27	8.72
	Max	490.50	3639.60	166.80	425.60	487.50	253.80	11.29	24.66	71.54
	Median	129.90	1,478.90	79.02	175.80	190.90	12.43	0.59	1.76	24.05
	Mean	159.21	1,416.05	81.62	186.73	216.70	38.56	1.32	4.28	28.71
	Standard deviation (SD)	87.96	685.09	29.13	92.04	103.49	59.00	2.11	5.83	13.87
	Coefficient of variation (CV)/%	55.25	48.38	35.69	49.29	47.76	153.02	159.01	136.33	48.32
	Skewness	2.09	0.86	0.32	0.71	1.06	2.49	3.96	2.32	1.38
	Kurtosis	5.75	2.44	1.92	0.55	0.78	6.11	17.56	5.07	2.04
Weining	Min	32.32	113.00	15.63	5.32	93.69	0.28	0.20	0.28	10.02
	Max	400.70	4368.00	129.60	400.80	1,291.40	50.60	20.58	9.35	575.90
	Median	135.50	1,145.90	67.83	80.61	182.10	17.06	1.08	1.56	47.82
	Mean	150.04	1,319.14	70.74	123.70	270.40	18.92	2.47	2.17	83.71
	Standard deviation (SD)	82.89	829.71	24.92	97.66	228.83	14.00	3.65	1.98	109.97
	Coefficient of variation (CV)/%	55.25	62.90	35.23	78.95	84.63	74.03	147.53	91.55	131.36
	Skewness	1.39	1.50	0.34	1.32	2.85	0.54	3.60	1.93	3.05
	Kurtosis	2.13	3.61	0.33	0.98	10.12	−0.59	16.06	4.20	10.52
	Soil background values in Guizhou Province	95.90	794.00	39.10	32.00	99.50	20.00	0.66	2.24	35.20

average geoaccumulation index of heavy metal elements in Libo and Chishui was less than 0, indicating a clean state. The average Igeo value of heavy metals in Panxian was Cu (1.96) > Zn (0.54) > Ni (0.48) > Cd (0.42) > As (0.36) > Sb (0.35) > Mn (0.25) > Cr (0.15). The average Igeo value of heavy metals in Weining was Cu (1.37) > Cd (1.32) > Zn (0.86) > Pb (0.66) > Ni (0.27) > Mn (0.15) > Cr (0.06). It could be seen that the Cu in Panxian indicates significant contamination, and the Cu, Cd, Zn, and Pb in Weining also indicate significant contamination. Nazeeram et al. (2021) used the geoaccumulation index method to evaluate the status of heavy metals as pollutants in rural soils in Urümqi, China, and found that the average degree of pollution by heavy metals was in the order of Hg > Cd > Pb > Zn >

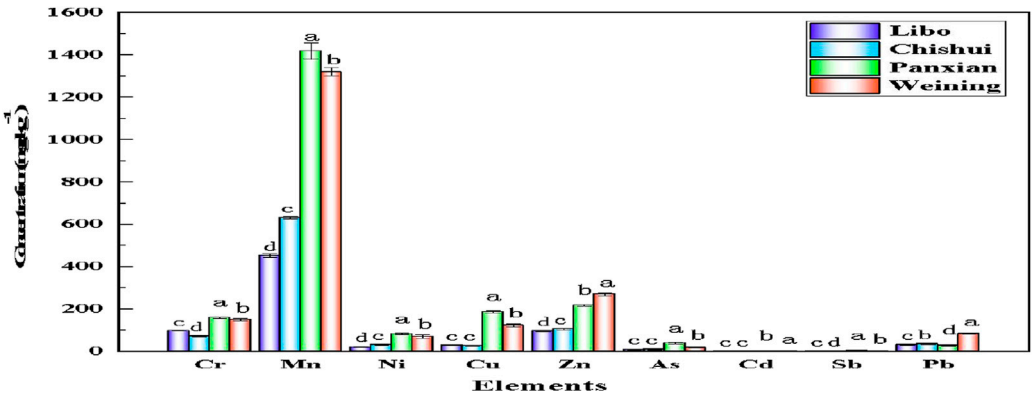

FIGURE 2
The concentrations of heavy metals in soil in different study areas (different letters indicate significant differences at $p < 0.05$)

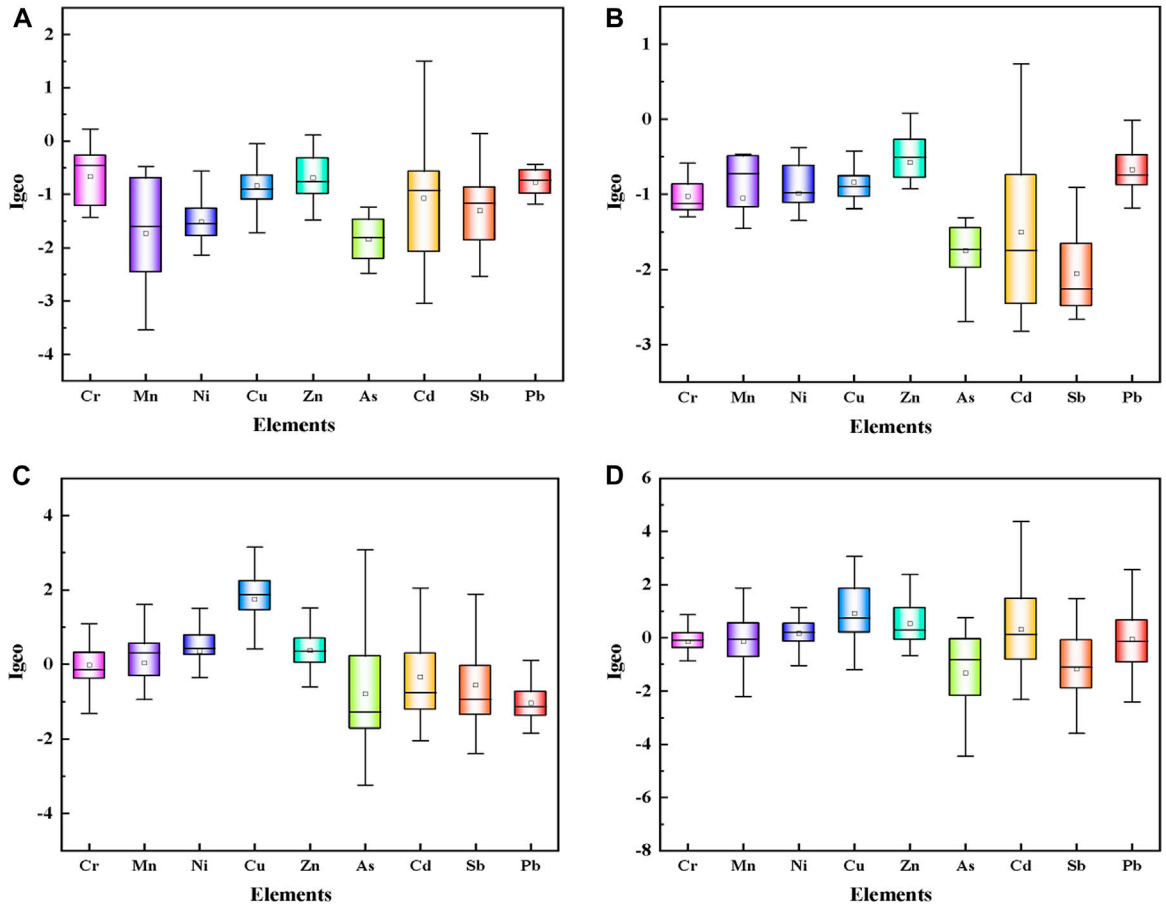

FIGURE 3
Evaluation results of the geoaccumulation index
Note: **(A–D)** represent Libo, Chishui, Panxian, and Weining in Guizhou Province, China.

Cu > Ni > As > Cr. The average I_{geo} values of Hg, Cd, and Pb was >0, and Hg and Cd had different degrees of pollution. Zhang et al. (2015) evaluated the amount of heavy metal contamination in the soil in the potato production area of Panxian and found that the soil was free of contamination from Cu and As, while there was slight contamination from Cd. A comparison of their findings with those of this study indicates that the levels of Cu, As, and Cd are increasing over time. Morteza et al. (2019) evaluated the amount of heavy metal contamination in soil in the Persian Gulf (southern Iran), and the EF and I_{geo} values indicated that the sediments were contaminated

TABLE 2 Results of evaluation by the pollution load index.

Region	Cr	Mn	Ni	Cu	Zn	As	Cd	Sb	Pb	
	I_{PL}									I_{PLzone}
Libo	0.94	0.45	0.53	0.84	0.93	0.42	0.71	0.61	0.88	0.67
Chishui	0.73	0.70	0.77	0.84	1.03	0.44	0.55	0.37	0.95	0.67
Panxian	1.47	1.53	1.91	5.03	1.94	0.87	1.18	1.03	0.73	1.47
Weining	1.35	1.35	1.68	2.83	2.17	0.60	1.86	0.66	1.44	1.39

with Cd and Pb. Contamination with Pb was more serious in this area compared with the findings of this study, which found that the contamination with Pb was relatively light and contamination with Cd was more serious.

3.2.2 Evaluation of the pollution load index

The results of an evaluation of the soil in each study area using the heavy metal pollution load index are shown in Table 2. The soil in Libo was slightly polluted with Cr, Cu, Zn, Cd, and Pb. In Chishui, the soil was lightly polluted with Zn and slightly polluted with Cr, Ni, Cu, and Pb. In Pan County, the soil was extremely polluted with Cu, lightly polluted with Cr, Mn, Ni, Zn, Cd, and Sb, and slightly polluted with As. In Weining, the soil was moderately polluted with Cu and Zn and slightly polluted with Cr, Mn, Ni, Cd, and Pb. The regional pollution degree was as follows: Panxian (1.47)>Weining (1.39)>Libo (0.67), and Chishui (0.67).

A comparison with the evaluation results of the geoaccumulation index method indicates that the pollution load index was more stringent at evaluating the degree of pollution of each heavy metal. In addition, the division was more detailed, which enabled the evaluation of each pollution point in the region. This method is suitable to compare the evaluation of regional pollution in several areas and can also reflect the contribution of each heavy metal to the region. The results of different heavy metals in soil under the various evaluation methods differed slightly, primarily owing to the different emphasis of varying evaluation methods. Alternatively, the geoaccumulation index method includes the influence of natural geological effects and anthropogenic activities on heavy metals in soil, and its results are more intuitive. Hadi et al. (2022) evaluated the degree of heavy metal contamination in the soil of the site around Moghan'stannery, Ardabil, Iran, by examining the levels of As, Cd, Cr, Cu, Ni, Pb, and Zn. The average levels of all the heavy metals in the soil, except for Pb, were below the maximum allowable levels. Among them, the levels of Cd and Zn were the lowest and highest, respectively, which showed that contamination with Zn was more serious at this site, while Cd caused less contamination. This differs from the results of this study, which identified higher levels of contamination with Cd, probably owing to differences in the areas studied. Pan et al. (2022) used the pollution load index and health risk evaluation methods to analyze the characteristics of heavy metals in surface sediments of autumnal mangrove wetlands of different origins in eastern Fujian, China, and assess their health risks. They found that the regional pollution load index of heavy metals in the surface sediments of natural mangrove forests was lower than that of artificial mangrove forests. The corresponding pollution levels were all one, which indicates moderate pollution. The non-carcinogenic risk of heavy metals in the surface sediments of autumnal mangrove wetlands was very low for adults, and Cd posed a serious non-carcinogenic risk for children. Pb posed a non-carcinogenic risk to children, and Cd posed a serious carcinogenic risk to adults and children. Ghazaryan et al. (2018) determined and assessed the impact of mining on soil contamination by utilizing various contamination indices. Soil was selected for sampling from 13 points, eleven elements were determined, and the levels of soil contamination were determined using a pollution load index, contamination level (Cd), and a geoaccumulation index. The Cd-based assessment showed that 33.3% of the soil samples had very high levels of contamination.

3.2.3 Human health risk evaluation

3.2.3.1 Potato risk evaluation

The results of the potato health risk assessment are shown in Supplementary Table S4. In the four production areas of Libo, Chishui, Panxian, and Weining, the ADD of potatoes to adults and children was less than one, indicating that the potatoes would not cause risk to the human body after eating. Local residents do not have to worry about the risks posed by consuming potatoes. Although the soil of potato-producing areas was polluted with heavy metals to varying degrees, the potatoes planted showed no obvious harm to human health. The reason might be related to the absorption characteristics of potatoes to heavy metals, and to the fact that people peel potatoes before eating them, thus reducing the intake of heavy metals. Rattan et al. (2005) showed that in addition to oral intake of vegetables, the human body can also ingest heavy metals through other channels, so ADD is not solely responsible for all the health risks of heavy metals found in the human body.

The ADD in children is greater than in adults, indicating a greater potential for food risk in children; thus care is needed to ensure potato food safety to protect children's health. Therefore, measures should be taken to effectively prevent heavy metal pollution sources.

Selahvarzi and Ardakani (2020) evaluated the risk to human health from heavy metals found in the potatoes grown in the Lorestan Province, Iran, and found that the average levels of Cd, Cu, Pb, and Zn in the potato samples were 0.154, 0.148, 0.250, and 0.143 mg kg^{-1}, respectively, which were below the maximum allowable limits established by the World Health Organization, meaning that those potatoes exhibited no obvious potential health risks to human health. However, to ensure food security and reduce the health risks associated with food consumption, special attention should be paid to the content of Cd and Pb.

3.2.3.2 Carcinogenic risk evaluation

The carcinogenic evaluation indices of soil heavy metals for adults and children following different pathways of exposure in each study area are shown in Table 3. As shown in this table, in the study areas of

TABLE 3 Carcinogenic health risk index.

Region	Heavy metal	R ingestion		R dermal contact		R inhalation	
		Adult	Children	Adult	Children	Adult	Children
Libo	Cr	1.37×10^{-4}	3.19×10^{-4}	2.18×10^{-5}	3.57×10^{-5}	0.1	1.25×10^{-7}
	As	3.70×10^{-5}	8.64×10^{-5}	3.60×10^{-7}	5.90×10^{-7}	7.20×10^{-10}	3.21×10^{-10}
	Cd	1.19×10^{-5}	2.77×10^{-5}	4.73×10^{-8}	7.75×10^{-8}	—	—
Chishui	Cr	1.01×10^{-4}	2.35×10^{-4}	1.60×10^{-5}	2.63×10^{-5}	7.56×10^{-2}	9.24×10^{-8}
	As	4.12×10^{-5}	9.12×10^{-5}	4.01×10^{-7}	6.57×10^{-7}	5.01×10^{-10}	2.23×10^{-10}
	Cd	8.25×10^{-6}	1.93×10^{-5}	3.30×10^{-8}	5.39×10^{-8}	—	—
Panxian	Cr	2.24×10^{-4}	5.23×10^{-4}	3.58×10^{-5}	5.86×10^{-5}	0.17	2.06×10^{-7}
	As	1.63×10^{-4}	3.80×10^{-4}	1.59×10^{-6}	2.60×10^{-6}	1.38×10^{-9}	6.14×10^{-10}
	Cd	2.27×10^{-5}	5.29×10^{-5}	9.05×10^{-8}	1.48×10^{-7}	—	—
Weining	Cr	2.11×10^{-4}	4.94×10^{-4}	3.37×10^{-5}	5.52×10^{-5}	0.16	1.94×10^{-7}
	As	7.80×10^{-5}	1.87×10^{-4}	7.79×10^{-7}	1.27×10^{-6}	2.58×10^{-9}	1.15×10^{-9}
	Cd	4.25×10^{-5}	9.91×10^{-5}	1.69×10^{-7}	2.77×10^{-7}	—	—

Libo, Chishui, and Weining, the carcinogenic health risk of Cr to adults and children was greater than that of As and Cd under ingestion exposure. Cr had a very strong carcinogenic risk for adults through inhalation. In the four study areas, Cr had a weak carcinogenic risk to the human body under dermal contact. Cr had an extremely strong carcinogenic risk to adults, and the carcinogenic risk to children was not obvious, while As and Cd had no obvious carcinogenic risk to the human body under the inhalation pathway.

The human health evaluation focuses more on the health risk hazards caused by the intake of soil heavy metals into the human body through different pathways. The results of the carcinogenic risk evaluation in this study indicated that the three heavy metals Cr, As, and Cd that were found in the soil in the four study areas all had different degrees of carcinogenic risk for adults and children through ingestion, and the order of risk was Cr > As > Cd. The carcinogenic risk for humans was greater for children than adults, which is consistent with the results of Xu et al. (2021) and Wang et al. (2021). Exposure to Cd through dermal contact for both adults and children resulted in a carcinogenic risk of Cd that was not significant in the four study areas, while As had some carcinogenic risk for adults or children in some of the study areas. In contrast, Cr had some carcinogenic risk for both adults and children, and the carcinogenic risk for humans was greater for children than adults, which Yang C. C. et al. (2018) attributed to the tendency of children to suck their fingers and play with soil. Children are easily exposed to contaminated heavy metal particles. Only Cr presented a strong carcinogenic risk for adults through inhalation, and the carcinogenic risk for humans was greater for adults than for children. Cr in the soil was the main influencing factor of carcinogenic risk in each study area, and efforts to prevent and control the management of Cr pollution should be undertaken.

3.2.3.3 Non-carcinogenic risk evaluation

The non-carcinogenic evaluation indices of soil heavy metals for adults and children following different pathways of exposure in each study area are shown in Supplementary Table S5, and the total non-carcinogenic health risks (HI) for adults and children following the three pathways of exposure in each study area were 0.36 and 5.74 for Libo, respectively, 0.36 and 5.14 for Chishui, respectively, 1.33 and 16.60 for Panxian, respectively, and 0.74 and 10.95 for Weining, respectively. The non-carcinogenic risk only applied to adults in Panxian. The non-carcinogenic risk was stronger for children in all the study areas, and the non-carcinogenic risk for children was greater than that for adults.

In the study area of Libo, Chishui, and Weining, Cr and As had non-carcinogenic risks to the health of children but insignificant non-carcinogenic risks to the health of adults under ingestion exposure. In the study area of Panxian, the HQ of Cr in the soil to children under ingestion exposure was greater than one, indicating a non-carcinogenic risk to the health of children but an insignificant non-carcinogenic risk to the health of adults under ingestion exposure. As had a non-carcinogenic risk to the health of both adults and children. The non-carcinogenic risk to humans for each heavy metal following exposure through dermal contact and inhalation was not significant. In the four study areas, the non-carcinogenic risk to humans for each type of heavy metal following exposure through dermal contact and inhalation was insignificant.

The results of the evaluation of non-carcinogenic risks in this study indicated that following exposure by ingestion, both the heavy metals Cr and As found in the soils of the four study areas would pose non-carcinogenic risks to the health of children, and As in Panxian would pose non-carcinogenic risks to the health of adults. The non-carcinogenic risks to humans from the heavy metals found in the soils of the four study areas were not significant following exposure by either dermal contact or inhalation. The HQ of soil heavy metals for children was greater than those of the adult HQ following all three routes of exposure, indicating that the non-carcinogenic health risks from soil heavy metals were more likely to affect children. Sarva et al. (2015) examined the risk of heavy metals, including Pb, Cd, Cr, and As, to human health in urban soils in Seri Kembangan, Malaysia. The mean values of the heavy metal hazard index were found to follow the

order of Pb (1.27) > Cr (0.11) > Cd (0.05) for non-cancerous patients. The total risk value for cancer from urban soil in Seri Kembangan owing to As (7.2×10^{-6}) was lower than the tolerable lifetime cancer risk for regulatory purposes (1×10^{-5}). Pb contamination was more serious in this area, while Cr and Cd posed health risks to humans as in this study. El-Alfy et al. (2017) evaluated drainage from the Nile Delta, in Egypt. The levels of Fe, Cd, Pb, Ni, Cr, and Co in the soil samples were determined. The HI calculations for HQ of the three different exposure pathways and metals from different locations were found to be >1, indicating the risk of non-carcinogenic effects. Only the CR of Co in the study area did not show a risk to humans. Azam K et al. (2020) evaluated heavy metals in agricultural soil irrigated with stable pond runoff in Birjand, Iran, using the human health risk index and found that the total hazard index values of heavy metals for adults and children through the three routes of exposure were 0.91 and 1.10, respectively, indicating a non-carcinogenic risk for children and less risk for adults, which is consistent with the results of this study. Many studies have shown that children have a higher health risk than adults (Rehman et al., 2017). These findings are also consistent with a study conducted by Karim and Qureshi, (2013). It has also been suggested that this is because children are at a developmental stage and have a higher sensitivity to health risks arising from heavy metals and are more vulnerable to hazards (Yang Q. Q. et al., 2018). This strongly suggests that greater effort should be conducted to protect the health of children from such risks.

4 Conclusion

Soils contaminated with heavy metals affect crop yields and quality and pose a potential threat to human health. In this study, the heavy metal pollution in the soil of some potato-producing areas of Guizhou Province was studied. We collected 89 soil samples from four potato-producing areas (Libo, Chishui, Panxian, and Weining), and the contents of nine heavy metals including Cr, Mn, Ni, Cu, Zn, As, Cd, Sb, and Pb were analyzed and determined. The heavy metal pollution in soil was evaluated by geoaccumulation index, pollution load index, and health risk assessment. The results revealed that Igeo<0 in Libo and Chishui, Igeo>0 in Panxian except for Pb. The Igeo of As and Sb were less than zero in Weining, and other elements had varying degrees of the index. The pollution load index in Panxian (1.47) > Weining (1.39) > Libo (0.67), Chishui (0.67). This showed that Libo and Chishui were not polluted in general, while some heavy metals in Panxian and Weining indicated the soils there were polluted. Human health risk assessment showed that potatoes in the four study areas will not harm the health of local residents through food ingestion. In terms of carcinogenesis, the risk of human carcinogenesis in all study areas under the ingestion pathway was Cr > As > Cd. Under the dermal contact pathway, Cr and As both have certain risks. In the inhalation pathway, Cr has a strong risk for adults. In terms of non-carcinogenic risk, children in the four study areas have a strong risk under each pathway. Heavy metals in the soil of the four study areas all pose health risks to the human body, so attention should be paid to the remediation of heavy metals in the contaminated areas to ensure human health. The data obtained in this study can be used by the public, including health assessors, educators, conservationists, and other stakeholders in Guizhou Province to assess health risks in the relevant areas and take series of measures in future work to minimize the health risks to local residents.

Data availability statement

The original contributions presented in the study are included in the article/Supplementary Materials, further inquiries can be directed to the corresponding author.

Author contributions

The study conception and design were mainly performed by JZ and KL. Material preparation was mainly performed by MZ and QC. Data collection and analysis were mainly performed by XH and WL. The revision and editing of the revised manuscript were mainly performed by JZ.

Funding

This research was supported by the National Natural Science Foundation of China (21866008), the Science and Technology Planning Project of Guizhou Province, China [Qiankehehoubuzu No. (2020)3001], and Renjihezi of Guizhou university NO. (2017)51.

Conflict of interest

The authors declare that the research was conducted in the absence of any commercial or financial relationships that could be construed as a potential conflict of interest.

The reviewer JZ declared a shared affiliation with the authors to the handling editor at the time of review.

Publisher's note

Supplementary material

The Supplementary Material for this article can be found online at: https://www.frontiersin.org/articles/10.3389/fenvs.2023.1071353/full#supplementary-material

References

Azam, K., Ali, N., Hamed, B., Roya, P., Aliyeh, G., and Ahmad, Z. (2020). Assessment of human health risks and pollution index for heavy metals in farmlands irrigated by effluents of stabilization ponds. *Environ. Sci. Pollut. Res.* 27, 10317–10327. doi:10.1007/s11356-020-07642-6

Bao, S. D. (2000). *Soil agrochemical analysis [M*. 3 edition. Beijing: China Agricultural Press.

Brewer, R., Peard, J., and Heskett, M. (2017). A critical review of discrete soil sample data reliability: Part 1-field study results. *SOIL and SEDIMENT Contam.* 26 (1), 1–22. doi:10.1080/15320383.2017.1244171

China General Environmental Monitoring Station (1990). *Background values of soil elements in China [M]*. Beijing: China Environmental Science Press.

Doabi, S. A., Karami, M., Afyuni, M., and Yeganeh, M. (2018). Pollution and health risk assessment of heavy metals in agricultural soil, atmospheric dust and major food crops in Kermanshah province. *Ecotoxicol. Environ. Saf.* 163, 153–164. Iran. doi:10.1016/j.ecoenv.2018.07.057

Du, M., Zhang, Q. Y., Ren, P., Gao, S., and Bu, D. (2021). Evaluation of heavy metal distribution and ecological risk in agricultural land in Nianchu River Basin, Tibet. *J. Environ. Eng. Technol.*, 1–13.

El-Alfy, M. A., El-Amier, Y. A., and El-Hamid, H. T. A. (2017). Soil quality and health risk assessment of heavy metals in agricultural areas irrigated with wastewater from Kitchener Drain, Nile Delta, Egypt. *J. Sci. Agric.* 1, 158–170. doi:10.25081/jsa.2017.v1.50

Fakhri, Y., Saha, N., Ghanbari, S., Rasouli, M., Miri, A., Avazpour, M., et al. (2018). Carcinogenic and non-carcinogenic health risks of metal (oid) s in tap water from Ilam city, Iran. *Food Chem. Toxicol.* 118, 204–211. doi:10.1016/j.fct.2018.04.039

Ferreira-Baptista, L., and De Miguel, E. (2005). Geochemistry and risk assessment of street dust in Luanda,Angola: Atropical urban environment. *Atmos. Environ.* 39 (25), 4501–4512. doi:10.1016/j.atmosenv.2005.03.026

GB/T 17141-1997, Determination of soil quality of lead and cadmium by graphite furnace atomic absorption spectrophotometry.

GB/T 22105.2-2008, Determination of total mercury, total arsenic and total lead in soil quality Atomic fluorescence method Part 2: Determination of total arsenic in soil.

GB/T 22105.3-2008, Determination of total mercury, total arsenic and total lead in soil quality Atomic fluorescence method Part 3: Determination of total lead in soil.

Ghazaryan, K. A., Movsesyan, H. S., Khachatryan, H. E., and Ghazaryan, N. P. (2018). Geochemistry of potentially toxic trace elements in soils of mining area: A case study from zangezur copper and molybdenum combine, Armenia. *Bull. Environ. Contam. Toxicol.* 101 (6), 732–737. doi:10.1007/s00128-018-2443-0

Hadi, S., Mehdi, F., Ahmad, Z., Amir, H. M., and Shahrokh, N. (2022). Spatial distribution and contamination of heavy metals in surface water, groundwater and topsoil surrounding Moghan's tannery site in Ardabil, Iran. *Int. J. Environ. Anal. Chem.* 102 (5), 1049–1059. doi:10.1080/03067319.2020.1730342

TUCLHe, T. B., Liu, c. Q., and Lu, X. H. (2013). Effects of land use and parent materials on trace elements accumulation intopsoil. *J. Environ. Qual.* 42 (1), 103–110. doi:10.2134/jeq2012.0057

HJ -2019, Determination of copper, zinc, lead, nickel and chromium in soil and sediment by flame atomic absorption spectrophotometry.

Huang, S., Li, Q., Yang, Y., Yuan, C., Ouyang, K., and You, P. (2017). Risk assessment of heavy metals in soils of a lead-zinc mining area in Hunan Province (China). *Chem. Ind.* 66, 173–178. doi:10.15255/kui.2016.049

Jia, Z., Li, S., and Wang, L. (2018). Assessment of soil heavy metals for eco-environment and human health in a rapidly urbanization area of the upper Yangtze Basin. *Sci. Rep.* 8, 3256. doi:10.1038/s41598-018-21569-6

Jiang, S. Y. (2008) Distribution characteristics of heavy metals in soil, plants and human body in the area around Guixi Smelter (Sumen Village) and its pollution evaluation.

Kamani, H., Mirzaei, N., Ghaderpoori, M., Bazrafshan, E., Rezaei, S., and Mahvi, A. H. (2018). Concentration and ecological risk of heavy metal in street dusts of Eslamshahr, Iran. *Hum. Ecol. Risk Assess.* 24, 961–970. doi:10.1080/10807039.2017.1403282

Kamunda, C., Mathuthu, M., and Madhuku, M. (2016). Health risk assessment of heavy metals in soils from Witwatersrand gold mining basin, South Africa. *Int. J. Environ. Res. Public Health* 13, 663. doi:10.3390/ijerph13070663

Karim, Z., and Qureshi, B. A. (2013). Health risk assessment of heavy metals in urban soil of Karachi, Pakistan. *Hum. Ecol. Risk Assess.* 20, 658–667. doi:10.1080/10807039.2013.791535

Long, J. H., and TanJ, Wu Y. J. (2013). A comparative study on the detection of heavy metal in soil with differentdigestion methods[J]. *Environ. Monit. China* 29 (1), 123–126.

Lü, Y., Zhang, K., Chai, F. H., Cheng, T., Yang, Q., Zheng, Z., et al. (2017). Atmospheric size-resolved trace elements in a city affected by non-ferrousmetal smelting:Indications of respiratory deposition and health risk. *Environ. Pollut.* 224, 559–571. doi:10.1016/j.envpol.2017.02.039

Ma, H. H., Peng, M., Liu, F., Guo, F., Tang, S. Q., Liu, X. Q., et al. (2020). Biological effectiveness and transport enrichment characteristics of heavy metals in soil-crop systems of agricultural fields in typical carbonate rock areas of Guangxi[J]. *Environ. Sci.* 41 (01), 449–459. doi:10.13227/j.hjkx.201905040

Ministry of Environmental Protection (2014). *Ministry of land and resources national soil pollution status survey bulletin*. Beijing: Ministry of Environmental Protection, Ministry of Land and Resources.

Mohmand, J., Eqani, S. A. M. A., Fasola, M., Alamdar, A., Mustafa, I., Ali, N., et al. (2015). Human exposure to toxic metals via contaminated dust:Bio-accumulation trends and their potential risk estimation. *Chemosphere* 132 (8), 142–151. doi:10.1016/j.chemosphere.2015.03.004

Morteza, S., Amir, H. M., Seyed, Y. H., Hossein, A., Hasan, P., Ahmad, Z., et al. (2019). Spatial distribution, enrichment and geo-accumulation of heavy metals in surface sediments near urban and industrial areas in the Persian Gulf. *Desalination Water Treat.* 158, 130–139. doi:10.5004/dwt.2019.24238

Müller, G. (1969). Index of geoaccumulation in sediments of the rhine river. *Geol. J.* 2, 108–118.

Nazeeram, Y. S. F. J., Zhang, J. Z., Leng, B. B., and Wang, T. (2021). Evaluation of heavy metal pollution characteristics and potential ecological risk in rural soils of Urumqi city. Proceedings of the Annual Scientific and Technical Conference of the Chinese Society of Environmental Sciences, 491–498.

Neyestani, M. R., Bastami, K. D., Esmaeilzadeh, M., Shemirani, F., Khazaali, A., Molamohyeddin, N., et al. (2016). Geochemical speciation and ecological risk assessment of selected metals in the surface sediments of the northern Persian Gulf. *Mar. Poll. Bull.* 109 (1), 603–611. doi:10.1016/j.marpolbul.2016.05.024

Ngole-Jeme, V. M., and Fantke, P. (2017). Ecological and human health risks associated with abandoned gold mine tailings contaminated soil. *PLoS One* 12, e0172517. doi:10.1371/journal.pone.0172517

Pan, H., Zheng, K. J., You, W. B., Wang, R., Cai, J. B., and He, D. J. (2022). Evaluation of heavy metal pollution and health risk in wetlands of different origins of autumn eggplant forests. *Guangxi Plant* 1-11.

Pan, L. B., Ma, J., Wang, X. L., and Hou, H. (2016). Heavy metals in soils from a typical county in Shanxi Province, China:Levels, sources and spatial distribution. *Chemosphere* 148, 248–254. doi:10.1016/j.chemosphere.2015.12.049

Pascaud, G., Leveque, T., Soubrand, M., Boussen, S., Joussein, E., and Dumat, C. (2014). Environmental and health risk assessment of Pb, Zn, as and Sb in soccer field soils and sediments from mine tailings: Solid speciation and bioaccessibility. *Environ. Sci. Pollut. Res.* 21 (6), 4254–4264. doi:10.1007/s11356-013-2297-2

Patlolla, A. K., Todorov, T. I., Tchounwou, P. B., van der Voet, G., and Centeno, J. A. (2012). Arsenic-induced biochemical and genotoxic effects and distribution in tissues of Sprague–Dawley rats. *Microchem. J.* 105, 101–107. doi:10.1016/j.microc.2012.08.013

Rahman, S. H., Khanam, D., Adyel, T. M., Islam, M. S., Ahsan, M. A., and Akbor, M. A. (2012). Assessment of heavy metal contamination of agricultural soil around dhaka export processing zone (DEPZ), Bangladesh: Implication of seasonal variation and indices. *Appl. Sci.* 2, 584–601. doi:10.3390/app2030584

Rattan, R. K., Datta, S. P., Chhonkar, P. K., Suribabu, K., and Singh, A. K. (2005). Long-term impact of irrigation with sewage effluents on heavy metal content in soils, crops and groundwater—A case study. *Agric. Ecosyst. Environ.* 109 (3), 310–322. doi:10.1016/j.agee.2005.02.025

Rehman, Z. U., Khan, S., Brusseau, M. L., and Shah, M. T. (2017). Lead and cadmium contamination and exposure risk assessment via consumption of vegetables grown in agricultural soils of five-selected regions of Pakistan. *Chemosphere* 168, 1589–1596. doi:10.1016/j.chemosphere.2016.11.152

Rezaei, H., Jafari, A., Kamarehie, B., Fakhri, Y., Ghaderpoury, A., Karami, M. A., et al. (2018). Healthrisk assessment related to the fluoride, nitrate, and nitrite in the drinking water in the Sanandaj, Kurdistan County, Iran. *Hum. Ecol. Risk Assess.* 25, 1242–1250. doi:10.1080/10807039.2018.1463510

Sarva, M. P., Sharifah, N. S. I., and Ahmad, Z. A. (2015). Health risk assessment of heavy metal exposure in urban soil from Seri Kembangan (Malaysia). *Arab. J. Geosci.* 8, 9753–9761. doi:10.1007/s12517-015-1895-3

Selahvarzi, S., and Ardakani, S. S. (2020). Analysis and health risk assessment of toxic (Cd and Pb) and essential (Cu and Zn) elements through consumption of potato (Solanum tuberosum) cultivated in Iran. *Int. J. Environ. Anal. Chem.* 102 (18), 6310–6320. doi:10.1080/03067319.2020.1807974

Sun, J. W., Huang, Y. Z., Shi, M. C., Cui, Y. S., Li, X. F., Zhao, L. J., et al. (2008). Progress in the study of soil heavy metal biotoxicity. *J. Ecol.* (06), 2861–2869.

US EPA (2011). *Exposure factors handbook*. Springfield,VA Washington: National Technical InformationService.

US EPA (2001). *Risk assessment guideance for superfund:volume I:human health EvaluationManual*. Washington, DC: Office of Emergency and Remedial Response.

US EPA (2002). *Supplemental guidance for developing soil screening levels for superfundsites[R]*. Washington, DC: Office of Emergency and Remedial Response.

US EPA (1994). *Uptake biokinetic model for lead in children (IEUBK)*. Washington DC: Office of Emergency and Remedial Response, 540–599.

Wang, G., Su, M. Y., Chen, Y. H., Lin, F. F., Luo, D., and Gao, S. F. (2006). Transfer characteristics of cadmium and lead from soil to the edible parts of six vegetable species in southeastern China. *Environ. Pollut.* 144 (1), 127–135. doi:10.1016/j.envpol.2005.12.023

Wang, G. X., Guan, C., Wu, W., Chen, Z. Y., and Li, H. P. (2022). *Establishment of a method for the determination of 15 heavy metals and hazardous elements in Chinese patent medicines containing natural copper and its uncertainty assessment*. Testing, China, 1–14.

Wang, Z., Guo, Y., Zheng, X. Z., Zhou, X. J., and Shi, X. L. (2021). Environmental geochemical evaluation and health risk assessment of a landfill site in Guangzhou City. *J. Guizhou Univ. Nat. Sci. Ed.* 38 (04), 52–59+74.

Wilding, L. P. (1985) Spatial variability: Its documentation, accomodation and implication to soil surveys[J].Spatial variations.

Xu, S. M., Pan, Z. D., and He, H. K. (2021). Evaluation of ecological health risk of heavy metals in soil of Selian mining area[J]. *Contemp. Chem. Res.* (22), 85–88.

Xu, Y. X., Peng, Z. K., Wang, Q. H., and Xue, L. (2013). Evaluation of soil heavy metal pollution around a lead-zinc smelting area in Western Guanzhong by applying the ground accumulation index method and ecological hazard index method[J]. *Sichuan Environ.* 32 (04), 79–82.

Yang, C. C., Zhao, W. T., Gao, X. F., Cheng, S. G., Xie, D., and Ma, P. T. (2018). Distribution characteristics and health risk evaluation of metal elements in water bodies of drinking water sources in Luhun Reservoir. *Environ. Sci.* 39 (01), 89–98.

Yang, J. Y. (2019). *Geochemical characteristics of heavy metal elements in arable land and its pollution evaluation in Aga Town, Liupanshui, Guizhou*. Chengdu, China: Chengdu University of Technology.

Yang, L., Li, Y., Peng, K., and Wu, S. (2014). Nutrients and heavy metals in urban soils under different green space types in Anji, China. *Catena* 115, 39–46. doi:10.1016/j.catena.2013.11.008

Yang, Q. Q., Duan, Q., Huang, L., Bi, J., and Lu, X. N. (2018). A review of soil heavy metal pollution from industrial and agricultural regions in China: Pollution and risk assessment: Pollution and risk assess-ment. *Sci. Total Environ.* 642, 690–700. doi:10.1016/j.scitotenv.2018.06.068Li

Yousefi, M., Dehghani, M. H., Nasab, S. M., Taghavimanesh, V., Nazmara, S., and Mohammadi, A. A. (2018). Data on trend changes of drinking groundwater resources quality: A case study in abhar. *Data Brief.* 17, 424–430. doi:10.1016/j.dib.2018.01.032

Zeng, Q. Q., Fu, T. L., Zou, H. Q., Teng, L., Wu, K., Xie, T., et al. (2021). Spatial distribution and source analysis of heavy metals in soil of a pepper planting area in Guizhou Province. *J. Agro-Environmental Sci.* 40 (01), 102–113.

Zhang, J., Lang, X. D., and Chen, R. (2015). Status and evaluation of soil heavy metal content in potato growing area in Liupanshui, Guizhou. *Guangdong Agric. Sci.* 42 (17), 6–1.

Zhang, S. Y. (2021). GIS-based evaluation of soil heavy metal pollution and health risk assessment in different functional areas [J]. *J. Environ. Eng. Technol.*, 1–13.

Zhao, L., Hu, Y., Zhou, W., Liu, Z. H., Pan, Y. C., Shi, Z., et al. (2018). Estimation methods for soil mercury content using hyperspectral remote sensing. *Sustainability* 10 (7), 2474. doi:10.3390/su10072474

frontiers | Frontiers in Environmental Science

TYPE Original Research
PUBLISHED 22 February 2023
DOI 10.3389/fenvs.2023.1132268

OPEN ACCESS

EDITED BY
Xiaohu Wen,
Northwest Institute of Eco-Environment and Resources (CAS), China

REVIEWED BY
Yuanfeng Qi,
Qingdao University of Technology, China
Wenjun Huang,
Shanghai Jiao Tong University, China
Jia Duo,
Xinjiang Institute of Ecology and Geography (CAS), China

*CORRESPONDENCE
Qiankun Wang,
wang_qiankun@zijinming.com

SPECIALTY SECTION
This article was submitted to Toxicology, Pollution and the Environment, a section of the journal Frontiers in Environmental Science

RECEIVED 27 December 2022
ACCEPTED 01 February 2023
PUBLISHED 22 February 2023

CITATION
Zhao P, Chen J, Liu T, Wang Q, Wu Z and Liang S (2023), Heavy metal pollution and risk assessment of tailings in one low-grade copper sulfide mine.
Front. Environ. Sci. 11:1132268.
doi: 10.3389/fenvs.2023.1132268

Heavy metal pollution and risk assessment of tailings in one low-grade copper sulfide mine

Pingping Zhao[1,2,3], Jinghe Chen[1], Tianfu Liu[3], Qiankun Wang[1]*, Zengling Wu[1] and Shuqin Liang[2]

[1]State Key Laboratory of Comprehensive Utilization of Low-Grade Refractory Gold Ores, Zijin Mining Group Co., Ltd., Shanghang, China, [2]Fujian Province Colleges and University Engineering Research Center of Solid Waste Resource Utilization, Longyan University, Longyan, China, [3]State Key Laboratory of Structural Chemistry, Fujian Institute of Research on the Structure of Matter, Chinese Academy of Sciences, Fuzho, China

Analyzing the pollution level and ecological risk of heavy metals in tailings is a necessary step for conducting revegetation after a tailings pond's closure. Herein, we determined the heavy metal pollution status and ecological risk in one low-grade copper sulfide tailings pond using chemical and mineralogical analysis, chemical extraction, and ecological risk assessment. The results showed that the low-grade copper sulfide tailings displayed a low pollution status and exhibited a very low ecological risk. Among six heavy metals (Cu, Pb, Zn, As, Cr, and Cd), only Cu (53.7 mg/kg) slightly exceeded its standard value limit (50 mg/kg), and was the main pollutant in the tailings. Due to its high toxicity, As had the maximum contribution to the potential ecological risk in the tailings. Pb, Zn, Cr, and Cd in the tailings were practically of no pollution, and at low or none potential ecological risk. In order to conduct revegetation in the tailings pond, more attention should be paid to the acidity change of tailings and its impact on the chemical activity and bioavailability of Cu and As. This research provides a theoretical basis for heavy metals risk control and revegetation in the low-grade copper sulfide tailings pond.

KEYWORDS

mine tailings, heavy metal, chemical fraction, pollution level, ecological risk assessmemt

1 Introduction

Mineral resources provide an important material foundation for society development and national security (Wu et al., 2021). However, the mining processes generate a large amount of tailings, which is about 2–12 times of the metal extracted from the ore (Jiang et al., 2021). At present, over 10 billion tons of mine tailings are produced globally each year (Xie and van Zyl, 2020). Billions of tons of tailings are increasingly accumulated in tailings ponds and are inevitably exposed to the environment for a long-term period. These tailings usually contain various kinds of heavy metals such as Pb, As, Cr, Cd, Mn, Zn, and Cu, which are commonly associated with the metal ore and would be released into the surrounding farmland soil, groundwater system and nearby rivers by directly penetrating, surface runoff and/or groundwater recharge (Barcelos et al., 2020). Therefore, heavy metal contents in the environment near tailings ponds might continue to increase, leading to severe environmental pollution (Khoeurn et al., 2019; Wang et al., 2019; Kan et al., 2021; Luo et al., 2021; Qi et al., 2022a).

Previous studies have demonstrated the great impacts of tailings on environmental quality and the ecological landscape (Nie et al., 2022). For example, affected by Hg mining deposits, the average contents of Hg and Ni in agricultural soil in Gongguan of Shaanxi province exceeded the national secondary standard value by 3.9, and 4.0 times, respectively (Zhu et al., 2018). Affected by artisanal gold mining, the mean concentrations of Hg and Cd in six villages in Tongguan (east of Shaanxi Province of China) were respectively 3.9 and 5.1 times of their maximum allowable concentrations for agricultural soils (Xiao et al., 2017). The translocation and accumulation of heavy metals in tailings may not only threaten the regional ecological security (Dubey et al., 2018; Ismail et al., 2019), but also affect the human health through food chain *via* causing some chronic diseases, metabolism disorders, deformities, and cancers (Al osman et al., 2019; Sanaei et al., 2021). For instance, Wang et al. found that Cu, Cr, Pb, Cd, and As in vegetables and crops near four typical mining and smelting zones in central China were 6.7%, 6.7%, 66.7%, 80.0%, and 26.7% higher than the national standards, respectively (Wang et al., 2021b).

It is worth noting that only the total contents of heavy metals are not enough for assessing the ecological risk of tailings (Moore et al., 2014; Jiang et al., 2021). The toxicity, bioavailability, mobility, or potential risks of heavy metals should also depend on their chemical fractions (Zhao et al., 2021). Heavy metals' chemical fractions in tailings can be determined by various extractants with different leaching strength (Cheng et al., 2018; Gitari et al., 2018; Roebbert et al., 2018; Wu et al., 2018). Among the various extraction protocols, the modified BCR sequential extraction is one of the most widely used method and applied in various environmental components such as soil, sediment, sewage sludge, and mining waste (Matong et al., 2016; Li et al., 2018; Wang et al., 2021a; Gao et al., 2021; Liu et al., 2022). By using this technique, the bioavailability of As, Cr, Cd, Mn, Pb, and Zn were also successfully estimated from environmental matrices (Barcelos et al., 2020). In addition, in the farmland soils around several typical mining areas, Zhao et al. (2021) analyzed the association relationship between multiple heavy metals and Fe fractions.

For characterizing the ecological risk of contaminants to the environment, various risk assessment methods have been developed in many studies under multiple matrices (Wu et al., 2018; Buch et al., 2021; Dash et al., 2021; Masri et al., 2021; Demirak et al., 2022; Zhang et al., 2022). Among these methods, risk assessment code (*RAC*), geo-accumulation index (I_{geo}), and potential ecological risk index (*RI*) have been widely used based on the total content and chemical fraction of heavy metals. For example, Cheng et al. reported a moderate soil Cd contamination around a coal mining area of Huaibei coalfield by applying *RAC*, I_{geo} and *RI* (Cheng et al., 2018). Using the improved I_{geo} and *RI*, Luo et al. (2021) found that Sb and As exhibited a serious risk and Cr, Cd, Cu, Pb, and Zn posed a low risk in Qinglong antimony mine tailings. In addition, the Nemerow integrated pollution index (P_N) is also frequently applied to assess the pollution level of multiple heavy metals (Zhang et al., 2018; Chai et al., 2021).

Currently, one low-grade copper sulfide mine tailings pond has to face the problem of ecological restoration after its closure. In addition to copper, this low-grade copper sulfide ore consists of a large number of minerals, which contain potentially toxic elements, such as As, Pb, Zn, Mn, Cr, and Cd. In the process of copper mining, these coexisting heavy metals are discarded and enter the mine tailings pond. Heavy metals play a significant impact on the quality of the soil, and can be enriched in organisms (Xing et al., 2022). In order to successfully achieve ecological restoration of the tailings pond, investigating the pollution levels in the tailings and assessing the potential ecological risks has become an urgent problem.

Therefore, the objectives of this study are as follows: 1) performing the chemical and mineralogical analysis of the low-grade copper sulfide mine tailings; 2) determining the concentrations and chemical fraction of various heavy metals (Cu, Pb, Zn, As, Cr, and Cd); 3) investigating the pollution degree and ecological risk of these metals. This research is expected to provide a comprehensive information on heavy metals in the low-grade copper sulfide mine tailings and lay a basis for the tailings' pollution control and vegetation reconstruction.

2 Materials and methods

2.1 The tailings sample and reagents

About 5.0 t tailings slurry were sampled from the total outlet of the transfer pump of the low-grade copper sulfide mine tailings pond. The water content of tailings slurry was about 40%. The collected tailings were air-dried, evenly mixed, grinding and sieved by a 10-mesh nylon mesh screen.

All reagents used in this study were analytically pure and were directly used. Only hydrochloric acid (purity 37%), nitric acid (purity 65%), and perchloric acid (purity 70%) were purchased from Xilong Scientific Co., Ltd. (Chengdu, China), and other reagents, including standard metal solutions (1000 mg/L) were purchased from Macklin Biochemical Technology Co., Ltd. (Shanghai, China). All the solutions were prepared in deionized water.

2.2 Chemical and mineralogical analysis

Analysis of physicochemical properties is necessary to characterize the tailings sample. The pH was measured using a pH meter (PHS-3C, Ramag, China) at a 2.5:1 water-to-tailings ratio. The cation exchange capacity was estimated at pH equal to seven by ammonium acetate exchange method (Belay et al., 2022). The mineral phase of the tailings was determined by X-ray diffraction spectroscopy (X'Per Powder, PANalytical, Netherlands) scanning from 10° to 80° at a scan speed of 1°/min. The chemical composition of the tailings was determined by X-ray fluorescence spectroscopy (S8 TIGER, Bruker, Germany). The particle size analysis of the tailings was performed with a laser particle size analyzer (BT-9300H(T), China) with a detection limit of 0.01 μm.

2.3 Tailings digestion and chemical fraction

2.3.1 Tailings digestion

The total contents of various heavy metals in the tailings were analyzed by aqua regia and $HClO_4$ digestion method

TABLE 1 The degrees of contamination and ecological risk.

Degree	Speciation index	Total content indices			
	RAC	I_{geo}	P_N	E_r^i	*RI*
None	≤1%	≤0	$P_N < 0.7$	–	–
Alert level	–	–	$0.7 < P_N < 1.0$	–	–
Low	1%–10%	0–1	$1.0 < P_N < 2.0$	<40	<150
Moderate	10%–30%	1–2	$2.0 < P_N < 3.0$	40–80	150–300
Considerable	–	2–3	–	80–160	–
High	30%–50%	3–4	$P_N > 3.0$	160–320	300–600
Very high	>50%	4–5	–	>320	≥600
Extremely Serious	–	>5	–	–	–

(Ying et al., 2022). 30 ml of acid solutions (15 ml HCl and 5 ml HNO_3 + 10 ml $HClO_4$) was added to 0.5 g tailings, and then heated to 200°C. Digested solutions were diluted by 1% HNO_3 aquation into 100 ml volumetric flasks. All glassware was immersed in 20% nitric acid solution to at least 24 h before usage.

2.3.2 Chemical fractions of heavy metals

Chemical fractions of heavy metals in the low-grade copper sulfide tailings were determined by the modified BCR sequential extraction (Zhao et al., 2021; Demirak et al., 2022). This method separates the chemical fractions of heavy metals into four forms: weak acid soluble fraction, reducible fraction, oxidizable fraction and residual fraction (Jayarathne et al., 2018). Weak acid soluble fraction (F1): added 20 ml of 0.11 M CH_3COOH solution to one 50 ml tube containing 0.5 g of tailings, continuously shaken for 16 h at 25°C. Reducible fraction (F2): added 20 ml of 0.5 M $NH_2OH{\cdot}HCl$ solution (adjusted to pH = 1.5 with HCl) to the former tube and shook for 16 h at 25°C. Oxidizable fraction (F3): added 3 ml of 30% H_2O_2 solution, shook intermittently for 1 h at 25°C, and then continued to digest for another 1 h at 85°C until the volume in the tube dropped to 2–3 ml. Repeated the above steps until the volume was reduced to 1 ml. Finally, put 20 ml of 1.0 M CH_3COONH_4 solution into the cooled tube and shook for 16 h. Residual fraction (F4): used aqua regia and $HClO_4$ to extract the residual heavy metals.

Centrifuged all the above suspensions at 1500 r/min for 10 min, and then filtered by 0.45 μm membrane. The dissolved heavy metals were determined by a flame atomic absorption spectrophotometer (Shimadzu AA-7000F, Japan), while As was measured by atomic fluorescence spectrophotometer (AFS-9800, Beijing KeChuang HaiGuang Instrument Co., Ltd, China), and reported on a dry weight basis (mg/kg).

The accuracy of the modified BCR sequential extraction method was verified by comparing the sum of four chemical fractions with the total contents obtain from direct tailings digestion. The recovery of the sequential extraction method was calculated according to Eq. 1 (Demirak et al., 2022):

$$\text{Recovery rate} = (C_{F1} + C_{F2} + C_{F3} + C_{F4}) \Big/ C_{\text{total digestion}} \times 100\% \quad (1)$$

where $C_{\text{total digestion}}$ is the total concentration of heavy metal; C_{F1}, C_{F2}, C_{F3}, and C_{F4} are the contents of F1, F2, F3 and F4 forms of heavy metals in the low-grade copper sulfide tailings.

2.4 Pollution status and ecological risk of heavy metals

The risk assessment code (*RAC*), geo-accumulation index (I_{geo}), Nemerow integrated pollution index (P_N), and potential ecological risk index (*RI*), were performed to comprehensively evaluate the pollution status and ecological risk of various heavy metals in the low-grade copper sulfide tailings. The degrees of *RAC*, I_{geo}, P_N and *RI* are shown in Table 1 (Demirak et al., 2022). The details of the above-mentioned methods are described as follows.

2.4.1 Risk assessment code (*RAC*)

Chemical fractions of heavy metals largely affect their harm to the environment (Moore et al., 2014). In particular, the weak acid soluble fraction of metals is weakly bound to the minerals in soil, they would easily enter aqueous solution and affect the organisms. Therefore, the *RAC* is defined as the percentage of the weak acid soluble fraction within the total metal concentration (Nemati et al., 2011; Demirak et al., 2022).

$$RAC = \left(C_{F1} \Big/ C_{\text{total digestion}}\right) \times 100\% \quad (2)$$

where C_{F1} is the weak acid soluble fraction concentration of certain heavy metal; $C_{\text{total digestion}}$ is the total concentration of certain heavy metal. *RAC* is one of the most important environmental risk assessment methods for soils and sediments.

2.4.2 Geo-accumulation index (I_{geo})

The geo-accumulation index (I_{geo}), known as the Muller Index, is widely used to characterize the sediment pollution level by comparing current heavy metals contents with pre-industrial values (Dash et al., 2021; Su et al., 2022). Unlike of other methods, I_{geo} takes into account the impact of the geochemical background values on the heavy metals' pollution status. Since the low-grade copper sulfide mine locates in Fujian Province, China, the geochemical background values in the

Fujian province were used here. The calculation formula is as follows (Ma et al., 2016):

$$I_{geo} = \log_2\left(\frac{C_n}{1.5B_n}\right) \quad (3)$$

where C_n is the total digestion concentration of metal n in the soil, B_n is the geochemical background value of heavy metal n. The factor 1.5 is a conversion coefficient to eliminate variations in background value that might be caused by differences in rocks.

2.4.3 The Nemerow integrated pollution index (P_N)

The Nemerow integrated pollution index (P_N), proposed by American scholar Nemerow, is widely employed to assess the comprehensive pollution status of various heavy metals (Wang et al., 2022). P_N is calculated by the average value and the maximum value of single factor pollution index. The calculation formula are expressed as follows (Chai et al., 2021):

$$P_i = \frac{C_i}{S_i} \quad (4)$$

$$P_N = \sqrt{\frac{(\bar{P}_i)^2 + (P_{imax})^2}{2}} \quad (5)$$

where P_i is the single factor pollution index of heavy metal i; C_i is the total concentration of heavy metal i; S_i is the evaluation standard of heavy metal i, taking the national soil pollution risk screening value (GB 15618-2018, denoted as "standard" below) as the reference standard. P_N is the Nemerow integrated pollution index, $\bar{P}_i$ represents the average value of all P_i, P_{imax} shows the maximum value of all P_i.

2.4.4 Potential ecological risk index (*RI*)

The potential ecological risk index (*RI*), proposed by Hakanson, is widely used to assess the soil environmental ecological risk caused by heavy metals. This method not only considers the influence of concentration and toxicological characteristics of heavy metals in a specific environment, but also eliminates the difference caused by the background value of heavy metals. The calculation formula are as follows (Qi et al., 2022b):

$$RI = \sum E_r^i \quad (6)$$

$$E_r^i = T_r^i \times C_f^i \quad (7)$$

$$C_f^i = C_s^i / C_n^i \quad (8)$$

where RI is the potential ecological risk index; E_r^i is the individual coefficient of potential ecological risk of heavy metal i; T_r^i is the toxicity response coefficient of heavy metal i; C_f^i is the single factor pollution index of heavy metal i; C_s^i is the total concentration of heavy metal i in the surface soil; C_n^i is the reference standard of heavy metal i. The toxicity response coefficient T_r^i of heavy metals are: Cu = Pb = 5, Zn = 1, As = 10, Cr = 2, and Cd = 30 (Jiang et al., 2021).

3 Results and discussion

3.1 Physicochemical properties of tailings

The physicochemical characteristics of tailings affect the accumulation and mobility of the heavy metals in tailings. The low-grade copper sulfide mine tailings was found to be acidic with a pH of 4.5. Cation exchange capacity was determined to be 13.1 cmol/kg. The d_{10}, d_{50}, and d_{90} values of the tailings particle sizes were 1.61, 16.18, and 72.4 μm, respectively. According to the particle size distribution results, it can be seen that the permeability of the tailings is very poor.

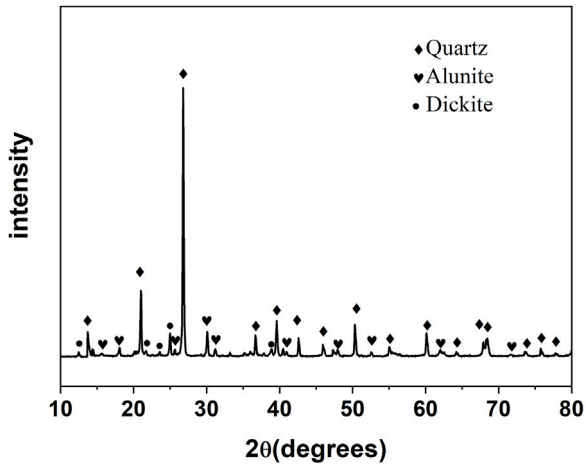

FIGURE 1
The XRD patterns of the low-grade copper sulfide tailings.

The XRD test (Figure 1) indicated that the tailings in the low-grade copper sulfide mine was composed by quartz, alunite, dickite, pyrite, and sericite. The results obtained by XRF (Table 2) showed that heavy metal elements in the tailings included Cu, Pb, Ba, As, Mn, Cr, Zn, Ni, and so on. Considering the content and the toxicity of various heavy metals, Cu, Pb, Zn, As, Cr, and Cd were chosen to be analyzed by tailings digestion and the modified BCR protocol.

3.2 Contents and chemical fractions of heavy metals in the low-grade copper sulfide tailings

3.2.1 Contents of heavy metals

Heavy metal concentrations, as shown in Table 3, were investigated to reveal the pollution status in the low-grade copper sulfide tailings pond. In comparison to the national soil pollution risk screening value limit (GB 15618-2018), only the Cu content (53.7 mg/kg) in tailings slightly exceeded the standard limit (50 mg/kg). The As content (33.9 mg/kg) in tailings was close to the standard limit (40 mg/kg), so more attention should be paid to it. The contents of Pb and Zn were significantly less than their relevant standard limits. The Cr and Cd contents in tailings were not detected. Based on the above analysis, Cu was considered to be the main pollutant in the tailings.

3.2.2 Chemical fractions of heavy metals

Chemical fractions of heavy metals in the tailings were carried out to characterize their chemical activity and bioavailability as well as their risks to the environment. As shown in Table 3, recovery rates of all heavy metals were 93.2%–98.3%, suggesting that the sums of

TABLE 2 Chemical compositions of the low-grade copper sulfide tailings by XRF analysis (wt%).

Element	Si	Al	S	K	Fe	Ca	Ti	Na	Cu	Pb	P	Mg
Result	29.9	5.35	4.05	1.88	1.50	0.217	0.132	0.109	0.0768	0.0454	0.0350	0.0341
Element	Ba	Sr	Zr	As	Mn	Cl	Cr	Zn	Nb	Ga	Ni	Rb
Result	0.0338	0.0295	0.0107	0.0078	0.0074	0.00695	0.00541	0.00326	0.00310	0.00296	0.00143	0.00142

TABLE 3 Contents of six heavy metals in the tailings obtained by digestion and BCR, background values in Fujian Province and national soil pollution risk screening value (mg/kg).

Element	Content	BCR	Recovery (%)	Background value	Standard (GB15618-2018) pH ≤ 5.5
Cu	53.7	52.9	98.5	21.6	50
Pb	4.09	3.81	93.2	34.9	70
Zn	13.0	12.3	94.6	82.7	200
As	33.9	32.4	95.6	5.78	40
Cr	–	–	–	41.3	150
Cd	–	–	–	0.054	0.3

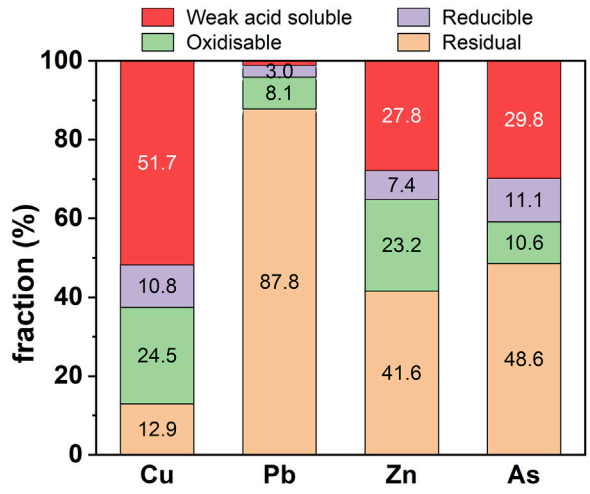

FIGURE 2
Heavy metals chemical fractions in the low-grade copper sulfide tailings using the modified BCR sequential extraction.

four chemical fractions were consistent with the total contents. Therefore, the modified BCR sequential extraction was reliable and repeatable. The chemical fractions of heavy metals were depicted in Figure 2. Various chemical fractions of Cr and Cd were not detected; thus, they were not provided here.

Cu. As shown in Figure 2, Cu was distributed in all four chemical fractions, and the considerable proportion (51.7%) of total Cu existed in the weak acid soluble fraction. This part of Cu existed in the form of ion-exchange and carbonate binding, and was loosely combined with soil matrices. Once the environmental conditions change, such as the pH, Cu in the weak acid soluble fraction would easily release into the environment. Therefore, among four kinds of chemical fractions, the weak acid soluble metal fraction is the most unstable, toxic, and bioavailable component (Matong et al., 2016; Demirak et al., 2022). The portion (24.5%) of oxidizable fraction was also noticeable. In oxidizable fraction, Cu combined with various organics and sulfide to form highly stable organic-copper compounds (Ma et al., 2016). About 12.9% and 10.8% of Cu had been found in residual and reducible fractions, respectively.

Pb. A proportion of 87.8% of Pb existed in the residual fraction, which was hard to release into pore-waters through dissociation due to its combination with aluminosilicate minerals (Burachevskaya et al., 2019; Ying et al., 2022). Only 8.1%, 3.0%, and 1.1% of Pb were found in oxidizable, reducible, and weak acid soluble fraction, respectively. Therefore, it is believed that Pb has weak chemical activity and bioavailability in the low-grade copper sulfide tailings.

Zn and As. Zn and As were very similar in chemical fractions, and mainly existed in the residual fraction with the proportions of 41.6% and 48.6%. This part of Zn and As were difficult to re-enter into the environment. In addition, there were about 30% of Zn and As in the weak acid soluble fraction, which were labile and easy to release under acidic conditions. 23.2% of Zn and 10.6% of As were observed in the oxidizable fraction. The reducible fractions of Zn and As were 7.4% and 11.1%, indicating that only small amounts of Zn and As were bound with Fe and Mn (oxyhydr) oxides.

3.3 Heavy metal pollution and ecological risk assessment

3.3.1 Risk assessment code (*RAC*)

Based on the chemical fraction results obtained by the modified BCR sequential extraction, the potential risks to the environment were estimated using the *RAC* method. Only the weak acid soluble fraction was considered here due to its easy entry into the environment. As displayed in Table 4, Cu posed

TABLE 4 The degrees of contamination and ecological risk of heavy metals in the low-grade copper sulfide tailings.

Element	*RAC* (%)		I_{geo}		P_N		Potential ecological risk			
							E_r^i		*RI*	
Cu	51.7	Very high	0.728	Low	1.13	Low	5.4	Low	14.2	Low risk
Pb	1.1	Low	−3.68	None			0.29	Low		
Zn	27.8	Medium	−3.25	None			0.065	Low		
As	29.8	Medium	1.97	Moderate			8.5	Low		
Cr	–	None	−∞	None			0	None		
Cd	–	None	−∞	None			0	None		

very high risk to the environment, while Zn and As posed the medium risks, and Pb posed the low risk, Cr and Cd posed no risk. Meanwhile, only Cu content in tailings slightly exceeded the national soil pollution risk screening value limit (GB 15618-2018), As content was close to the standard, other four heavy metals were much lower than their standard limit. Therefore, considering the *RAC* values and concentrations of heavy metals in the tailings, special attention should be paid to the environmental/ecological impacts caused by Cu. It is suggested that several amendments to the tailings may be required to passivate Cu (i.e., reducing the weak acid soluble fraction) before establishing revegetation in the low-grade copper sulfide tailings pond. Furthermore, in the process of revegetation, Cu enrich plants should not be selected unless they could be properly treated.

3.3.2 Geo-accumulation index (I_{geo})

For the purpose of determining heavy metals contamination levels in the tailings, the geo-accumulation index I_{geo} values of six heavy metals were calculated, as shown in Table 4. The level of I_{geo} from high to low was As > Cu > Zn ≈ Pb ≈ Cr ≈ Cd. Only the I_{geo} value of As exceeded 1, indicating that As fell into the "moderately polluted" level. The I_{geo} value of Cu was less than 1, indicating that Cu belonged to "unpolluted to moderately polluted". Furthermore, the I_{geo} values of Zn, Pb, Cr, and Cd were below 0, suggesting that these four kinds of heavy metals were practically of "no pollution". In this study, the I_{geo} values were calculated according to the soil background value in the Fujian province. However, while the low-grade copper sulfide mine is rich in copper element, it may also contain some other heavy metals, such as As, Pb and Zn. Therefore, the background values of heavy metals in the low-grade copper sulfide mine may be different from the soil background values in the Fujian province. It is speculated that the main reason why the As content in the tailings (33.9 mg/kg) is higher than its background value (5.78 mg/kg) is due to natural contribution rather than anthropogenic activities. The pollution status of Cu and As reflected by the high I_{geo} values only indicated the impact of heavy metals to ecological environment.

3.3.3 The Nemerow integrated pollution index (P_N)

The Nemerow integrated pollution index (P_N) was applied to assess the comprehensive pollution levels of heavy metals in the tailings. This index highlights the impacts of high concentrations of pollutants on soil environment quality. As shown in Table 4, the P_N obtained by six heavy metals was equal to 1.13, suggesting that the tailings sample showed low pollution to the environment. The P_{imax} value was determined by the content of Cu, indicating that Cu was the main contributor to heavy metals pollution of the tailings.

3.3.4 Potential ecological risk index (*RI*)

The potential ecological risk index (*RI*) was applied based on the national soil pollution risk screening value (GB 15618-2018) to assess the ecological risk. This method can reflect the comprehensive impacts of multiple pollutants. As illustrated in Table 4, the individual coefficient of potential ecological risk E_r^i values in decreasing order were As > Cu > Pb > Zn > Cr ≈ Cd. According to E_r^i values of six heavy metals, As and Cu were the main sources of potential ecological risk of the low-grade copper sulfide tailings. Although single factor pollution index C_f^i of Cu was larger than that of As, due to the higher toxicity of As, As had a higher E_r^i, indicating that As posed a higher potential ecological risk than Cu. Even so, all E_r^i values of six heavy metals were far below 40, as well as *RI* value (14.2) was far less than 150, indicating that there was a very low potential ecological risk in the low-grade copper sulfide tailings. The results of *RI* were basically the same as those of the P_N index.

4 Conclusion

Chemical and mineralogical analysis, chemical extraction, and ecological risk assessment were employed to evaluate the pollution level and ecological risk in the low-grade copper sulfide tailings pond. According to the results of P_N and *RI*, the low-grade copper sulfide tailings displayed a low pollution status and exhibited a very low ecological risk.

Among the six heavy metals (Cu, Pb, Zn, As, Cr, Cd) contained in the tailings, only Cu content exceeded the standard limit. Furthermore, the *RAC* of Cu was high than 50%. Cu was the main pollutant in the low-grade copper sulfide tailings. Although the content of As was below its standard limit, its high toxicity led to the largest potential ecological risk in the tailings. Based on the I_{geo} and E_r^i values, Pb, Zn, Cr, and Cd in the tailings were practically of no pollution, and exhibited low or none potential ecological risk.

It is urgent to pay more attention to the acidity change of tailings and its impact on the chemical activity and bioavailability of Cu and

As for conducting revegetation in the low-grade copper sulfide tailings pond.

Data availability statement

The original contributions presented in the study are included in the article/supplementary material, further inquiries can be directed to the corresponding author.

Author contributions

PZ: Conceptualization, methodology, formal analysis, data curation, writing-original draft, visualization, supervision, funding acquisition. JC: Writing-review and editing. TL: Writing-review and editing. QW: Conceptualization, resources, project administration. ZW: Validation, resources. SL: Investigation, resources, data curation.

Funding

The study was financially supported by the Natural Science Foundation of Fujian Province (No. 2022J05250), and the Qimai Natural Science Foundation of Longyan City, China (No. XLQM002).

Acknowledgments

The authors express special thanks to doctor Dean Song and Ruiming Zhang for their efforts in the revision of the manuscript. The authors would like to thank the editors and reviewers for their pertinent comments and suggestions.

Conflict of interest

PZ, JC, QW, and ZW were employed by the company Zijin Mining Group Co., Ltd.

The remaining authors declare that the research was conducted in the absence of any commercial or financial relationships that could be construed as a potential conflict of interest.

Publisher's note

References

Al osman, M., Yang, F., and Massey, I. Y. (2019). Exposure routes and health effects of heavy metals on children. *BioMetals* 32 (4), 563–573. doi:10.1007/s10534-019-00193-5

Barcelos, D. A., Pontes, F. V. M., da Silva, F. A. N. G., Castro, D. C., dos Anjos, N. O. A., and Castilhos, Z. C. (2020). Gold mining tailing: Environmental availability of metals and human health risk assessment. *J. Hazard. Mater.* 397, 122721. doi:10.1016/j.jhazmat.2020.122721

Belay, S. A., Assefa, T. T., Worqlul, A. W., Steenhuis, T. S., Schmitter, P., Reyes, M. R., et al. (2022). Conservation and conventional vegetable cultivation increase soil organic matter and nutrients in the Ethiopian highlands. *Water* 14 (3), 476. doi:10.3390/w14030476

Buch, A. C., Niemeyer, J. C., Marques, E. D., and Silva-Filho, E. V. (2021). Ecological risk assessment of trace metals in soils affected by mine tailings. *J. Hazard. Mater.* 403, 123852. doi:10.1016/j.jhazmat.2020.123852

Burachevskaya, M., Minkina, T., Mandzhieva, S., Bauer, T., Chaplygin, V., Zamulina, I., et al. (2019). Study of copper, lead, and zinc speciation in the Haplic Chernozem surrounding coal-fired power plant. *Appl. Geochem.* 104, 102–108. doi:10.1016/j.apgeochem.2019.03.016

Chai, L., Wang, Y., Wang, X., Ma, L., Cheng, Z., and Su, L. (2021). Pollution characteristics, spatial distributions, and source apportionment of heavy metals in cultivated soil in Lanzhou, China. *Ecol. Indic.* 125, 107507. doi:10.1016/j.ecolind.2021.107507

Cheng, S., Liu, G., Zhou, C., and Sun, R. (2018). Chemical speciation and risk assessment of cadmium in soils around a typical coal mining area of China. *Ecotoxicol. Environ. Saf.* 160, 67–74. doi:10.1016/j.ecoenv.2018.05.022

Dash, S., Borah, S. S., and Kalamdhad, A. S. (2021). Heavy metal pollution and potential ecological risk assessment for surficial sediments of Deepor Beel, India. *Ecol. Indic.* 122, 107265. doi:10.1016/j.ecolind.2020.107265

Demirak, A., Kocakaya, M., and Keskin, F. (2022). Chemical fractions of toxic metals and assessment of risks on the environment and health in Mugla topsoils. *Int. J. Environ. Sci. Technol.* 19 (6), 5631–5648. doi:10.1007/s13762-021-03547-0

Dubey, S., Shri, M., Gupta, A., Rani, V., and Chakrabarty, D. (2018). Toxicity and detoxification of heavy metals during plant growth and metabolism. *Environ. Chem. Lett.* 16 (4), 1169–1192. doi:10.1007/s10311-018-0741-8

Gao, Y., Jia, J., Xi, B., Cui, D., and Tan, W. (2021). Divergent response of heavy metal bioavailability in soil rhizosphere to agricultural land use change from paddy fields to various drylands. *Environ. Sci. Process. Impacts* 23 (3), 417–428. doi:10.1039/D0EM00501K

Gitari, M. W., Akinyemi, S. A., Ramugondo, L., Matidza, M., and Mhlongo, S. E. (2018). Geochemical fractionation of metals and metalloids in tailings and appraisal of environmental pollution in the abandoned Musina Copper Mine, South Africa. *Environ. Geochem. Health* 40 (6), 2421–2439. doi:10.1007/s10653-018-0109-9

Ismail, A., Riaz, M., Akhtar, S., Goodwill, J. E., and Sun, J. (2019). Heavy metals in milk: Global prevalence and health risk assessment. *Toxin Rev.* 38 (1), 1–12. doi:10.1080/15569543.2017.1399276

Jayarathne, A., Egodawatta, P., Ayoko, G. A., and Goonetilleke, A. (2018). Assessment of ecological and human health risks of metals in urban road dust based on geochemical fractionation and potential bioavailability. *Sci. Total Environ.* 635, 1609–1619. doi:10.1016/j.scitotenv.2018.04.098

Jiang, L., Sun, H., Peng, T., Ding, W., Liu, B., and Liu, Q. (2021). Comprehensive evaluation of environmental availability, pollution level and leaching heavy metals behavior in non-ferrous metal tailings. *J. Environ. Manag.* 290, 112639. doi:10.1016/j.jenvman.2021.112639

Kan, X., Dong, Y., Feng, L., Zhou, M., and Hou, H. (2021). Contamination and health risk assessment of heavy metals in China's lead–zinc mine tailings: A meta–analysis. *Chemosphere* 267, 128909. doi:10.1016/j.chemosphere.2020.128909

Khoeurn, K., Sakaguchi, A., Tomiyama, S., and Igarashi, T. (2019). Long-term acid generation and heavy metal leaching from the tailings of Shimokawa mine, Hokkaido, Japan: Column study under natural condition. *J. Geochem. Explor.* 201, 1–12. doi:10.1016/j.gexplo.2019.03.003

Li, Y.-C., Min, X.-B., Ke, Y., Chai, L.-Y., Shi, M.-Q., Tang, C.-J., et al. (2018). Utilization of red mud and Pb/Zn smelter waste for the synthesis of a red mud-based cementitious material. *J. Hazard. Mater.* 344, 343–349. doi:10.1016/j.jhazmat.2017.10.046

Liu, H., Qu, M., Chen, J., Guang, X., Zhang, J., Liu, M., et al. (2022). Heavy metal accumulation in the surrounding areas affected by mining in China: Spatial distribution patterns, risk assessment, and influencing factors. *Sci. Total Environ.* 825, 154004. doi:10.1016/j.scitotenv.2022.154004

Luo, G., Han, Z., Xiong, J., He, Y., Liao, J., and Wu, P. (2021). Heavy metal pollution and ecological risk assessment of tailings in the Qinglong Dachang antimony mine, China. *Environ. Sci. Pollut. Res.* 28 (25), 33491–33504. doi:10.1007/s11356-021-12987-7

Ma, X., Zuo, H., Tian, M., Zhang, L., Meng, J., Zhou, X., et al. (2016). Assessment of heavy metals contamination in sediments from three adjacent regions of the Yellow River using metal chemical fractions and multivariate analysis techniques. *Chemosphere* 144, 264–272. doi:10.1016/j.chemosphere.2015.08.026

Masri, S., Lebron, A., Logue, M., Valencia, E., Ruiz, A., Reyes, A., et al. (2021). Risk assessment of soil heavy metal contamination at the census tract level in the city of santa ana, CA: Implications for health and environmental justice. *Environ. Sci. Process. Impacts* 23, 812–830. doi:10.1039/d1em00007a

Matong, J. M., Nyaba, L., and Nomngongo, P. N. (2016). Fractionation of trace elements in agricultural soils using ultrasound assisted sequential extraction prior to inductively coupled plasma mass spectrometric determination. *Chemosphere* 154, 249–257. doi:10.1016/j.chemosphere.2016.03.123

Moore, F., Nematollahi, M. J., and Keshavarzi, B. (2014). Heavy metals fractionation in surface sediments of Gowatr bay-Iran. *Environ. Monit. Assess.* 187 (1), 4117. doi:10.1007/s10661-014-4117-7

Nemati, K., Bakar, N. K. A., Abas, M. R., and Sobhanzadeh, E. (2011). Speciation of heavy metals by modified BCR sequential extraction procedure in different depths of sediments from Sungai Buloh, Selangor, Malaysia. *J. Hazard. Mater.* 192 (1), 402–410. doi:10.1016/j.jhazmat.2011.05.039

Nie, W., Luo, M., Wang, Y., and Li, R. (2022). 3D visualization monitoring and early warning system of a tailings dam—gold copper mine tailings dam in zijinshan, fujian, China. *Front. Earth Sci.* 10, 800924. doi:10.3389/feart.2022.800924

Qi, Y., Fan, C., Quan, X., Xi, F., Liu, Z., Cao, Q., et al. (2022a). *In-situ* recycling strategy for co-treatment of antimony-rich sludge char and leachate: Pilot-scale application in an engineering case. *Chem. Eng. J.* 446, 137315. doi:10.1016/j.cej.2022.137315

Qi, Y., Wei, X., Zhao, M., Pan, W., Jiang, C., Wu, J., et al. (2022b). Heavy metal pollution characteristics and potential ecological risk assessment of soils around three typical antimony mining areas and watersheds in China. *Front. Environ. Sci.* 10. doi:10.3389/fenvs.2022.913293

Roebbert, Y., Rabe, K., Lazarov, M., Schuth, S., Schippers, A., Dold, B., et al. (2018). Fractionation of Fe and Cu isotopes in acid mine tailings: Modification and application of a sequential extraction method. *Chem. Geol.* 493, 67–79. doi:10.1016/j.chemgeo.2018.05.026

Sanaei, F., Amin, M. M., Alavijeh, Z. P., Esfahani, R. A., Sadeghi, M., Bandarrig, N. S., et al. (2021). Health risk assessment of potentially toxic elements intake via food crops consumption: Monte Carlo simulation-based probabilistic and heavy metal pollution index. *Environ. Sci. Pollut. Res.* 28 (2), 1479–1490. doi:10.1007/s11356-020-10450-7

Su, C., Meng, J., Zhou, Y., Bi, R., Chen, Z., Diao, J., et al. (2022). Heavy metals in soils from intense industrial areas in south China: Spatial distribution, source apportionment, and risk assessment. *Front. Environ. Sci.* 10. doi:10.3389/fenvs.2022.820536

Wang, J., Shi, L., Zhai, L., Zhang, H., Wang, S., Zou, J., et al. (2021a). Analysis of the long-term effectiveness of biochar immobilization remediation on heavy metal contaminated soil and the potential environmental factors weakening the remediation effect: A review. *Ecotoxicol. Environ. Saf.* 207, 111261. doi:10.1016/j.ecoenv.2020.111261

Wang, L., Zeraatpisheh, M., Wei, Z., and Xu, M. (2022). Heavy metal pollution and risk assessment of farmland soil around abandoned domestic waste dump in Kaifeng City. *Front. Environ. Sci.* 10. doi:10.3389/fenvs.2022.946298

Wang, P., Sun, Z., Hu, Y., and Cheng, H. (2019). Leaching of heavy metals from abandoned mine tailings brought by precipitation and the associated environmental impact. *Sci. Total Environ.* 695, 133893. doi:10.1016/j.scitotenv.2019.133893

Wang, Z., Bao, J., Wang, T., Moryani, H. T., Kang, W., Zheng, J., et al. (2021b). Hazardous heavy metals accumulation and health risk assessment of different vegetable species in contaminated soils from a typical mining city, central China. *Int. J. Environ. Res. Public Health* 18 (5), 2617. doi:10.3390/ijerph18052617

Wu, J., Lu, J., Li, L., Min, X., and Luo, Y. (2018). Pollution, ecological-health risks, and sources of heavy metals in soil of the northeastern Qinghai-Tibet Plateau. *Chemosphere* 201, 234–242. doi:10.1016/j.chemosphere.2018.02.122

Wu, W., Zhou, J., Niu, J., and Lv, H. (2021). Study on coupling between mineral resources exploitation and the mining ecological environment in Shanxi Province. *Environ. Dev. Sustain.* 23 (9), 13261–13283. doi:10.1007/s10668-020-01209-8

Xiao, R., Wang, S., Li, R., Wang, J. J., and Zhang, Z. (2017). Soil heavy metal contamination and health risks associated with artisanal gold mining in Tongguan, Shaanxi, China. *Ecotoxicol. Environ. Saf.* 141, 17–24. doi:10.1016/j.ecoenv.2017.03.002

Xie, L., and van Zyl, D. (2020). Distinguishing reclamation, revegetation and phytoremediation, and the importance of geochemical processes in the reclamation of sulfidic mine tailings: A review. *Chemosphere* 252, 126446. doi:10.1016/j.chemosphere.2020.126446

Xing, J., Gao, L., and He, L. (2022). Species distribution and concentration pollution of soil heavy metals in coal mine reclamation areas. *Front. Environ. Sci.* 10. doi:10.3389/fenvs.2022.925074

Ying, H., Zhao, W., Feng, X., Gu, C., and Wang, X. (2022). The impacts of aging pH and time of acid mine drainage solutions on Fe mineralogy and chemical fractions of heavy metals in the sediments. *Chemosphere* 303, 135077. doi:10.1016/j.chemosphere.2022.135077

Zhang, P., Qin, C., Hong, X., Kang, G., Qin, M., Yang, D., et al. (2018). Risk assessment and source analysis of soil heavy metal pollution from lower reaches of Yellow River irrigation in China. *Sci. Total Environ.* 633, 1136–1147. doi:10.1016/j.scitotenv.2018.03.228

Zhang, X., Gong, Z., Allinson, G., Xiao, M., Li, X., Jia, C., et al. (2022). Environmental risks caused by livestock and poultry farms to the soils: Comparison of swine, chicken, and cattle farms. *J. Environ. Manag.* 317, 115320. doi:10.1016/j.jenvman.2022.115320

Zhao, W., Gu, C., Ying, H., Feng, X., Zhu, M., Wang, M., et al. (2021). Fraction distribution of heavy metals and its relationship with iron in polluted farmland soils around distinct mining areas. *Appl. Geochem.* 130, 104969. doi:10.1016/j.apgeochem.2021.104969

Zhu, D., Wei, Y., Zhao, Y., Wang, Q., and Han, J. (2018). Heavy metal pollution and ecological risk assessment of the agriculture soil in xunyang mining area, Shaanxi province, northwestern China. *Bull. Environ. Contam. Toxicol.* 101 (2), 178–184. doi:10.1007/s00128-018-2374-9

frontiers | Frontiers in Environmental Science

TYPE Original Research
PUBLISHED 13 April 2023
DOI 10.3389/fenvs.2023.1163422

OPEN ACCESS

EDITED BY
Jun Wu,
Harbin Engineering University, China

REVIEWED BY
Chen Tu,
Institute of Soil Science (CAS), China
S. Suresh,
Sona College of Technology, India

*CORRESPONDENCE
Amal An-nori,
amal.an-nori@um6p.ma

SPECIALTY SECTION
This article was submitted to Toxicology, Pollution and the Environment, a section of the journal Frontiers in Environmental Science

RECEIVED 10 February 2023
ACCEPTED 27 March 2023
PUBLISHED 13 April 2023

CITATION
An-nori A, El Mejahed K, Fels LE, Touhami D, Ezzariai A, El Gharous M and Hafidi M (2023), Assessment of the agronomic value of solar-dried sludge and heavy metals bioavailability based on the bioaccumulation factor and translocation index.
Front. Environ. Sci. 11:1163422.
doi: 10.3389/fenvs.2023.1163422

Assessment of the agronomic value of solar-dried sludge and heavy metals bioavailability based on the bioaccumulation factor and translocation index

Amal An-nori[1,2]*, Khalil El Mejahed[1,2], Loubna El Fels[3], Driss Touhami[2], Amine Ezzariai[2], Mohamed El Gharous[1,2] and Mohamed Hafidi[2,3]

[1]Agricultural Innovation and Technology Transfer Center (AITTC), Mohammed VI Polytechnic University, Benguerir, Morocco, [2]College for Sustainable Agriculture and Environmental Science, Mohamed VI polytechnic University, Benguerir, Morocco, [3]Laboratory of Microbial Biotechnologies, Agrosciences and Environment (BioMAgE) Labeled Research Unit-CNRST N°4, Cadi Ayad University, Marrakesh, Morocco

This study aimed to assess the agronomic value of solar-dried sludge (SDS) and the transfer of Cr, Ni, Pb, and Cu to wheat (*Triticum aestivum*) and faba bean (*Vicia faba*). A greenhouse experiment was performed involving two rates of SDS (15 t/ha and 30 t/ha) from an activated sludge-based wastewater treatment plant. In addition to the single use of an SDS amendment, co-application of SDS and mineral fertilizers was also included to determine the best scenario resulting in high yields and less negative implications on the environment. Data for both wheat and faba bean showed that applying SDS at 30 t/ha led to competitive yields compared to the ones obtained previously, while 15 t/ha of SDS and mineral fertilizers were co-applied. The use of SDS increased soil organic matter, slightly decreased the pH value, and increased soil salinity. The contents of Ni, Cu, and Pb were not significantly affected by the application of SDS. Only Cr showed high soil concentrations in proportion to the increasing rates of SDS. The bioaccumulation of heavy metals in roots was more important in 30 t/ha than that in 15 t/ha amended soil. In the case of wheat, the bioconcentration factor (BCF) root values correspond to the following order: Cr (0.89) >Cu (0.85)> Ni (0.28)> Pb (0.22). In the case of faba bean, BCF roots were observed as follows: Cu (1.04 > Ni (0.37)> Cr (0.16)> Pb (0.15). Wheat excluded Cr, Ni, and Pb from the uptake by shoots, and Cu was translocated from roots to shoots with a percentage of 11% at 30 t/ha of applied SDS. Faba beans demonstrated more important values of HM's translocation by respecting this order (Ni (37.7%) > cu (30.24%)> Cr (17.59%), while Pb was excluded from the translocation. No significant difference was observed regarding the translocation index when the sludge rate has been duplicated from 15 t/ha to 30 t/ha. Based on these outcomes, SDS used at the rate of 30 t/ha is the best scenario to amend the soil and provide nutrients to plants. Wheat is

Abbreviations: SDS, solar-dried sludge; WWTP, wastewater treatment plant; FAO, Food and Agriculture Organization; HMs, heavy metals; AFNOR, Association Française de Normalisation; TKN, total Kjeldahl nitrogen; ICP-AES, inductively coupled plasma atomic emission spectrometry; RCBD, randomized complete block design; GP, germination percentage; CCI, chlorophyll content index; HI, harvest index; BCF, bioconcentration factor; and TI, translocation index.

translocating less heavy metal to the edible part; it is, thus, the most suitable crop to be involved in the current context.

KEYWORDS

solar-dried sludge, organic amendment, heavy metal, uptake, toxicity, soil, wheat, faba bean

1 Introduction

Due to the rapid population growth, which is estimated to reach 9 billion by 2050 (WPP, 2017), ensuring food security around the world has become a challenge. To deal with this concern, yields have been improved through crop intensification, inducing soil quality degradation. This intensification involves an excessive use of mineral fertilizers and results in organic matter depletion of soils. Moreover, intensified agriculture with conventional tillage affects soil's structural stability and increases its vulnerability to erosion. According to Rasmussen et al. (1998), conventional tillage practices can reduce soil organic carbon at the top 7.5 cm of a soil by 25%–30%. Thus, meeting the global food demand without affecting soils, associated resources, and the environment, while moving food and agricultural systems toward sustainability, has become an urgency. Indeed, sustainable agricultural intensification was suggested to achieve more food, produced from the same land, reducing negative environmental impacts, and then, providing positive societal and economic benefits.

On the other hand, sewage sludge production is being increased proportionally to the widespread adoption of advanced technologies of wastewater treatment. The management of such a byproduct, without negative implications on the environment, constitutes a major concern for all the stakeholders including researchers from all fields. Several practices have been adopted for sewage sludge final disposal such as landfilling, incineration, and application on agricultural soils, while awareness about sewage sludge as a valuable resource is increasing. Therefore, landfilling started to phase out in many countries (Kroiss et al., 2007; Raheem et al., 2018) in parallel with the search for alternative ways of valorization.

Knowing that sewage sludge contains plant nutrients (N, P, and K among others) and more than 50% of organic matter, its use as an organic amendment and fertilizer can contribute to soil property enhancement and soil nutrient availability. This practice is crucial for Africa, mainly in arid and semi-arid regions, where soils have very low organic matter content (Albaladejo et al., 2013) and most crop residues are removed. For instance, in Morocco, the mean value of organic matter content is below 2% and the annual agricultural soil loss is estimated to 100 million tons (FAO, 2015). Thus, agricultural recycling of sewage sludge consists of a particular relevance for soil organic matter improvement and associated physical and chemical benefits. According to several research studies, incorporating sludge into agricultural soils leads to atmospheric CO_2 concentration reduction and soil organic carbon increase. This may, consequently, contribute to carbon sequestration and improve soil fertility (Soriano-Disla et al., 2010). Indeed, the applied organic matter can be associated with clay to form the clay–humus complex, which promotes soil aeration and increases nutrients availability. However, to be applied on agricultural soils, sewage sludge should be neutralized and stabilized as it includes some hazardous materials, such as pathogens, heavy metals (HMs), and other organic micropollutants (Fijalkowski et al., 2017).

In the latest trends, with regard to the field of sewage sludge treatment, the solar-drying process is involved with particular emphasis, especially where solar radiation is available as it is the case in Morocco (3000 h/year of sunshine). Throughout the literature, the solar-drying process has been proven to not affect the agronomic value of sewage sludge (Lem et al., 2017; An-nori et al., 2020a; An-Nori et al., 2022). Moreover, its significant ability to remove pathogens, namely, indicators of fecal contamination and helminths, has been reported in several research studies (Shanahan et al., 2010; Paluszak et al., 2012; An-Nori et al., 2021). However, less information is available on the behavior of heavy metals in solar-dried sludge, especially in terms of bioavailability and transfer to plants. Furthermore, HM accretion within the comestible parts of crops is a limitation to sewage sludge application on arable soil (Eid et al., 2021). According to several authors, plant uptake is one of the major pathways by which the essential and non-essential HMs enter the food chain (Karami et al., 2009). The uptake of HMs by plants is influenced by numerous parameters including the physical and chemical characteristics of the soil, the sewage sludge composition and its application rate, plant species and their physiology, rhizosphere biochemistry, climatic parameters, HMs, and their speciation (Dolgen et al., 2007). Contrary to the bioaccumulation of HMs in root systems, translocation from roots to shoots is controlled mainly by plant physiology (Kalis et al., 2008; Chimie, 2014; Chopra, 2014). The concentration of HMs in roots has been widely used as an indication of metal bioavailability (Chaignon et al., 2003), while the concentration measured in shoots determines which fraction may potentially enter the food chain and undergo biomagnification, having concomitant impacts on human health and alterations to the environment.

Throughout the literature, several investigations focused on the composted sewage sludge application on agricultural soils. However, solar-dried sludge and its implications on crops' yields and quality was not addressed, especially in Morocco. Additionally, the behavior and traceability of the included HMs in solar-dried sludge, after recycling in agriculture, is not yet addressed in the literature. In this study, we aimed to assess (i) the agronomic value of solar-dried sludge as an organic amendment on crop yields and (ii) HM transfer to different parts of wheat and faba bean crops.

2 Materials and methods

2.1 Solar-dried sludge characteristics

The solar-dried sewage sludge used in the present experiments has been sampled from the wastewater treatment plant (WWTP) of Marrakech city, which is an activated sludge-based WWTP. Before

solar drying, the sludge was digested (37°C) and mechanically dewatered using belt filters and was then solar-dried for 45 days in summer under a semi-arid climate (An-nori et al., 2020a). Physicochemical analysis of solar dried sludge was performed in three replicates, in a previous investigation (An-nori et al., 2020a). The main characteristics of solar-dried sludge (SDS) are shown in Table 1.

The used sewage sludge is an important source of organic matter (61.5%) and total nutrients (4%, 2.62%, and 0.5% of N, P, and K, respectively) (Table 1); thus, it can importantly be used as a fertilizer complement or a fertilizer depending on the rate of application. Regarding HM analysis, high concentrations of Cr, Ni, Cu, and Pb have been recorded (3008 mg/kg, 31.84 mg/kg, 181.19 mg/kg, and 68.98 mg/kg, respectively). In comparison with the international limits for agricultural use of SS, namely, the EC Directive 86/278/EEC (Supplementary Table S1), Cu, Ni, and Pb did not exceed these limits. As for Cr, it is only a few ppm above the maximum admitted load considered by the U.S. Environmental Protection Agency (Supplementary Table S1). However, the speciation analysis of this element in a previous investigation indicated low mobility potential of Cr (An-nori et al., 2020a). Indeed, the oxidizable fraction, which was initially predominant in the sludge before undergoing a solar drying process, decreased very significantly after 45 days of solar drying, and the residual fraction, the most stable in the environment, became the most important in SDS. This leads to the assumption that Cr may not be relatively bioavailable to plants. However, guidelines or limits are different from one country to another; they are based on the total content of metals in sewage, soil, and plant, and hence, more investigations are needed by integrating soil, plant, climate, and HM total content and speciation in solar-dried sludge to decide rationally on its safe use in agriculture.

TABLE 1 Physicochemical characteristics of solar-dried sludge used as an organic amendment (An-nori et al., 2020a).

Parameter	Value
pH[a]	7.07 ± 0.0
EC[a] (mS/cm²)	2.20 ± 0.2
DM[b] (%)	93.46 ± 0.3
OM[b] (%)	61.5 ± 0.7
Ash content[b](%)	38.5 ± 0.7
TOC[b] (%)	34.8 ± 1.4
C/N	9.06
TKN[b] (%)	4.02 ± 0.0
P[b] (%)	2.68 ± 0.0
K[b] (%)	0.50 ± 0.0
Mg[b] (mg/kg)	0.51 ± 0.0
Ca[b] (g/kg)	26.21 ± 1.0
Mn[b] (mg/kg)	224.33 ± 3.2
Fe[b] (g/kg)	9.97 ± 0.5
Na[b] (g/kg)	4.9 ± 0.2
Cr[b] (mg/Kg)	3008.23
Ni[b] (mg/Kg)	31.84
Cu[b] (mg/Kg)	181.19
Pb[b] (mg/Kg)	68.98

[a]Results expressed per fresh matter.
[b]Results expressed per dry matter; OM: organic matter, TOC: total organic carbon, TKN: total Kjeldahl nitrogen. The values correspond to the means of three replicates (± standard deviation).

2.2 Soil physicochemical characteristics

Samples from the 20 cm topsoil were collected from the experimental farm of UM6P in Ben Guerir, Morocco (31.6295° N, 7.9811° W). Soil samples were air-dried, mechanically grinded, and then sieved to obtain less than 2 mm fraction. Soil texture was determined by Robinson's pipette method, and pH and electrical conductivity were measured on an aqueous extract of soil (1/10 w/v, distilled water, 30 min of shaking) (AFNOR NF T90-008). Equivalent calcium carbonate (CO_3^{2-}) was determined by using the Bernard calcimeter (Hulseman, 1966). OM was determined by muffle calcination (600 C for 6 h). Total Kjeldahl nitrogen (TKN) was assayed in 0.5 g samples by using the classical Kjeldahl procedure by steam distillation according to the AFNORT90-110 standard. The content of HMs and major essential elements in the soil were determined after mineralization with tri-acid mixture (7 mL HNO_3, 2 mL HF, and 1 mL $HClO_4$) in the DigiPREP system (3 h at 120°C) (Hanay et al., 2008). After digestion, the solutions were filtered (0.45 µm mesh) and then diluted to 50 mL with distilled water. After digestion, the filtrates were acidified (2% HNO_3) to undergo the analysis by inductively coupled plasma optical emission spectroscopy (ICP-OES) using the Agilent Technologies 5110 ICP-OES. All the physicochemical analyses were performed in triplicate, and all the chemicals used were of analytical reagent grade. Standards of soil and sewage sludge were used for quality control in the quantification of HMs. Soil analysis was performed before planting and after harvest. All the analyses were performed at the Agricultural Innovation and Technology Transfer Center laboratories of UM6P. The main characteristics of the used soil in the present investigation are shown in Supplementary Table S2.

2.3 Experimental design

Two agricultural trials were carried out in pots between January and May 2021 under greenhouse conditions at the experimental farm of Mohammed VI Polytechnic University (UM6P) in Ben Guerir, Morocco, involving two crops: faba bean (*Vicia Faba*) and wheat (Triticum *aestivum*). Six treatments have been used separately for both wheat and faba bean, as shown in Table 2. They consist of SDS rates with and without fertilizer complement and include a treatment having mineral fertilizers (F) only. The treatments were arranged in a randomized complete block design (RCBD), with four repetitions.

The applied F is equivalent to 50 kg N/ha, 20 kg P/ha, and 90 K kg/ha for wheat and 10 kg N/ha, 20 kg P/ha, and 40 K kg/ha for faba bean, and it was calculated based on soil N, P, and K availability tests. These two trials were set in 4 kg-sized plastic pots filled with 3 kg of soil and 1 kg of gravel, at their bottom, to allow

TABLE 2 Involved treatments in agronomic trials.

0	Control
F	Treatment with mineral fertilizers
D1	15 t/ha of SDS
D1+F	15 t/ha of SDS + F
D2	30 t/ha of SDS
D2+F	30 t/ha of SDS + F

water drainage. Ten wheat seeds were sown in each pot. As for faba bean, two seeds were rinsed using deionized water and germinated in the dark on moist filter paper for 48 h at 24 C prior to sowing. Irrigation was regularly carried out to maintain approximately 60% water holding capacity (Foster, 1995) during the whole cycle of faba bean and during the four first months for wheat.

2.4 Plant parameter measurements

2.4.1 Emergence percentage

The germinated seeds were counted after 2 weeks to calculate the emergence percentage (GP), as follows:

$$GP = \left(\frac{Number\ of\ germinated\ seeds}{total\ number\ of\ planted\ seeds}\right) x\ 100. \quad (1)$$

2.4.2 Chlorophyll content index

Chlorophyll is highly involved in photosynthesis, the process by which the plant makes carbohydrates. Photosynthesis is reported to be one of the most sensitive plant physiological processes, and it is known to be vulnerable to metallic stress. Hence, CCI values may be an indicator in case sludge induces phytotoxicity in the present experiments. Starting from 2 months after sowing, the CCI was measured in the vegetative stage, from the middle part of the five youngest leaves (n = 20) by using a CCM-300 chlorophyll meter (Hansatech instruments).

2.4.3 Yield and its components

At harvest, in each pot (n = 4), the total biomass yield, straw yield, grain yield, and thousand seed weight were determined for wheat. The harvest index (HI) was calculated as the ratio of grain yield over total above-ground biomass.

$$Harvest\ Index\ (HI) = \left(\frac{Grain\ yield}{Total\ biomass}\right) x\ 100. \quad (2)$$

As for faba bean, the total biomass yield and grain yield were determined in each pot (n = 4).

2.5 Heavy metal analysis in plants

At the end of the growing cycle (5 months after sowing), the plants were harvested, threshed, and separated into straw roots and seeds. Roots were thoroughly rinsed with tap water followed by deionized water. Afterward, shoots and roots were dried at 40°C for 2 days until they reach a constant weight. For HM analysis in shoots and roots, samples (0.5 g) were mixed with 8 mL of HNO_3 and 2 mL of H_2O_2 and placed in a hot plate at 100 °C until total evaporation of the extracting solvents. The mineralized material was recovered by the addition of ultrapure water and filtered with an ashless filter. The volume was adjusted to 25 mL with ultrapure water and acidified with 2% HNO_3. The concentrations of metals in shoots and roots were determined by using the ICP-OES spectrophotometer from Agilent Technologies.

2.6 Bioconcentration factor and translocation index

The bioconcentration factor (BCF) represents the quotient of the concentration in plants and the concentration in soil of a given metal (Karami et al., 2009).

$$BCF = \left(\frac{C\ tissue}{C\ soil}\right), \quad (3)$$

where C_{tissue} represents metal concentrations in the tissues of the plant (either above-ground or underground organs) and C_{soil} represents metal concentrations in soil (Ali et al., 2013). The metal concentrations in the extracts of the soil and plants were calculated based on dry weight.

2.6.1 Translocation index

$$TI = \left(\frac{C\ shoots}{C\ roots}\right) x\ 100, \quad (4)$$

where C_{shoots} represents metal concentrations in the tissues of organs above-ground plant (mg/Kg) and C_{roots} represents metal concentrations in the tissues of the plant roots (mg/Kg) (Marchiol et al., 2004).

2.7 Statistical analysis

Soil physicochemical properties, yield components, HM concentrations in different plant organs, and the BCF and TI were used as variables to test the effects of sludge and/or fertilizer application on wheat and faba bean. The impact of different treatments on the studied variables was analyzed using the one-way analysis of variance (ANOVA) using SPSS 20 software. When the ANOVA null hypothesis was rejected, Tukey's test at $p < 0.05$ was performed to determine significant differences among means.

3 Results and discussion

3.1 Physiological assessment of plant growth

3.1.1 Wheat emergence percentage

The emergence percentage of wheat is shown in Figure 1; an average of 90% was recorded. No significant difference was observed between different treatments. This is likely due to the fact that this

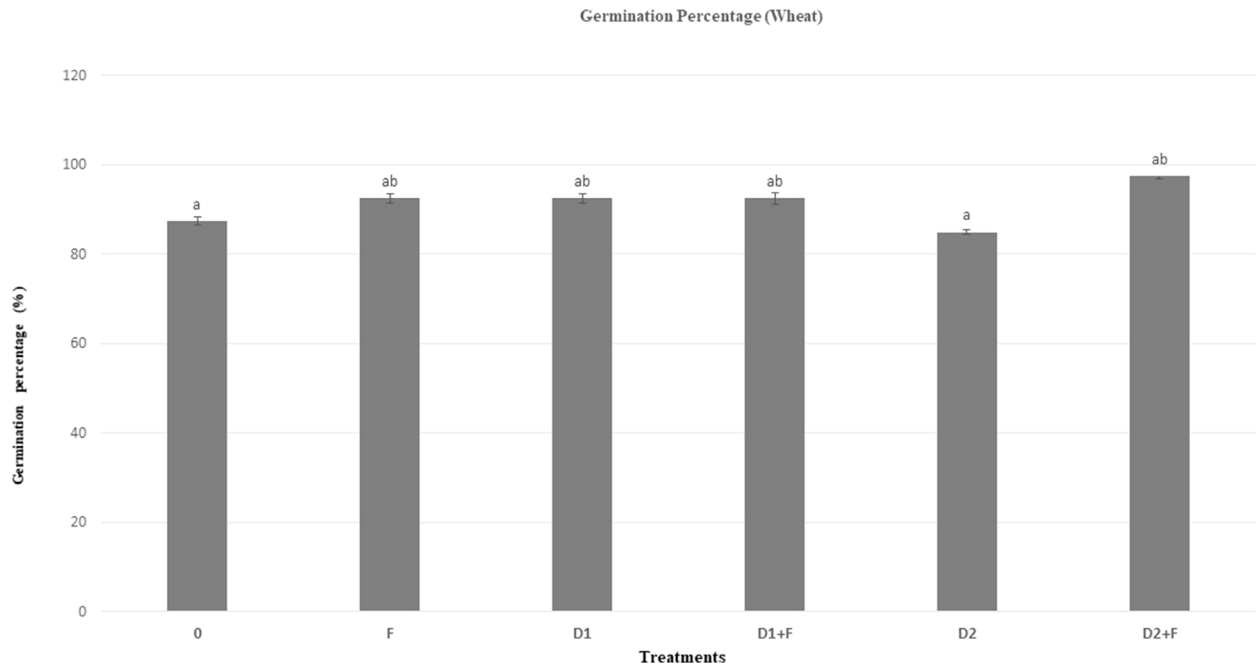

FIGURE 1
Emergence percentage of wheat. Results are the mean of four replicates. Bars represent standard errors (n = 4). Means with the same letter are not significantly different at ($p < 0.05$).

stage of plant growth, including germination and emergence, does not require nutrients and organic matter existing initially in the soil and provided by SDS and fertilization. In fact, seed germination is known to be vulnerable to metal phytotoxicity (Amin et al., 2013) and high salt concentration in case of high fertilizer application (especially the one containing nitrogen). The current results indicate that SDS incorporation into the soil did not induce any phytotoxicity in seeds during the germination stage. Despite its high content in the incorporated sludge (3008.23 mg/kg), chromium had no effect on the germination process.

3.1.2 Chlorophyll content index

Chlorophyll content showed a significant difference between different treatments for wheat (Figure 2A). The application of SDS separately or in combination with fertilizers significantly increased wheat's CCI when compared to the control and applied fertilizers alone (F). However, there was no significant difference between SDS treatments and the control and mineral-fertilized soils (Figure 2A). Our data are in agreement with Pascual et al. (2008), who found increased photosynthesis in pepper plants amended with digested sewage sludge compared to the control plants. This may be due to the nitrogen input, which was higher in SDS than the mineral fertilizer since chlorophyll content is approximately proportional to leaf nitrogen content (Evans, 1983; Bojovi and Markovi, 2009). In fact, the equivalent of 4% nitrogen rate in SDS in the two used rates (15 t/ha and 30 t/ha) exceeded the amount of nitrogen provided by the mineral fertilizer (50 kg/ha).

In the case of faba bean, there was no significant difference between all the treatments involving both mineral fertilizers and organic amendments (Figure 2B). Compared to wheat, faba bean presented an important value of CCI even for the control. The difference between wheat and faba bean in terms of the CCI pattern is likely due to the physiological difference between the two species. Indeed, due to its biological nitrogen fixation capacity, faba bean, like other food legumes, can fix the atmospheric nitrogen and convert it into ammonia that can be used for its growth (Fan et al., 2006).

Chlorophyll content in plants is among the symptoms related to heavy metal phytotoxicity. Several authors attributed chlorosis to a high concentration of Cr in soil (Amin et al., 2013; Mahdi, 2015). In the present context, considering the CCI increase due to SDS use as an organic amendment, it can be concluded that SDS did not induce phytotoxicity in both faba bean and wheat. This leads to the assumption that either the included metals in SDS were not available in plants or the applied rates were probably not high enough to induce phytotoxicity.

3.2 Yield assessment

The chemical composition of the sewage sludge used in the experiments (shown in Table 1) indicates that this material is an important source of organic matter and nutrients for agricultural soils, which justified its use as a fertilizer (Figure 3). Harvest index, biomass, straw, and grain yields were calculated for wheat in order to assess the agronomic added value of the applied SDS. The application of sewage sludge had significantly increased the total biomass production proportionally to the rate of sludge (160 qx/ha) instead of almost 50 qx/ha recorded in the control. As for straw, the recorded yield increased very significantly when SDS rate increased. 80 qx/ha was measured for the 30 t/ha applied sewage sludge compared to 60 qx/ha linked to the 15 t/ha of applied sludge and 40 qx/ha for the control. Furthermore, the co-application of chemical fertilizers and SDS at a rate of 15 t/a resulted

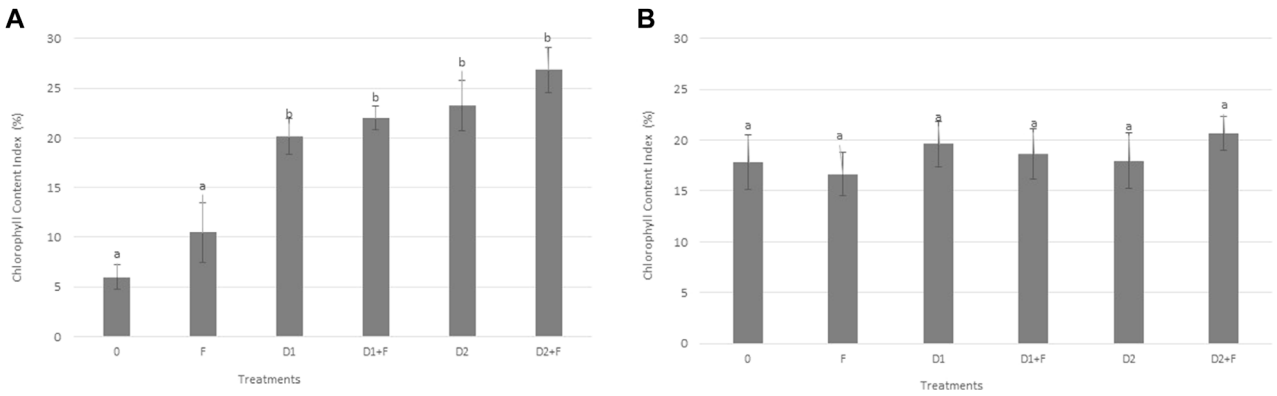

FIGURE 2
Chlorophyll content index measured in plants under different treatments: **(A)** wheat and **(B)** faba bean. Means with the same letters are not significantly different at $p = 0.05$.

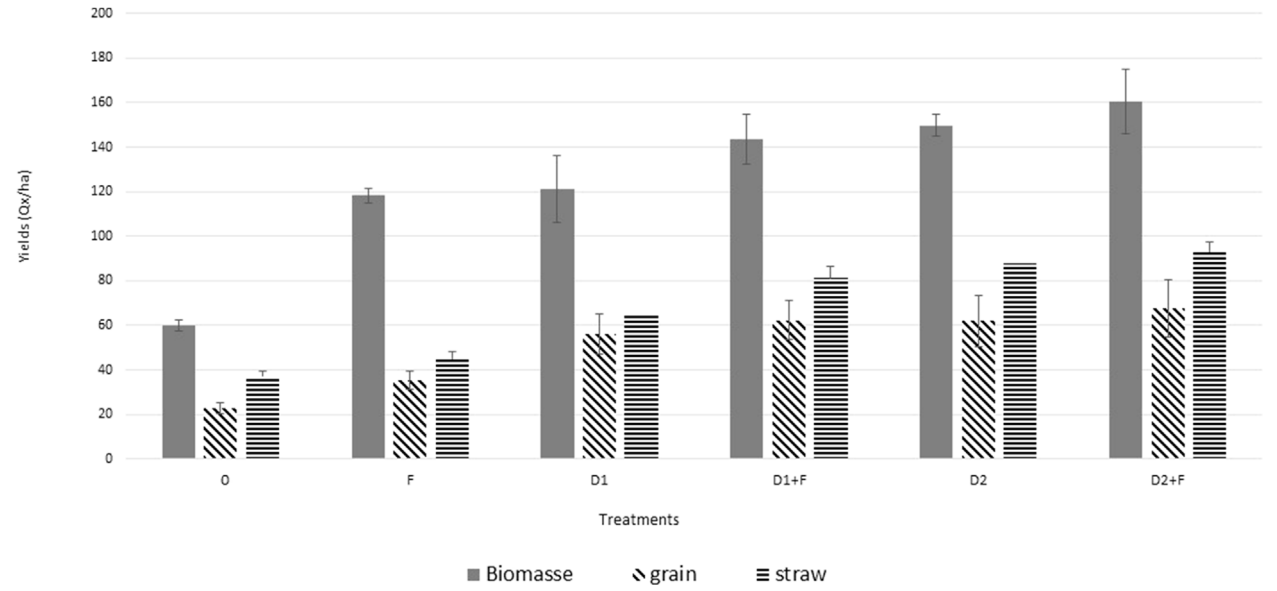

FIGURE 3
Biomass yield (qx/ha), straw yield (qx/ha) and grain yield. Results are mean of 4 replicates. Bars represent standard errors ($n = 4$).

in an important increase of both biomass and straw yields (Figure 3). However, no significant difference between the combined application of SDS and fertilizers and the single use of SDS was observed, especially when the application rate was high (30 t/ha). This leads to conclude that SDS application with an important rate may satisfy the needs of the plants in terms of nutrients. Hence, applying SDS on agricultural soils may contribute to limit the overuse of mineral fertilizers and then reduce their related cost and potential negative impacts on the environment.

The two rates of SDS and F enhanced the harvest index but without being significantly different from the control (Figure 4). The 1000 grain weight was not significantly affected by SDS, F, and their combination (Figure 4B). These outcomes helped understand that the applied treatments did not affect the yield quality.

The total biomass production and grain yield of faba bean are shown in Figure 5. Biomass yields were enhanced with the use of SDS as an organic amendment (Figure 5A). However, increasing the SDS application rate did not induce a significant effect on the biomass yield. The co-application of 30 t/ha SDS and mineral fertilizers provided the most important biomass yield with a significant difference when compared to other treatments. The single use of mineral fertilizers, when compared to the control, did not affect the biomass, but it significantly increased the grain yield over the control (Figure 5B). The co-application of 30 t/ha SDS with mineral fertilizers allowed an important grain yield (equivalent to 21.65 qx/ha).

Overall, sewage sludge application on agricultural soil increases crop production due to its high nutrient content, as demonstrated

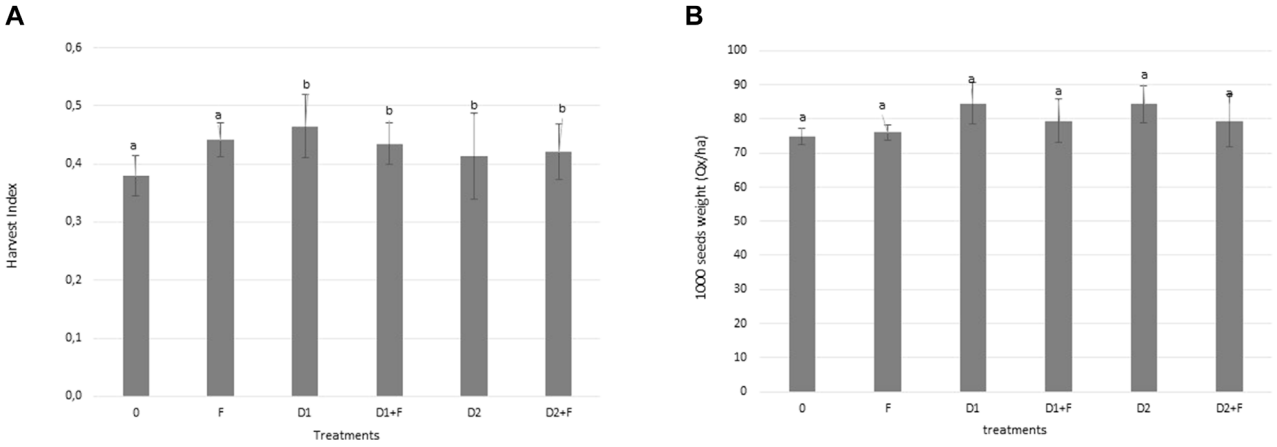

FIGURE 4
Harvest index evolution accordingly in the conduced treatments. Results are means of four replicates. Bars represent standard errors (n = 4). Letters indicate significant differences between treatments ($p < 0.05$).

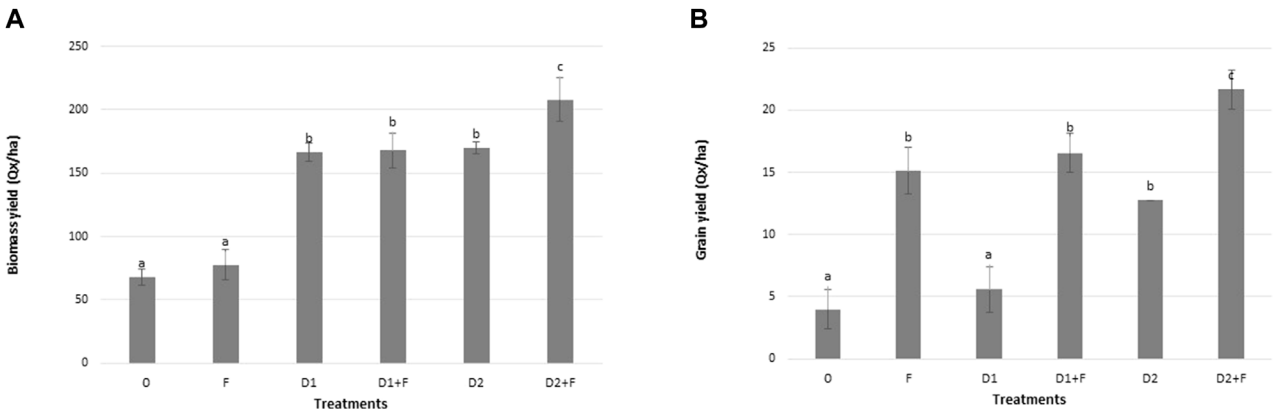

FIGURE 5
(A) Biomass yielld and **(B)** grain yields for faba beans in the different conducted treatments. Results are means of four replicates. Bars represent standard errors (n = 4). Means with the same letters are not significantly different at $p < 0.05$.

previously by several investigations (Latare et al., 2014; Samara et al., 2017; Eid et al., 2019). The present study showed that there is a trend of production increase while increasing the rates of sludge and demonstrated that an important rate of sludge without the addition of mineral fertilizers can support plant growth and development, which may reduce fertilizer applications to soil. However, the impact on soil properties, mainly the HM content, must be controlled according to the existing guidelines.

3.3 Soil physicochemical properties after harvest

The SDS application as an organic amendment increased the EC of the soil. Furthermore, after faba beans are harvested in the 30 t/ha amended pots, it reached 1.20 ms/cm compared to 0.87 ms/cm in the control. After wheat harvesting, the 30 t/ha of the applied SDS increased the EC up to 0.95 ms/cm against 0.53 ms/cm in the control (Table 3). Such observations may be explained by the high salt load brought by SDS to soil. Our findings are in accordance with Epstein E (1975), Chopra et al., and Samara et al. (2017), who reported increasing soil salinity while incorporating SDS as an organic amendment. However, it is worth emphasizing that the measured EC within the 30 t/ha amended soil reached neither the critical limit for sensitive field crops (2 mS/cm) nor the limit detrimental for most field crops (4 mS/cm) (Brady and Weil, 2008).

In our investigation, soil OM increased with the rate of SDS addition, achieving its highest value with the maximum dose (30 t/ha). After faba bean harvesting, OM reached 4.04% instead of 1.8% in the control. After wheat harvesting, soil OM reached 3.28%

TABLE 3 Physicochemical characteristics of the post harvested soil and heavy metals accumulation after solar-dried sludge application. Values are means of four replicates. Letters indicate significant differences between treatments ($p < 0.05$).

Soil	Sludge dose (T/HA)	pH	Electrical conductivity (MS/CM)	Organic matter (%)	Manganese (mg/kg)	Iron (mg/kg)	Cations exchange capacity (CEC)	Chromium (CR) (mg/kg)	Cooper (CU) (mg/kg)	Nickel (NI) (mg/kg)	Lead (PB) (mg/kg)
Post-harvest soil (faba bean)	0	8.73^{ab}	0.87^{ab}	1.84^{ab}	6.87	3.5525^{a}	14.15^{a}	26.47^{a}	13.38^{ab}	20.62^{a}	16.25^{a}
	15	8.6^{ab}	0.94^{ab}	3.09^{cde}	6.95	6.94^{abcd}	12.35^{a}	76.04^{b}	16.51^{ab}	20.31^{a}	16.70^{a}
	30	8.34^{a}	1.20^{b}	4.04^{e}	7.43	10.81^{cd}	15.58^{a}	141.04^{c}	19.84^{b}	20.65^{a}	17.86^{a}
Post-harvest soil (wheat)	0	8.97^{b}	0.53^{ab}	1.29^{a}	4.73	4.6325^{ab}	14.55^{a}	26.50^{a}	12.21^{a}	20.28^{a}	14.39^{a}
	15	8.70^{ab}	0.82^{ab}	2.14^{bc}	5.90	9.95^{bcd}	16.75^{a}	76.18^{b}	15.87^{ab}	21.29^{a}	30.68^{a}
	30	8.54^{ab}	0.95^{ab}	3.28^{de}	6.83	12.75^{d}	17.38^{a}	91.88^{b}	16.21^{ab}	21.40^{a}	17.59^{a}

compared to 1.29% in the control. These findings support the existing literature, which previously reported increases of soil organic matter upon addition of sewage sludge (Samaras et al., 2008; Heras et al., 2009; Carbonell et al., 2011; Rafael et al., 2011). These observations in terms of OM elevation due to SDS is for a significant relevance, especially in arid and semi-arid countries, such as Morocco, where soils are poor in OM. Regarding soil pH, a slight decrease was observed in the SDS-amended pots and the control for both crops. After faba beans were harvested in the 30 t/ha amended pots, pH reached 8.97 compared to 8.54 in the control. After wheat harvesting, pH is 8.54 in soil subjected to 30 t/ha of SDS compared to 8.73 to in the control (Table 3). Throughout the literature, some studies reported that sewage sludge incorporation into soil leads to an increase in soil pH. For instance, Samara et al. (2017) reported a significant increase in pH while incorporating limed sewage sludge (pH = 10). Others highlighted a decrease in pH while involving sewage sludge as an organic amendment. In fact, pH depends on the initial soils' pH, the buffering capacity of the soil, and the pH of the used sewage sludge (Garrido et al., 2005; Fawy et al., 2018). In the current study, soil pH was almost two units higher than SDS's pH. Hence, we can assume that the slight decrease in soil pH after SDS application is due to its buffering capacity. Moreover, these observations may also be attributed to the mineralization of organic nitrogen added by SDS, which produces protons by the nitrification process (Eid et al., 2019). As for nutrient content, they increased with the increasing rates of the applied SDS in soil under faba bean and wheat crops. Concentrations of HMs such as Cr, Cu, Pb, and Ni increased due to SDS application (Table 3). Particularly, a significant level or content of Cr resulted from SDS application for faba beans (141 mg/kg) and wheat (92 mg/kg) when compared to the negative control under faba beans and the one under wheat (25.47 mg/kg and 26.50 m/kg, respectively). However, the accumulated HMs (Cr, Ni, Pb, and Cu) in soil remain under the maximum permissible values (Supplementary Table S3) set by the commission of the European Communities directive (commission of the European Communities 1986).

3.4 Transfer of heavy metals from solar-dried sludge-amended soil to faba bean and wheat

Figure 6 shows the concentrations of Cr, Ni, Pb, and Cu in shoots and roots of wheat according to the conducted treatments. It can be observed that excluding Cu, the concentration of these metals were under the quantification limit in wheat's shoots. However, high values were recorded in roots which seemed to be in accordance with Karami et al. (2009) and Mazen et al. (2010), who concluded that metals accumulated mostly in roots rather than in other wheat tissues. Figure 6A shows the concentrations of Cr that are markedly higher in roots than shoots. The concentration of Cr in roots increased significantly when sludge rate increased (91.45 mg/kg and 14.28 mg/kg at 30 t/ha and 15 t/ha applied SDS, respectively). In addition, the combination of SDS and mineral fertilizers resulted in a significant increase of Cr uptake by roots (146 mg/kg against 59.74 mg/kg in the D2+F and D1+F treatments, respectively).

Ni showed the same pattern within the used treatments; an increase in root concentration was recorded when the SDS rate increased (5.7 mg/kg and 3.37 mg/kg when SDS was applied at 15 t/ha and 30 t/ha, respectively). The combined application of SDS and mineral fertilizers increased Ni concentration from 4.76 to 7.21 mg/kg. Figure 6C shows a slight increase in Pb root concentrations when the SDS rate increased (2.01 mg/kg against 3.66 mg/kg). Contrary to the previously reported metals, copper content in shoots was high enough to be quantified through plant analysis. However, shoot concentrations remained very low when compared to those of roots (3.41 mg/kg in shoots against 35.45 mg/kg in roots within the D2+F treatment). Figure 6D shows that Cu concentration increased in both shoots and roots when the SDS rate increased. Additionally, a significant increase in Cu concentration in roots was recorded while involving mineral fertilizers with the 30 t/ha of SDS.

Contrary to wheat, Figure 7 shows that Cr, Cu, and Ni have been quantified in faba bean's shoots although their concentrations remain less important than those measured in roots. Lead was not quantified in faba bean's shoots, but an important concentration was recorded in roots (Figure 7C). The concentrations of Cr, Cu, and Ni in roots increased with the increase in SDS rates. Moreover, a significant difference was observed between the single application of SDS and its co-application with mineral fertilizers in terms of HM concentration in faba bean roots. Copper concentration in roots also showed a very significant difference among the applied treatment. An average concentration of 45 mg/kg was measured when 30 t/ha of SDS and mineral fertilizers were applied together (Figure 7D).

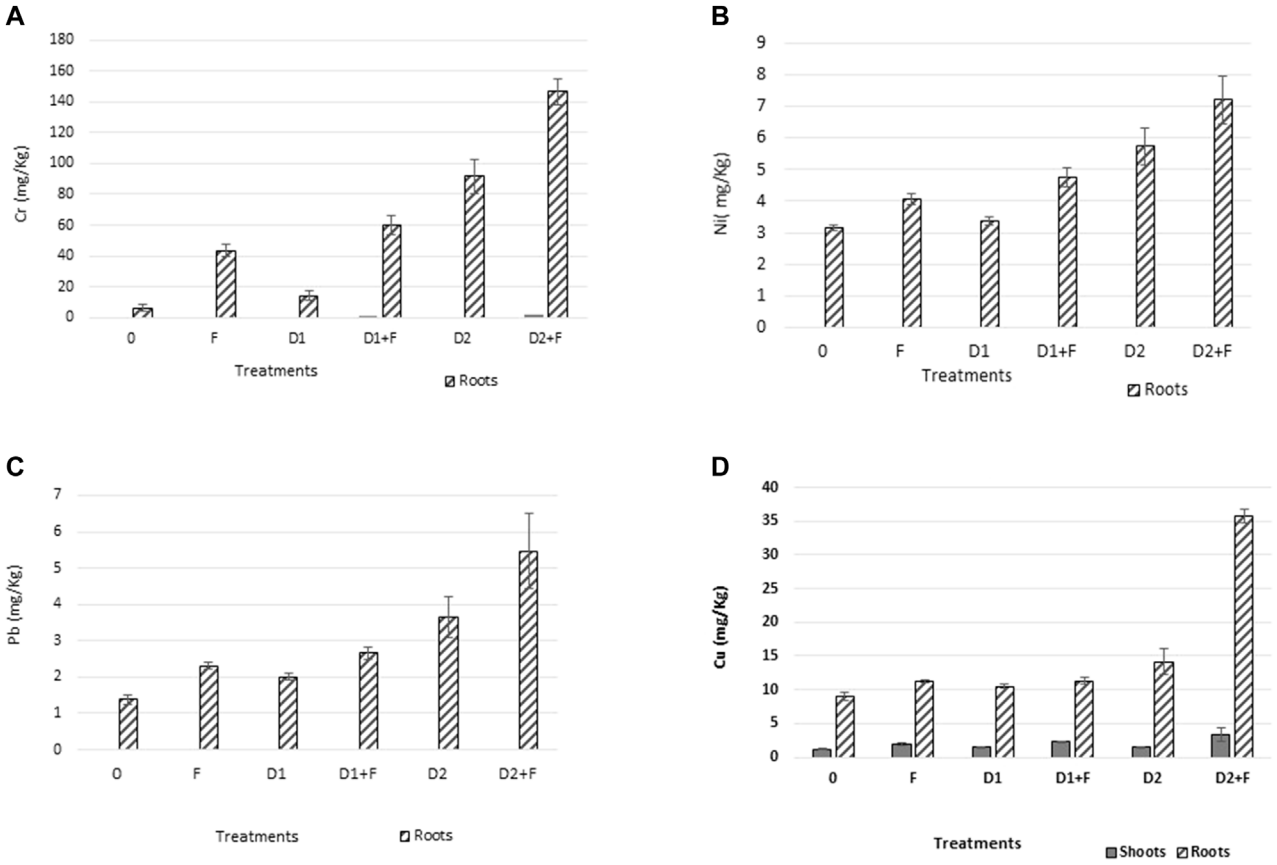

FIGURE 6
Concentration of metals in shoots and roots of wheat in the different conducted treatments: **(A)** Cr, **(B)** Ni, **(C)** Pb, and **(D)** Cu. Results are means of four replicates. Bars represent standard errors (n = 4).

From the aforementioned results, it can be assumed that the increase of metal contents, mainly in roots when the SDS rate increased, is likely due to the additional concentrations of these metals brought to the soil by SDS, as demonstrated previously by several authors (Bose and Bhattacharyya, 2008; Soriano-disla and Gómez, 2014; Eid et al., 2019). Moreover, this may be a consequence of an interesting root development enhanced by the nutrient input of the applied SDS as an organic fertilizer.

3.5 Bioaccumulation and phytoextraction assessment of heavy metals by wheat and faba bean

3.5.1 Bioaccumulation of metals assessed by the bioconcentration factor

The previously presented data emphasized that the roots exhibited markedly elevated heavy metal concentrations compared to the above-ground plant components. In order to assess more accurately the HM uptake by roots, bioaccumulation is a commonly involved concept. Bioaccumulation defines the ability of the plant tissue to accumulate HMs, while allowing for their initial substrate content (Pachura et al., 2015). In other words, the higher the content of metal is in soil, the higher the concentration of the element is observed in plant tissues. As a basis for HM's bioaccumulation assessment, the BCF is commonly used (Guo-hang et al., 2018; Eid et al., 2021). The four-degree scale described by Michałowski and Gołas (2001) and Pachura et al. (2015) was adopted. If the BCF >1, the plants have accumulated elements, and the ratios around 1 indicate that the plants are not influenced by the elements, and a BCF <1 shows that plants exclude the elements from the uptake (Soriano-disla and Gómez, 2014; Agic et al., 2015). If the plants have higher BCF values, they can be used for soil remediation.

The previously described results compare well with BCF values, as shown in Table 4. BCF shoots for wheat in all the conducted treatments helped understand that the above-ground part of wheat does not accumulate metals. However, in the case of faba beans, in the non-amended trial (absence of SDS), BCF shoots also meant that faba beans did not accumulate metals in the shoots. However, BCF values showed medium bioaccumulation of Cu in shoots but a high bioaccumulation of that metal in roots for both wheat and faba beans. When SDS is applied at 30 t/ha, a high bioaccumulation of Cr in roots was observed. As for Pb, medium bioaccumulation in roots was recorded for both wheat and faba beans. A significant difference in terms of the bioaccumulation of the studied HMs in roots was

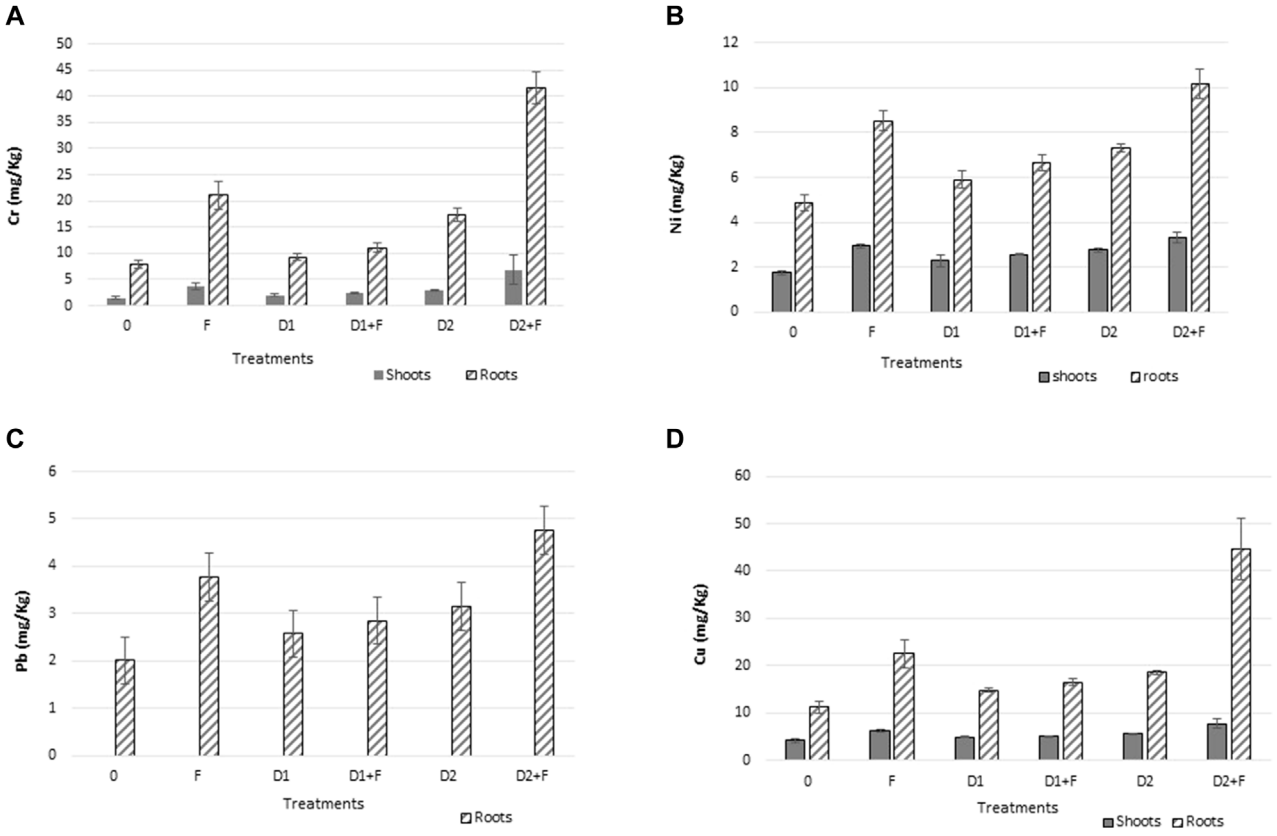

FIGURE 7
Concentration of metals in shoots and roots of faba beans in the different conducted treatments: **(A)** Cr, **(B)** Ni, **(C)** Pb, and **(D)** Cu. Results are means of four replicates. Bars represent standard errors (n = 4). Letters indicate significant differences between treatments ($p < 0.05$).

observed between the single use of SDS and the combined treatment involving SDS and mineral fertilizers.

The current data demonstrated that the assayed HMs were in a higher concentration within the root system than in the above-ground plant components (shoots). This compared well with the literature as the root system has been demonstrated to be the principal site of accumulation of HMs because of their high binding affinity in this type of tissue (Karamooz et al., 2016). Roots behave as a filter with respect to the uptake of HMs, acting, thus, as an obstruction to their absorption or decelerating their passage to shoots (Ahmed et al., 2018; Eid et al., 2021). Moreover, the plants have a range of processes that enables them to deal with the presence of HMs in the substrate. For instance, binding the metals to the root cells and/or sequestering them in vacuoles are among the tools by which the active regions of the cells are kept away from HMs (Zhou et al., 2015).

The metal concentration in roots is known to be highly related to the metal speciation in the soil solution (Yang et al., 2019). Prior to this study, we have assessed HM speciation in SDS. We have demonstrated, through a BCR scheme, a low mobility of the studied HMs (Cr, Ni, Pb, and Cu) since the residual fraction was found to be predominant compared to the exchangeable, reducible, and oxidizable ones (An-nori et al., 2020a). Although the recorded results in the present study regarding BCF roots seemed to be in accordance with the speciation results, it may be more rational to investigate HM speciation in the soil solution, after the incorporation of SDS, to explain the mechanisms behind the bioaccumulation of HMs in the root system.

3.5.2 Phytoextraction of metals assessed by the translocation index

The translocation index (TI) is a measure of the phytoextraction capacity of plants. It indicates the efficiency of the internal translocation of HMs from the root system to the stems, leaves, and fruits (Marchiol et al., 2004). This transfer is governed by a number of factors but mostly by the plant, its physiology, and its water transport system (Kalis et al., 2008). By analyzing the values of the TI for both faba beans and wheat (Table 5), Cu was most importantly translocated into shoots among the studied metals. Moreover, the translocation of Cu was more important in faba beans compared to wheat. As for Cr and Ni, they were not translocated into wheat shoots within the conducted treatments. Pb was excluded from translocation in both wheat and faba beans. This means that the mobility of lead in the root-above-ground part system is very low, as demonstrated previously by Pachura et al. (2015). The translocation index of Cr increased proportionally to the

TABLE 4 Bioconcentration factor for roots and shoots in wheat and faba beans under the different treatments. Values are means of four replicates. Letters indicate significant differences between treatments ($p < 0.05$).

Plant	Dose of sludge (t/ha)	BCF shoots				BCF roots			
		Cr	Ni	Pb	Cu	Cr	Ni	Pb	Cu
Wheat	0	0	0	0	0,10^{a}	0,24^{a}	0,16^{a}	0,10^{a}	0,74^{a}
	D1	0	0	0	0,09^{a}	0,19^{a}	0,16^{a}	0,10^{a}	0,68^{a}
	D2	0	0	0	0,09^{a}	0,89^{b}	0,28^{c}	0,22^{b}	0,85^{ab}
	F	0	0	0	0,16^{b}	1,65^{c}	0,20^{ab}	0,15^{ab}	0,92^{ab}
	D1+F	0	0	0	0,15^{b}	0,77^{b}	0,23^{bc}	0,15^{ab}	0,74^{a}
	D2+F	0	0	0	0,26^{c}	1,05^{b}	0,36^{d}	0,32^{c}	0,94^{b}
Faba bean	0	0,02^{a}	0,13^{a}	0	0,27^{a}	0,18^{a}	0,37^{a}	0,10^{a}	0,71^{a}
	D1	0,03^{a}	0,14^{a}	0	0,30^{a}	0,13^{a}	0,36^{a}	0,12^{a}	0,90^{a}
	D2	0,03^{a}	0,13^{a}	0	0,31^{ab}	0,16^{a}	0,37^{a}	0,15^{b}	1,04^{ab}
	F	0,16^{b}	0,22^{b}	0	0,40^{b}	0,18^{a}	0,64^{b}	0,18^{bc}	1,48^{b}
	D1+F	0,02^{a}	0,15^{a}	0	0,31^{ab}	0,38^{b}	0,39^{a}	0,14^{ab}	0,98a^{b}
	D2+F	0,12^{b}	0,17^{a}	0	0,35^{ab}	0,33^{b}	0,52^{b}	0,23^{c}	2,04^{b}

TABLE 5 Translocation index in wheat and faba beans under the different treatments. Values are mean of four replicates. Letters indicate significant differences between treatments ($p < 0.05$).

Plant	Dose of sludge (t/ha)	TI (%)			
		Cr	Ni	Pb	Cu
Wheat	0	0	0	0	12,95^{a}
	D1	0	0	0	13,62^{ab}
	D2	0	0	0	11,21^{a}
	F	0	0	0	16,97^{ab}
	D1+F	0	0	0	20,34^{bc}
	D2+F	0	0	0	24,00^{c}
Faba bean	0	11,195^{a}	36,346^{bc}	0	38,20^{b}
	D1	27,145^{ab}	38,63^{c}	0	33,47^{ab}
	D2	17,596^{a}	37,699^{c}	0	30,24^{ab}
	F	19,927^{ab}	34,49^{ab}	0	27,63^{a}
	D1+F	22,95^{ab}	38,421^{c}	0	31,35^{ab}
	D2+F	39,31^{b}	32,64^{a}	0	29,45^{a}

increasing rate of SDS (30 t/ha). The significant increase in the TI when mineral fertilizers were used (20% instead of 10% in non-amended pots and 40% instead of 19% in the amended ones) helped understand that the use of mineral fertilizers increased the translocation values of Cr in the root-above-ground part system of both wheat and faba beans. This is likely due to the root-above-ground part system development, which was enhanced when SDS and mineral fertilized were co-applied to soil. Overall, despite being enhanced by the co-application of SDS amendment and the mineral fertilizers, the recorded values of the TI for both wheat and faba beans in all the conducted treatments remain far less than 100%.

Knowing that the phytoextraction is likely to be related to the plant physiology, it can be assumed from the aforementioned data that faba bean involves phytoextraction mechanisms more than wheat. Since the translocated metal into shoots (the edible part) is most likely to cause health issues, it can also be concluded that wheat may be more suitable to be grown in an SDS-amended soil.

4 Conclusion

The present study markedly reveals the important added value of SDS in terms of agronomic yields of both faba beans and wheat. The crop production increased with the increasing rates of SDS. The use of SDS as an organic amendment showed competitive results in terms of biomass and grain yields compared to the single use of mineral fertilizers. The chlorophyll and germination percentage assessments did not indicate any phytotoxicity associated to SDS. Regarding soil properties, the use of SDS as an organic amendment enhanced soil organic matter, slightly decreased pH, and increased electrical conductivity. The contents of Ni, Cu, and Pb were not significantly affected by the application of SDS as an organic amendment. Only Cr showed increased concentrations in soil proportionally to the increasing rates of SDS, but the recorded concentrations remained under the limits set by the U.S. Environmental Protection Agency. The bioaccumulation of the studied HMs assessed by the BCF showed higher values in roots compared to shoots. When SDS is applied at 30 t/ha, it resulted in medium bioaccumulation of Cr in roots in both wheat and faba beans. When 30 t/ha of SDS was co-applied with mineral fertilizers, high bioaccumulation of Cr was observed. The phytoextraction assessment showed that wheat excluded Cr, Ni, and Pb from the translocation and

only Cu was found to be translocated into the above-ground part. On the contrary, faba beans translocated HMs to the above-ground part except Pb. All the translocation index values were far less than 100%. Neither SDS rates nor mineral fertilizers affected the translocation index values for both faba beans and wheat. Furthermore, this may be recommended more in the present context as the edible part did not include HMs. On the basis of the present study, it appeared that the risk associated to SDS regarding HM uptake by wheat and faba bean tissues can be considered less significant than its agronomic value and its positive effects on soil fertility. Therefore, it is recommended in the present context to use SDS at 30 t/ha as the best scenario to amend the soil and provide nutrients to plants. As a perspective to this study, a long-term field monitoring must be engaged in order to assess the long-term effect of SDS application on soil quality and the related implications on the environment.

Data availability statement

The original contributions presented in the study are included in the article/Supplementary Material, further inquiries can be directed to the corresponding author.

Author contributions

Conceptualization was completed by AA-n and MH. Methodology was created by AA-n. Software and research activities were handled by AA-n. Original draft preparation was handled by AA-n, while writing—corrections and editing were completed by KE, LE, DT, AE, ME, and MH and supervision was conducted by MH.

Funding

This study was financially supported by the Sustainability Platform (OCP Group), as part of the AS146 "*Physicochemical and microbiological characterization of sewage sludge for agricultural recycling.*" The funder was not involved in the study design, collection, analysis, interpretation of data, the writing of this article, or the decision to submit it for publication.

Acknowledgments

The authors would like to thank Mohammed VI Polytechnic University (UM6P) and the OCP group for their technical and financial support. They would also like to thank the experimental farm and the laboratory teams of the Agricultural Innovation and Technology Transfer Center (AITTC).

Conflict of interest

The authors declare that the research was conducted in the absence of any commercial or financial relationships that could be construed as a potential conflict of interest.

Publisher's note

All claims expressed in this article are solely those of the authors and do not necessarily represent those of their affiliated organizations, or those of the publisher, the editors, and the reviewers. Any product that may be evaluated in this article, or claim that may be made by its manufacturer, is not guaranteed or endorsed by the publisher.

Supplementary material

The Supplementary Material for this article can be found online at: https://www.frontiersin.org/articles/10.3389/fenvs.2023.1163422/full#supplementary-material

References

Agic, R., Milenkovic, L., and Ilic, Z. S. (2015). Transfer factor as indicator of heavy metals content in plants. *Fresenius Environ. Bull.* 24 (11), 4212–4219.

Ahmed, D. A., Slima, D. F., and Ahmed, D. A. (2018). *Heavy metal accumulation by Corchorus olitorius L. irrigated with wastewater 14996–15005.*

Albaladejo, J., Ortiz, R., Garcia-franco, N., Pintado, J. G., and Martínez-mena, M. (2013). Land use and climate change impacts on soil organic carbon stocks in semi-arid Spain. *J. Soils Sediments* 13, 265–277. doi:10.1007/s11368-012-0617-7

Amin, H., Arain, B. A., Amin, F., and Surhio, M. A. (2013). Phytotoxicity of chromium on germination, growth and biochemical attributes of Hibiscus esculentus L. *Am. J. Plant Sci.* 4, 2431–2439. doi:10.4236/ajps.2013.412302

An-nori, A., El Fels, L., Ezzariai, A., El Gharous, M., El Mejahed, K., and Hafidi, M. (2020a). Effects of solar drying on heavy metals availability and phytotoxicity in municipal sewage sludge under semi-arid climate. *Environ. Technol. Innov.* 19, 101039. doi:10.1016/j.eti.2020.101039

An-Nori, A., El Fels, L., Ezzariai, A., El Gharous, M., El Mejahed, K., Hafidi, M., et al. (2021). Effectiveness of helminth egg reduction by solar drying and liming of sewage sludge. *Environ. Sci. Pollut. Res.* 28, 14080–14091. doi:10.1007/s11356-020-11619-w

An-Nori, A., El Fels, L., EzzariaiEl Gharous, A. M., El Mejahed, K., and Hafidi, M. (2022). Solar drying as an eco-friendly Technology for sewage sludge stabilization: Assessment of micropollutant behavior, pathogen removal, and agronomic value. *Front. Environ. Sci.* 10. doi:10.3389/fenvs.2022.814590

Brady, N. C., and Weil, R. R. (2008). *The nature and properties of soil.* 14 ed. Upper Saddle River, NJ: Prentice-Hall.

Bojovi, B., and Markovi, A. (2009). Correlation between nitrogen and chlorophyll content in wheat (triticum aestivum l). 31, 69–74.

Bose, S., and Bhattacharyya, A. K. (2008). Heavy metal accumulation in wheat plant grown in soil amended with industrial sludge. *Chemosphere* 70, 1264–1272. doi:10.1016/j.chemosphere.2007.07.062

Carbonell, G., Miralles, R., Imperial, D., Torrijos, M., Delgado, M., and Antonio, J. (2011). Effects of municipal solid waste compost and mineral fertilizer amendments on soil properties and heavy metals distribution in maize plants (Zea mays L). *Chemosphere* 85, 1614–1623. doi:10.1016/j.chemosphere.2011.08.025

Chaignon, V., Sanchez-Neira, I., Herrmann, P., Jaillard, B., and Hinsinger, P. (2003). Copper bioavailability and extractability as related to chemical properties of contaminated soils from a vine-growing area. *Environ. Pollut.* 123, 229–238. doi:10.1016/s0269-7491(02)00374-3

Chimie, R. R. De (2014). Translocation of heavy metals from sewage sludge amended. *SOIL PLANT* 59, 81–89.

Chopra, V. K. A. K. (2014). Accumulation and translocation of metals in soil and different parts of French bean (Phaseolus vulgaris L.) amended with sewage sludge. *Amend. Sew. Sludge* 92, 103–108. doi:10.1007/s00128-013-1142-0

Eid, E. M., Alrumman, S. A., El-bebany, A. F., Fawy, K. F., Taher, M. A., Hesham, A. E., et al. (2019). Evaluation of the potential of sewage sludge as a valuable

fertilizer for wheat (*Triticum aestivum* L.) crops. *Environ. Sci. Pollut. Res.* 26, 392–401.

Eid, E. M., Shaltout, K. H., Alamri, S. A. M., Alrumman, S. A., Hussain, A. A., Sewelam, N., et al. (2021). Prediction models based on soil properties for evaluating the uptake of eight heavy metals by tomato plant (Lycopersicon esculentum Mill.) grown in agricultural soils amended with sewage sludge. *J. Environ. Chem. Eng.* 9, 105977. doi:10.1016/j.jece.2021.105977

Evans, J. R. (1983). Nitrogen and photosynthesis in the flag leaf of wheat (*Triticum aestivum* L.) *Plant Physiol.* 72, 297–302. doi:10.1104/pp.72.2.297

Fan, F., Zhang, F., Song, Y., Sun, J., and Bao, X. (2006). *Nitrogen fixation of faba bean (vicia faba L.) interacting with a nonlegume in two contrasting intercropping systems nitrogen fixation of faba bean (vicia faba L.) interacting with a non-legume in two contrasting intercropping systems 2016–2020*. doi:10.1007/s11104-006-0019-y

FAO (2015). *Boosting Africa's Soils; from the Abuja Declaration on Fertilizers to a sustainable soil management framework for food and nutrition security in Africa by 2030*.

Fawy, K. F., Taher, M. A., Hesham, A. E., Eid, E. M., El-bebany, S. A. A. A. F., and Ahmed, G. A. E. M. T. (2018). The evaluation of sewage sludge application as a fertilizer for broad bean (Faba sativa Bernh.) crops. *Food Energy Secur.* 7, e00142. doi:10.1002/fes3.142

Fijalkowski, K., Rorat, A., Grobelak, A., and Kacprzak, M. J. (2017). The presence of contaminations in sewage sludge – the current situation. *J. Environ. Manage.* 203, 1126–1136. doi:10.1016/j.jenvman.2017.05.068

Garrido, S., Campo, G. M. D. E. L., Esteller, M. V., Vaca, R., and Lugo, J. (2005). Heavy metals in soil treated with sewage sludge composting, their effect on yield and uptake of broad bean seeds (Vicia faba L.) *Water, Air, Soil Pollutionh* 166, 303–319. doi:10.1007/s11270-005-5269-4

Guo-hang, Y., Guang-yun, Z. H. U., He-lian, L. I., Xue-mei, H. A. N., Ju-mei, L. I., and Yi-bing, M. A. (2018). Accumulation and bioavailability of heavy metals in a soil-wheat/maize system with long-term sewage sludge amendments. *J. Integr. Agric.* 17, 1861–1870. doi:10.1016/S2095-3119(17)61884-7

Hanay, Ö., Hasar, H., Kocer, N. N., and Aslan, S. (2008). Evaluation for agricultural usage with speciation of heavy metals in a municipal sewage sludge. *Bull. Environ. Contam. Toxicol.* 81, 42–46. doi:10.1007/s00128-008-9451-4

He, Q., Ren, Y., Mohamed, I., Ali, M., and Hassan, W. (2013). Assessment of trace and heavy metal distribution by four sequential extraction procedures in a contaminated soil. *Soil Water Res.* 8 (2), 71–76. doi:10.17221/20/2012-SWR

Heras, J. D., Castro, E., and Man, P. (2009). A comparison of the application of different waste products to a lettuce crop: Effects on plant and soil properties. *Eff. plant soil Prop.* 123, 148–155. doi:10.1016/j.scienta.2009.08.013

Hulseman, J. (1966). An inventory of marine carbonate materials. *J. Sediment. Petrol.* 36 (2), 622–625. doi:10.1016/j.scienta.2009.08.013

Kalis, E. J. J., Temminghoff, E. J. M., and Riemsdijk, W. H. V. (2008). Relationship between metal speciation in soil solution and metal adsorption at the root. *Surf. Ryegrass* 2231, 2221–2231. doi:10.2134/jeq2007.0543

Karami, M., Afyuni, M., Rezainejad, Y., and Rainer, S. (2009). Heavy metal uptake by wheat from a sewage sludge-amended calcareous soil. *Nutrient Cycl. Agroecosyst.* 83, 51–61. doi:10.1007/s10705-008-9198-7

Karamooz, H., Akbar, S. A., Saeid, F. N., and Rainer, S. (2016). *Tolerance and accumulation of heavy metals by Descurainia sophia L.*

Kroiss, H., Zessner, M., Management, M., and View, C. B. (2007). *Ecological and economical relevance of sludge treatment and.*

Latare, A. M., Kumar, O., Singh, S. K., and Gupta, A. (2014). Direct and residual effect of sewage sludge on yield, heavy metals content and soil fertility under rice – wheat system. *Ecol. Eng.* 69, 17–24. doi:10.1016/j.ecoleng.2014.03.066

Lem, L., Collard, M., and Teychen, B. (2017). Comparison of three different wastewater sludge and their respective drying processes: Solar, thermal and reed beds. *e Impact Org. matter Charact.* 203, 760–767.

Mahdi, W. (2015). *Influence of chromium metal on chlorophyll content in leaves of paddy oryza influence of chromium metal on chlorophyll content in leaves of paddy oryza sativa L.*

Marchiol, L., Assolari, S., Sacco, P., and Zerbi, G. (2004). Phytoextraction of heavy metals by canola (Brassica napus) and radish (Raphanus sativus) grown on multicontaminated soil. *Environ. Pollut.* 132 (1), 21–27. doi:10.1016/j.envpol.2004.04.001

Mazen, A., Faheed, F. A., and Ahmed, A. F. (2010). Study of potential impacts of using sewage sludge in the amendment of desert reclaimed soil on wheat and jews mallow plants. *Soil Wheat Jews Mallow Plants* 53, 917–930. doi:10.1590/s1516-89132010000400022

Michałowski, M., and Gołas, J. (2001). The contents of selected heavy metals of willow organs as an indicator of their use in sewage sludge utilization. *Workbooks Basic Prob. Agric. Sci.* 477, 411e419.

Pachura, P., Ociepa-kubicka, A., and Skowron-grabowska, B. (2015). Assessment of the availability of heavy metals to plants based on the translocation index and the bioaccumulation factor Assessment of the availability of heavy metals to plants based on the translocation index and the bioaccumulation factor. *Desalin. Water Treat.* 57, 1469–1477. doi:10.1080/19443994.2015.1017330

Paluszak, Z., Skowron, K., Sypuła, M., and Skowron, K. J. (2012). Microbiological evaluation of the effectiveness of sewage sludge sanitization with solar drying technology. *Int. J. Photoenergy* 2012, 341592. doi:10.1155/2012/341592

Pascual, I., Avilés, M., and Aguirreolea, J. (2008). Effect of sanitized and non-sanitized sewage sludge on soil microbial community and the physiology of pepper plants. *Plant Soil* 310, 41–53. doi:10.1007/s11104-008-9626-0

Rafael, J., Bueno, P., Berton, R. S., Dias, P., Chiba, M. K., Alberto, C., et al. (2011). *Chemical and microbiological attributes of an oxisol treated with successive applications of sewage sludge*, 1461–1470. 1.

Raheem, A., Singh, V., He, J., Dastyar, W., Dionysiou, D. D., Wang, W., et al. (2018). Opportunities and challenges in sustainable treatment and resource reuse of sewage sludge: A review. *Chem. Eng. J.* 337, 616–641. doi:10.1016/j.cej.2017.12.149

Rasmussen, P. E., Albrecht, S. L., and Smiley, R. W. (1998). Soil C and N changes under tillage and cropping systems in semi-arid Pacic Northwest agriculture. *Soil tillage res.* 47, 197–205. doi:10.1016/S0167-1987(98)00106-8

Samara, E., Matsi, T., and Balidakis, A. (2017). Soil application of sewage sludge stabilized with steelmaking slag and its effect on soil properties and wheat growth. *Waste Manag.* 68, 378–387. doi:10.1016/j.wasman.2017.06.016

Samaras, V., Tsadilas, C. D., and Stamatiadis, S. (2008). Effects of repeated application of municipal sewage sludge on soil fertility, cotton yield, and nitrate leaching. *Agron. J.* 100, 477–483. doi:10.2134/agronj2007.0162

Shanahan, E. F., Roiko, A., Tindale, N. W., Thomas, M. P., Walpole, R., and Ipek Kurtböke, D. (2010). Evaluation of pathogen removal in a solar sludge drying facility using microbial indicators. *Int. J. Environ. Res. Public Health* 7, 565–582. doi:10.3390/ijerph7020565

Soriano-disla, J. M., and Gómez, I. (2014). The transfer of heavy metals to barley plants from soils amended with sewage sludge with different heavy metal burdens. *J. Soils Sediments* 14, 687–696. doi:10.1007/s11368-013-0773-4

Soriano-Disla, J. M., Navarro-Pedreño, J., and Gómez, I. (2010). Contribution of a sewage sludge application to the short-term carbon sequestration across a wide range of agricultural soils. *Environ. Earth Sci.* 61, 1613–1619. doi:10.1007/s12665-010-0474-x

WPP (2017). "World populations prospects," in *Key findings and advance table* (New York, NY, USA: United Nations), 1. [Google Scholar].

Yang, Y., Zeng, L., and Chen, L. (2019). Chemical speciation and bioavailability of cadmium and lead in the gray calcium soil. *Environ. Pollut. Bioavailab.* 31, 306–315. doi:10.1080/26395940.2019.1685908

Zhou, L., Zhao, Y., and Wang, S. (2015). *Cadmium transfer and detoxification mechanisms in a soil – mulberry – silkworm system: Phytoremediation potential*, 18031–18039. doi:10.1007/s11356-015-5011-8

Frontiers in Environmental Science

Explores the anthropogenic impact on our natural world

An innovative journal that advances knowledge of the natural world and its intersections with human society. It supports the formulation of policies that lead to a more inhabitable and sustainable world.

Discover the latest Research Topics

See more →

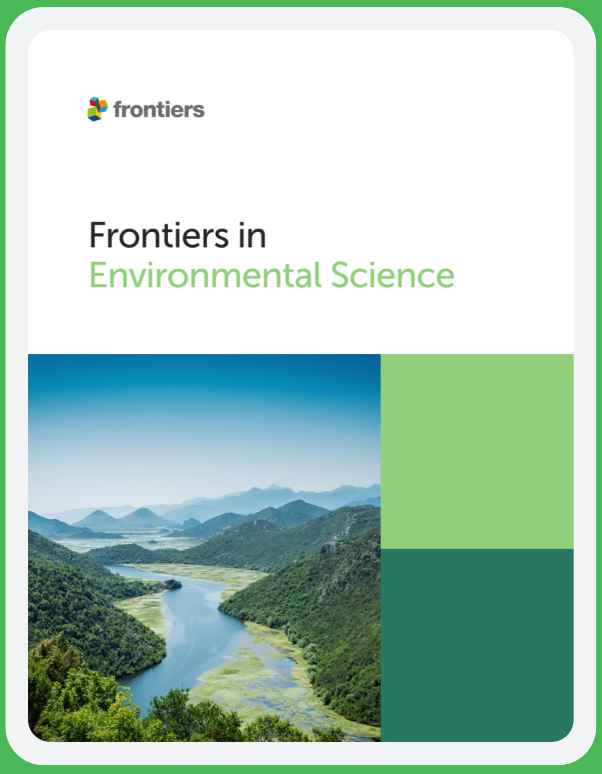

Frontiers

Avenue du Tribunal-Fédéral 34
1005 Lausanne, Switzerland
frontiersin.org

Contact us

+41 (0)21 510 17 00
frontiersin.org/about/contact